

56 Copies

NATIONAL AERONAUTICS AND SPACE ADMINISTRATION

Technical Memorandum 33-382

26

Proceedings
of the
3rd Aerospace Mechanisms Symposium

Held at the Jet Propulsion Laboratory
Pasadena, California
May 23-24, 1968



71 00-17001-826

FACILITY FORM 602

(ACCESSION NUMBER)	232	(THRU)	1
(PAGES)	CR-97758	(CODE)	31
(NASA CR OR TMX OR AD NUMBER)		(CATEGORY)	



JET PROPULSION LABORATORY
CALIFORNIA INSTITUTE OF TECHNOLOGY
PASADENA, CALIFORNIA

October 1, 1968

Reproduced by the
CLEARINGHOUSE
for Federal Scientific & Technical
Information Springfield Va. 22151

NATIONAL AERONAUTICS AND SPACE ADMINISTRATION

Technical Memorandum 33-382

Proceedings
of the
3rd Aerospace Mechanisms Symposium

Held at the Jet Propulsion Laboratory
Pasadena, California
May 23-24, 1968



JET PROPULSION LABORATORY
CALIFORNIA INSTITUTE OF TECHNOLOGY
PASADENA, CALIFORNIA

October 1, 1968

REPRODUCED BY
NATIONAL TECHNICAL
INFORMATION SERVICE
U.S. DEPARTMENT OF COMMERCE
SPRINGFIELD, VA. 22161

Preface

The 3rd Aerospace Mechanisms Symposium, held at the Jet Propulsion Laboratory, California Institute of Technology, on May 23-24, 1968, was sponsored by the University of Santa Clara, Lockheed Missiles & Space Company, and the Jet Propulsion Laboratory. The Symposium brought together approximately 300 representatives from 68 organizations concerned with the use of mechanisms in space.

The organizing committee included Richard K. Pefley and Stein Weissenberger, University of Santa Clara; Alfred L. Rinaldo and George G. Herzl, Lockheed Missiles & Space Company; Paul Bomke and Peter T. Lyman, Jet Propulsion Laboratory; and James L. Adams, Stanford University. The review panel for papers submitted at this Symposium consisted of James L. Adams, Peter T. Lyman, and George G. Herzl, chairman, who edited the submitted papers in cooperation with Mrs. Mary Fran Buehler of the Jet Propulsion Laboratory.

Management representatives of the sponsoring organizations who gave active support and encouragement were the Very Reverend Patrick Donohoe and Robert Parden of the University of Santa Clara, William H. Pickering and Geoffrey Robillard of the Jet Propulsion Laboratory, and Wayland Griffith and Elmer Wheaton of Lockheed Missiles & Space Company.

Additional assistance in preparing for this Symposium was provided by Mrs. Marilyn Buck of the Jet Propulsion Laboratory, who handled many of the details of the meeting.

The meeting was divided into four sessions with the following chairmen:

- | | |
|-------------------------------|---|
| I. May 23, Morning Session | Robert Debs, NASA Ames Research Center |
| II. May 23, Afternoon Session | Robert F. Steidel, University of California at Berkeley |
| III. May 24, Morning Session | Bernard Roth, Stanford University |
| IV. May 24, Afternoon Session | Francis J. Carroll, NASA Electronics Research Center |

A feature of this Symposium was a panel discussion, "Bearings and Suspensions in Space." Members of the panel were D. L. Kirkpatrick, General Electric Company; William J. Kurzeka, Atomics International Division of North American Rockwell Corporation; H. I. Silversher, Lockheed Missiles & Space Company; and George G. Herzl, Lockheed Missiles & Space Company. The moderator was William J. Schimandle of the Jet Propulsion Laboratory. The introductory remarks of the four panel members are a part of these *Proceedings*.

Prior Symposia in This Series

First Aerospace Mechanisms Symposium

May 19–20, 1966
University of Santa Clara
Santa Clara, California

Proceedings, AD 638 916, are available from:

The Clearinghouse for Federal Scientific and Technical Information
Department of Commerce
Washington, D.C.

2nd Aerospace Mechanisms Symposium

May 4–5, 1967
University of Santa Clara
Santa Clara, California

Proceedings, TM 33-355, are available from:

Jet Propulsion Laboratory
California Institute of Technology
Pasadena, California

Contents

Session I

A Brushless Despin Drive and Control for a Communication Satellite Antenna	3
<i>M. F. Fleming and D. D. Phinney</i>	
Flexural Pivots for Space Applications	9
<i>F. A. Seelig</i>	
High-Response Electromechanical Control Actuator	19
<i>G. D. Goldshine and G. T. Lacy</i>	
Minimum-Weight Springs	27
<i>H. O. Fuchs</i>	
The Radio Astronomy Explorer 1500-ft-Long Antenna Array	37
<i>E. D. Angulo and W. P. Kamachaitis</i>	
The Development Philosophy for SNAP Mechanisms	45
<i>O. P. Steel, III</i>	

Session II

Mechanisms for Restraining and Deploying a 50-kW Solar Array	55
<i>Theron Haynie and Abraham Kriger</i>	
Lubrication of DC Motors, Slip Rings, Bearings, and Gears for Long-Life Space Applications	65
<i>B. J. Perrin and R. W. Mayer</i>	

Panel Discussion: Bearings and Suspensions in Space

Evaluation of Dry Lubricants and Bearings for Spacecraft Applications	77
<i>D. L. Kirkpatrick and W. C. Young</i>	
Development of Bearings for Nuclear Reactors in Space	85
<i>William J. Kurzeka</i>	
Controlled-Leakage Sealing of Bearings for Fluid Lubrication in a Space Vacuum Environment	93
<i>H. I. Silversher</i>	
Mechanical Suspensions for Space Applications	101
<i>George G. Herzl</i>	

Session III

Mechanical Design of the Spin-Scan Cloud Camera	117
<i>D. T. Upton</i>	
A Passive Solar Panel Orientation Servomechanism	125
<i>R. L. Samuels</i>	
Mechanical Aspects of the Lunar Surface Magnetometer	133
<i>William Schwartz and William L. Nelms</i>	
Torsionally Rigid and Thermally Stable Boom	139
<i>F. C. Rushing, A. B. Simon, and C. I. Denton</i>	
A Torsion Wire Damping System for the DODGE Satellite	145
<i>Darnley M. Howard</i>	
Introduction to Rolamite	153
<i>J. P. Ford</i>	
Nonmagnetic, Lightweight Oscillating Actuator	163
<i>Dennis K. McCarthy</i>	

Session IV

The Surveyor Shock Absorber	171
<i>F. B. Sperling</i>	
Unique Mechanism Features of ATS Stabilization Boom Packages	179
<i>R. A. Lohnes, D. N. Matteo, and E. R. Grimshaw</i>	
Mechanism Design—A Test Laboratory Viewpoint	189
<i>J. M. Haley</i>	
Ball-Lock-Bolt Separation System	197
<i>J. I. Moulton</i>	
Fluid Thermal Actuator	203
<i>B. A. Shepherd and K. R. Johnson</i>	
Development of Gravity-Gradient Dampers	211
<i>M. E. Johnson and S. H. Marx</i>	
List of Attendees	219

Opening Remarks

P. T. Lyman

Jet Propulsion Laboratory

It is my pleasure to welcome you, on behalf of the organizing committee, to the 3rd Aerospace Mechanisms Symposium. This Symposium is sponsored by the University of Santa Clara, the Lockheed Missiles & Space Company, and the Jet Propulsion Laboratory of the California Institute of Technology. We have here today attendees from many areas of the United States and Canada, representing industry, universities, and various government agencies.

The prime purpose of this Symposium is to provide a forum for the open discussion and interchange of the real world problems of interest to the designer of aerospace mechanisms. The organizing committee believes that this Symposium is unique in this purpose, inasmuch as other mechanisms conferences are, in most part, oriented toward new theory. If one is willing to consider knowledge as an expanding sphere as a function of time, one can then argue that the designer's job is far more difficult than the theoretician's. The designer must consider all knowledge, past and present; in other words, the *volume* of the knowledge sphere. On the other hand, the theoretician worries primarily about new knowledge only; in other words, the *surface* of the knowledge sphere. It is the recognition of this kind of situation which has led to this series of Symposia.

In response to the Symposium's call for papers, many fine papers were submitted. Unfortunately, due to the limited time available for presentation and the requirement to present a broad but balanced spectrum of topics, we were not able to accept all submitted papers for presentation.

Papers on flight and development failures were encouraged primarily. Such papers are often more valuable than reports of successful efforts, since they prevent others from following blind alleys and making costly mistakes.

We encourage your aggressive and critical discussion to draw this information from the authors.

If the interchange of ideas at this Symposium plays a role in preventing a major problem or a failure in a flight program, then the cost effectiveness of this Symposium will be incalculable.

**Organizations Represented
at the 3rd Aerospace Mechanisms Symposium**

Aeroflex Laboratories, Inc.	McDonnell Douglas Corporation
Aerospace Corporation	Mechanics Research, Inc.
Applied Research Laboratories	Metal Improvement Company
Ball Brothers Research Corporation	Mounteer Instrument Company
Bell Telephone Laboratories, Inc.	NASA Ames Research Center
The Bendix Corporation	NASA Electronics Research Center
The Boeing Company	NASA Goddard Space Flight Center
California Institute of Technology	NASA Headquarters
California State College at Los Angeles	Naval Research Laboratory
DynaMetric, Inc.	North American Rockwell Corporation
Electro-Optical Systems, Inc.	Ohio State University
Emerson Electric Company	Perkin-Elmer Corporation
ESSA National Environmental Satellite Laboratory	Philco-Ford Corporation
Fairchild Hiller Corporation	Purdue University
Farrington and Light Associates	Pyronetics, Inc.
The Garrett Corporation	Quantic Industries, Inc.
General Dynamics Corporation	Radio Corporation of America
General Electric Company	Ryan Aeronautical Company
General Motors Corporation	Sandia Corporation
AC Electronics Division	Santa Barbara Research Center
Defense Research Laboratories	Seattle University
General Precision, Inc.	SKF Industries, Inc.
Georgia Institute of Technology	SPAR Aerospace Products, Ltd.
Goodyear Aerospace Corporation	Stanford University
Hughes Aircraft Company	Sylvania Electric Systems
Hycon Manufacturing Company	TRW Systems Group
Jet Propulsion Laboratory	United States Air Force
The Johns Hopkins University	United States Naval Postgraduate School
Lockheed Aircraft Corporation	United Technology Center
Lockheed Missiles & Space Company	University of California, Berkeley
Lockheed Technical Services	University of California, Los Angeles
Martin Marietta Corporation	University of Santa Clara
<i>Machine Design</i> Magazine	Western Gear Corporation
The Marquardt Corporation	Westinghouse Electric Corporation



Session 1

OVERLEAF: Robert Debs, NASA Ames Research Center, Session Chairman

N 69-11302

A Brushless Despin Drive and Control for a Communication Satellite Antenna

M. F. Fleming

Philco-Ford Corporation
Space & Re-entry Systems Division
Palo Alto, California

D. D. Phinney

Ball Brothers Research Corporation
Boulder, Colorado

This paper describes a brushless despin mechanical drive and control system used to orient a high-gain communications antenna from a spin-stabilized satellite. This drive scheme can be readily adapted to applications requiring three-axis stabilization and high reliability. The paper reviews both the design and the performance test results.

I. Introduction

One of the promising techniques for communications satellite operation is to employ a steerable antenna to achieve high gain and still retain the inherent advantages of spin stabilization. This paper describes a mechanically despun antenna developed at Philco-Ford Space & Re-entry Systems Division, with Ball Brothers Research Corporation acting as the subcontractor for the mechanical subassembly. This antenna, designed for operation in the 7- to 8-GHz frequency band, consists of three major elements: the motor drive assembly, the control electronics, and the RF antenna. The total system weight is approximately 12 lb, including redundant control electronics, while the average power is less than 5 W. The unit has been designed for a 5-year lifetime and possesses features readily adaptable to a variety of despin applica-

tions. The antenna is designed to provide earth coverage from synchronous altitude. The required peak gain is 18.0 dB with the half-power point at 9.5 deg off axis.

Figure 1 shows the general arrangement of the antenna in the spacecraft. The despun horn-reflector combination is concentric with the spacecraft spin axis. Radiated energy is focused on the reflector by means of a horn and RF lens and then reflected through an angle of 90 deg so that the beam is continually directed toward the center of the earth as the satellite spins. Also shown in the figure is the location of earth sensors which provide the basic steering signal for the antenna motor drive. Radial and axial thrusters are used to maintain longitudinal station and to periodically correct spin axis attitude as required for proper earth coverage.

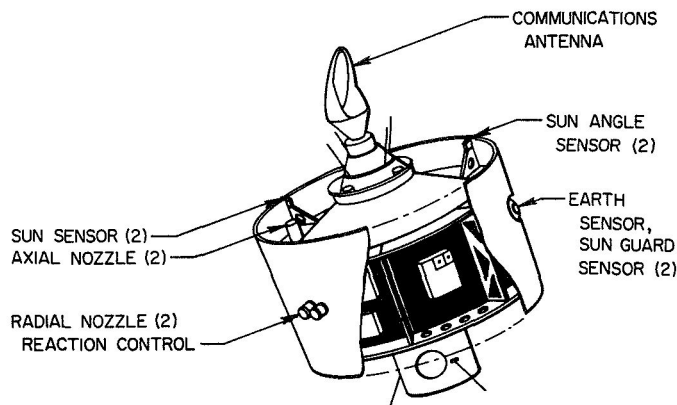


Fig. 1. Spacecraft arrangement showing antenna and drive assembly

II. Despun Antenna System

The despun antenna system consists of the following major subassemblies:

- (1) RF subassembly, consisting of radiating aperture (horn, lens, reflector), orthomode-transducer, polarizer, and rotary joint (not discussed in this paper).
- (2) Motor drive assembly, consisting of bearings with lubrication provisions, motor, resolver, angular rate pickoff, and position pickoff.
- (3) Control system, consisting of an earth sensor assembly, which provides the earth center reference signal, and control logic circuitry, which drives the motor with respect to the earth reference signal.

A. Motor Drive Assembly

The antenna is supported and positioned by the motor drive assembly. There are two pertinent considerations in the mechanical design of this component: (1) the requirement to withstand the launch environment without the complexity of a caging mechanism and (2) the requirement of a mission lifetime of 5 years, which influences the selection of lubrication and bearing configuration and the selection of a drive motor that avoids sliding electrical contacts. The final configuration is shown in Fig. 2.

1. Bearings and lubrication. The basic bearing size is dictated by the RF waveguide, which has a 1-in. bore. Bearings chosen were of the thinnest available cross section large enough to go over the waveguide and have a capacity sufficient to withstand launch loads with a large safety factor.

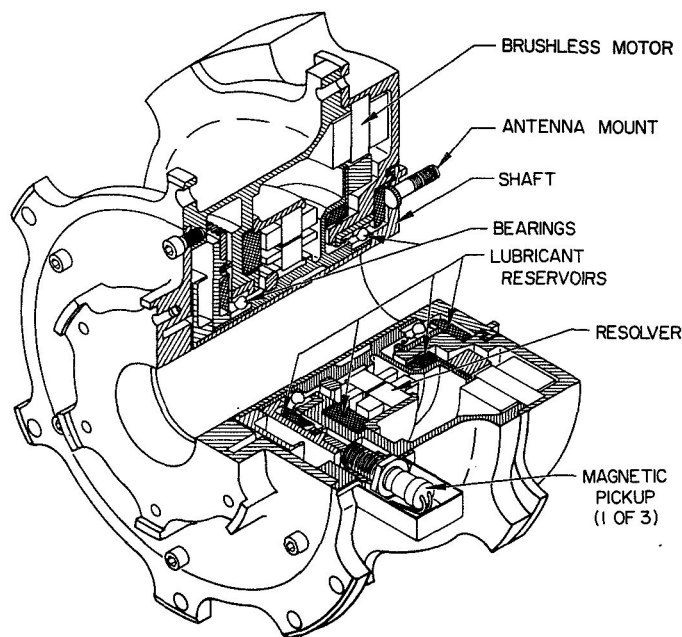


Fig. 2. Cutaway of drive assembly

In order to have a one-piece ball separator with fully enclosed pockets, one shoulder of the outer race is relieved to permit assembly. The bearings are placed back-to-back on opposite ends of the shaft. The outer race of the antenna-end bearing is slip-fitted in the housing and preloaded axially outward by a light spring. The spring is installed in a cup that is cut to length at assembly to give just enough axial play on the shaft to compensate for differential expansion between the housing and shaft when the unit heats to its maximum operating temperature. Spring preload is sufficient to locate the shaft firmly and is well below the minimum thrust capacity of the bearings for 5 years of operation at 110 rpm and maximum achievable reliability. The bearings are made of consumable electrode-vacuum melted 440 C corrosion-resisting steel to provide maximum fatigue capacity and resistance to atmospherically induced corrosion with a standard available material.

The lubricant consists of a low-vapor-pressure organic liquid with metallo-organic additives. It is applied in a thin film on all bearing surfaces and is impregnated into the ball separator, which is specified with a controlled porosity in order to provide it with lubricant capacity. The lubricant and application method bear the designation Vac Kote by Ball Brothers Research Corporation,¹

¹For more information on Vac Kote, see "Lubrication of DC Motors, Slip Rings, Bearings, and Gears for Long-Life Space Applications," by B. J. Perrin and R. W. Mayer, in these *Proceedings*.

who developed the process for use on the Orbiting Solar Observatory (OSO) series of satellites.

Lubricant replenishment is accomplished by oil stored in porous nylon reservoirs located on both sides of each bearing. Oil in the reservoirs outgasses slowly until equilibrium is reached between the oil-coated surfaces of the assembly and the oil vapor in the closed compartment. As an oil molecule is lost by evaporation from any surface, it is replaced by one striking and being captured by the temporarily depleted area. At equilibrium there is a continuous interchange of lubricant molecules between the bearing surfaces, the space around them, and the oil-coated internal walls of the assembly. Oil molecules finding their way through the labyrinth seals are replaced by ones from the reservoirs. The thin lubricant films which this system deploys have been proved capable of lubricating lightly loaded ball bearings at moderate speeds and temperatures by hundreds of spaced components, many operating for thousands of hours.

2. Overall construction. As seen in Fig. 2, the motor and resolver rotors are mounted on an inner shaft with journals for the bearing inner races. This shaft is titanium to eliminate differential expansion effects on the resolver rotor which could affect its output. The titanium shaft is sleeved with an aluminum tube which is flanged at one end to mount the antenna and which forms the waveguide through the center of the assembly. The toothed wheel, which excites the magnetic pickups, and the rotary RF joint flange complete the shaft assembly. The

magnetic pickup exciter wheel and the waveguide flange have integral rings which fit closely in grooves in the housings to form labyrinth seals that retard the escape of lubricant.

The housing is in two parts, both magnesium with Dow 17 surface treatment. Bearing outer ring mounting bores are sleeved with 416 corrosion-resistant steel to provide increased resistance to assembly damage and to reduce differential expansion effects on the bearing fits. An AND10050-2 boss is provided for attachment of a nitrogen purge line for prelaunch operation during periods of high relative humidity, which might cause bearing corrosion.

B. Control System

The control for despinning and stabilizing the antenna with respect to the earth is shown in the functional block diagram of Fig. 3. The IR earth sensor mounted on the spinning portion of the satellite provides the basic pointing reference for the despun antenna. The sensor used in this system operates in the 14- to 16-micron IR band and is free of cloud-induced interference. Such a sensor was manufactured by Lockheed Missiles & Space Company initially for the P-11 Program, the Despun Antenna Test Satellite, and the Intelsat Program. The sensor in use on the present program is a high-reliability version having a calculated mean time to failure of 90 years. The Lockheed sensor provides an earth center reference accurate to within 0.2 deg.

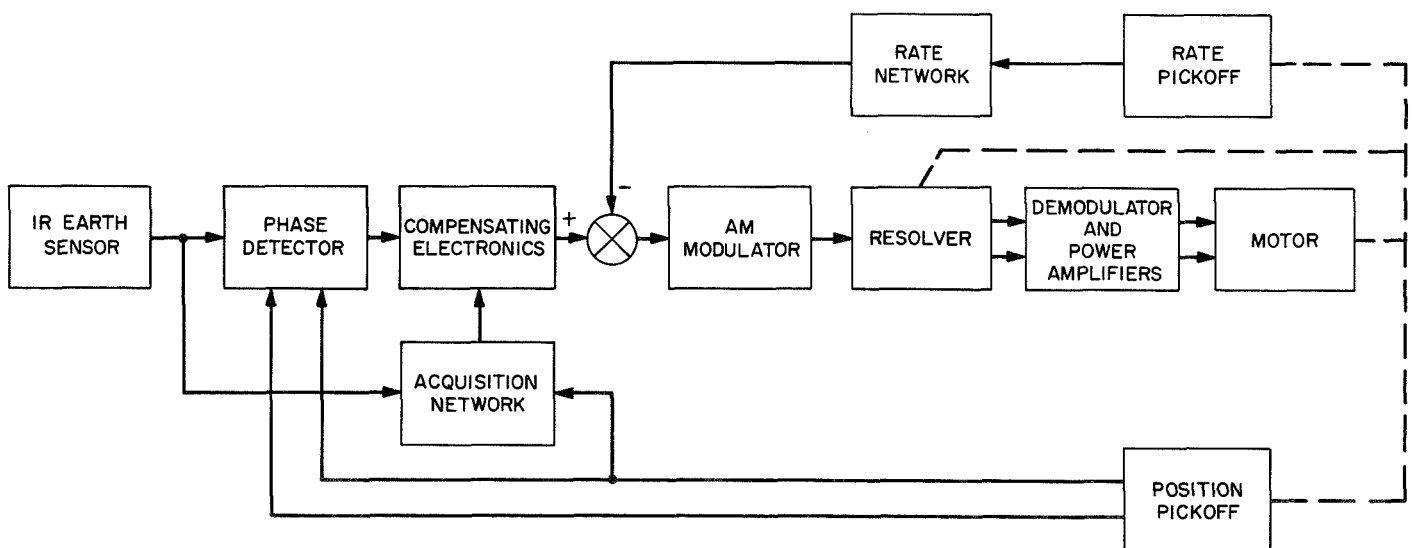


Fig. 3. Despun antenna control loop functional block diagram

Antenna position with respect to the spinning spacecraft is obtained by the use of two magnetic pickups and a steel tooth attached to the drive shaft. Angular rate data are delivered by a third magnetic pickup which is excited by a multiple-toothed steel disc. It was found during development that a high-performance tachometer is necessary to accomplish the pointing accuracy requirement. Two position sensors are used: the signal from the first is used as a prime reference, while the second, mounted 180 deg from the prime, accomplishes sign inversion for the control circuitry. The output of the angular rate magnetic pickup is in the form of a pulse train with a frequency proportional to rotor speed. To avoid the need for a digital frequency lock loop and phase detector, the signal-processing technique converts the pulse train to a speed-proportional signal having a form analogous to the output of a tachometer. Implementation becomes simple in principle and design.

The resolver-commutated synchronous motor affords the system maximum efficiency without the complexity of a special starting circuit and without compromising the long life objectives through the introduction of sliding contacts.

The drive employs a rotary transformer-type resolver which, when properly aligned, acts to commutate the synchronous permanent magnet motor. The resolver has an input winding which is excited at 1000 Hz and two output windings which have an output proportional to the input at the input carrier frequency modulated with a trigonometric function of the angular position of the rotor. The rotor is a variable reluctance element having shorted windings, whose turns and winding distribution are controlled to obtain an optimum modulated wave shape on the output winding and a desired phase relationship between the two windings. The resolver schematic is shown in Fig. 4. The figure also shows the relationship between input and output signals where ϕ is

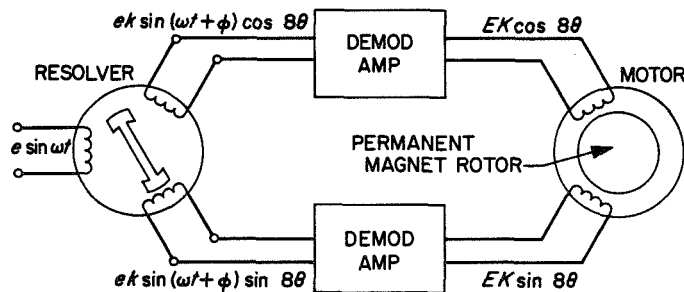


Fig. 4. Motor-resolver block diagram

an electrical phase shift between the carrier frequency input and output and θ is the angular position of the rotor.

The acquisition network consists of a speed differential circuit. The earth sensor output triggers a monostable to generate a speed-dependent signal as described above for the rate network. This signal is compared with the output of a similar tachometer circuit operated by the position feedback magnetic pickup. The output error is proportional to the speed differential, after filtering, and is fed to the compensating electronics.

III. Test Results

Performance data available at the time of publication reflect results of two successful breadboard systems and one model constructed of flight quality components in flight model configuration. The data represent the cumulative effort of approximately 10 months of intensive design, simulation, test, evaluation, and redesign.

The power required to operate the mechanically de-spun antenna is described in two respects, starting transients and tracking. The maximum power input during the starting is limited by the dc-dc converter and is no greater than 7.5 W lasting no more than 10 s. The running or tracking power varies with bearing drag and speed of rotation. The bearing drag varies inversely with temperature and is practically independent of speed in the range of 76 to 105 rpm. A plot of total power versus temperature is shown in Fig. 5. The power includes the requirements for (1) a shunt regulator to reduce bus current ripple to 15 mA peak to peak, (2) the dc-dc converter losses, and (3) the control power for the motor

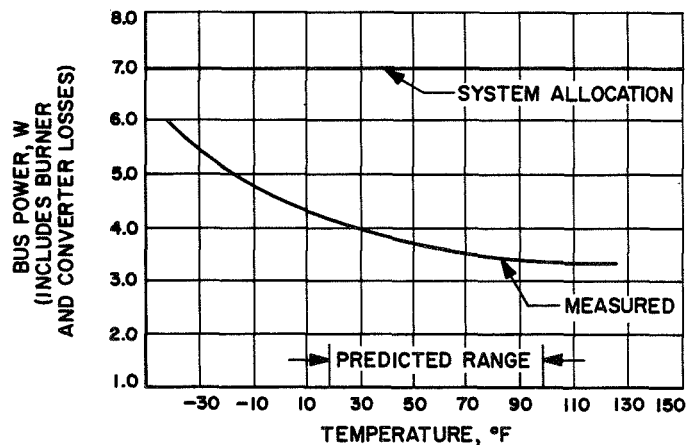


Fig. 5. Bus power vs temperature

drive assembly. The design margins in Fig. 5 result from specifying a 30°F temperature range in excess of the predicted limits. The control circuitry can drive the motor at 180% of the most severe drag torque predicted.

The tracking error varies with speed. Slower speeds result in a greater sensitivity to tachometer errors caused by runout. Electronic drift errors also increase, although slightly. Temperature-induced drift errors are of second-order consequence, with the test data reflecting the jitter error caused by resolver-motor nonconformity and mechanical runout. The results of measurements made on the development model are shown in Fig. 6. In order to

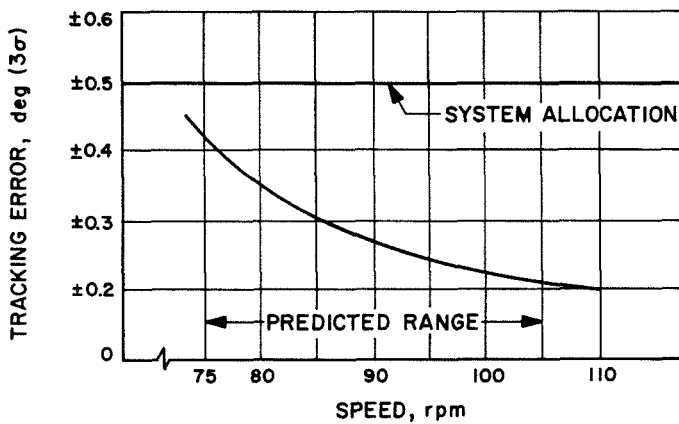
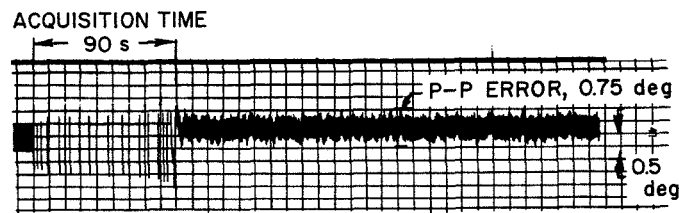


Fig. 6. Acquisition and tracking performance

demonstrate the context of information shown in Fig. 6, a sample of the acquisition transient is included. The acquisition transient shows the time (≈ 90 s) from turn-on to tracking at the ± 0.5 -deg level. The 0.5-deg allocation is from a total system requirement of ± 1 deg and is proportioned between mechanical alignment (± 0.1 deg), earth sensor errors (± 0.2 deg) and the despun antenna control.

IV. Summary and Conclusions

A despin drive making use of what is believed to be a unique application of a resolver-commutated synchronous motor to a speed servomechanism has been described. The total system is simple, has a minimum of moving surfaces in contact with each other, and consequently has a high reliability for the long space mission it is designed for. All these characteristics make the drive well suited to its intended mission as well as to others that may arise in the future.

Salient conclusions drawn from this design experience are:

- (1) A resolver-commutated synchronous motor is practicable for high-precision orientation requirements.
- (2) Sliding electrical contact surfaces can be avoided, enhancing confidence in a long mission lifetime objective.
- (3) The system weight and electrical power requirements are extremely attractive, particularly when compared with other schemes.
- (4) The system can be readily adapted to related despin applications.

Discussion

H. Smallen: Why was not beryllium used instead of magnesium for the housing of the drive assembly (Fig. 2)?

Beryllium has physical and mechanical properties which enhance its use for bearing housings for aerospace applications. These include:

- (1) Coefficient of expansion comparable to steel bearings and races.
- (2) High stiffness.
- (3) Light weight.
- (4) High-precision elastic limit.
- (5) High damping capacity.
- (6) Better corrosion resistance than magnesium (does not require protective coating as does magnesium).
- (7) High thermal conductivity.
- (8) High specific heat.

The use of magnesium for the drive assembly housing necessitated the use of a titanium shaft to eliminate differential expansion effects on the resolver rotor. This, along with an aluminum tube, complicated the device. In spite of the high beryllium cost com-

pared to that of magnesium, it is believed that a better and less expensive drive assembly would have resulted.

VHPB (vacuum hot-press block beryllium) would be the logical choice. This material is easy to machine and many intricate housings have been fabricated for space applications.

Table D-1 compares beryllium and titanium for bearing housing application.

D. D. Phinney: Beryllium has excellent characteristics for use as a structural material in despin drives. Our investigations show, however, that the cost differential is significant and cannot be justified in all instances. Titanium and magnesium were used in the subject drive instead of beryllium because of lower cost and better availability, at a penalty of a few ounces of weight. When all requirements were considered, no significant design simplification appeared possible by using beryllium that would offset its high cost. Use of magnesium for the housing, on the other hand, simplified handling procedures, since magnesium is not notch sensitive while beryllium requires any surface scratches to be etched out to prevent cracks.

Table D-1. Physical and structural property comparisons for beryllium and magnesium

Alloy	Density, lb/in. ³	Young's modulus, 10 ⁶ psi	Typical tensile strength, ksi		Thermal conductivity, Btu ft/h ft ² °F	Specific heat, Btu/lb/°F	Thermal expansion, 10 ⁻⁶ in./in./°F
			<i>F_{tu}</i>	<i>F_{ty}</i>			
VHPB beryllium	0.067	42-44	50	40	110	0.40	6.2
Magnesium	0.066	6.4	36	29	35	0.25	13.5

F_{tu} ultimate tensile strength.
F_{ty} tensile yield strength.

NU9 33803

Flexural Pivots for Space Applications

F. A. Seelig

The Bendix Corporation Fluid Power Division
Utica, New York

Design considerations and problems encountered in fabricating flexural pivots for use as structural members are discussed. Applications described include engine mounts, camera telescope mounts, missile support systems, gimbal assemblies, and trunnion pivots.

I. Introduction

Flexural pivots have been successfully applied in space programs by many NASA contractors and other agencies. It is intended here to discuss some of the design considerations and problems encountered in fabrication of pivots for those applications where flexural pivots are utilized as structural support members (as opposed to those used in instrument sensing devices). Typical applications are engine mounts (*Lunar Orbiter*), camera telescope mounts (ATS¹ satellites), support system (Transtage Engine, *Titan III C* Missile), support system (ERNO Third Stage Engine, ELDO Missile), gimbal assembly (Directional Control Test Missile Test Stand), and the trunnion pivots (X-ray Telescope *Apollo* Applications Program, AAP).

¹*Applications Technology Satellite*. See also "Mechanical Design of the Spin-Scan Cloud Camera," by D. T. Upton, in these *Proceedings*.

These applications will be discussed in the sequence mentioned above to show the interrelationship of one design to another and how improvements of one design were subsequently incorporated in another.

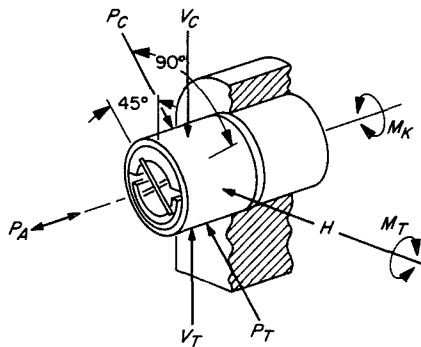
II. Basic Components of Flexural Pivots

All flexural pivots consist of three basic elements: flexures, core or inner housing, and mounting means or outer housing. The heart of any flexural pivot is the flexure; it must have first priority of design consideration. The configuration and the orientation within the assembly with respect to the major force vectors applied must be optimized for a particular specification. The core, or inner housing, is the member to which flexures are directly attached. It fixes the orientation of flexures while providing reinforcement of the flexures. It is fastened to the outer housing, which is the mounting member for the complete, self-contained pivot.

III. Flexure Designs

Normally one thinks of flexures in terms of flat rectangular pieces of spring steel cut from lengths of rolled sheet stock. This is the simplest form that can be fabricated and stress-analyzed. The means by which to use these simple members most efficiently is the challenge to the designer. What behavior patterns do they follow when combined and used in pairs or sets of various dimensions? How are their load-carrying capabilities affected by force vector combinations? What conditions of load are design limitations?

In order to consider flexure design, one must first decide what is required of the assembly with respect to its structural capacity. As a place to start, let's consider that there are six fundamental force vectors and two basic moments shown on Fig. 1. All force vectors here are assumed to be of equal magnitude. The flexure proportions for various loading conditions may be related to each other approximately as shown in Fig. 2 with respect to length, width, and thickness. Orientation is related to the force vectors. For example: if only a P_c is considered (Fig. 2c), it can easily be seen that one



- V_C VERTICAL FORCE SHARED BY ALL FLEXURES IN COMPRESSION
- P_C ALL FORCE CARRIED BY ONE FLEXURE (OR PAIR IN SAME PLANE) IN COMPRESSION
- H HORIZONTAL FORCE PUTS ONE FLEXURE (OR PAIR IN SAME PLANE) IN COMPRESSION
- P_A AXIAL FORCE PUTTING ALL FLEXURES IN SHEAR
- V_T VERTICAL FORCE SHARED BY ALL FLEXURES IN TENSION
- P_T ALL FORCE CARRIED BY ONE FLEXURE (OR PAIR IN SAME PLANE) IN TENSION
- M_T MOMENT APPLIED TO BEND PIVOT AXIS (NOT INCLUDING OVERHUNG MOMENT FROM TRANSVERSE FORCES ABOVE)
- M_K MOMENT APPLIED TO ROTATE PIVOT AND CAUSE BENDING OF FLEXURES

RADIAL FORCES SHOWN TO BE CONSIDERED IN PLANE OF M_T AXIS
ILLUSTRATION SHOWS ORIENTATION WITH FLEXURE ANGLES ONLY

Fig. 1. Primary force vectors, flexural pivot design

relatively thick flexure will suffice. If the direction of the load relative to the flexures is as shown in Fig. 2e, the tension flexure may be relatively thin and the compression member somewhat thicker (to prevent buckling). Similarly, the flexure thickness of Fig. 2d is greater than that of Fig. 2b. (The flexure configurations for individual load conditions shown here are not realistic, since it would indeed be unusual to find such simple load systems for a given application.)

More realistically, most applications require an investigation of complex combinations of these force vectors. For example, let's assume that flexures must be designed to support a small variable-thrust engine in the third stage of a missile. The engine, supported on a gimbal ring which is not completely rigid, is held in a fixed position by locked-up actuators during the launch phase, with its center of gravity off the centerline of its thrust vector. Also assume that the engine must be fired and gimballed through maximum operating angles at full thrust. It is obvious that the force vectors in this application require careful study to determine which force combinations are applied simultaneously and cause the most stress on the flexures. These combined loads set the design limits.

In order to consolidate the infinite number of configuration possibilities, three basic concepts will be considered, each permitting variations of flexure length, width, and thickness for design adjustment. These basic arrangements are shown in Figs. 2g, h, and i, respectively: the 90-deg symmetrical universal system, the 60-deg symmetrical nonuniversal system, and the "plus design" or unsymmetrical system. The latter uses the wide flexure as the main load-carrying member, with the narrow flexures as stabilizing elements. It has been our experience that most pivot applications for space structures can be satisfied with these three concepts. It is not intended to imply that other configurations of flexures and pivot concepts are not to be considered, but only that these form a simple, realistic design approach. We normally use the formulas developed in papers by Fred Eastman (Refs. 1-3), W. H. Wittrick (Ref. 4), Henry Troeger (Ref. 5) and others which deal with simple flat flexures. There are other possibilities, such as triflexures, cruciforms, contoured cross sections, and wire. All of these can be designed for specific requirements, but they also have limitations which may or may not be desirable. It is not intended to discuss these at this time.

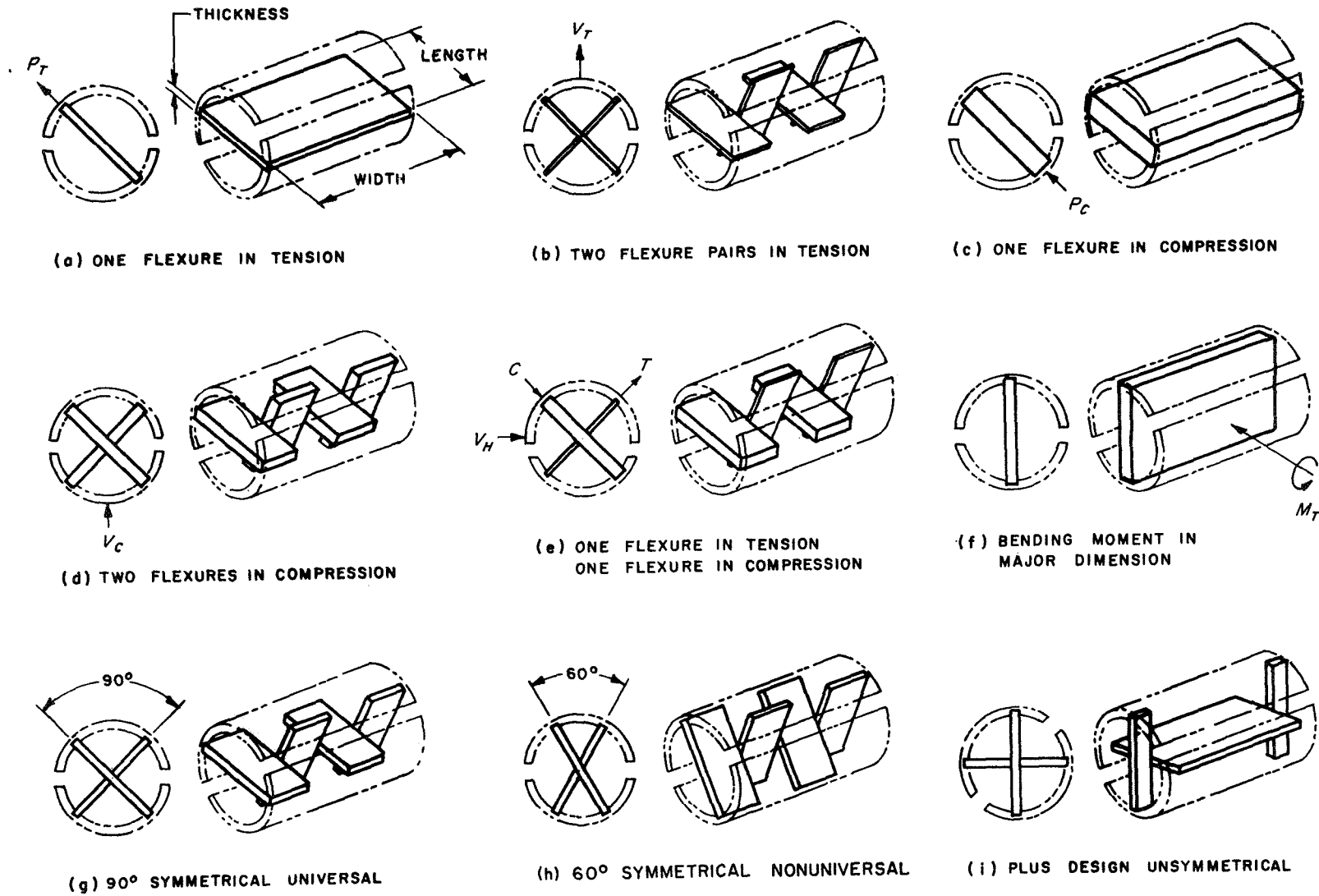


Fig. 2. Flexure configuration and orientation with respect to load

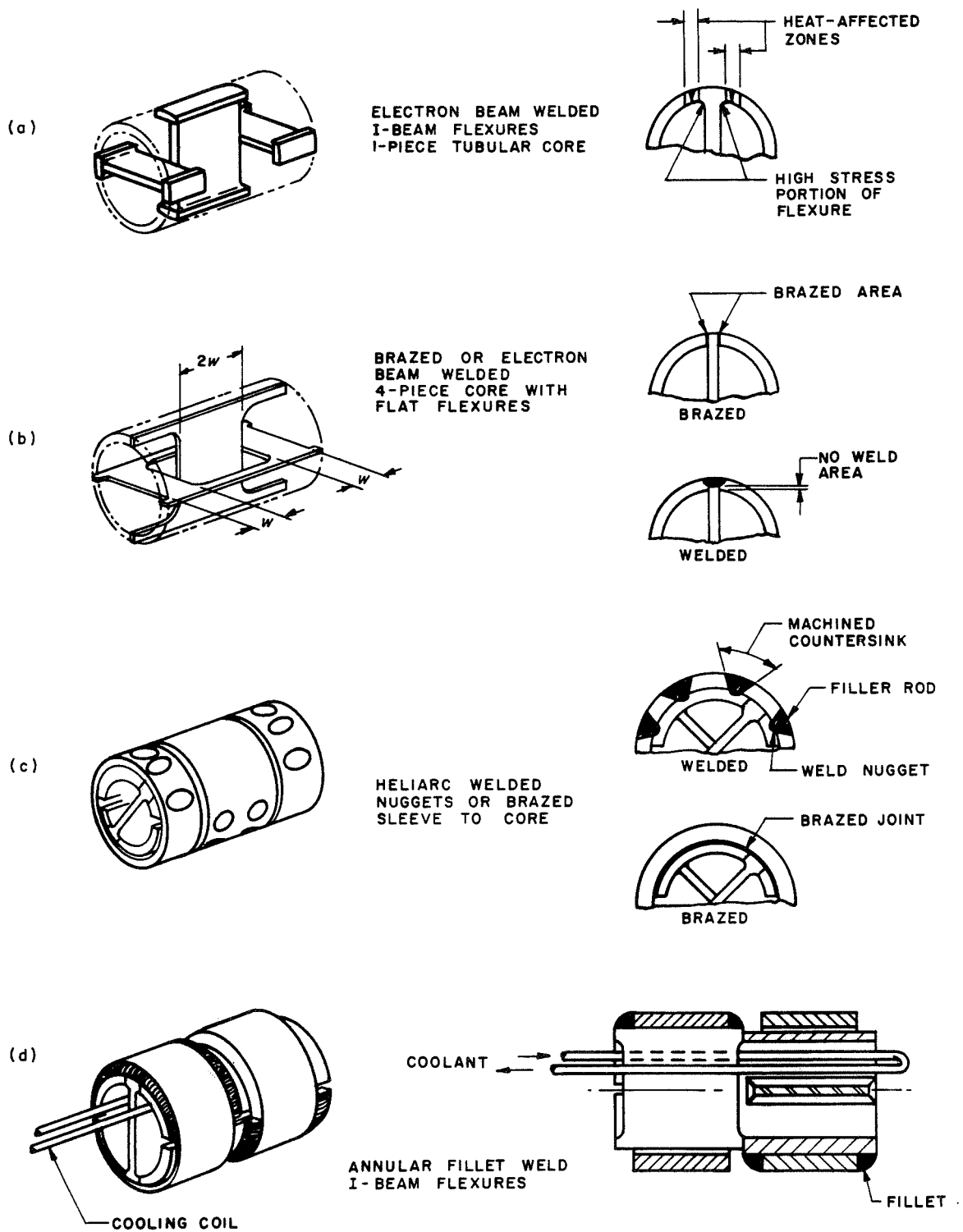


Fig. 3. Fabrication of brazed and welded assemblies

IV. Core or Inner Housing

The inner pivot housing or core can be as important for structural integrity as the flexure. Flexural pivots can be designed so that the forces are applied with the housing acting either as a cantilever beam or as a double-end-supported beam. The whole concept of mounting must be considered, particularly if weight or radial stiffness limitations are involved. The thickness of the housing depends on the method of attachment of the flexures and must be reasonably proportional to the flexure configuration. As a rule of thumb, we have used a thickness at least equal to flexure thickness for welded construction and at least $1\frac{1}{2}$ to 2 times the flexure thickness for brazed construction (Fig. 3). This assumes the braze joints to be extended beyond the individual flexure widths, as shown in Fig. 3b. The core may be rectangular, square, octagonal, or round to suit the mounting conditions. The round tubular shape seems to have the greatest advantage for utilization of material and lends itself to simple machine operations such as turning, boring, and centerless grinding. It also permits the use of tubing, which reduces material cost and machine time. This type of housing may also be made from die-formed cylindrical segments or quadrants, brazed or welded together with the flexures. The housing configuration may be adjusted to suit the fabrication techniques intended.

V. Mounting Member, Outer Housing

This member of the flexural pivot is primarily an adapter to fit the flexures included in the core assembly to the other hardware. In some cases, a heavy core can incorporate tapped holes, studs, or partial flanges, eliminating the need for the outer member. The cylinder outer sleeve provides a more readily adaptable member for mounting without complicating the fabrication of the core assembly. It can be easily modified to include flanges or mounting lugs. The round shape has the same machining advantages as the core.

VI. Fabrication

A variety of fabrication methods are utilized in making a pivot assembly. Joining processes demand careful consideration in the design configuration of the basic components. For example, if temperature and load conditions are moderate, pivots of brazed construction with flat flexures and quadrant-type housing are adequate (Fig. 3b). However, if the design is likely to carry high transverse loads creating high flexure stresses, I-beam flexures with

a one-piece tubular core are a more practical and more reliable design (Fig. 3a). This permits welding and keeps the heat-affected zone of the weld away from the highly stressed portion of the flexures.

There are several possibilities for attaching the outer housing or sleeve to the core. One method is by countersinking through holes from the outside of the sleeve, welding the inner edge of the countersunk holes to the outer surface of the core, and then filling the countersunk holes with filler material (Fig. 3c). This involves good welding technique to avoid overheating the flexures. Another method is to braze the sleeve and core together (Fig. 3c). A third method, utilizing annular fillet welding at each edge of the outer housing, has proved to be the most reliable (Fig. 3d). The illustration shows four separate welds on a cantilever pivot. The double-end type requires two additional welds on the third section of the outer sleeve. This method uses a heat sink or cooling method to avoid overheating the flexures.

VII. Applications

The foregoing paragraphs have covered structural considerations and fabrication methods employed to attain the structural integrity of flexural pivots. These are not the only problems involved in pivot design, as will be shown by discussion of applications in the following paragraphs. Pivots for these are depicted in Fig. 4.

The first two applications involve standard off-the-shelf-type pivots which, incidentally, are a slightly modified version of the 90-deg symmetrical universal system flexures in Fig. 2g. Instead of having two pairs of equal flexures, this design has one pair of two equal flexures on the outboard ends of the housing and one double-width flexure on a 90-deg intersecting plane in the center. The flexures are flared out as they enter the brazed joint in a quadrant-type housing, as shown in Fig. 3b. This gives higher axial capacity, higher transverse stiffness, and a slightly higher torsional stiffness than the simpler configuration.

The *Lunar Orbiter*² utilized a cantilever pivot $\frac{5}{8}$ in. in diameter by 1 in. long for the gimbal support system of a 100-lb thrust engine. Reports from the Boeing Company and NASA confirm excellent performance of the flexural pivots in all five *Lunar Orbiter* flights. These

²Work on this program was conducted for the NASA Langley Research Center under NASA Contract NAS 1-3800.

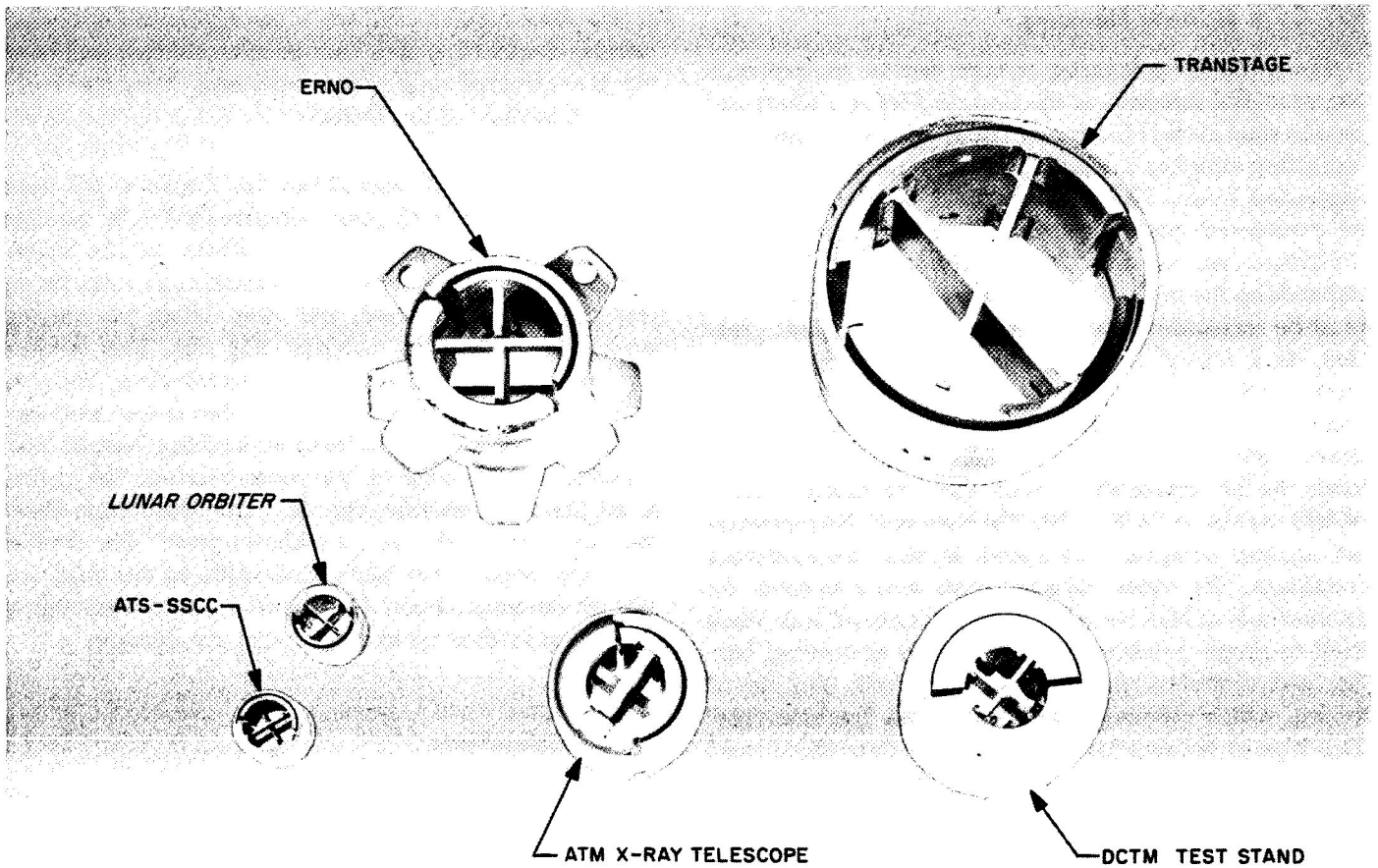


Fig. 4. Flexural pivots

pivots were purchased from stock with a 100% reliability load test prior to shipment.

Specifications for these pivots were as follows:

- (1) Rate of motion: 0.05 to 10 deg/ s.
- (2) Temperature: 400° F maximum to +35° F minimum.
- (3) Nominal angular motion: ± 4 deg, maximum ± 15 deg at no load.
- (4) Life: 5,000 nominal angular cycles at maximum temperature and nominal radial load; 200 nominal angular cycles at maximum temperature, maximum radial load and maximum axial load.
- (5) Torsional spring rate through maximum angular motion: 13 lb in./rad $\pm 10\%$.
- (6) Radial load: 200 lb maximum, 110 lb nominal.
- (7) Axial load: 35 lb maximum.

- (8) Pressure environment: 1×10^{-14} to 760 torr maximum.

The reasons for selection of these pivots were: (1) no lubrication requirements, (2) elimination of the effect of varying operating temperatures on bearing clearances, and (3) small required angular motion (see Fig. 5).

The ATS Spin-Scan Cloud Cameras utilize a double-end-type pivot $\frac{5}{8}$ in. in diameter and 1 in. long. These pivots are used in both the black-and-white and the color versions of the camera. They provide trunnion mounts for the camera telescopes, which oscillate ± 7.5 deg and ± 9 deg respectively at a rate of 1 cycle every 24 min. These applications demand extremely accurate position repeatability as the telescope moves through its angular travel. Figure 6 is a sectional view of the color camera assembly showing the pivot locations. Transverse forces applied to the pivots in both of these applications were relatively small, permitting the use of the flat flexure brazed fabrication.

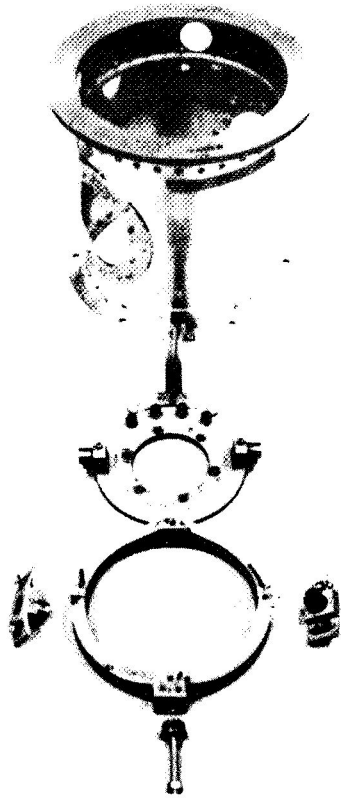


Fig. 5. Lunar Orbiter gimbal and bearing assembly, thrust vector control, photograph courtesy of The Boeing Company

The Engine Gimbal System for the Transtage Engine (*Titan III C* Missile), Fig. 7a, involved a breakthrough in the development of the weld fabrication techniques discussed in earlier parts of this paper. Several earlier unsuccessful fabrication attempts provided the experience and pointed to the need for new design and fabrication approaches. This program started with some basic investigations of the joining process. Weight was important, as were high strength, low torsional stiffness, and low radial deflections. After preliminary investigations, the 60-deg symmetrical nonuniversal system of flexures was selected with a double-end pivot configuration. The previous unsuccessful attempts at joining both by brazing and welding of flat flexures into a cylindrical housing led to the development of the I-beam type flexure and electron beam welding.

The housing joining method shown in Fig. 3c (heli-arc with countersunk holes) was used. A weld failure on the first prototype made it necessary to increase weld size. For weight reduction, it was also mandatory to remove a considerable amount of the core thickness and outer sleeve material, which further limited the available weld area. In spite of these requirements, the welding technique solved the problem.

The ERNO Engine (ELDO Third Stage) gimbal pivots (Fig. 7b) required a flexure configuration change due to

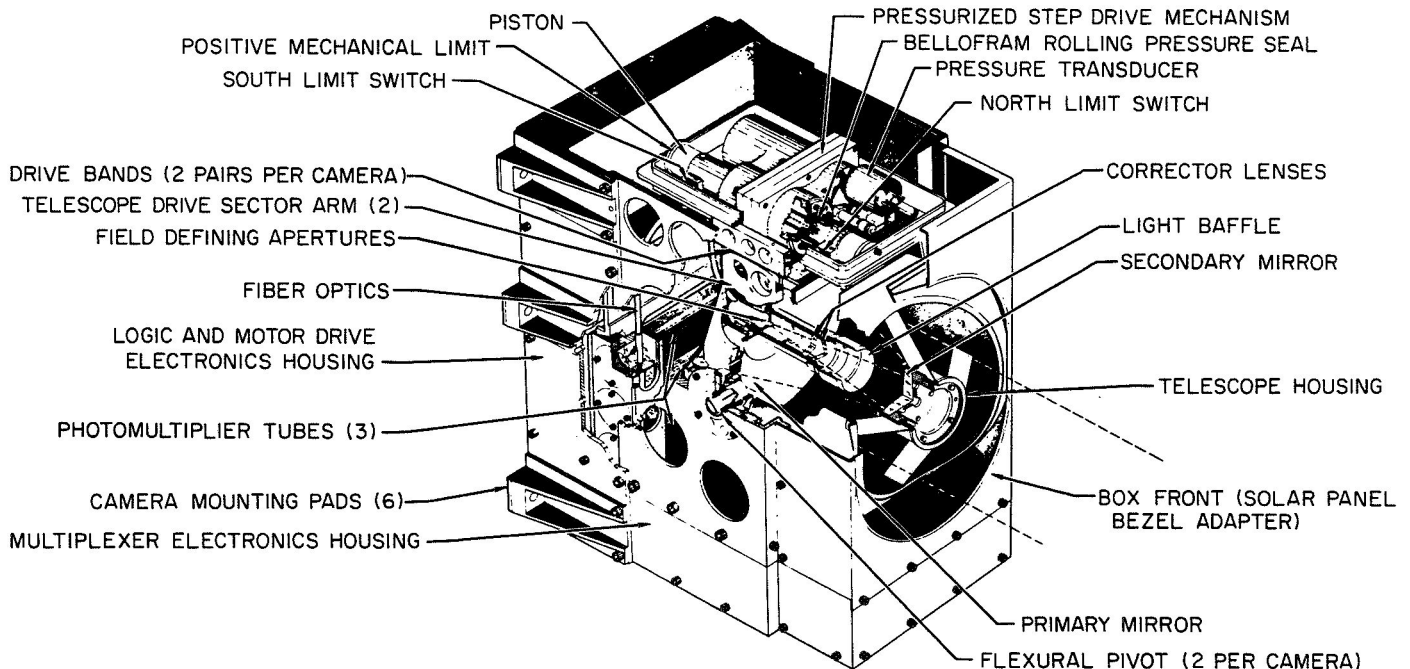


Fig. 6. ATS Spin-Scan Cloud Camera, photograph courtesy of the University of Wisconsin

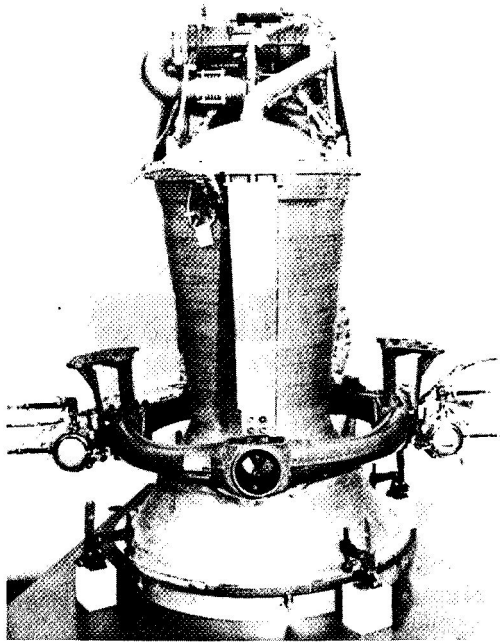


Fig. 7a. Transtage engine and gimbal, photograph courtesy of Aerojet General Corporation

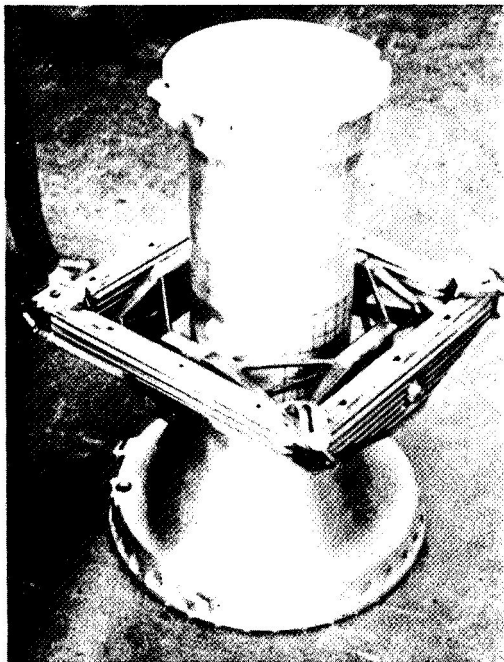


Fig. 7b. ERNO engine and gimbal, photograph courtesy of ERNO GmbH, Bremen, Germany (designer and producer of the main rocket motor and the structure of the third-stage *Europe I* rocket)

the limited envelope allowed for the pivot. The square gimbal ring tends to reduce the M_T type of moment (see Fig. 1), allowing a cantilever design in the space available. Normally a double-end-type pivot would be recommended for this high load application to better distribute the major forces on the flexures. The "plus design" configuration solved this problem. The outer housing-to-core welds had passed acceptance load tests but failed in a static load test when installed in the customer's hardware. Available area for welding was limited by the flexures and four large mounting lugs on each half of the outer housing. After some development, we adopted the annular weld shown in Fig. 3d. This approach was successful—both static and vibration tests were performed satisfactorily and the system was approved for flight status.

The Directional Control Test Missile (DCTM) Wiggle Test Stand (Fig. 8), involved another gimbal system with much higher radial stiffness and smaller deflection angle than the two previous gimbals. In spite of high radial stiffness requirements, it appeared that the flexures would be sufficiently stiff with the 90-deg symmetrical universal system. Weight was no limitation, and a double-end pivot with a square gimbal ring was designed. From this job we learned that the influence of the housing thickness on the radial stiffness of the pivot was of prime importance. The diameter had to be increased from an original diameter of $1\frac{1}{8}$ in. to $1\frac{3}{4}$ in. to provide satisfactory results for the application.

The most recent pivot application for structural space hardware is the AAP telescope mount. These pivots support the X-ray telescope and are used to minimize stresses in the telescope tube, particularly during the launch phase of the program. Figure 9 shows the arrangement of the pivots on the X-ray telescope. The specifications required small deflection angles, moderate loads, and high radial stiffness. The experience gained from investigating the core stiffness on the DCTM test stand application and from the annular weld method used on the ERNO gimbal pivots was utilized in the design of the X-ray telescope mount, resulting in only minimal development testing. In fact, this application was satisfied without the benefit of a prototype unit.

VIII. Summary

It has been attempted here to demonstrate some of the primary considerations in the design and fabrication of flexural pivots as structural members. The purpose was

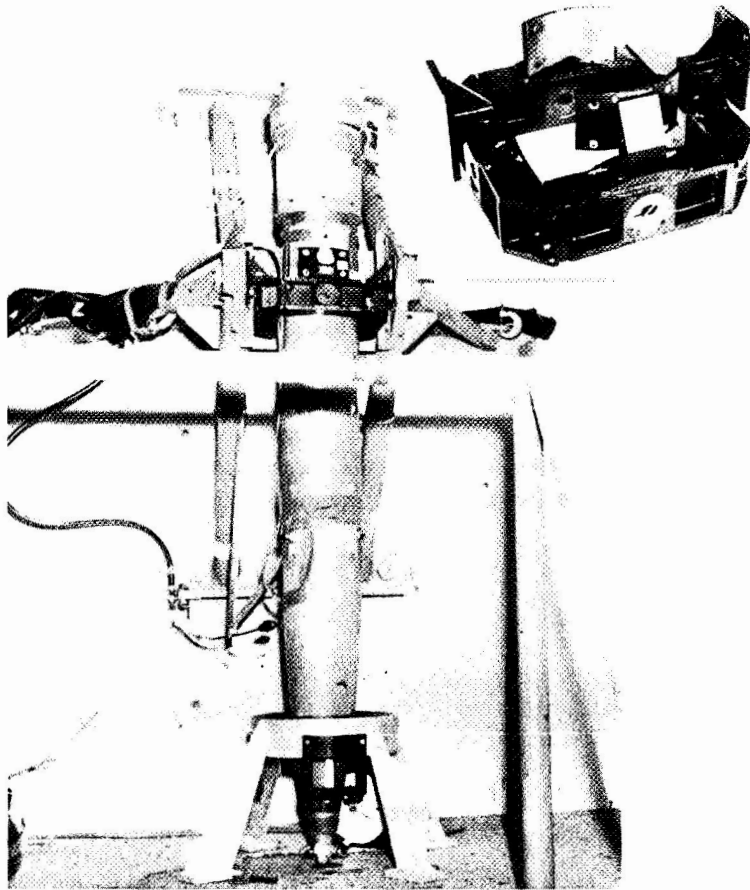


Fig. 8. DCTM Wobble Test Stand, photograph courtesy of Grumman Aircraft Engineering Corporation

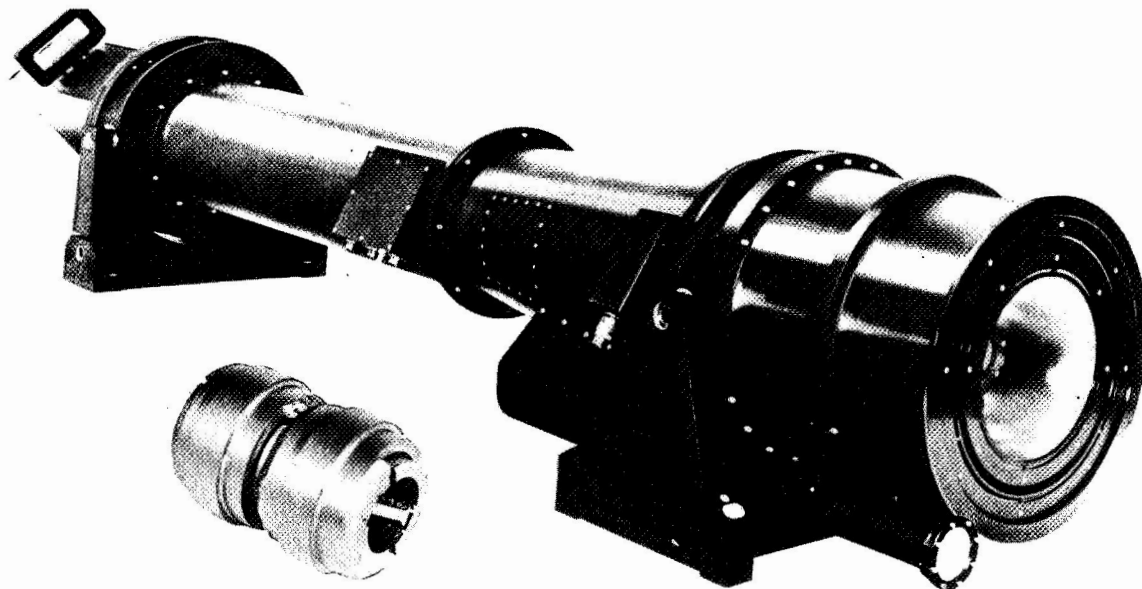


Fig. 9. ATM X-ray telescope, photograph courtesy of American Science and Engineering Company

to demonstrate the necessity to thoroughly investigate all conditions of load and environment before deciding on a pivot size and configuration. The fabrication methods cannot be separated from design requirements, since they often dictate the feasibility of the use of flexural pivots – both from design and cost considerations.

Acknowledgments

The author acknowledges the courtesy of the companies that have given permission for publication of photographs in this paper, as listed in the figure captions. Acknowledgment for publication of the Spin-Scan Cloud Camera photograph is made to the NASA Goddard Space Flight Center and to V. E. Suomi and R. J. Parent of the University of Wisconsin, prime investigator and co-investigator, respectively, for the camera.

References

1. Eastman, F. S., *Flexural Pivots to Replace Knife Edges in Ball Bearings*, Eng. Exp. Sta. Bull. No. 86. University of Washington, Seattle, 1935.
2. Eastman, F. S., "Design of Flexural Pivots," *J. Aeronaut. Sci.*, Vol. 5, pp. 16–21, Nov. 1937.
3. Eastman, F. S., "The Unique Properties of Flexural Pivots," *The Trend in Engineering*, Vol. 12, No. 1, University of Washington, Seattle, 1960.
4. Wittrick, W. H., *The Theory of Symmetrical Crossed Flexure Pivots*, Department of Aeronautical Engineering, University of Sydney, Australia, 1948.
5. Troeger, H., "Considerations in the Application of Flexural Pivots," *Automatic Control*, Vol. 17, No. 4, pp. 41–46, Nov. 1962.

N 69-11804

High-Response Electromechanical Control Actuator

G. D. Goldshine and G. T. Lacy
General Dynamics Corporation
Pomona, California

Because the need for advanced missile system performance required increased propulsion space, the space available in the missile for the control section was decreased by two-thirds. At the same time, long-term storage without maintenance required an all-electric control system. Prime objectives were to achieve substantial weight, power, and cost reductions while attaining significant increase in control capability. The resulting design of a high-performance electromechanical actuator developed at the Pomona Division of General Dynamics is described. An analytical model for investigating the internal characteristics of the actuator is shown, and some significant performance features are discussed. Development flight testing of the system has been completed, and the actuator is being mass-produced in the STANDARD MISSILE and ARM programs.

I. Introduction

The increased performance requirements for tactical missile systems initiated the development of adaptive control techniques for achieving the control-system parameter requirements. Before these techniques could be applied, a bistable control actuator with performance characteristics exceeding those available from any previous actuator development was required. The present study developed such an electromechanical actuator.

II. System Constraints

There were three principal system constraints on the control actuator:

- (1) The reduced space envelope.
- (2) The reduction in weight.
- (3) The control parameters.

A. Space Envelope

The basic necessity for increasing advanced missile system performance dictated the need for increased propulsion system performance. The propulsion increase was gained by the use of a longer rocket motor. Since the overall missile was not elongated, it became necessary to package the control section in a space envelope approximately two-thirds the length of previous section volumes. At the same time, from the standpoint of maintainability and producibility, it was necessary to provide a modular design that would be packaged by quadrant, so that four identical actuators were provided per missile. (The missile is controlled by four tail control surfaces, each driven by a separate actuator.)

B. Weight

Each actuator weighs approximately 12.8 lb; the entire control section weighs 68 lb, which represents about a

40% reduction in weight from the control section previously used in missile designs.

C. Control Parameters

The principal control parameters for the electromechanical actuator are given in Table 1.

Table 1. Control parameters

Parameter	Requirement
Transport delay time (from applied control signal to actuator reversal at full rate)	3 ± 1 ms
No-load tail rate	200 ± 50 deg/s
Tail drift rate (under no-load conditions in the bistable open-loop mode)	≤ 5 deg/s
Input power (nominal/ambient)	520 W
Load sensitivity (tail drift rate/in.-lb of applied external hinge moment)	0.05 deg/s/in.-lb
Operating life cycle (3 min on, 60 min off; 4 min for ARM)	1 h total on time

III. System Description

Each actuator, in combination with a bistable switching amplifier situated in the autopilot electronics, operates in a bistable mode such that the output is a maximum CW or CCW rate of change of tail incidence angle. The overall missile control system is adaptive by virtue of including the bistable switch/actuator combination in cascade with the missile dynamics in a closed loop, such that a limit cycle mode is sustained. Changes in gain in the forward path of the loop (i.e., aerodynamic parameter changes) will then be automatically compensated for by a resulting inverse change of nonlinear gain in the bistable switch/actuator combination. The limit cycle characteristics are fully determined only by including missile loop parameters together with the internal dynamics of the actuators themselves. (A full description of the adaptive loop is outside the scope of this paper.) The absence of the more conventional closed-loop position feedback directly around the actuator also introduces a need for special consideration of tail position drift errors due to internal unbalance within the actuators and external loading applied to the tails.

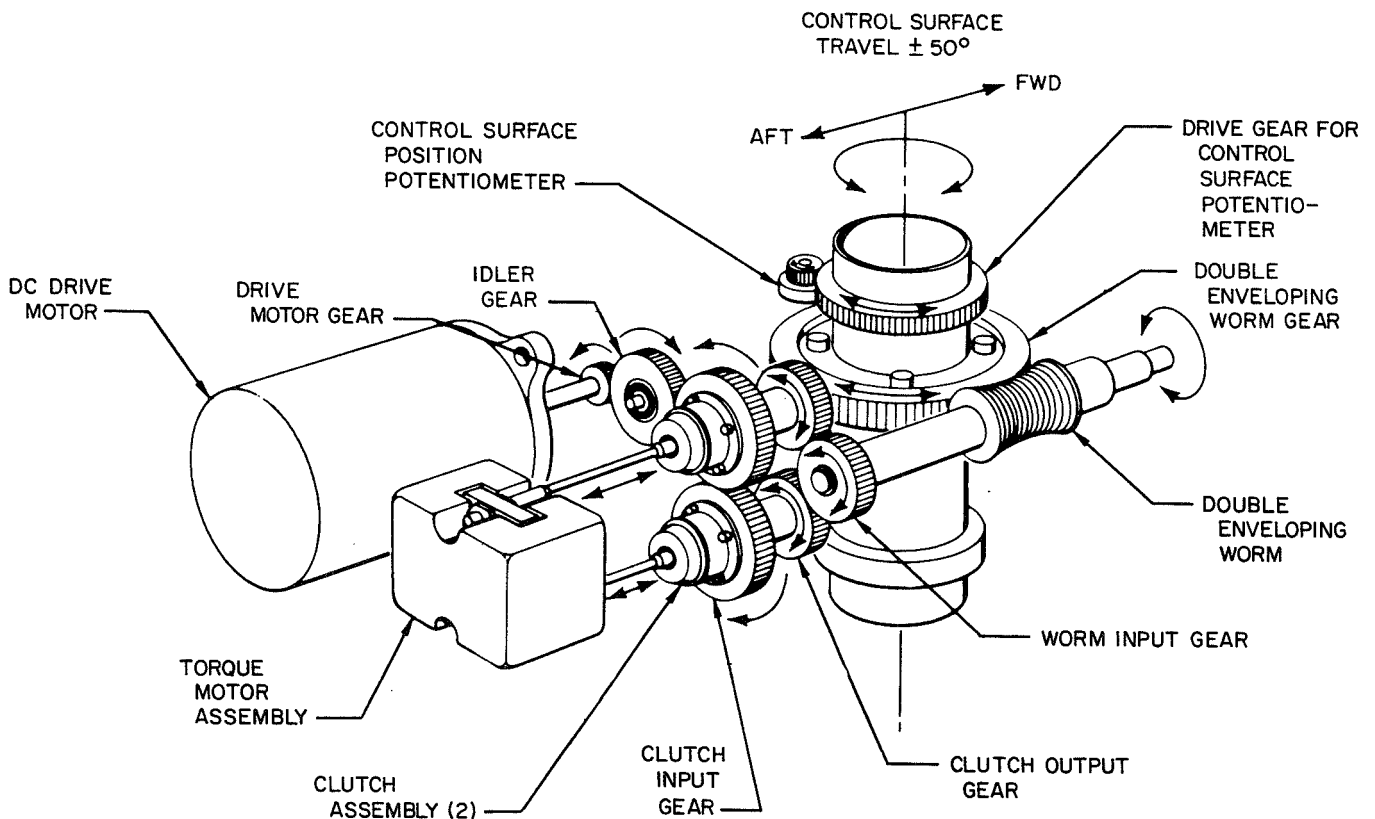


Fig. 1. Actuator mechanical schematic

The electromechanical actuator consists of the following parts: two contra-rotating capstan spring clutches with actuating cones, a torque motor, a unidirectional dc drive motor, a reduction gear train, a worm output drive, and a control surface position potentiometer (see Fig. 1).

Operation of the actuator is as follows: the contra-rotating clutch input gears that mount the capstan springs are driven at an essentially constant speed by the drive motor and reduction gear train. Both clutch output shafts are geared through a further spur gear stage to a single worm shaft. The actuator output shaft carries a sector gear in mesh with the worm and provides a direct mounting for the aerodynamic control surface. Engagement of either one of the clutches closes the drive path between the drive motor and the control surface (tail),

thus imparting maximum velocity to the surface in a direction depending upon which clutch is engaged.

IV. Analytical Model

An analytical model of the system suitable for analog computer simulation was developed, as shown in Fig. 2.

A. Drive Motor

The torque developed as a function of applied voltage and rotational speed may be expressed approximately as

$$M_e = N_1 \frac{K_T}{R} (V_e - K_b N_1 \dot{\theta}_e)$$

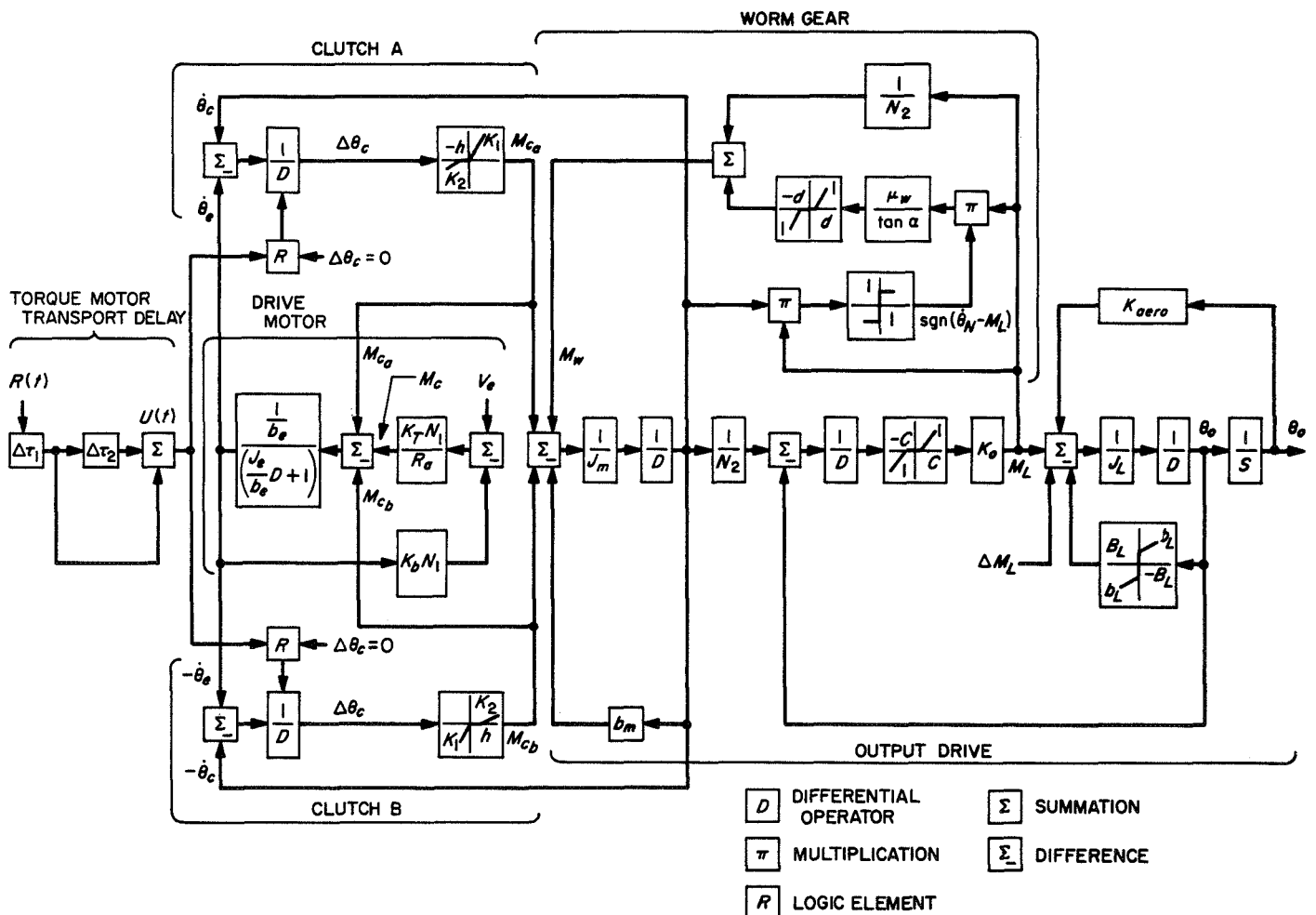


Fig. 2. Functional block diagram, electromechanical clutch actuator

Inertia and viscous friction of the unidirectional rotating parts are considered as lumped parameters J_e and b_e . Further neglecting compliance and backlash in this part of the drive, the velocity of the clutch input gears may be written

$$\dot{\theta}_e = \frac{1}{\frac{J_e}{b_e} D + 1} (M_e - M_c)$$

B. Clutch

Each clutch is represented in both the engaged and disengaged modes. In the disengaged mode, no contact is possible between spring and clutch output and, therefore, no torque is transmitted. In the engaged mode, the clutch cone is assumed to be fully depressed by the torque motor so as to accomplish complete coil windup, and maximum torque is transmitted in accordance with the clutch torsional stiffness K_1 .

C. Torque Motor

The torque motor function is expressed as a pure transport delay time of $\Delta\tau_1$ and $\Delta\tau_2$ as follows:

$\Delta\tau_1$ = time from application of input voltage to first armature motion

$\Delta\tau_2$ = time to transfer the engagement mode from one clutch to the other

The output $U(t)$ is used on the control signal for the engagement/disengagement mode and is depicted as a square wave of dead time ($\Delta\tau_1$) and phase lag ($\Delta\tau_2$) with respect to a driver signal $R(T)$.

D. Worm Gear

The characteristic of coulomb friction at the worm mesh is depicted here. Since this is dependent on the magnitude of transmitted torque, it can be expressed as

$$M_{ic} = \frac{M_L}{N_2} \left[1 - \frac{\mu_{ic}}{\tan \alpha} \cdot \text{sgn}(\dot{\theta}_{ic} \cdot M_L) \right]$$

where

$\text{sgn}(M_L) = \text{sgn}(\theta_{ic})$ when load torque is in the direction of rotation

$\text{sgn}(M_w) = \text{sgn}(M_L)$ when the input torque is opposite to the load torque.

E. Output Drive

All of the reversing parts of the actuator are included here. Backlash and compliance are assumed across the worm mesh in combination with inertia and friction on each side of the mesh. Then the clutch output torque can be expressed as

$$M_c = (J_m D + b_m) \dot{\theta}_c + M_w$$

and torque developed at the worm mesh output can be depicted as

$$M_L = J_L D \dot{\theta}_o + b_L \dot{\theta}_o + B_L \text{sgn} \dot{\theta}_o$$

Owing to drive backlash and compliance, the angular deflection between the actuator output shaft and worm output gear may be expressed as

$$\theta_o = \frac{1}{D} \left(\frac{\dot{\theta}_w}{N_2} - \dot{\theta}_o \right)$$

The torque transmitted across the drive may be written as

$$M_L = K_o (\Delta\theta_o - C), \quad \Delta\theta_o > C$$

and

$$M_L = 0, \quad \Delta\theta_o < C$$

One of the prime factors of the computer study has been to investigate the effect of various parameters on waveform and torque sensitivity. The internal dynamics of the actuator are severely affected by the friction in the various stages of the mechanism which, in turn, affect the distortion characteristic of the actuator output. A typical computer run is shown in Fig. 3. The dynamic overshoot characteristics of the clutch output velocity are illustrated. This occurs because of the release of strain energy during the engagement and the backing-off of the spring as the output velocity exceeds the input. Thus, the clutches transmit torque in very sharp impulses.

In general, the frictional characteristics of the output shaft bearings appear to have the greatest effect on the waveform characteristics of the actuator.

Typical computer results for actuator characteristics under hinge moment loading are shown in Fig. 4. The knee is a strong function of μ_{ic} (worm mesh friction).

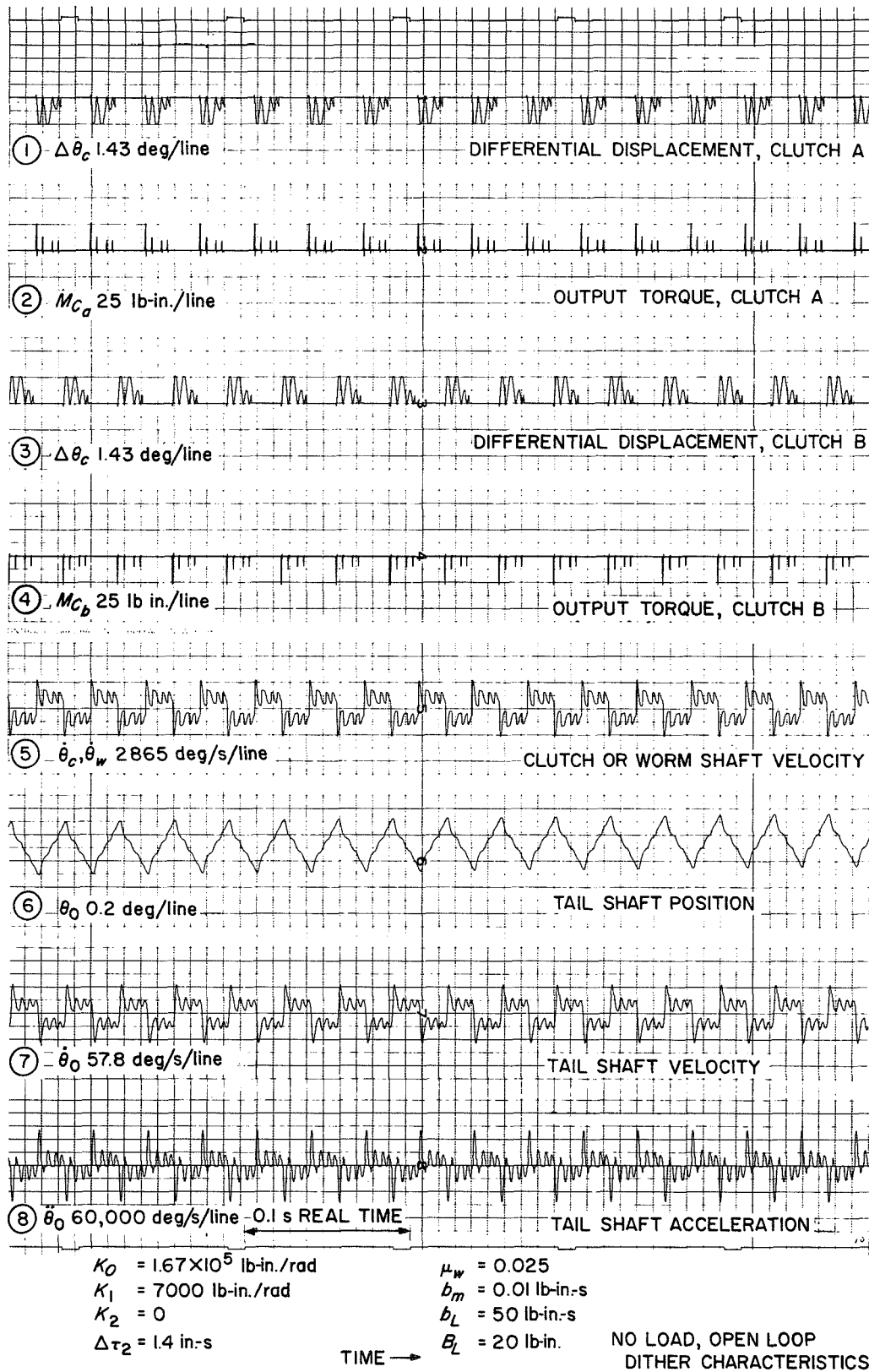


Fig. 3. Typical computer run, actuator output

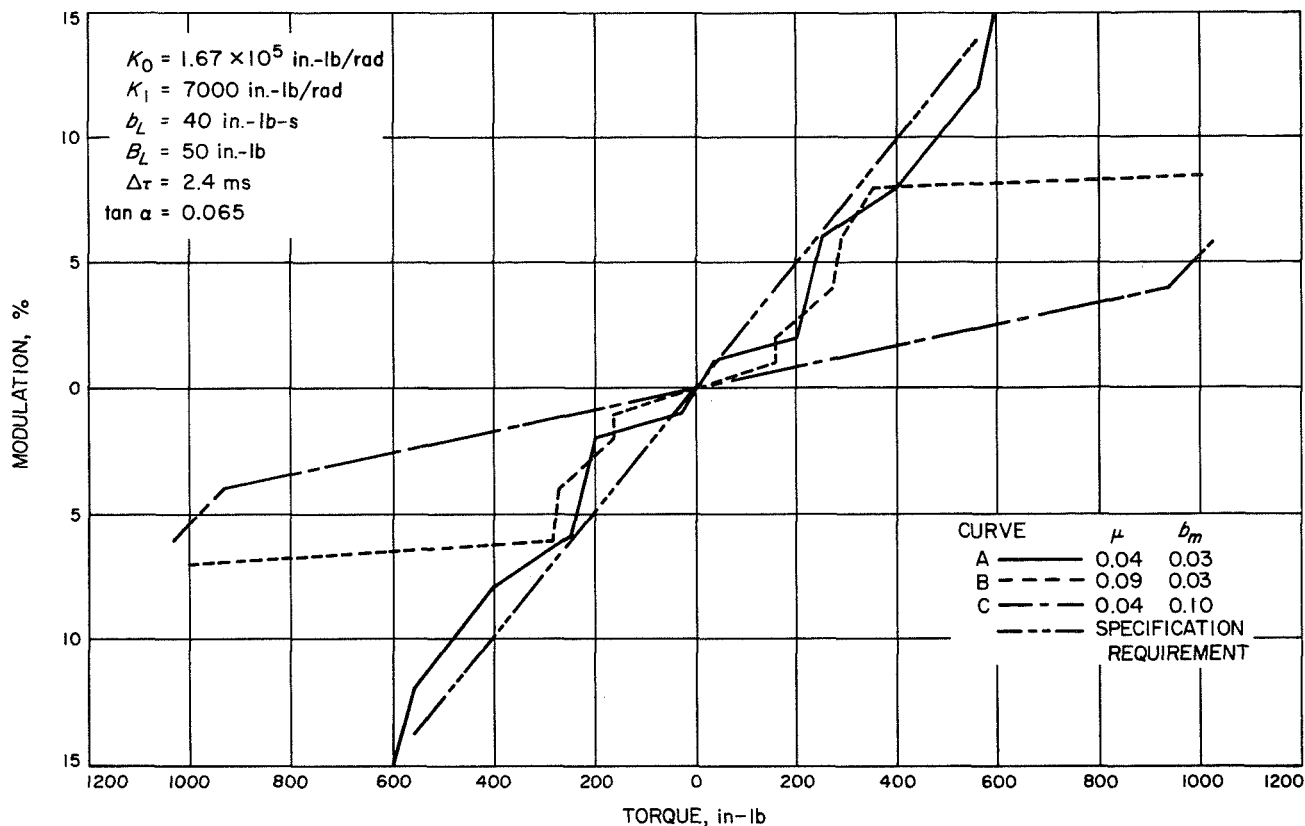


Fig. 4. Analytical hinge moment characteristic

V. Performance Characteristics

The basic characteristic parameters of the actuator fall in the category of waveform shape, power input and output, torque motor performance, transport delay time, drift, and torque sensitivity.

A typical performance trace of a developmental model under no-load operating conditions is shown in Fig. 5. Of prime interest here is the smooth trace and the operation of the actuator within the transport delay time, consistently and repeatably. The tail-rate performance is well within specification for all conditions.

The basic necessity for the hinge-moment sensitivity requirement is to control the drift of the actuator under hinge-moment loading effect. This requirement results from the method of utilizing the actuator in an effective open-loop operation as part of the adaptive control technique. The actuator's sensitivity to drift is accentuated by the differential number of clutch engagements in each half cycle. Under loading effects which either aid or oppose the actuator motion during the cycle, there is a resultant drift known as hinge-moment sensitivity.

The effect of actuator parameters on hinge-moment sensitivity is shown in Fig. 4, taken from the computer simulation. For case A where $\mu_{10} < \tan \alpha$, a steep slope indicates a strong influence of external torque. Case B for $\mu_{10} > \tan \alpha$ (i.e., irreversible worm condition) has the characteristic knee. Performance is improved for higher torques, indicated by the flatter slope beyond the knee. A reduction of μ_{10} and an increase in viscous friction b_m at the worm shaft, in C, results in a flat slope throughout the design torque range. The increase in b_m is obtained by including a simple plate damper to the worm shaft. Typical actuator test data, with and without the dampers, are shown in Fig. 6. Computer data points also included in Fig. 6 show good correlation between the test data and theoretical results.

VI. Program Status

The present program has undergone flight testing of development prototype missiles. This is, in essence, a reproduction evaluation program leading to final production models.

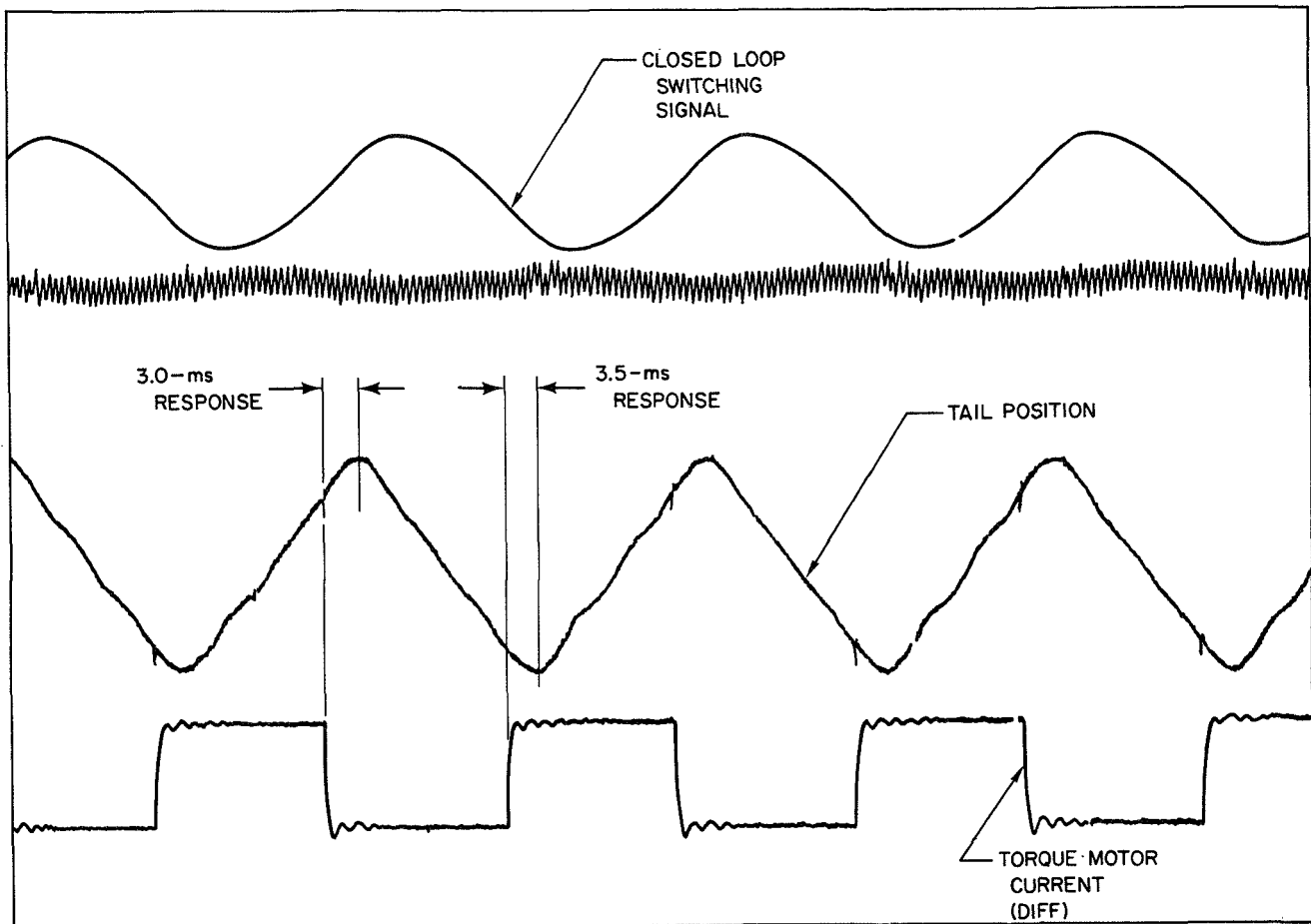


Fig. 5. Typical waveform diagram

The actuator is fully developed and qualified. It is in current production on the STANDARD ARM and STANDARD MISSILE programs. The number of production units manufactured is in excess of 700 devices.

Nomenclature

b_e	drive motor friction, viscous	J_m	clutch + worm shaft inertia
b_L	output shaft friction, viscous	K_o	output drive stiffness
b_m	clutch + worm shaft friction, viscous	$K_{1,2}$	clutch spring stiffness
B_L	output shaft friction, coulomb	K_{aero}	external load spring constant
C	output drive backlash	K_b	drive motor back emf
d	displacement	K_T	drive motor torque sensitivity
D	differential operator	M_c	clutch output torque
J_e	drive motor inertia	M_e	drive motor torque at the clutch
J_L	output shaft inertia	M_L	external load torque

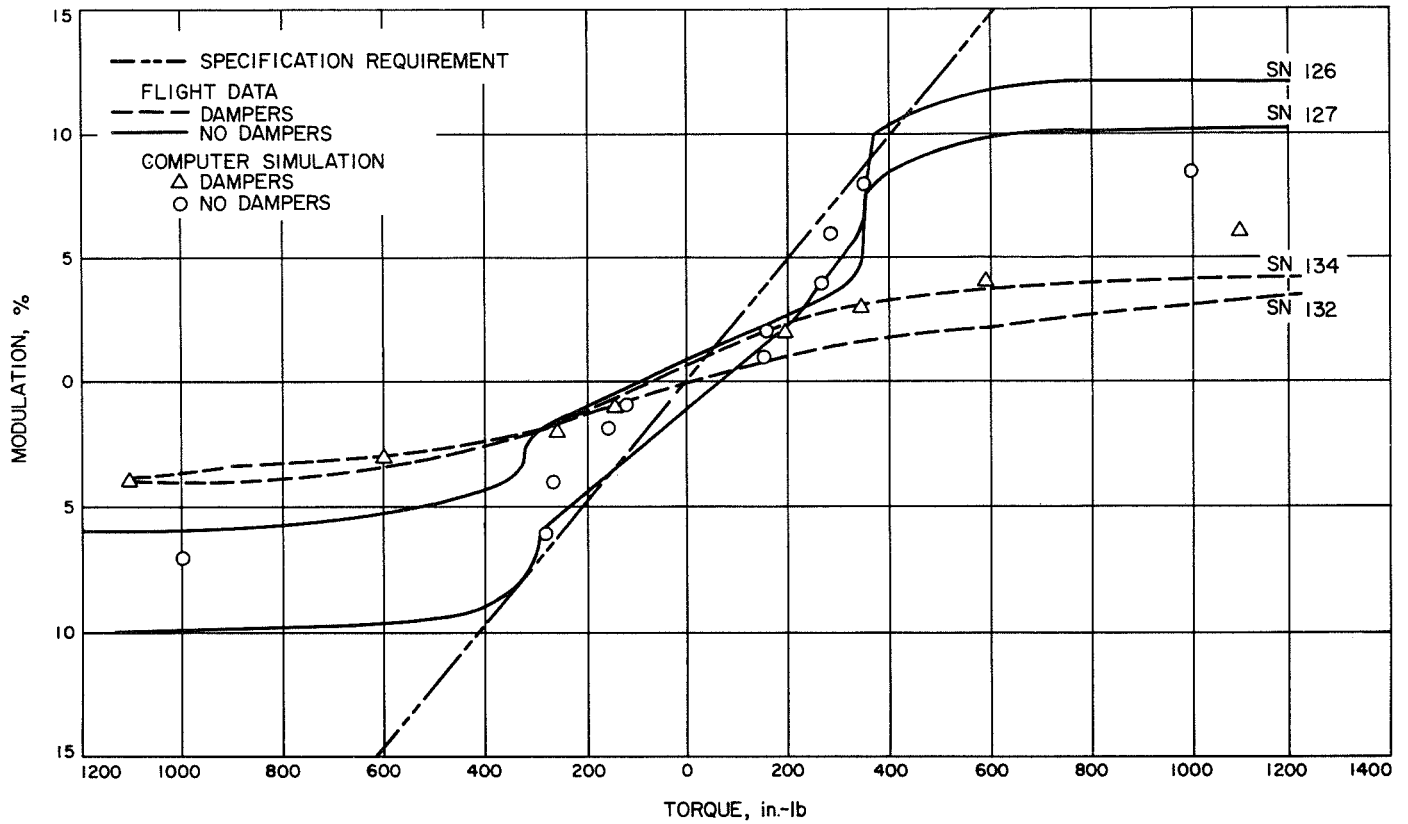


Fig. 6. Typical data, flight actuator hinge moment

Nomenclature (contd)

M_w	torque at worm shaft	α	worm lead angle
N_1	input drive gear reduction	$\dot{\theta}_c$	clutch output shaft speed
N_2	output drive gear reduction	$\dot{\theta}_e$	clutch input shaft speed
R	drive motor armature resistance	$\dot{\theta}_o$	output shaft speed
$U(t)$	transport function	$\dot{\theta}_w$	worm shaft speed
V_e	voltage input	μ_{wv}	worm mesh friction

NO 9-11805

Minimum-Weight Springs

H. O. Fuchs
Stanford University
Stanford, California

Springs are considered as energy accumulators. Efficient load-deflection curves and ways of obtaining them are shown. The resilience of different materials in different modes of stressing and methods of increasing the apparent resilience are discussed. Formulas are given for the design of torsion bars with rectangular cross section and of coil springs with egg-shaped cross section, which are very efficient springs.

I. Introduction

The weight of a spring is determined by the amount of energy that must be absorbed in the spring, by the qualities of the spring material, by the stress distribution in the cross sections of the spring, and by the extent to which all the cross sections are active in performing spring duties. We will denote these factors as

- R material resilience
- f_1 efficiency of the cross section
- f_2 efficiency of the configuration
- ρ density
- U maximum energy stored in the spring

so that the total weight required for a spring will be

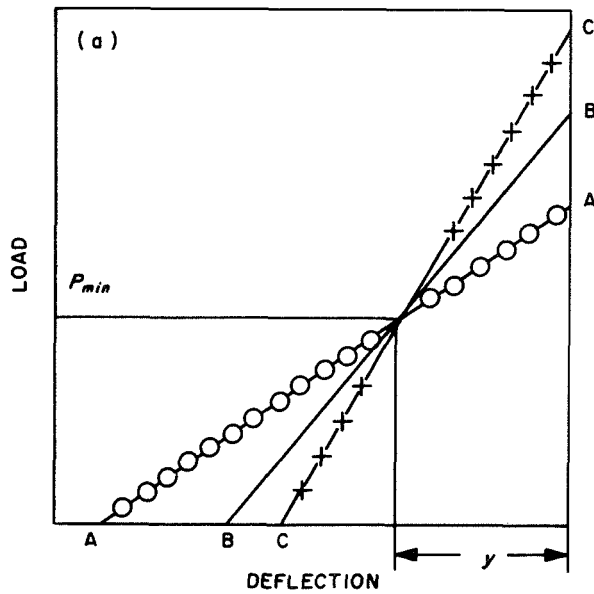
$$\frac{\rho U}{R f_1 f_2}$$

This formula is trivial by itself. Our interest will be in minimizing the energy U , maximizing the efficiency factors f , choosing a material of high resilience R , looking for tricks to coax more resilience R out of a given material, and keeping in mind that the performance of associated functions such as the provision of leverage has a large effect on the overall efficiency of the device.

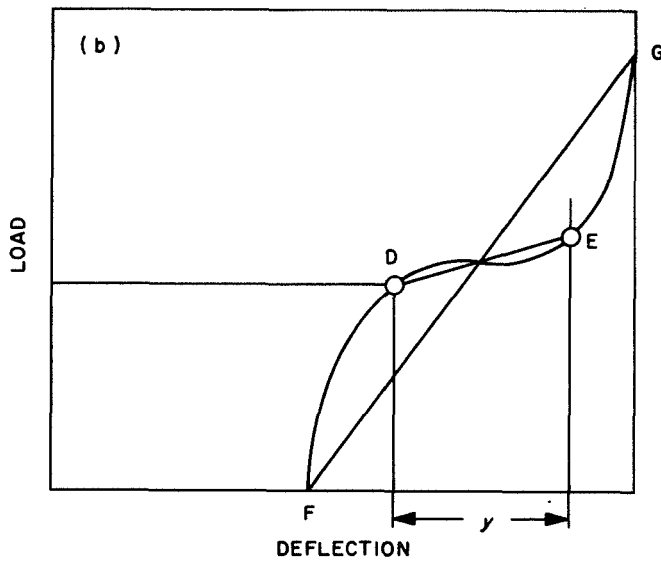
To dispose of this last point first, we remember that a torsion bar may be more efficient by itself than a coil spring, but that the levers and anchors which are required to transmit forces into the torsion bar may reverse the situation. We observe that springs are most manageable when they incorporate leverage, such as the distance from coil center to wire center in a coil spring.

II. Minimizing the Absorbed Energy

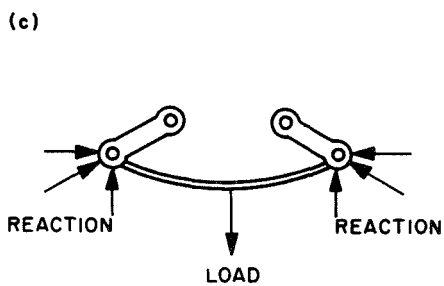
The maximum energy stored in a spring depends primarily on the maximum load and the travel from zero



B-B = MINIMUM-ENERGY CURVE. A-A, STIFFNESS IS TOO LOW. C-C, STIFFNESS IS TOO HIGH. y = REQUIRED WORKING STROKE.



F-G = MINIMUM-ENERGY CURVE. D AND E DEFINE REQUIRED LOADS AND REQUIRED WORKING STROKE y . F-D-E-G IS OBTAINED BY "SOFTENING" FG BY BUCKLING LOADS.



ONE POSSIBLE METHOD OF "SOFTENING" A STIFF SPRING BY APPLYING BUCKLING LOADS

Fig. 1. Minimizing the energy stored in a spring

load to maximum load. It also depends on the shape of the load-deflection curve.

With the usual constraints, namely, a given minimum load P_{min} , a given working stroke y , and a linear load-deflection curve, the minimum energy condition is defined by the equation

$$U_{min} = 2yP_{min}$$

which implies

$$P_{max} = 2P_{min}$$

This follows from symmetry considerations (Fig. 1a).

Fortunately this minimum condition is not very sensitive, as shown by Table 1.

Table 1. Variation of maximum energy U stored in linear springs of equal minimum load P_{min} and different maximum loads P_{max}

P_{max}/P_{min}	1.1	1.3	1.5	2	3	5	10
U/U_{min}	3	1.4	1.12	1	1.12	1.56	2.77

The ratios of P_{max}/P_{min} between 1.5 and 3 are quite innocuous. For the low ratios that are sometimes required, the situation is more serious, and we are well advised to deviate from the usual linear load-deflection relation. This can be done in two ways: to use the spring piece-wise, as in the Negator, or to approach buckling. To do the latter, we use a basically stiff spring, of somewhat longer stroke, with the ratio $P_{max} = 2P_{min}$, and we soften this spring by applying a buckling load (Fig. 1b).

In leaf springs, the buckling load can be provided by a suitable shackle arrangement (Ref. 1); in Belleville springs, the action is built in. The low lateral stiffness of coil springs near their buckling load has also been used. All these can be regarded as modifications of snap actions like those in oil cans, light switches, or micro-switches. They can be very useful where a low ratio of P_{max}/P_{min} is required.

For cushioning springs with nonlinear load-deflection curves, it is well to remember that increasing the stiffness by bottoming out some of the spring before it has reached the maximum permissible stress is bound to be wasteful. Clever ways can be devised to overcome this, but in general it is more effective and more efficient to

simply add bumper springs which come into action later in the working stroke.

III. Maximizing Resilience

The energy that must be stored in a spring is the integral under the entire load-deflection curve, from zero load to maximum deflection. We have seen how this integral can be minimized. Now we want to find the material which can store the energy in the smallest mass. If all the spring material could be stressed up to the permissible limit, then the specific resilience of the springs (energy stored per unit mass) would equal the specific resilience of the material.

We define the specific resilience as R/ρ and the resilience as

$$R_1 = \frac{\sigma^2}{2E}$$

or

$$R_2 = \frac{\tau^2}{2G}$$

depending on the type of stressing, normal or shear. The permissible stress in tension or shear is σ or τ respectively; the corresponding modulus of elasticity is E or G .

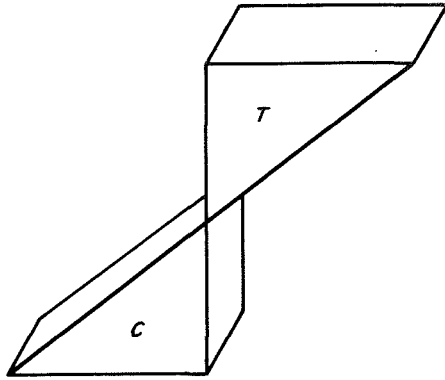
In springs, the stresses are fortunately either predominantly normal, as in bending, or predominantly shear, as in torsion; we need not here be concerned about intermediate cases and triaxial states of stress. We define R as energy stored per unit volume mainly to postpone the nuisance of pounds force and pounds mass. The units of R are inch pounds per cubic inch or lb/in^2 . The units of R/ρ , with ρ in pounds mass per cubic inch, are inches \times standard acceleration.

If we compare the two resilience, we find that they would be equal if

$$\frac{\sigma}{\tau} = \left(\frac{E}{G}\right)^{1/2}$$

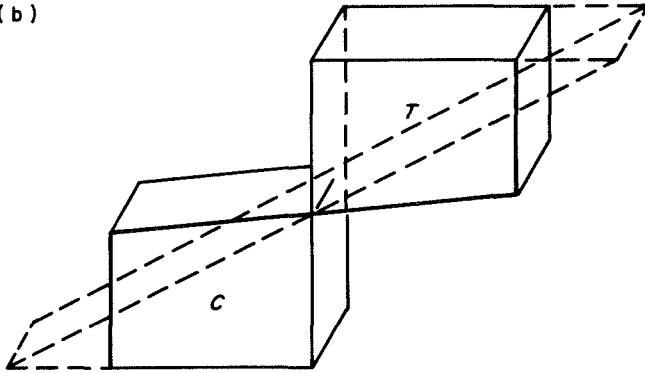
For steel, aluminum, titanium, magnesium, etc., E/G is about 2.8. We would be indifferent about using bending or shear if the ratio of permissible tensile stress to permissible shear stress were $2.8^{1/2}$ or about 1.7. This is not far from the ratio of yield stresses according to the Mises-Hencky or octahedral shear stress theory, but it may be very far from the ratio of permissible bending

(a)



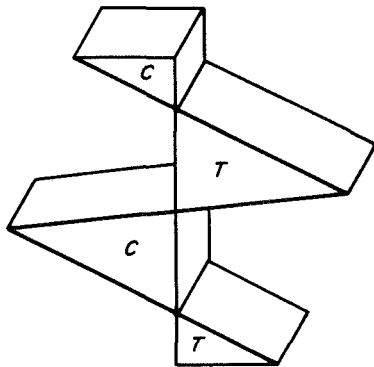
THEORETICAL ELASTIC STRESS DISTRIBUTION ON A
RECTANGULAR SECTION IN BENDING
T = TENSION
C = COMPRESSION

(b)



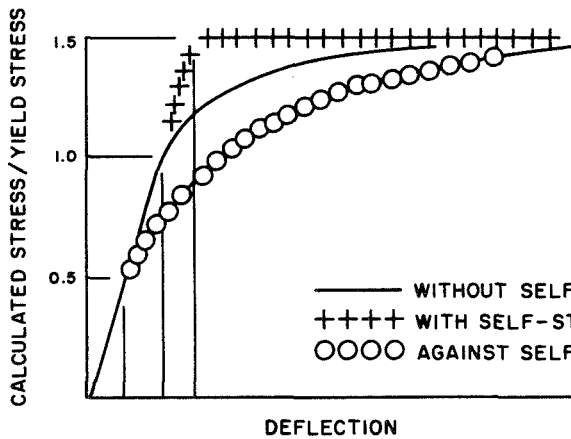
THEORETICAL LIMIT-STRESS DISTRIBUTION WITH
ENTIRE SECTION AT YIELD STRESS γ . DASHED LINE
SHOWS FICTITIOUS ELASTIC STRESS DISTRIBUTION
WHICH WOULD PRODUCE SAME BENDING MOMENT.
MAXIMUM FICTITIOUS STRESS = 1.5γ .

(c)



STRESS DISTRIBUTION AFTER RELEASE FROM
THE CONDITION OF 2(b). SELF-STRESS AT
EXTREME FIBER = 0.5γ .

(d)



THEORETICAL ELASTIC-PLASTIC
LOAD-DEFLECTION CURVES

— WITHOUT SELF-STRESS
++++ WITH SELF-STRESS
OOO AGAINST SELF-STRESS

Fig. 2. Self-stress

stress to permissible torsional stress in spring design. The permissible torsional stress in compression springs is much higher than would be expected on this basis. Comparing different materials, we find the following conservative values of permissible stresses recommended in the SAE Manual on Helical Springs (Ref. 2) and calculate the apparent values of resilience with the moduli given there, as shown in Table 2.

The apparent resiliences in the different modes of loading are far from equal. The high values for compression springs are explained by the existence of beneficial self-stresses. In those helical torsion springs (stressed in bending) which are cold-wound from small wire, beneficial self-stresses also exist, but are less effective. In the hot-wound 0.50-in. alloy steel spring, the self-stresses induced by coiling are removed by heat-treating. Figure 2 illustrates self-stresses.

The much higher apparent resilience that can be obtained from the material in compression springs explains why weight can be saved by replacing an extension spring by a pair of long "hooks" which compress a spring between their inner ends when the outer ends are pulled apart.

Table 2 also illustrates the fact that the level of permissible design stresses is much more important in springs than in structural members, because the weight of a spring will be inversely proportional to the *square of the stress*.

In music wire and in hard-drawn stainless, the decrease in diameter from 0.10 to 0.05 in. corresponds to

an increase in permissible stress of about 13%, but to an increase in resilience of about 28%. The dependence on the square of the stress explains also why springs were among the first products that utilized the stress increase made possible by shotpeening.

Steel is hard to beat as a spring material. Any competing material will have to be evaluated on the basis of specific resilience. Aluminum alloys, whose modulus of elasticity and density each are about 1/3 that of steel, will save weight only if their permissible stresses exceed 1/3 of the corresponding stresses for steel. Glass fiber, which has even lower values of modulus and of density, seems to be worthy of serious consideration for certain applications.

IV. Maximizing the Cross-Section Efficiency

We define the efficiency f_1 of a cross section as the ratio of the elastic energy stored per unit volume of the cross section in bending or in torsion to the resilience of the material. The factor f_1 is a measure of the uniformity of stress distribution in the cross section. Anything we can do to make the stress distribution more uniform will increase f_1 and decrease the weight of the spring.

The efficiencies of a few cross sections are shown in Table 3. Note that the data are restricted to sections that are free of stresses at zero load. The very important effect of self-stresses will be discussed later.

Table 2. Apparent resilience of spring material

Material	Modulus, Msi		Diameter, in.	Torsion springs		Compression springs		Tension springs	
	E	G		σ , ksi	R_0 , psi	τ_1 , ksi	R_1 , psi	τ_2 , ksi	R_2 , psi
Alloy steel (hot wound)	29	11	0.50	155	410	146	985	106	515
Music wire (cold wound)	30	11.5	0.10	212	750	154	1030	114	565
			0.05	240	960	174	1320	128	710
302 stainless hard drawn (cold wound)	25.5	10	0.10	148	430	106	560	91	415
			0.05	170	565	123	755	105	550
Phosphor bronze (cold wound)	15	6.2	0.10	90	270	70	395	55	245
			0.05	98	320	76	460	60	290

Msi = 10⁶ lb/in.²

Table 3. Efficiencies of cross sections of straight bars, free of stresses at zero load

Loading	Round	Square	Rectangle 2:1	Rectangle 10:1
Bending	0.25	0.33	0.33	0.33
Torsion	0.50	0.31	0.26	0.31

First, we note the good showing of round sections in torsion; they are more efficient than any of the others by a ratio of 3:2 or more. By extending uniformly all around the circumference, the high stresses cover a larger fraction of the total area than in other sections or other modes of loading. We know that we can redistribute the stresses at maximum load by introducing self-stresses. Their exact distribution depends on strain-hardening. For purposes of comparison we assume a perfect plastic-elastic material, prestressed to the extreme limit, and then find the efficiencies listed in Table 4.

Table 4. Efficiency of cross sections of straight bars, prestressed to a theoretical limit

Loading	Round	Square	Rectangle 2:1	Rectangle 10:1
Bending	0.72	0.75	0.75	0.75
Torsion	0.89	0.77	0.75	0.80

Comparing Table 4 with Table 3, we note that all cross-section efficiencies have increased dramatically, and that the differences between various cross sections have become much less. The most remarkable increase is for round sections in bending. The makers of roller shades and mouse traps were not as inefficient as one might think.

In passing, we note that these efficiencies apply only if the maximum stress is the failure criterion, not if the stress range is the failure criterion. For infrequent loading or for shotpeened springs in fatigue, the maximum stress is the better criterion. The stress values used in spring design calculations are the ranges from zero load (where we usually have a negative self-stress) to full load. The increase in section efficiency produced by prestressing is reflected by an increase in calculated permissible stress as in Table 2. The greater improvement by prestressing of the originally less efficient sections is reflected in the higher calculated stresses permissible for

these sections. The permissible design stress for round wire stressed in bending in a torsion spring will thus be 13% higher than the permissible stress for square wire of the same size and material (the increase in section efficiency is 50% greater). The stress values quoted in the literature include the effect of presetting. In choosing springs, one must take full advantage of presetting, but not make a double allowance for it, once by the efficiency factor and then again by the higher permissible stress. The efficiency factor is used to choose a cross-section shape in preliminary design, the stress value in final dimensioning of the chosen shape.

Returning now to the real implications of Table 4, we observe that in limit design all quoted cross sections are better in torsion than in bending. The table actually understates the case for torsion, because prestressing is easier in torsion than in bending.

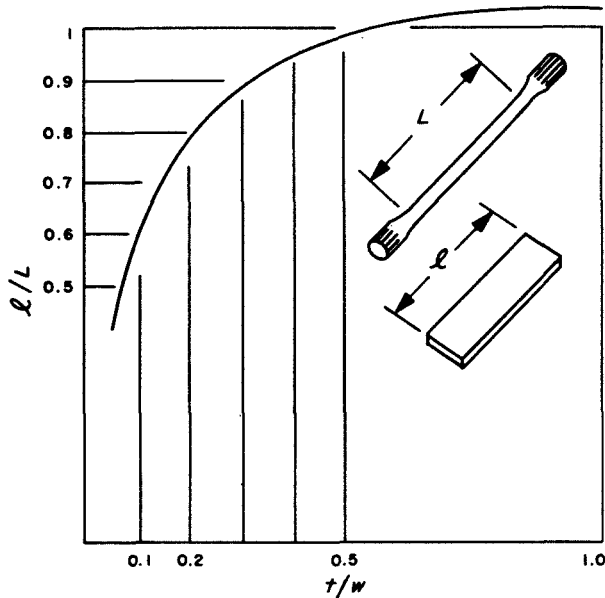
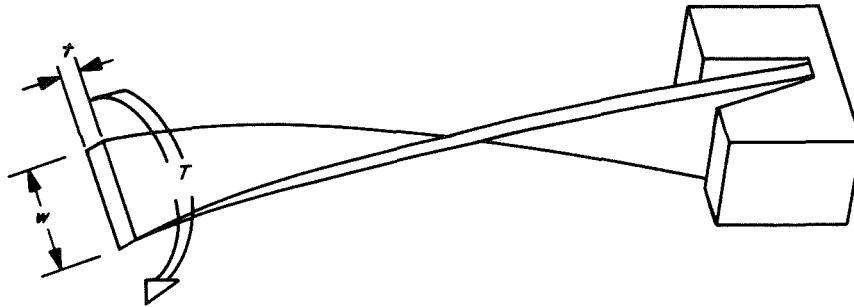
We also observe that with limit design the round section is only about 11% more efficient in torsion than a narrow rectangle. If we apply this to torsion bars, the narrow rectangle turns out to be a far better spring for the following reasons:

- (1) Flat torsion bars do not require inactive ends (Ref. 3).
- (2) The ends are easier to hold, with better leverage.
- (3) Flat torsion bars are far easier to manufacture.
- (4) For equal spring rates, flat torsion bars are shorter.
- (5) Several flat torsion bars can be used as a bundle in parallel.

To facilitate the use of flat torsion bars, a few relevant formulas are quoted in Fig. 3.

The efficiency factors of Tables 3 and 4 are calculated for straight bars. In coiled springs, we must modify these factors to allow for the higher strain on the shorter fibers near the coil center and for the direct shear in tension springs and in compression springs.

For the usual round wire of diameter d , coiled into a compression spring of mean diameter D , the combined correction factor for curvature and direct shear can be approximated as $K = 1 + 1.6d/D$. (A more accurate approximation is due to Wahl, Ref. 4.) Taking $D = 6d$, which is a very reasonable proportion, the efficiency of the cross section decreases in the ratio $(1/K)^2 = 0.63$. As



RATIO l/L OF LENGTH OF RECTANGULAR BAR OVER ACTIVE LENGTH OF ROUND BAR OF SAME STIFFNESS, SAME LOAD CAPACITY, AND SAME MAXIMUM STRESS (INCLUDING SELF-STRESS). BOTH BARS PRESET, CALCULATED BY LIMIT DESIGN.

FORMULAS FOR RECTANGULAR TORSION BAR SPRINGS

$$S/A = Gt/l$$

$$T/A = (0.333 - 0.2t/w)Gt^3w/l$$

$$T/S = (0.333 - 0.2t/w)t^2w$$

A = ANGLE OF TWIST
 G = SHEAR MODULUS
 S = STRESS (EXCLUDING SELF-STRESS)
 T = TORQUE

l = LENGTH
 t = THICKNESS
 w = WIDTH

Fig. 3. Rectangular torsion bars with active ends

a result, the efficiency of the round section without pre-setting is decreased from 0.5 to 0.31, a very substantial decrease. The efficiency of the heavily preset round section will be decreased by a lesser but still substantial amount.

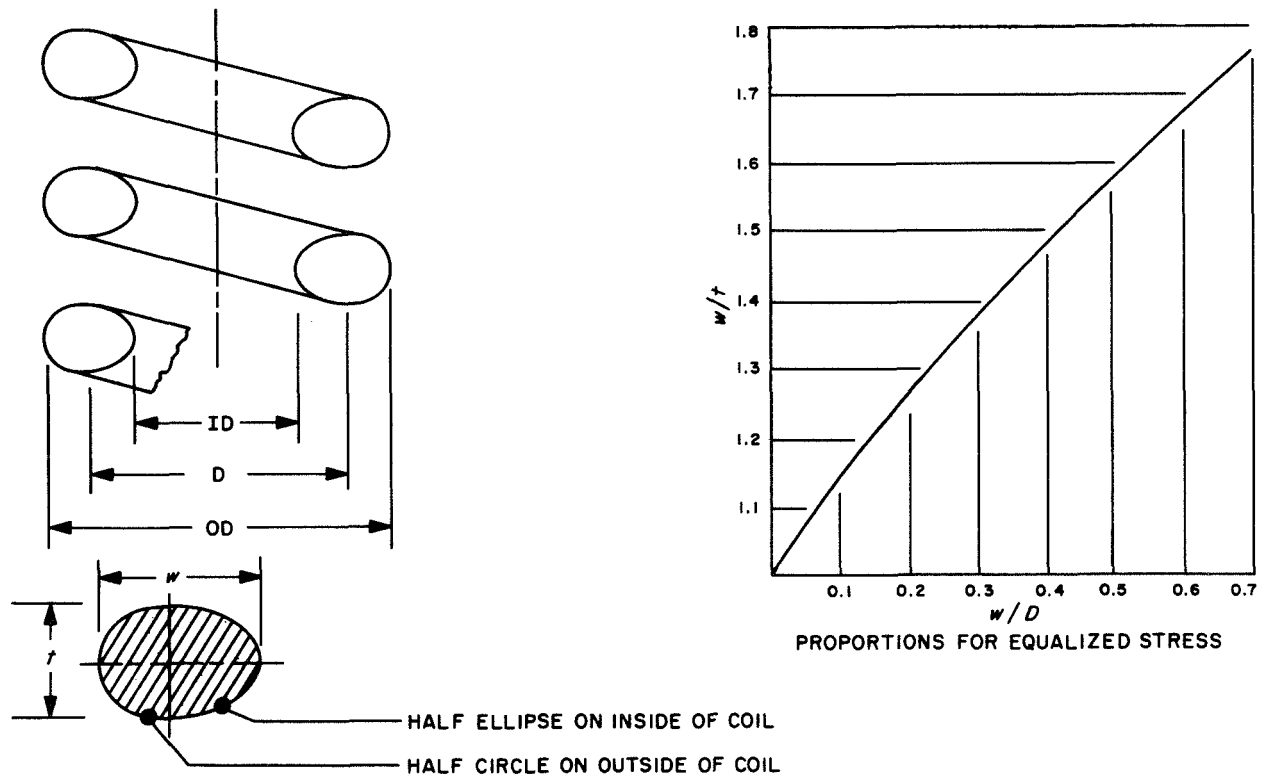
To overcome this unfavorable stress distribution, it has been proposed to make coil springs not from round wire

but from egg-shaped wire (Ref. 5). By this method, weight savings of 30% are readily obtainable without pre-setting, on the basis of calculations. With pre-setting, the difference becomes less. A series of tests was made, in which eight preset springs experimentally hot coiled from egg-shaped bars were fatigue tested and compared with preset production springs which had a better surface because of the more expeditious hot processing of

the production springs. The springs were not shot-peened. The tests showed the following values of energy stored per pound of spring at a median fatigue life of 200,000 cycles:

Round bars	325 in.-lb per lb of spring	100%
Egg-shaped bars	380 in.-lb per lb of spring	117%

Note that the greater resilience was obtained in spite of the poorer surface. The saving in steel weight was considered insufficient to justify the extra effort for railway use, but might be very attractive for aerospace. The saving increases rapidly when springs are coiled to smaller diameters. A collection of formulas relevant to the design of such coil springs is shown in Fig. 4.



$$S/P = 2.55D/wt^2$$

$$P/f = Gt^4(2.1w/t - 1.1)/8ND^3$$

$$A = \pi wt/4$$

$$D = 0.5(OD + ID) + 0.152(w - t)$$

- A = AREA OF CROSS-SECTION
- D = COIL DIAMETER (OF CENTROID OF SECTION)
- f = DEFLECTION
- G = SHEAR MODULUS
- N = NUMBER OF ACTIVE COILS
- P = LOAD
- S = MAXIMUM SHEAR STRESS (EXCLUDING SELF-STRESS)
- t = THICKNESS
- w = WIDTH

Fig. 4. Coil springs with cross section compensated for curvature correction

Knowing that hollow sections are more efficient than solid sections, one might be tempted to make springs of tubes instead of bars or wires. This approach is reasonable for springs which must only maintain a static load, but it will not work for springs in fatigue service because it is too difficult to shotpeen the inside of small straight hollow sections and impossible to shotpeen the inside of a coiled tube. Unless the surfaces are shotpeened, the permissible stress is so much less that a weight increase results instead of a weight saving.

Shotpeening works, of course, because surfaces need fatigue protection and because fatigue damage is propagated by tensile stresses. This suggests a potential improvement for sections stressed in bending: by making the section unsymmetrical, the neutral axis can be located closer to the tensile surface. Automotive leaf springs of this type have been used successfully (Ref. 1), archery bows have long been made of cross sections unsymmetric about the neutral axis, and skis used to be made with such sections, no doubt for the same reasons.

V. Configuration Efficiencies

We have already mentioned the superior configuration efficiency of flat torsion bars as compared with round torsion bars. Greater ease of force transmission and the absence of enlarged inactive ends account for it. It is difficult to give a general numerical ratio, but in a 1-in.-diameter torsion bar, 20 in. long, with 1.3-in.-diameter ends each 1.5 in. long, the inactive ends account for 25% of the total spring weight. With a value of $R = 985$ from Table 2, $f_1 = 0.50$ from Table 3, $f_2 = 0.75$ from the consideration of the inactive ends, and 0.28 lb/in.^3 for the density of steel, we obtain an overall energy/weight ratio of $985 \times 0.5 \times 0.75 / 0.28 = 1300 \text{ in.-lb/lb}$ for such a torsion bar. The SAE Manual (Ref. 1) gives 1000 to 1500 in.-lb energy per lb of spring for torsion bars.

A compression coil spring requires one or two inactive end coils, which will account for 10 to 20% of the weight of a spring with 10 coils. Heavy-duty die springs show energy/weight ratios quite close to those of torsion bars.

If minimum weight is a serious consideration, cantilever springs should not be clamped between plates at

their fixed ends, because the clamped part is obviously inactive, the end of the clamp introduces a stress concentration, and the clamp itself must be very rigid to perform its intended function. A three-point support is far superior because it leaves the material between support points active.

By themselves, flat springs in bending are not as efficient as springs stressed in torsion. They can be more efficient if the spring can also serve as a guide or link. Leaf springs in automobile suspensions are good examples of this: they compete successfully against a combination of coil spring plus guiding link.

We have already mentioned the importance of using high stresses in order to reduce spring weight in inverse proportion to the square of the stresses. As the spring weight is reduced, the spring becomes smaller and all attachments and enclosures also decrease in weight.

VI. Conclusion

The choice of material of high resilience is the paramount consideration in reducing spring weight. Anything that can be done to increase the permissible working stress will pay off doubly in decreased spring weight. Shotpeening and presetting are the chief tools in raising permissible levels of working stress. Permissible stresses are generally higher in smaller sections of material than in larger sections.

The fact that extension springs can not be preset and are difficult to peen decreases their utility. Compression springs and torsion bar springs are most amenable to presetting.

Flat torsion bar springs and compression springs made of egg-shaped wire deserve consideration where weight must be minimized. These two types of springs have the best overall efficiencies.

A value of 1000 in.-lb energy stored per pound of spring is a good round target figure. It can be exceeded with careful design, testing, and process control. Average design and manufacture may give as low as 300 in.-lb energy stored per pound of spring.

References

1. *Manual on Design and Application of Leaf Springs*, Society of Automotive Engineers, New York, 1945.
2. *Manual on Design and Application of Helical and Spiral Springs for Ordnance*, Society of Automotive Engineers, New York, 1943.
3. Anderson, P. Z., *Torsion Transmitting Mounting for Torsion Members Such as Rods and Springs*, U.S. Patent 2,606,020, Aug. 5, 1952.
4. Wahl, A. M., *Mechanical Springs*, Penton Publishing Company, Cleveland, O., 1944.
5. Schwarzbeck, J. G., and Fuchs, H. O., *Stress Equalized Coil Springs*, U.S. Patent 2,998,242, Aug. 29, 1961.

N 69-11306

The Radio Astronomy Explorer 1500-ft-Long Antenna Array*

E. D. Angulo

NASA-Goddard Space Flight Center
Greenbelt, Maryland

W. P. Kamachaitis

Fairchild Hiller Corporation
Germantown, Maryland

The mechanical components of the Radio Astronomy Explorer spacecraft main antenna array are described. Key components, such as the extendible antenna element and dispenser mechanism, are described in detail. System test techniques, development problems, and solutions are also presented.

I. Introduction

The science of radio astronomy is a relatively new tool for increasing man's knowledge of the universe. Until very recently, all observations had to be made from ground-based arrays. Such observations are severely limited by the ionosphere, the troposphere, and man-made radio noise. Much of the data obtained below 20 MHz is unreliable. With the advent of the space age, the possibility of placing a radio telescope in space was realized. The spacecraft should be able to compensate for its own influence on the incoming antenna signals and to monitor the strength of earth-generated noise. To fulfill these needs, the *Radio Astronomy Explorer* (RAE) spacecraft was developed.

The first RAE spacecraft is presently scheduled for launch in mid-year 1968 and has an expected life of one year. The main antenna array is X-shaped (Fig. 1) and

*All work described in this paper which was accomplished at the Space and Electronics Systems Division of Fairchild Hiller Corporation was performed under Contract NAS-5-11044 for the NASA Goddard Space Flight Center.

is diagonally 1500 ft long. This extreme length produces an inertia of over 200,000 slug-ft² and provides gravity-gradient capture. The array consists of four separate interlocked-seam tubular extendible elements (TEEs), each 750 ft long. Each V portion of the X configuration is electrically coupled, forming one antenna. The earth-oriented V antenna will be utilized to measure earth-generated noise. Solar and planetary emissions will be measured by the space-oriented V antenna. Prior to erection, each antenna element is stored in a 5.0 × 8.0 × 14.0-in. dispenser mechanism. The entire array, including dispensers, weighs 72 lb and can be erected in 25 min with 24 W of electrical power.

II. The Antenna Element

The basic material used in the antenna elements is precision-rolled beryllium copper. The elements are made from 0.002 × 2.00-in. continuous strip which is heat treated to form a 0.570-in.-diameter tube. This technique allows the tube to be wound flat on a spool for maximum compactness.

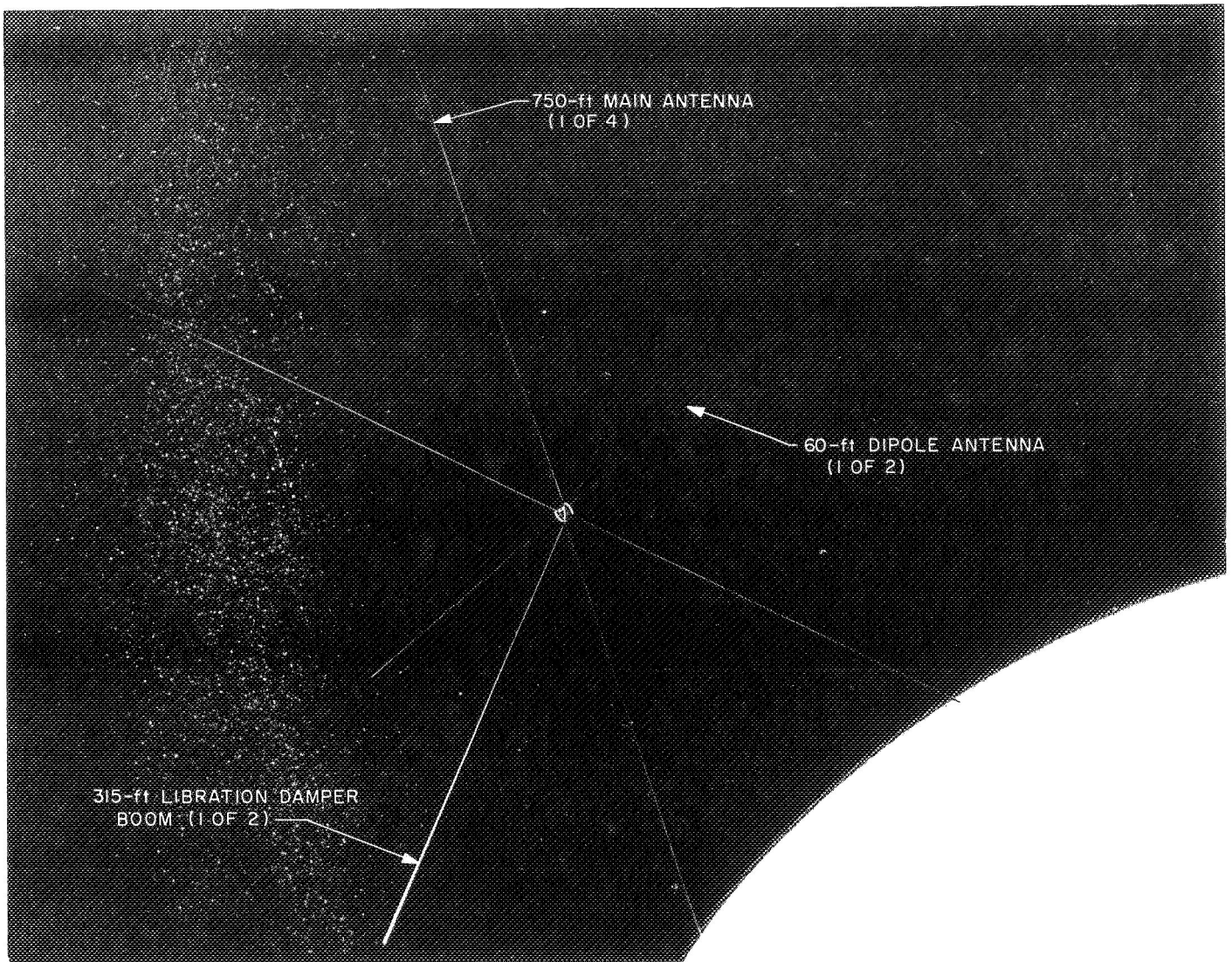


Fig. 1. Artist's conception of the RAE satellite, with antennas deployed

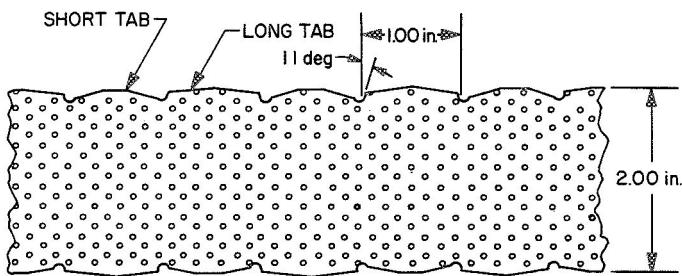


Fig. 2. Unformed antenna element

Figure 2 illustrates the antenna element prior to heat treating. The locked seam is made possible by punching a series of tabs on the edges of the flat element. Every

other tab has its apex flattened, i.e., the distance from the centerline of the element to the edge of the tabs alternates between long and short. When the flattened element springs into a tube, a short tab is presented to a long tab. The seam is "zippered" by tucking short tabs under long tabs. The "zipper" (Fig. 3) consists of a narrow-crowned roller mounted inside the half-formed tube on the centerline of the seam at a point just before the tabs to be mated touch each other. The pair of tabs move across the roller together as the element is dispensed but are restrained momentarily by the roller from curling into a tubular shape. The shorter tab springs clear of the roller first and curls into its normal position on the centerline of the seam. The longer tab clears the roller last so that when it springs down, it overlaps the

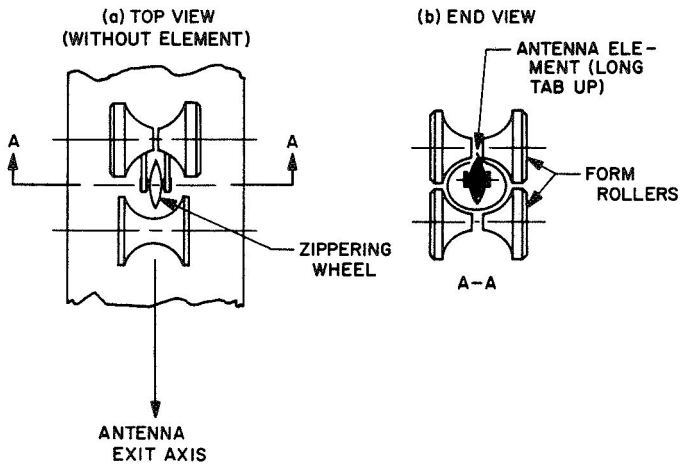


Fig. 3. Antenna element edge lock zipper

shorter tab already on the centerline. The process is reversed on the next pair of tabs. The end result is a row of interlocked tabs. Each tab is 1 in. long in the axial direction. To avoid play between adjacent tabs, an interference fit was achieved through the incorporation of an 11-deg wedge angle.

The antenna element also incorporates a system of thermal control coatings which are intended to minimize thermally induced deflections that could occur as a result of large diametral thermal gradients. (A ΔT of 2°C is considered prohibitive.) The outer surface has a coating of silver (0.0001 in.) which is polished to produce an absorptivity of less than 8%. To counteract the 8% thermal input that is being absorbed, the antenna is perforated to allow 8% of the solar energy to pass through the antenna and strike the back side. The inside of the element is coated with a film of highly absorptive black paint. Thus, 8% of the thermal input is absorbed on the front side of the antenna and 8% is absorbed on the back side, resulting in a theoretical zero gradient. Silver degradation and perforation passthrough is expected to occur because of extended operation in space. However, this combination of coatings and perforations is expected to maintain a diametral thermal gradient of 0.75°C .

III. The Antenna Dispenser Mechanism

The mechanism that is utilized to dispense each of the four RAE 750-ft-long antenna elements is illustrated in Fig. 4. It consists of a storage reel, drive train, element

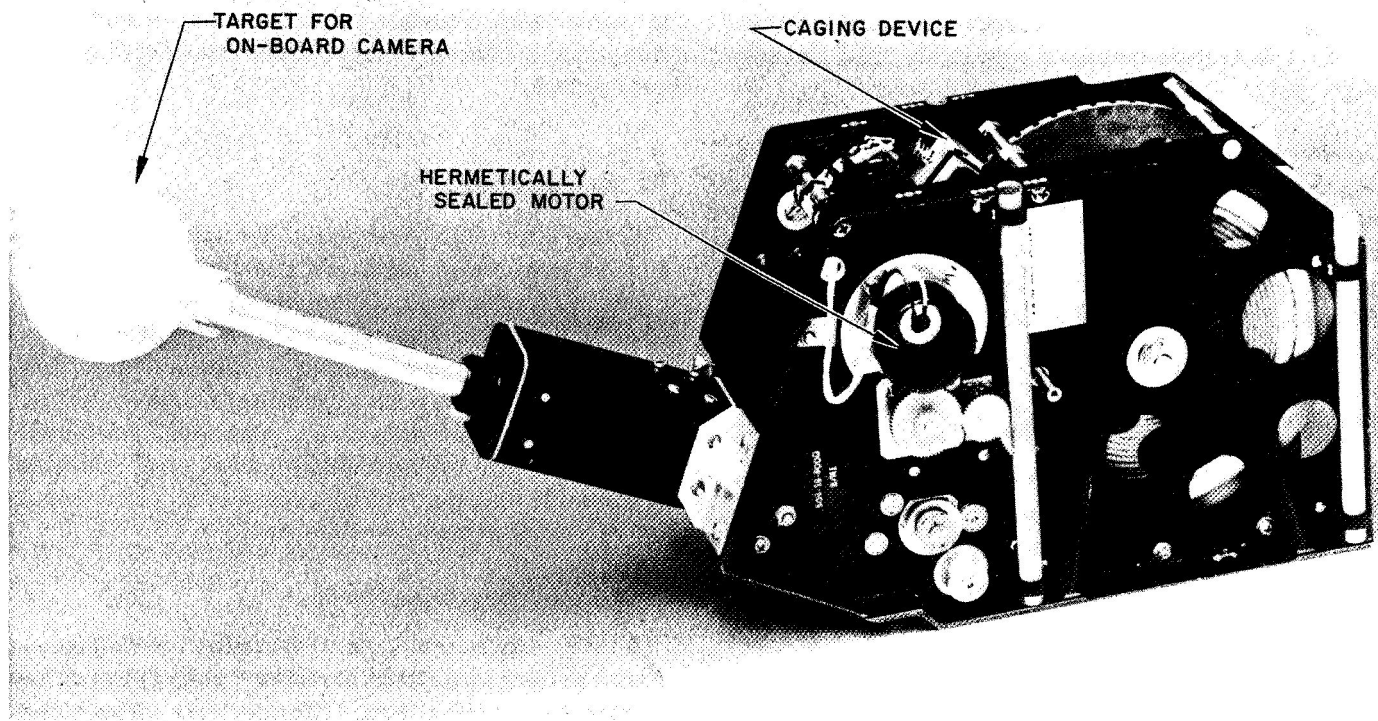


Fig. 4. Antenna dispenser mechanism

guide supports, antenna element edge locking device, launch caging mechanism, and analog instrumentation, mounted in a lightweight magnesium support structure. The mechanism is enclosed by an aluminum-foil-lined plastic cover that minimizes tarnishing of the silver-plated antenna element and provides the required RF shielding.

In the extend mode of operation, the element is pulled from the storage reel by a pinch drive roller while a small retarding force is applied to the storage reel through a friction clutch. This feature precludes buckling of the element, because it is in tension instead of compression. In addition, the pinch roller drive system maintains an essentially constant deployment speed without the complexity of a servo control system to compensate for the changing diameter of the spool-stored element. Furthermore, this unique drive feature eliminates the need for a translating main reel shaft because axial alignment of the extending element is achieved at the pinch drive roller.

Essentially the same drive principle is employed in the retraction mode. The basic difference in this mode is that the storage reel is driven with drive coupling derived through an electrically operated crown tooth clutch. During the retract mode, a slight retarding force is applied by a slip clutch at the pinch drive roller, which maintains element tension between it and the storage reel. This feature ensures a repeatably tight element storage wrap.

Ball-bearing-mounted rotating guide rollers are used exclusively to assist the antenna element in making the transition from flat to round. These rotating guides are contoured so as to achieve a smooth transition of the antenna element with no deformations after a minimum of 25 cycles. The contoured rollers also provide element bending root fixity. The output end of the guide system contains an adjustable pylon which has the edge-locking roller at its tip.

A redundant system is provided for electrical connection to the antenna. A spring-loaded, gold-plated, rotating wheel makes one RF contact directly on the antenna element at the pinch drive roller. The second RF contact is made through a spring-loaded clip that is used to attach the antenna root to the storage reel.

The mechanism design incorporates a ball detent, solenoid-actuated, reel-caging device so that the spring-like antenna material will remain tightly wrapped on the

storage spool during the launch vibration environment. This caging device consists of a spring-loaded plunger which engages with one of the slots provided on the periphery of the antenna element storage reel. After the desired orbit is achieved, the caging device is actuated. A telemetry switch is provided to verify uncaging of the reel. The switch also opens the solenoid circuit to conserve spacecraft electrical power. Inadvertent reset of the solenoid is precluded, since it requires a manual override.

An analog signal provides a direct readout of the length and speed of the antenna at all times during extension and retraction. The signal is derived from a 10-turn precision potentiometer driven from the pinch drive backup roller shaft. A gearhead speed reducer is interposed between the backup roller and the potentiometer to reduce the number of revolutions of the backup roller to slightly less than 10 turns at the potentiometer shaft for extension of 750 ft of antenna.

The limits of extension and retraction are sensed by a subminiature switch which has a spring-loaded contactor wheel that rides against the silver-plated surface of the element. This contact takes place at the backup roller adjacent to the antenna electrical connection. Switch actuation occurs when a slotted hole punched in the beginning and end of the antenna element passes under the switch roller, allowing the antenna to descend into a cutout in the backup roller, thereby opening the drive motor circuit.

IV. System Tests

Tubular extendible elements, like many other space-applied extensible systems, are unable to support their own weight in the earth's gravitational field. Regardless of this limitation, it was necessary to verify, first, that the antenna elements were straight as manufactured and, second, that the dispenser mechanism could in fact extend and retract the element in a simulated spatial environment with the required edge locking and unlocking. As a result, a unique straightness testing and element take-up device system was designed.

A. Antenna Straightness Testing

To date, straightness testing of tubular extendible elements has been conducted in water troughs several feet wide and up to 150 ft long. The specimen under test is usually supported by a row of saddles, each saddle being mounted on an individual float. The energy in a bowed

element is enough to displace the floats across the surface of the water until a two-dimensional reproduction of the curve is produced. Attempts have also been made to measure a three-dimensional displacement by incremental rotation of the element or by suspension on neutrally buoyant balloons. The prospect of scaling up one of these 150-ft facilities to meet the 750-ft RAE requirement presented formidable problems, particularly since the RAE specification permits a total tip deflection of 13 ft.

1. Test facility. The ideal test facility was located just 10 miles from the NASA Goddard Space Flight Center, at the Naval Ordnance Laboratory, White Oak, Maryland. The site is an underground ballistic missile range that is 1000 ft long, 10 ft in diameter, humidity controlled, and draft free, with the capability of having the air evacuated. Since the facility is underground, the temperature is stable. Because the range is in active use, its conversion to an RAE antenna straightness facility, together with the running of the test and removal of all gear, had to be accomplished during a weekend.

In order to keep the entire rig portable, it was decided to float the test antenna on small individual pans of water in lieu of one continuous trough. A spacing of 5 ft was selected. Since any bow in the floating element would cause it to strike the side of the pan, the pans had to be movable and were therefore suspended from overhead crossbars. The crossbars were attached to the steel walls of the range tunnel with magnets to avoid the need for any welding or other permanent modifications. Figure 5 illustrates the straightness test facility. Since there were 150 pan suspension systems, the cost of each had to be kept to a minimum. Thus, such things as cake pans, coat hangers, and beaded chains were used effectively throughout.

2. Test procedure. Each test is conducted as follows: First a ruby laser is mounted on the centerline of the tunnel and aimed down the row of suspended pans. To bring the water level in all pans to a uniform height, a target with cross hairs is floated in the first pan so that the laser produces a dot upon it. A technician with a pair of syringes, one empty and one filled with water, then adjusts the water level of that pan to bring the horizontal cross hair to the level of the laser beam. He then advances the target to the next pan and adjusts its water level. Since the target is made from a transparent material with scribed cross hairs, the laser shines through it and can be used simultaneously by other technicians leveling pans farther up the tunnel.

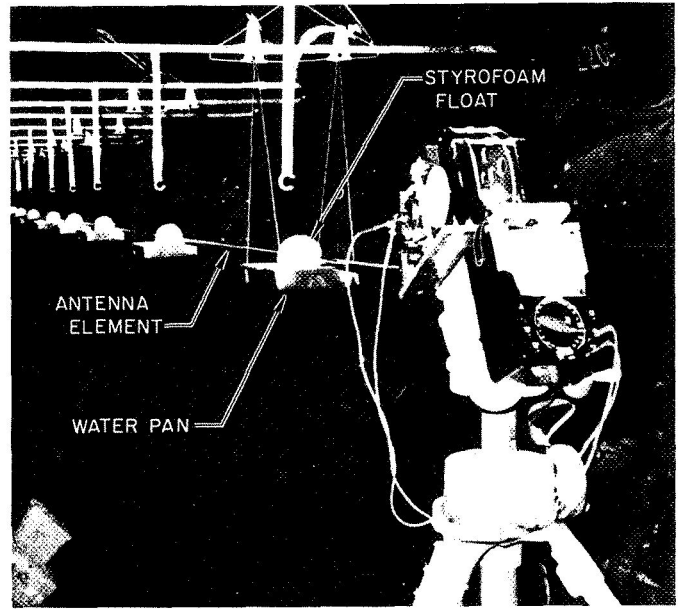


Fig. 5. RAE antenna element straightness testing

Once the pans have been leveled, the next step is to extend the antenna element to its full length and support it by Teflon hooks (prior to supporting it on floats). The antenna element with locked seam up is manually guided through all 150 hooks. The next step is to attach the floats, which are styrofoam cylinders 3 in. in diameter with a 0.570-in. hole on the axis. They are molded in halves and are secured around the antenna with a piece of tape wrapped once around the circumference of the float. The cylindrical design of the float is extremely important because it allows the antenna seam to twist. The antenna element is then removed from each successive hook and the float is placed in the water. Each pan is adjusted laterally as required to keep the float in the center of the pan. The off-axis deviation is then measured along the antenna element. Once these measurements are completed, the antenna element and mechanism are rotated 90 deg. Flotation adjustments are again made, and the off-axis deviations are measured. This technique therefore provides information that verifies that the manufacturing process is not resulting in excessively distorted antenna elements.

B. Dispenser Mechanism Testing

Verification of dispenser mechanism design integrity requires a device that can accept or release the antenna element without imparting an axial load on it. This was accomplished through the design of a bidirectional servo-controlled take-up mechanism. In effect, the take-up mechanism was designed as a mechanical symmetry of

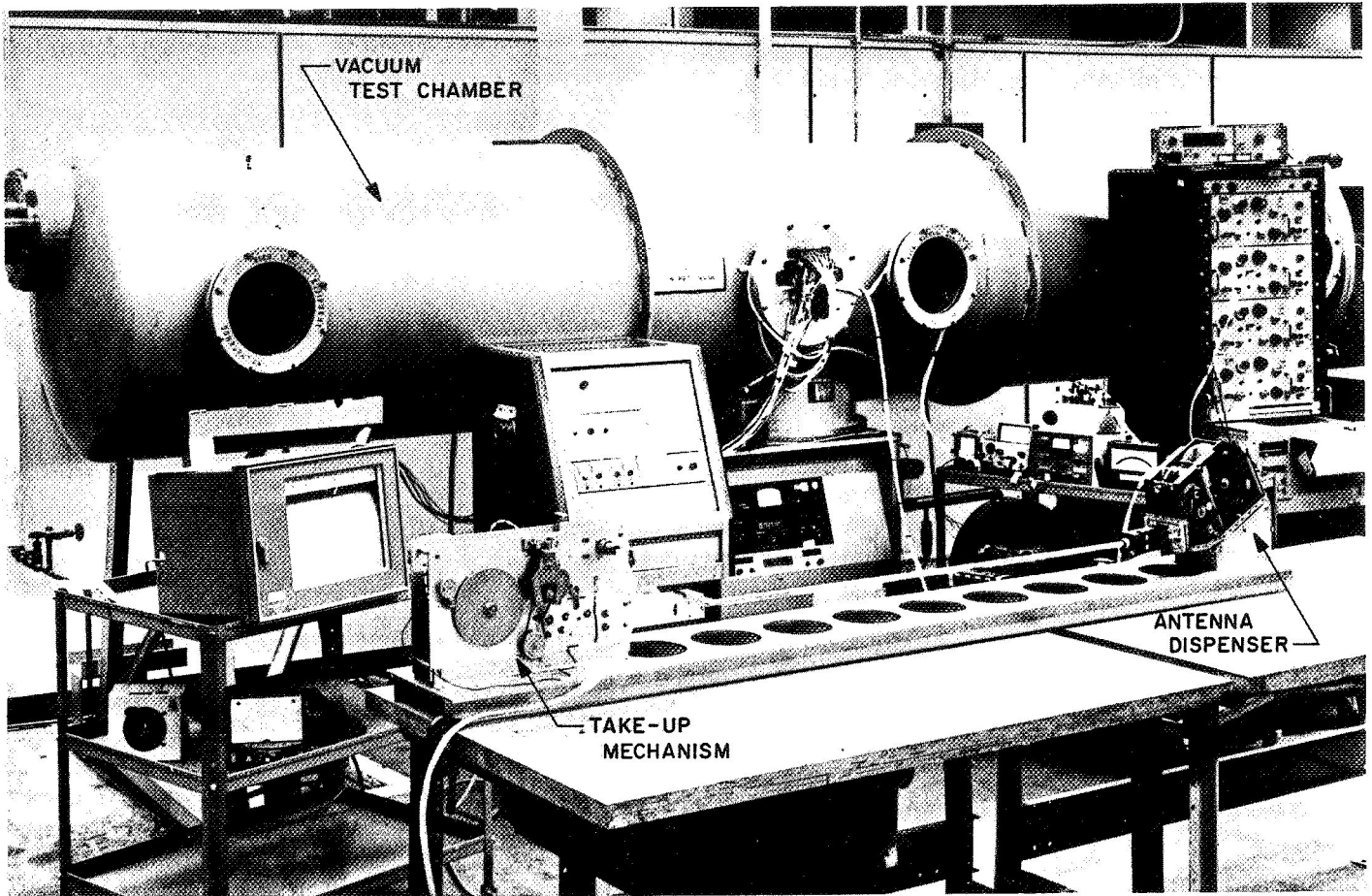


Fig. 6. Antenna dispenser mechanism testing

the flight dispenser. That is, drive principles such as motors, pinch drive rollers, drag clutches, rotating forming guides, etc., were preserved, since they were understood and known to function properly. A bidirectional servo system was designed to satisfy the velocity requirements of the flight units. Operation was simple, in that arming the electronics required only one switch closure. After this operation, the take-up device system simply responded to the flight units. The fixture length required the utilization of the 18-ft-long horizontal thermal vacuum test chamber at the Fairchild Hiller Space Technology Center. Figure 6 illustrates this test setup.

V. The Take-up Mechanism

Figure 7 illustrates the mechanical design concept of the take-up mechanism. The object of the device is to accept and/or release the antenna element without inducing an appreciable axial load in the formed tubular element section. To accomplish this, all forces acting in

the element must be nullified. As shown in Fig. 7, force F_1 is caused by the strain energy of the element which occurs as it translates from the flat to the tubular shape. When the flight mechanism is in the extend mode, the element is coming into the take-up mechanism at a constant rate. Drag forces D_1 , D_2 , and D_3 add to force F_1 . The spring must nullify these forces. Since the force-sensing roller is restrained by two strands of tape, only half of F_2 is applicable in calculating the element tension. Likewise, only half of D_3 is applicable. The equation then becomes

$$F_1 + D_1 + D_2 + \frac{D_3}{2} = \frac{F_2}{2} \quad (1)$$

Equation (1) is the equation that must be satisfied when the calibration system is in the extend mode. Since the tape velocity is constant, the various forces are constant, and the equation can be satisfied. The take-up mechanism motor does not enter into the calculations,

D = DRAG FORCE

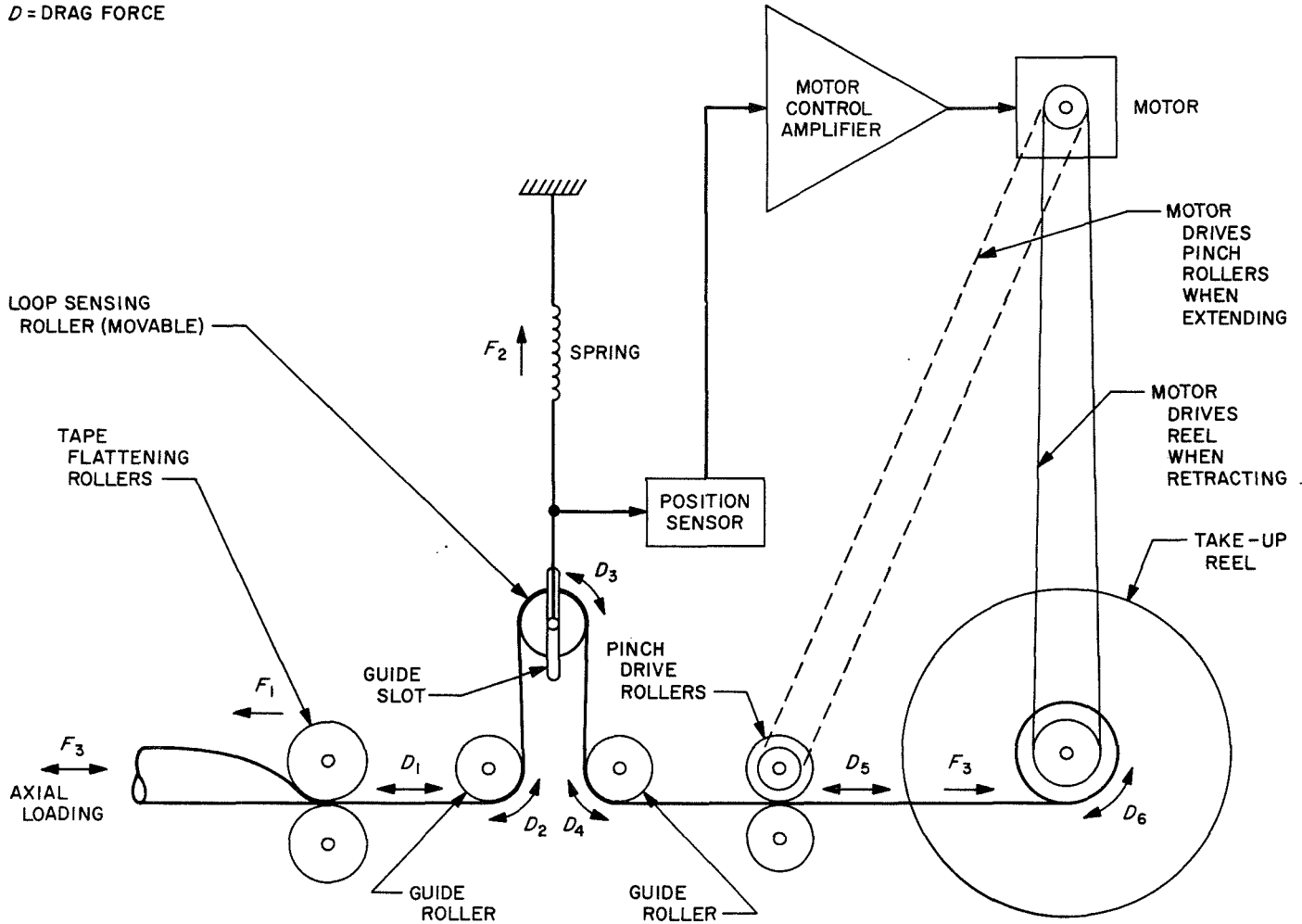


Fig. 7. Schematic diagram of take-up mechanism

since the spring is an effective buffer and tension regulator.

In the calibration system retract mode, the element is being pulled from the take-up mechanism storage reel by a pinch drive roller. The various forces now subtract from force F_1 . In addition, the element velocity is variable. Because of the buffer action of the spring, the force equation becomes

$$F_1 - D_1 - D_2 - \frac{D_3}{2} = \frac{F_2}{2} \quad (2)$$

Since the drag forces D_1 , D_2 , and D_3 are small and do not vary significantly with velocity, it is not necessary to change the spring force F_2 in order to accommodate Eq. (2).

This automatic calibration system was used extensively throughout the RAE mechanism design qualification and acceptance test program. Five full-length extensions and retractions were performed on each mechanism prior to installation in the spacecraft.

Operational integrity of the calibration system was verified visually by merely observing the position of the element loop sensing roller relative to the bearing slot extremities. As long as the roller shaft is not bottomed against either end of the slot, an axial force is not being transmitted to the translating antenna element.

VI. Conclusions and Recommendations

It can be concluded from the results of this development effort that compact lightweight tubular extendible

element systems (TEEs) can be employed for extremely long space antenna arrays. Furthermore, this activity has demonstrated that it is possible to adequately test very long antenna systems in the earth's gravitational field. In order that this segment of the technical community might benefit from this activity, the following development findings are mentioned:

- (1) Pinch driving of thin web material such as TEEs requires adequate tension control. Friction drag clutches can be utilized. Delrin friction plates should not be used. Recommended for use are composite bearing materials consisting of a brass backing onto which is sintered a thin porous layer of spherical bronze, which is, in turn, impregnated with a mixture of TFE fluorocarbon resin and lead powder.
- (2) The pinch drive roller elastomer should be chosen carefully. Viton should not be used because the durometer changes 90% at +5°F. Instead, we recommend a silicone elastomer per Federal Specification ZZ-R-765a, Class III Type 50.
- (3) Magnetically shielded, crown tooth, electrically operated, duplex clutches can be used for mode switching, provided mode coupling is isolated with one-directional mechanical clutches. This will prevent the front wheels from turning when the rear wheels are standing still.
- (4) Bidirectional servo-controlled TEE storage systems (take-up mechanisms) with narrow bandwidths can be devised. The designer should not attempt to compensate for inertia-caused jitter electronically. Instead, he can use viscous dampers, which are available for operation in a thermal vacuum environment.
- (5) Brush-type permanent magnet direct-current motors can be used for space applications without incorporating baffling schemes, O-rings, or wobble plates. Hermetic sealing can be achieved with bearing-supported eccentric shafting and a bellows. However, the shaft and bellows materials and bearing support system should be chosen with extreme conservatism.
- (6) Torsionally rigid, edge-locked TEE systems can be made simple. The designer should evaluate and understand his system geometry before launching into a complicated moving part system, and should provide sufficient adjustment to compensate for assembly and component tolerances. The RAE system uses a simple, fixed-shaft-mounted wheel, which reliably achieves edge-locking of 43,560 tabs per spacecraft.

N 69-11807

The Development Philosophy for SNAP Mechanisms*

O. P. Steele, III

Atomics International

A Division of North American Rockwell Corporation

Canoga Park, California

Mechanisms used in the control of SNAP (Systems for Nuclear Auxiliary Power) reactors face a life of many years in a hostile environment of high temperature (1000° F), high radiation (10^{20} nvt), and space vacuum (10^{-13} torr) without maintenance. The development approach for these mechanisms could either have been one of creating a congenial environment by a secondary support system or of producing mechanisms capable of direct operation in the hostile environment. For the SNAP reactors it was decided that this latter approach gave the highest overall system reliability.

This paper discusses this direct approach concept to hardware development and describes the steps taken for the successful development of the SNAP reactor control system mechanisms. The resulting whole new family of state-of-the-art mechanism components, such as actuators, bearings, gears, springs, limit switches, and position sensors, is briefly described.

The SNAP 10A system was successfully flown in 1965, and the SNAP 8 system is being readied for ground test later this year.

I. Introduction

During the last ten years, the Atomics International Division of North American Rockwell has been engaged in the development of the SNAP (Systems for Nuclear Auxiliary Power) reactor systems for the Atomic Energy

Commission. These are compact, liquid-metal-cooled, nuclear reactors coupled to various power conversion systems. The SNAP 10A system (Fig. 1), which was successfully flown in April 1965, was coupled to a thermal electric power conversion system and produced 500 W of electrical power. The SNAP 8 system, which is being readied for ground test later this year, will produce 700 kW thermal, and, when coupled to a mercury rankine

*This work was performed under Contract AT(04-3)-701 for the U. S. Atomic Energy Commission.

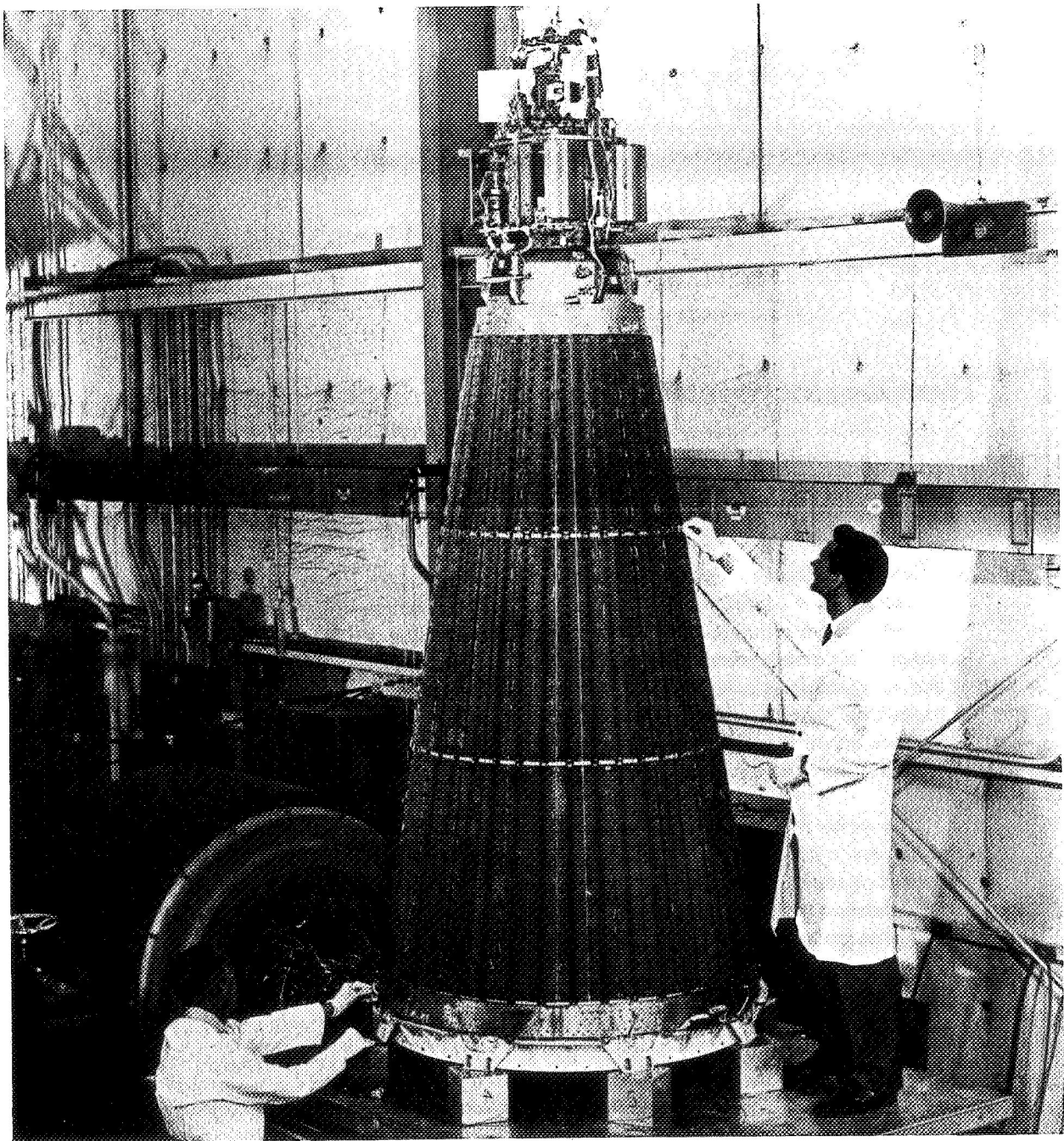


Fig. 1. SNAP 10A system being acceptance-tested prior to its successful space flight in April 1965

power conversion system, will produce 70 kW electrical power. If it is coupled to a thermal electric system similar to the 10A system, it will produce 15 kW electrical power.

II. Description of SNAP Reactors

These SNAP reactors provide a very strenuous environment in which mechanisms must operate, including space vacuum, high temperature, and high nuclear radiation after being subjected to launch, shock, and vibration. No repair or maintenance is possible during the several years that these nuclear reactors are operating. Size, weight, and reliability are naturally of prime importance. For weight consideration, it is desirable to omit or minimize both thermal insulation and nuclear shielding between the mechanism and the reactor. The components in close proximity to the reactor receive a radiation dose as high as 10^{20} nvt (fast neutrons) and 10^{11} rad (gammas) during a one-year period. The thermal heat generated by the reactor results in mechanism temperatures from 1000°F , near the bottom of the core vessel, to 1300°F at the top.

Because of space startup of the reactor, the mechanism must operate from subzero temperatures to the high steady-state temperatures above. Structural integrity, dimensional stability, and frictional characteristics of the mechanism must be kept within functional tolerances. Design requirements are further complicated by the vacuum of outer space. Exposed surfaces become "super" clean, providing opportunity for contacting surfaces to vacuum-weld together. The launch imposes shock loads up to 35 g, with accelerations to 100 g. Random noise vibrations can result in peaks up to 50 g, depending upon the launch vehicle.

The SNAP 10A and SNAP 8 reactors are cooled by liquid metal (NaK) and have homogeneous uranium hydride fuel (Fig. 2). The reactors are controlled by increasing or decreasing the leakage neutrons with external Be reflectors. The reflectors are semicylindrical drums that surround the reactor core vessel and rotate toward the core or away, as required.

III. The SNAP Reactor Control Mechanism

The reactor control mechanism is composed of an electromagnetic actuator that rotates the drums through a gear train upon command from an electronically pro-

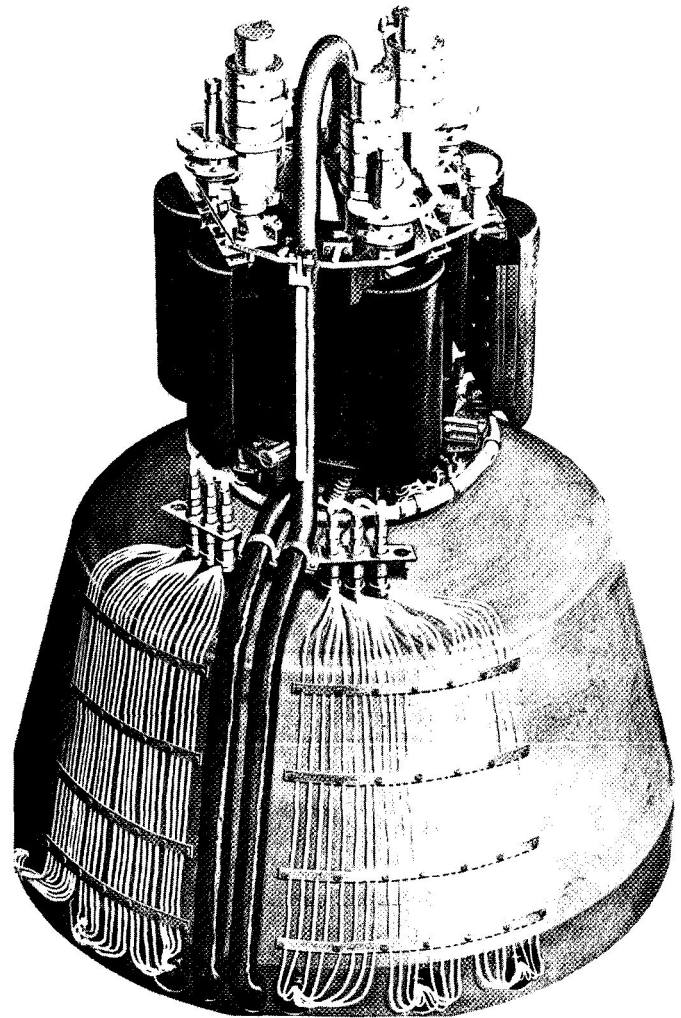


Fig. 2. Artist's sketch of the SNAP 8 reactor

grammed controller, along with the necessary auxiliaries such as position sensors and limit switches.

As soon as the space vehicle is in an established orbit, a ground command signal initiates reactor startup (Fig. 3). The electromagnetic controller is energized and controls the system by a programmed sequence of signals to the control drum actuators.

The direction, rate, and order of stepping action are preset in the programming. The coarse control drums are released and rotate to the full-in position. At this point the reactor is still subcritical, and the three fine control drums then start their rotation inward. Each drum is stepped sequentially.

During the startup, there are several preset rotational rates, with the rates decreasing as the reactor becomes

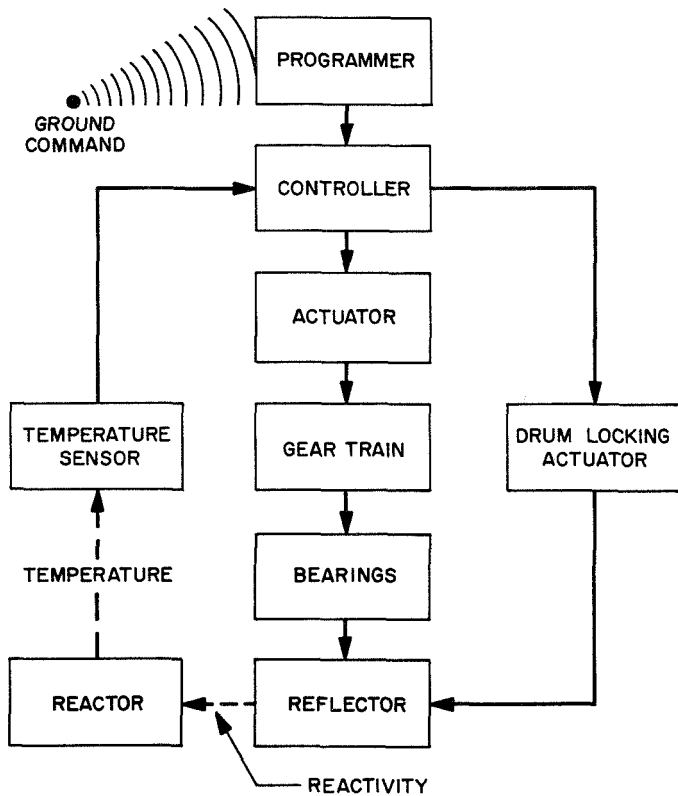


Fig. 3. SNAP 8 control system logic

critical and temperature or heat generation is established. When the reactor power level reaches the desired temperature, negative reactivity is introduced as a result of the temperature coefficients of the grid plate and fuel, thus dampening the power transient. After the initial temperature transient there is a gradual rise in power, with corresponding rises in the system temperature and coolant flow. This process continues until the reference temperature is reached. The temperature sensors then signal the controller, and the power to the control drum actuators is stopped. When the reactor outlet temperature varies from the design reference temperature, a temperature sensing switch signals the controller and the actuators step the drums to correct the reactivity.

IV. Design Philosophy

The detailed explanation of how this control system operates was given to show its simplicity. It is readily apparent that a mechanism to perform this function could have taken the form of a hundred different designs. The question is, then, why this one?

In the development of the control mechanisms for the SNAP reactor, we have established three basic philoso-

phies. The first of these is that we accept the fact that the shortest, most direct route to achieving the end objective may not be a direct line through the normal way of doing something. Second, the reliability is generally increased by the elimination of backup systems and by the reduction of the number of parts. Third, the fastest and least expensive development program is one that proceeds methodically from the understanding of the details to the evaluation of the completed assembly.

Let me illustrate each of these points. For the first, let us take the prime mover for our mechanism. We had available to us, from the prime system bus, both dc and 400-Hz ac. The rate of movement of the control drum for nuclear purposes is $\frac{1}{2}$ deg every 240 s. The generally accepted small prime mover for space applications is a high-speed ac motor, with 400 Hz being a common frequency. Were we to use a 4-pole, 400-Hz motor and a straight gear train reduction, we would end with a gear train with a ratio of two billion to one. Even if we were to use an 8- or a 12-pole motor, we would not have helped the situation significantly. Were we to pick some lower frequency, we still would end with a massive gear reduction system and still have a nonstandard prime mover.

If, however, we do not hamper our thinking by too much familiarity with how others are designing their space prime movers, but look at the basic end objectives, we quickly reach a different solution.

In the development of the hardware for the SNAP reactors, the starting point was a clear definition of the end functional requirements. The solution was then determined by the simplest and least amount of equipment to provide this function. In the point in question, the requirement is to move the control drum through small, incremental steps. The available power source is dc or 400-Hz ac. The objective is to couple these two points with the least number of incremental active components.

A dc stepper motor, with time delays between steps, represented the simplest approach. This solution circumvented many of the major problems such as lubricating the high-speed bearing and gears, the self-welding of rubbing parts, and high-speed position feedback. When this decision was reached, back in 1959, the dc stepper motors were far from the refined and widely used devices they are today.

By applying this same philosophy in the stepper motor design ("what is the basic physical law?" rather than

“what is the standard design?”) it has been possible to convert the dc stepper motor from a device that produces about 2.5 in.-oz/lb at room temperature to one that produces 24 in.-oz/lb at temperatures as high as 1300°F (Fig. 4).

This has been accomplished by such unorthodox design changes as the elimination of the permanent magnet rotor and the bifilar winding normally used. A design change giving the stator and rotor each the same number of teeth and moving these torque-producing teeth to the outside periphery has resulted in the greatest incremental torque increase. The development of a technique for wet winding the coils has allowed the fabrication of units with high reliability for long life at over 1200°F.

The second point can best be illustrated by the development of components to operate directly in their normal

environment. The alternative approach would have been to supply an artificial environment, less hostile to the component, by an auxiliary system: that is, to enclose the components within a sealed envelope, so that they do not see the vacuum environment, and to supply them with auxiliary cooling. This, however, results in the system reliability being a product of the reliability of the prime component and of the auxiliary system. Our experience has shown that our system reliability decreases with each additional item of hardware.

The third point is that of an orderly development program. The development program for the system components has proceeded from the detail material or component development testing, through the sub-assembly testing, and then to a prototype test. One illustration of this is bearing development (Fig. 5). When the

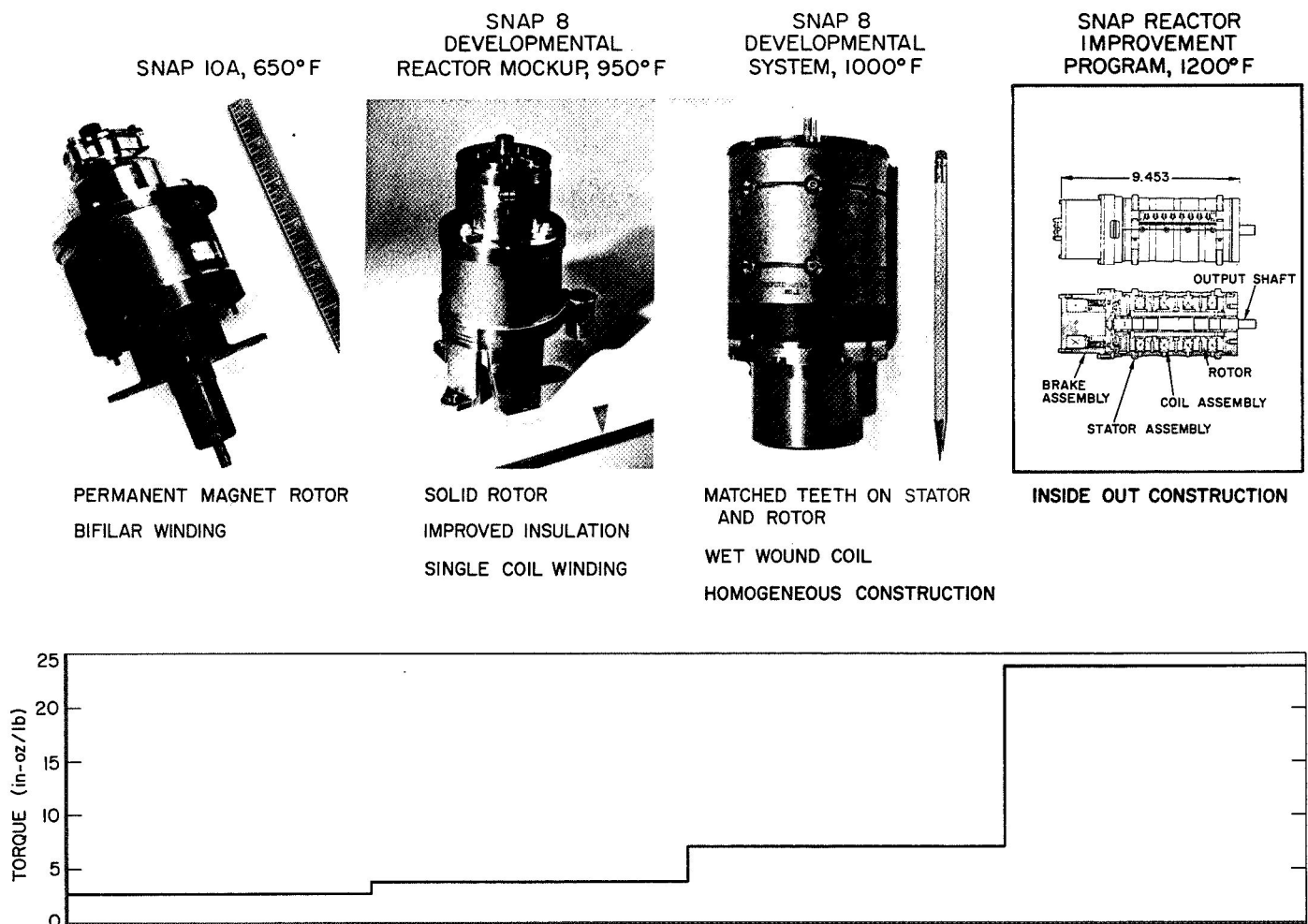


Fig. 4. Development of the dc stepper motor

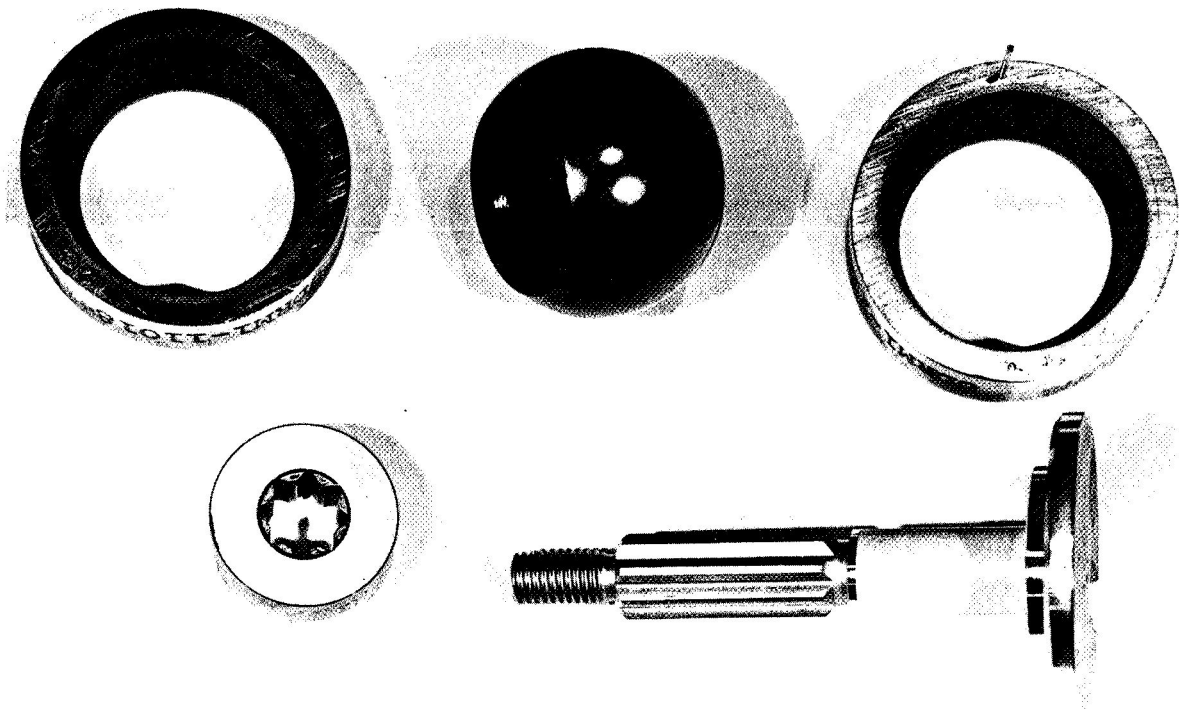
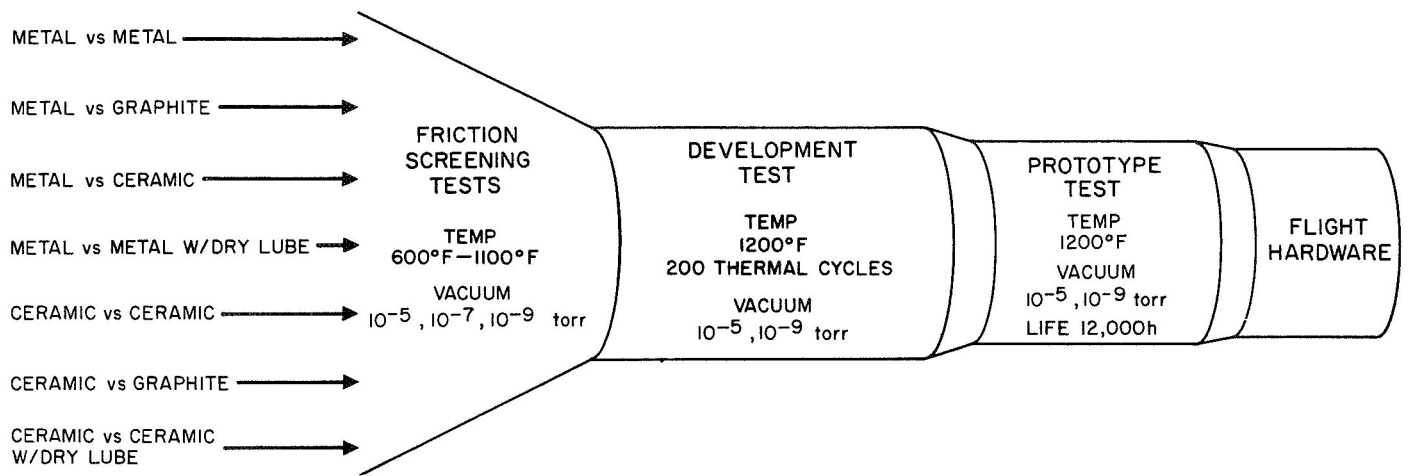


Fig. 5. Bearing material development

program started, no information was available on the friction of materials at 1000 to 1200°F in a vacuum environment. The initial tests were, therefore, material friction and self-adhesion tests. About 100 material combinations were tested to determine the ones with minimum friction and the least tendency to self-weld. Next, developmental bearings of the most promising materials were constructed and tested to verify the design calculations. Finally, prototype bearings were made and tested, under simulated conditions, for the full life requirement.

V. Thermal Environment

Because we have found that the thermal environment is the most strenuous, all prototypes are tested at 100° above the calculated operating temperature and to four times the expected thermal cycles. For the SNAP 8 reflector bearings, which are expected to operate at 1100°F and which are expected to experience 50 thermocycles during their life, prototype tests are conducted at 1200°F and through 200 thermocycles.

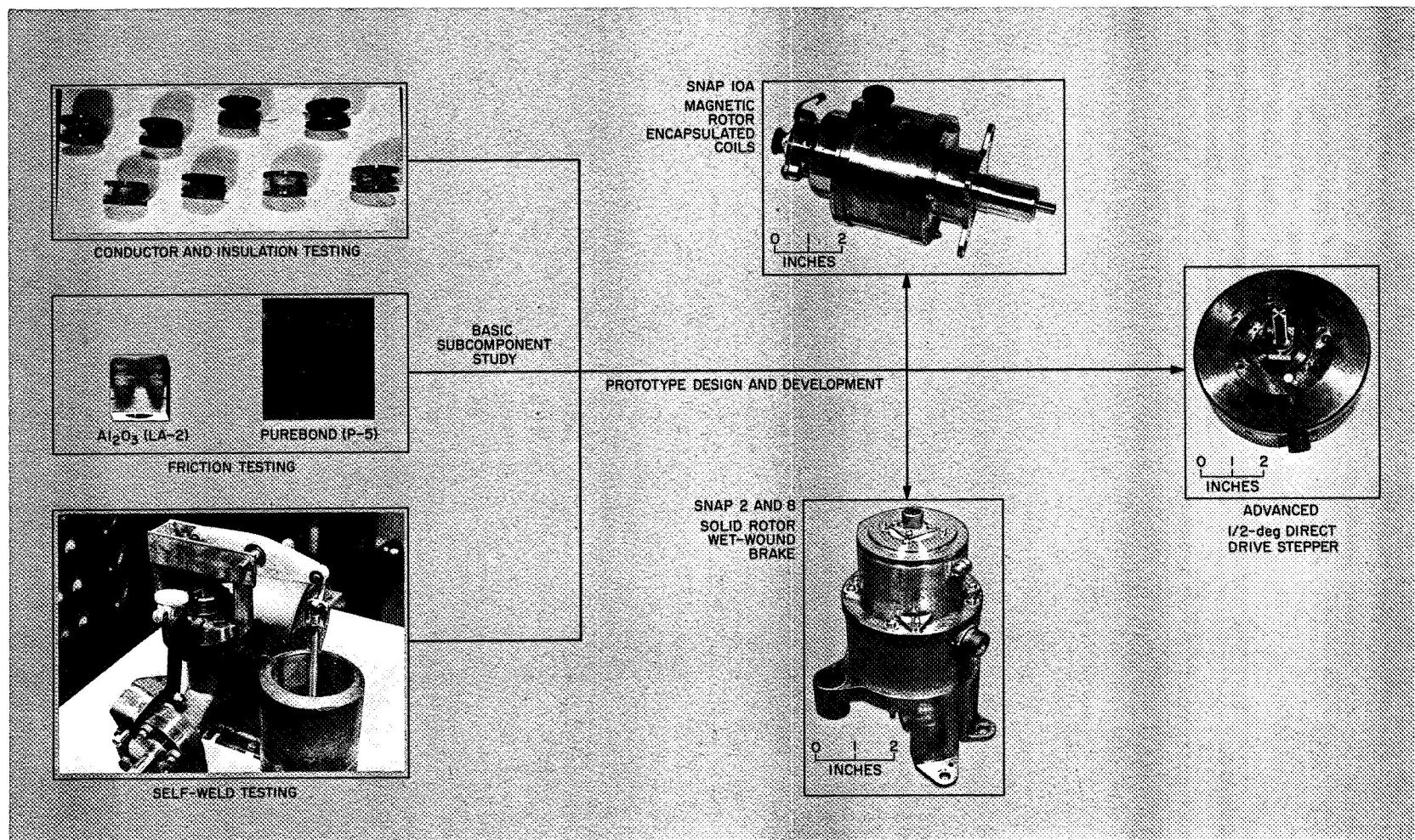


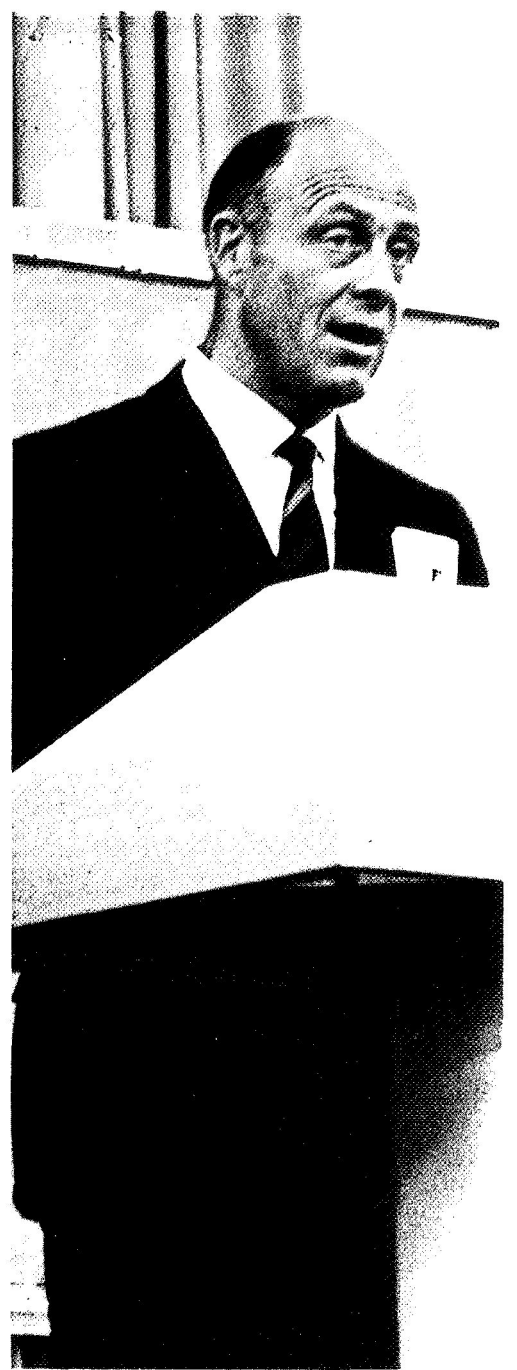
Fig. 6. Composite development plan, where component development is a common basic program to support current and proposed reactors, and the goal is maximum technology growth with minimum duplication

A more general illustration is shown in Fig. 6, where basic development tests on electrical conductors, high-temperature insulation, bearing friction, and self-welding are used as a foundation for the actuator prototype development.

VI. Flight Test Experience

The soundness and adequacy of this development approach is well illustrated by the SNAP 10A flight test.

During the preparation for launch and the count-down, not a single halt was caused by the reactor mechanism. During the 43 days of space operation, the reactor control mechanism functioned perfectly. (Paradoxically, it was the perfect functioning of the mechanism that resulted in the early shutdown of the reactor, when a spurious telemetry signal falsely triggered the "end-of-life" shutdown portion of the mechanism.) Similarly, perfect results have been achieved on ground tests where the space reactor systems have operated in similar environments for over a year.



Session II

**OVERLEAF: Robert F. Steidel, University of California
at Berkeley, Session Chairman**

N 69-11808

Mechanisms for Restraining and Deploying a 50-kW Solar Array*

Theron Haynie and Abraham Kriger
The Boeing Company
Seattle, Washington

A 5000-ft² folding modular solar array, designed by The Boeing Company for the Jet Propulsion Laboratory, can generate approximately 50 kW of power, with an efficiency greater than 20 W/lb, for a Mars flyby mission. To adequately stow and deploy this large-area solar array during boost and space flight, new mechanism-system design using conventional (1967 technology) light-duty mechanisms has been developed. The design requirements and hardware descriptions used to restrain, release, and deploy this large array are discussed.

I. Introduction

As spacecraft become more sophisticated and are required to perform more tasks, electrical power needs increase rapidly. While the *Explorer I* satellite required just a few milliwatts to complete its mission, a hypothetical ion-propelled spacecraft system, which has been studied for a Mars mission in the 1970s, indicates power demands approaching 50 kW. A 5000-ft² folding modular solar array, designed by The Boeing Company, has the capability to generate approximately 50 kW of power,

with an efficiency greater than 20 W/lb, for a Mars flyby mission.

The spacecraft that would utilize the solar array would be boosted by a *Saturn IB/Centaur* launch vehicle, and the array would be deployed within 3.5 h following launch (see Fig. 1). The design environments include steady-state and transient load conditions: sinusoidal, random, and acoustic excitation and extreme temperature and thermal shock conditions. The array configuration (Fig. 2) maximizes the live cell area within the shroud envelope. Four identical panel assemblies are positioned symmetrically about the spacecraft longitudinal axis. A panel assembly consists of 13 separate subpanels, each

*This work was performed for the Jet Propulsion Laboratory, California Institute of Technology, sponsored by the National Aeronautics and Space Administration under Contract NAS 7-100.

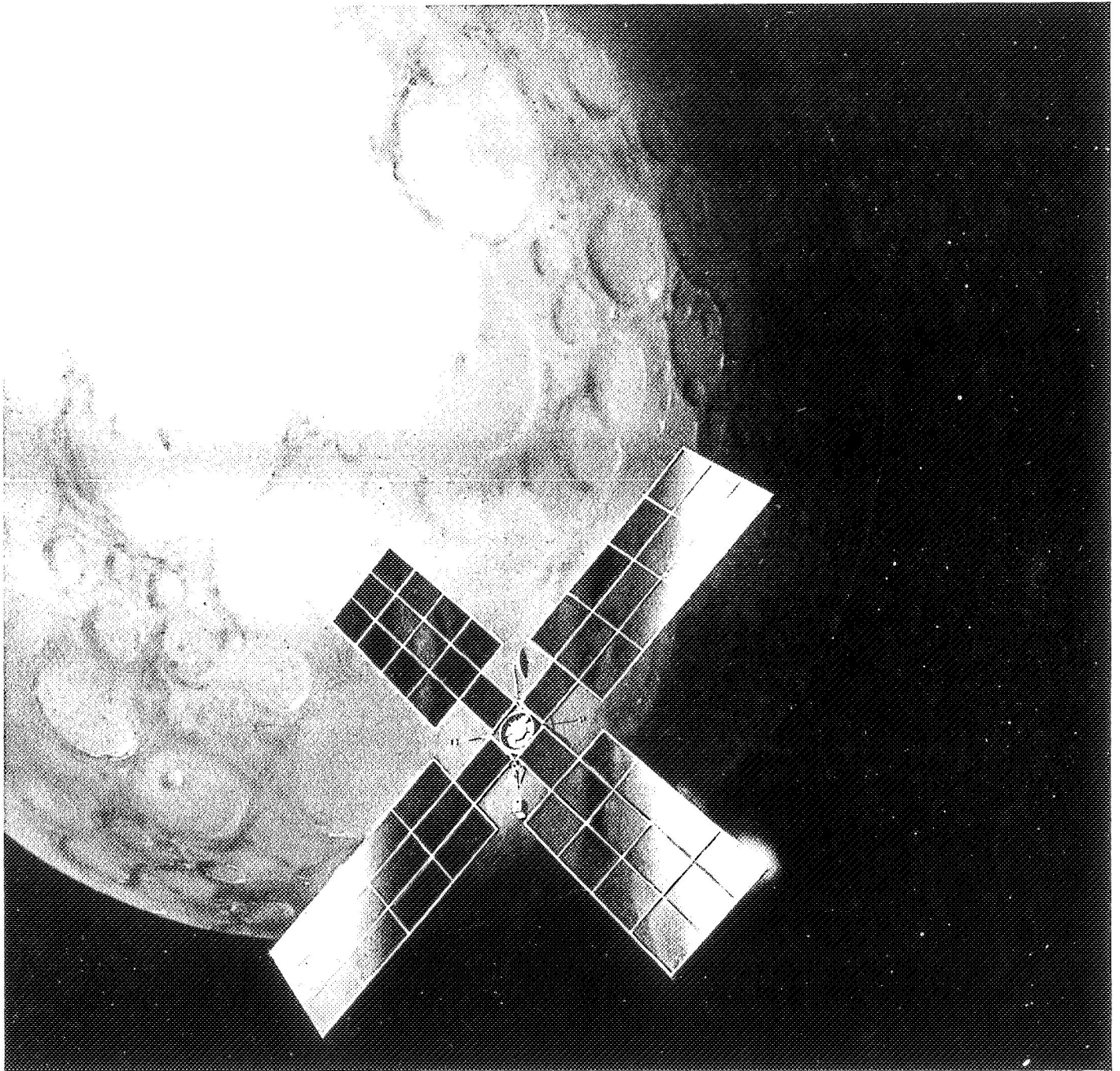


Fig. 1. Artist's conception of an ion-powered Mars flyby spacecraft utilizing a 5000-ft² solar array

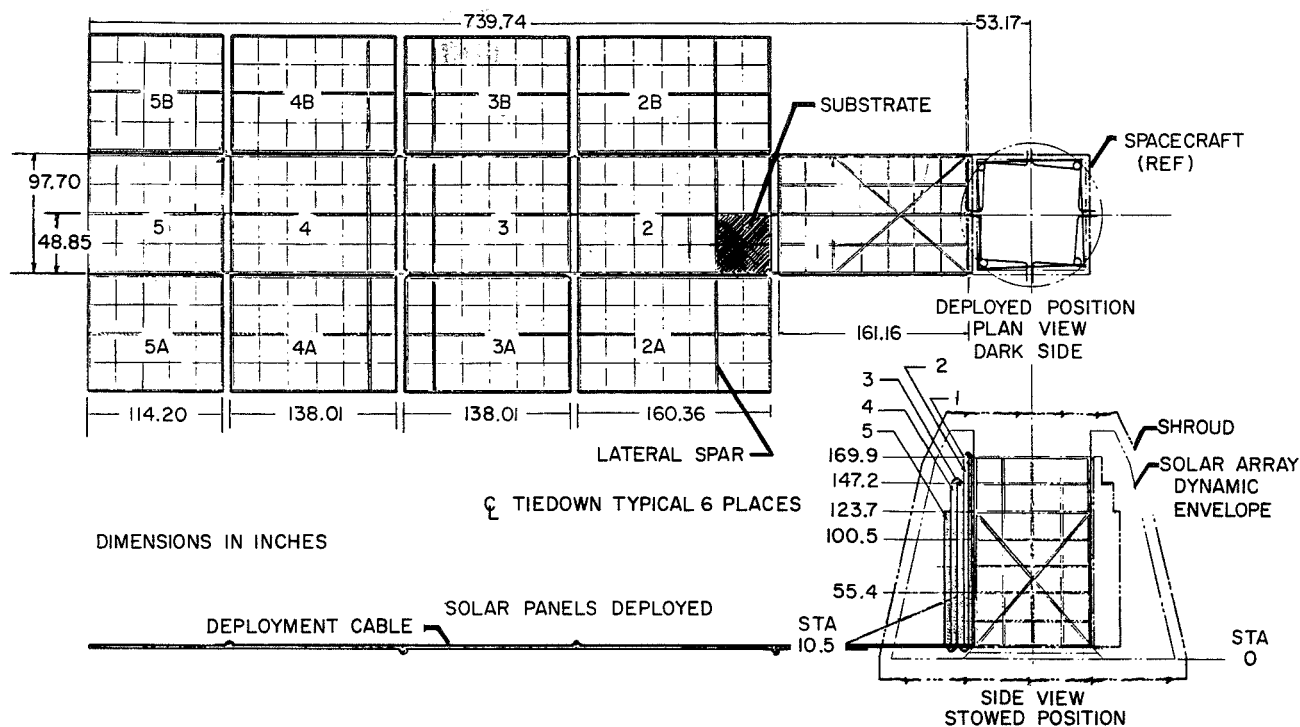


Fig. 2. Solar array, stowed and deployed

8 ft wide and varying in length from 9.5 to 13.5 ft. The first subpanel in each quadrant supplies 28 V power; all other panels supply 100 V power. When deployed, the array is firmly locked in a flat plane.

Beryllium is the primary structural material in the subpanel framework (Fig. 3) because of its excellent stiffness-to-weight ratio. Each framework consists of thin hot-formed beryllium channel and plate material bonded to form structural members. Adhesive bonding is used to eliminate possible stress risers that occur with mechanical fasteners. A diagonal matrix of 0.003- by 0.140-in. fiber glass tape is accurately positioned and bonded to the beryllium framework, providing a lightweight mounting surface for the solar cells. The tapes are pre-tensioned to increase substrate rigidity.

II. Boost Tiedown and Release System

The tiedown system allows the four panel assemblies to work together as a single structure during boost, increases the effective out-of-plane stiffness of each panel assembly, and reduces the loads inside the structure (Fig. 4). Mechanical release trains are used to minimize the number of pin-releases required for deployment.

To enhance its adaptability to different spacecraft configurations, the array-to-spacecraft interface is limited to a single array station plane. Three hinges per panel assembly transmit all boost loads from the array to the spacecraft and provide a hinge line for deployment. Each panel assembly is restrained from out-of-plane rotation about the hinge line during boost by linking it to its adjacent panel assemblies, which are inherently stiff in the in-plane direction; adjacent panel assemblies are joined by main tiedown fittings. To meet the boost phase frequency, envelope, strength, and weight environment, the 13 individual subpanels in each panel assembly act together as a type of "deep beam." A subpanel frame element is only 1.5 in. deep but may be as long as 13 ft.

By comparison, the entire panel assembly stack is 23 in. deep. A minimum of six shear transfer points along each longitudinal spar member is necessary to satisfy strength and stiffness requirements. By increasing the number of shear transfer points from one per longitudinal spar member to six, the fundamental frequency of the array is increased from 8 to 22 Hz, the peak deflection is decreased by over 10 times, and the maximum internal bending moments in the spar members are decreased over two times without changing the spar cross-sectional properties.

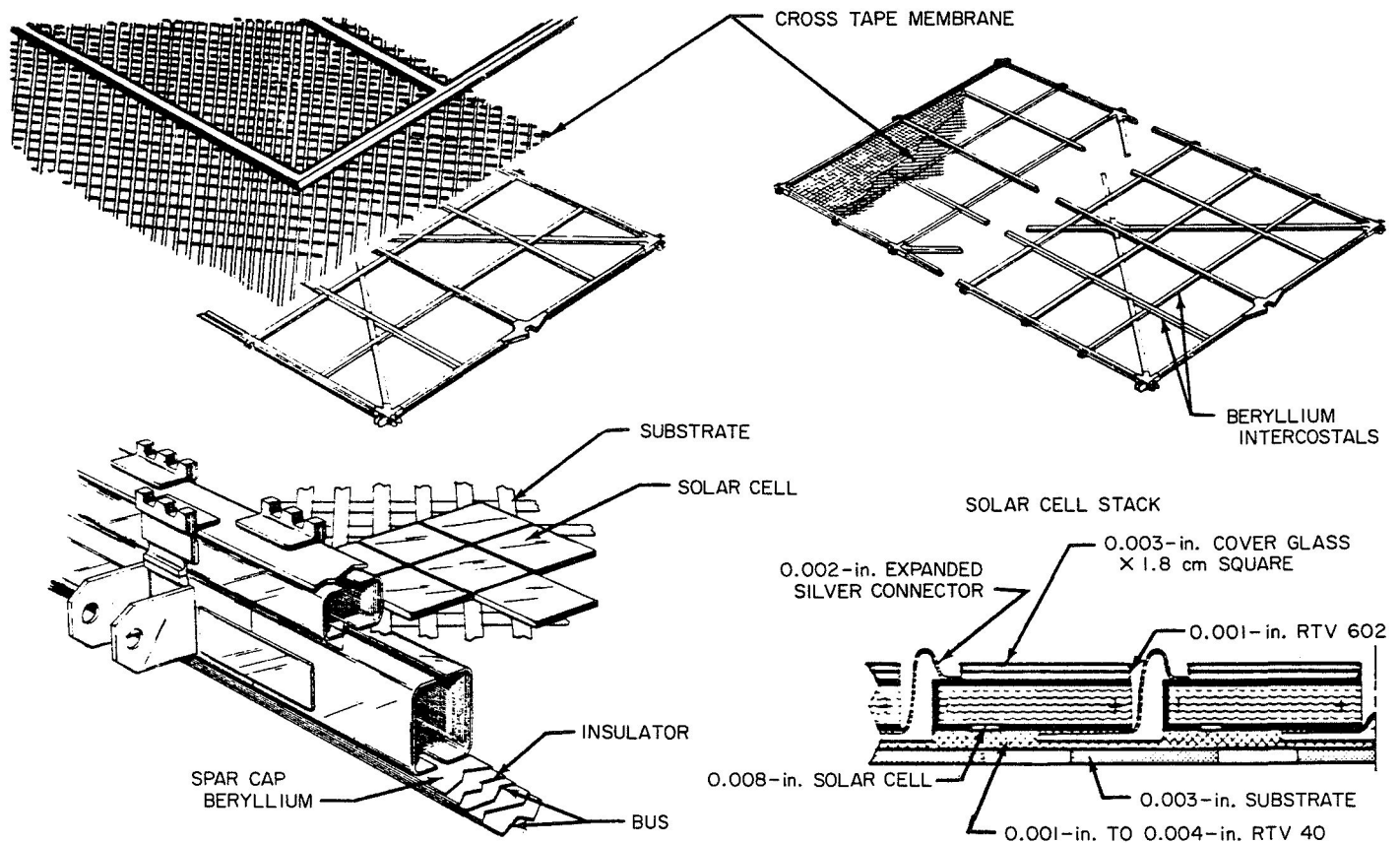


Fig. 3. Subpanel construction details

The net effect of using the tiedown and shear-tie system in this way is to make the individual subpanels work as an integrally stiffened panel assembly, where the individual panel assemblies work together as a more rigid unit basically independent of the spacecraft.

The shear ties provide load continuity between subpanels, both in a shearing and a normal direction. The shear teeth fitting minimizes localized loading effects into the beryllium spar members, thus improving the overall structural capability. The shear teeth are machined from 6Al-4V titanium plate with a multiple-tooth cutter to minimize the additive tolerance between mating parts. The teeth are bonded to the subpanels, but may be adjusted dimensionally along three axes. A preload at each shear-tie location maintains positive contact between mating shear teeth during critical loading conditions and is applied by three types of cable assemblies (Fig. 4): the circumferential cable, the corner cables, and the center tie cables. Additionally, release train cables run along each inboard edge of a panel assembly parallel to the longitudinal axis of the spacecraft and release the tiedown system on signal. In addition to these cable

assemblies, there are various fittings in the boost tiedown and release system that transfer loads between adjacent panel assemblies, serve as the termination point for the tiedown cables, transmit the component of cable loads inward into the panel stack, and react the center tie preloads.

The materials used for the system include stainless steel control cables for all external tiedown cables, organic Nomex cables for all center spar ties, and 7075-T6 aluminum for all fittings. Hard-anodize and molybdenum disulfide are used for bearing surfaces.

Rigging procedures require that center tie cables are installed and pre-tensioned initially, followed by installation and pre-tensioning of the outer cables in a predefined order to minimize wracking of the panel assembly. Rigging tests will be made to establish an optimum sequence to obtain the desired preloads in all cables. The mechanics of operation for the boost tiedown and release system during the rigging, operation, and release phases of the mission are examined and verified by ground tests as the overall program progresses.

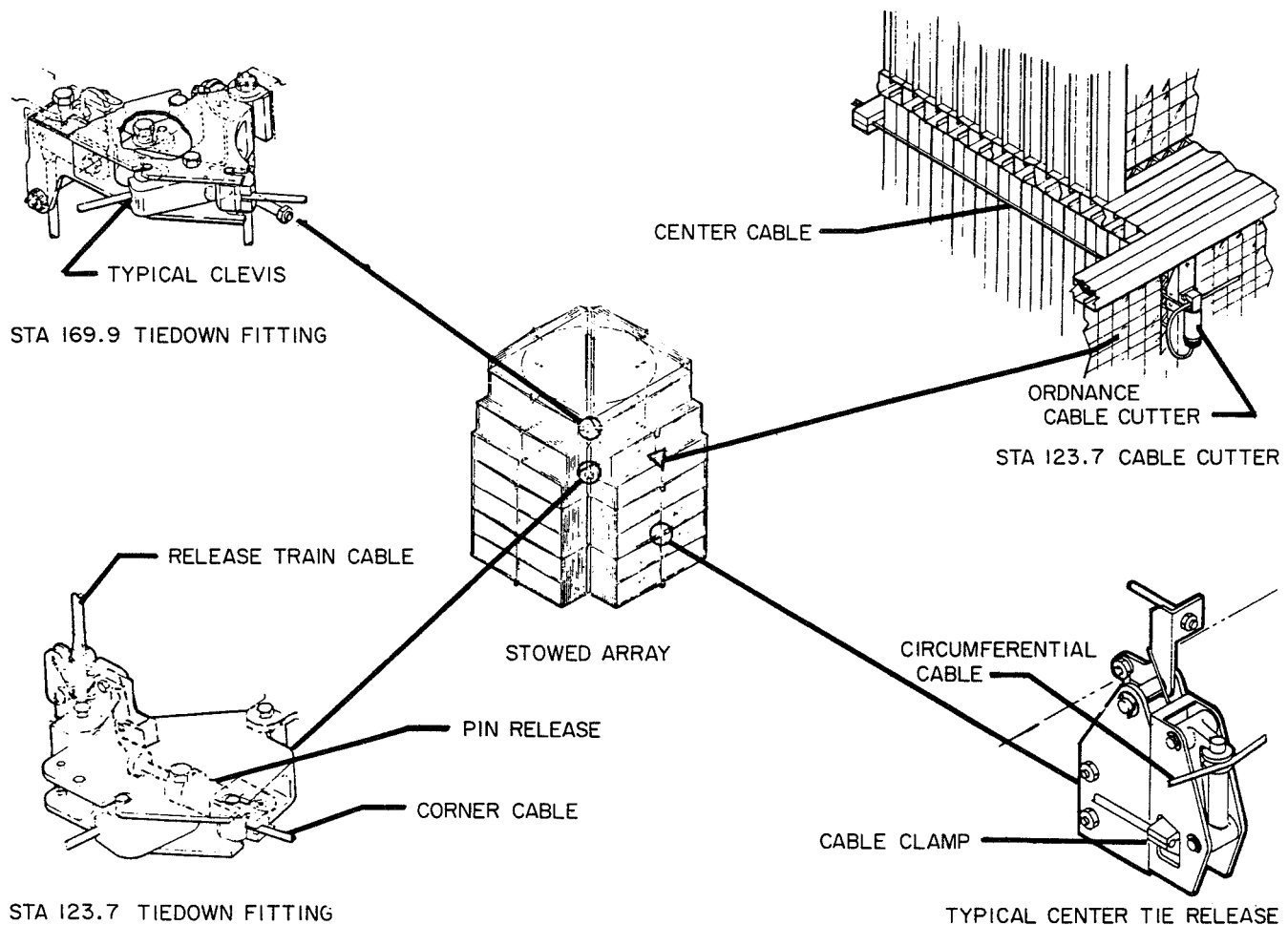


Fig. 4. Boost tiedown and release system

In a typical mission profile, the nose shroud is discarded before the final-stage burn. After burnout, when all significant boost loads have ceased to exist, the tiedown releasing sequence is initiated. An ordnance pin-release mechanism at each of the four major fittings is detonated, setting off a series of mechanical motions throughout the release train system. (The ordnance pin-releases selected are identical to those previously qualified on the *Lunar Orbiter* program.) All cables are released and discarded except for a single center tie cable that is retained on each of the four panel assemblies to prevent premature deployment. All significant stored strain energy is dissipated before panel deployment.

III. Panel Deployment

The main panels are deployed sequentially by an electric-motor-driven cable drum (Fig. 5). Four cable drum motor units mounted inside the spacecraft provide

a primary drive for each panel assembly. The cabling is rigged to make opposite panel motors operationally redundant, thus ensuring symmetrical deployment of each panel assembly pair even if one motor and cable drum assembly fails. Deployment velocity is controlled by the cable drum speed. On each main subpanel a control quadrant converts cable tension to hinge moment and controls the deployment sequence using a geneva drive mechanism to keep the panel stack secure until the adjacent inboard subpanels are open.

When the spacecraft is properly oriented, cable cutters sever the remaining center tie cables and release the panels for deployment. Power is supplied concurrently to the four deployment motor-cable drum assemblies. As the cable is drawn in, each panel assembly rotates 90 deg from the spacecraft centerline until a diagonal strut extends fully. Cam action on the center hinge unlatches the outboard 12-subpanel stack from the inboard panel, allowing deployment to continue. The subpanel stack

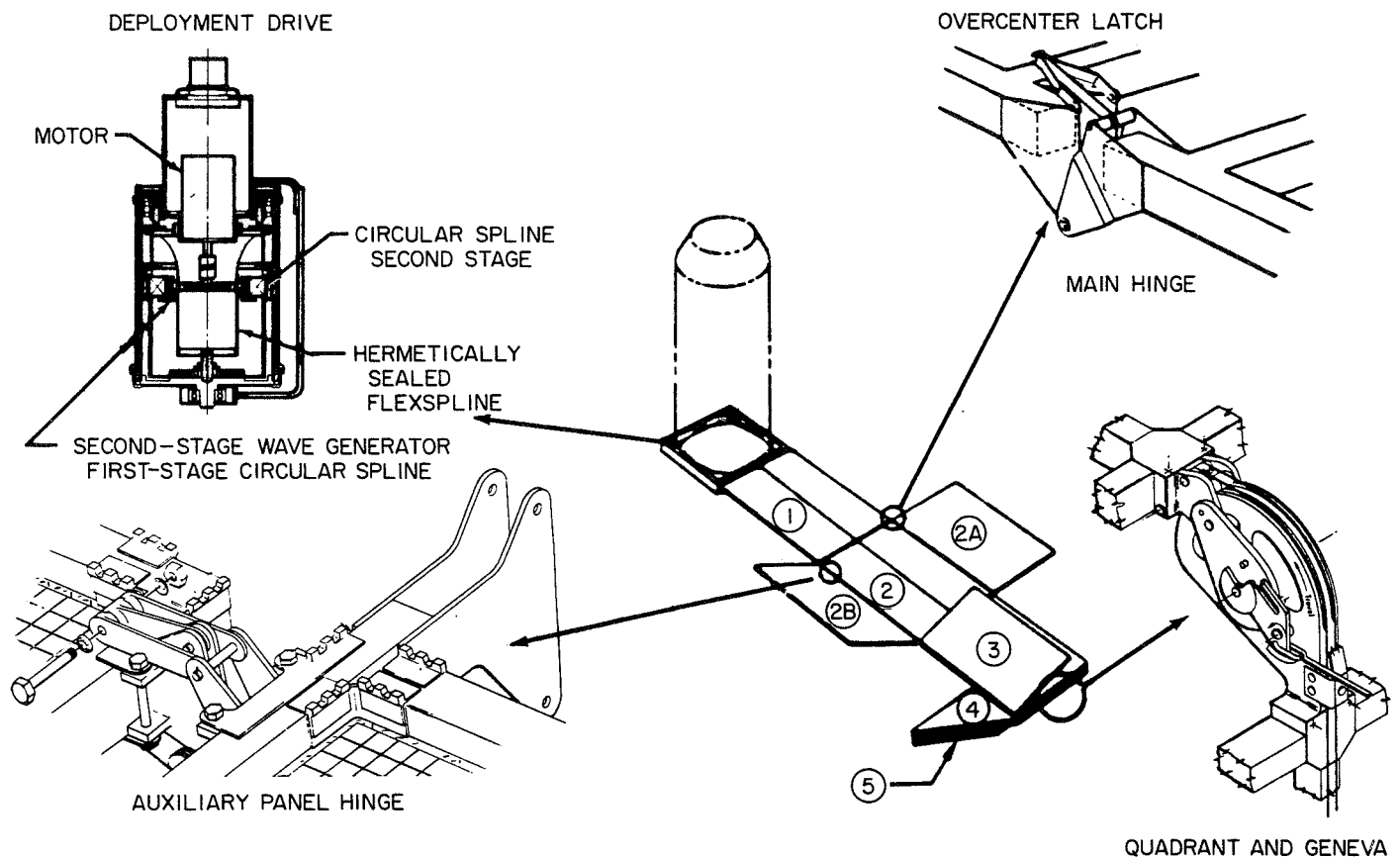


Fig. 5. Mechanisms and deployment sequence

rotates through 180 deg, at which time a four-bar linkage, integrated within the main hinges, snaps over center to securely latch Panel 2 to Panel 1 in a flat plane.

As the second subpanel reaches the full open position, the control-quadrant geneva rotates to release the outboard 9-panel stack. The sequence continues through successive 180-deg unfolding maneuvers until all main panels are deployed. Runaway deployment is prevented and passive damping provided by resistive torsion springs inside each main panel hinge assembly.

Each main subpanel four-bar linkage latch connects to a pin, which, when withdrawn from a fairlead in the end of the auxiliary A and B panels, allows each to deploy independently about its hinge axis. The deployment energy is supplied by a torsion spring in each hinge. Light-duty four-bar overcenter linkage latches lock the auxiliary subpanels in a flat plane. The angular velocity at latching is limited by a rotary viscous damper on each auxiliary subpanel. The dampers provide a damping ratio of 12 in.-lb/rad/s. Since the dampers are not temperature-compensated, thermal-control coatings are applied to

prevent excessively high temperatures. High-temperature operation causes a reduction in the damping capability, allowing excessive closing velocities at latching. Dampers exposed to deep space during the 3.5-h coast period are not protected from reduced temperatures. A warming period is required, after the main panels are deployed, before the oil flows freely within the damper passages. The dampers have sun exposure over 50% of their surface once the spacecraft locks on the sun and the main panels are deployed. If the spacecraft tumbles during coast, cooling of dampers is reduced.

IV. Deployment Design Details

The motor-cable drum assembly is composed of a 1/250-hp electric motor with a speed of 9700 rpm under load. The motor drives a 2.75:1 smooth ball bearing planetary reduction. The sun ring forms the wave generator for a middle-stage harmonic drive reducer with a ratio of 72:1. The output of the middle reducer is the wave generator of the third-stage harmonic drive with reduction of 140:1 for a total reduction of about 37,700:1.

The third stage output directly drives the cable drum, which is the outside housing for the motor and reducing train. The effective pitch diameter of the cable on the drum is 2.46 in.; the drum revolves at 0.259 rpm, providing a cable speed of 0.033 in./s. The motor, the planetary reduction, and the middle-stage wave generator are hermetically sealed, and the third-stage reduction has a rotary seal. Four drive units, each weighing 2.50 lb, are used. Batteries in the spacecraft electrical subsystem supply 28 V electric power. Space is provided within the spacecraft to route deployment cables and mount the motor-cable drum units.

The deployment cable used is 1/16-in.-diameter Monel, coated with molybdenum disulfide (MoS_2) dry-film lubricant, and has a breaking strength of 304 lb. It becomes a spring of reducing stiffness as deployment progresses to panel stacks of decreasing mass moment of inertia (803 slug ft² initially and 92 slug ft² for Subpanels 5, 5A, and 5B).

The control quadrants are made from aluminum alloy and provide an effective moment arm of 2.88 in. The cable groove is coated with MoS_2 , preventing adherence of the cable to the quadrant. The cable is retained on the quadrant by a Negator under a hoop tension load. As the quadrant and outboard panel stack rotate, the Negator spring is rolled onto a ball bearing take-up spool. These ball bearings, for space vacuum service, are stainless races and balls with a Teflon ball separator that deposits a minute quantity of Teflon to the rotating balls for lubrication and prevents vacuum welding.

The hinges between the spacecraft and the panel stack are the only ones that must withstand boost burnout loads. Outboard hinges support the deployed panels only under spacecraft maneuvers, ion engine thrust, and the panel loads introduced as they latch in place during deployment. Outboard hinges are made of simple flat aluminum plates riveted to mounting plates bonded on the outboard beryllium spars. Each hinge-half forms one leg of a four-bar linkage overcenter latch with pin joints. Bearing surfaces are prepared by first hard-anodizing the hole area and grinding to size. A baked-on coating of MoS_2 dry-film lubricant is then applied. The use of pin joints for latching eliminates sliding and mating surfaces, and backlash is limited to a tolerance buildup of the pin joints. Drilling of one hole on final assembly of the latch ensures perfect alignment. Striker plates, shear pins, and other precision-fitted parts are eliminated.

Auxiliary subpanel hinges use the same hard-anodize and dry-film pin bearings. Auxiliary subpanel deployment drive is provided by torsion springs. In the deployed state, the bending moment between panels is carried across the hinge as a couple between the hinge pin and the overcenter latch pins.

The diagonal strut between the spacecraft and the first subpanel maintains the angle between the spacecraft and the solar array. It also is a panel deployment lock. The strut is made up of four articulated links that stow nested together between the panel assembly and the spacecraft. As the panel deploys, two links straighten to form a tension-compression member maintaining angular control. Two smaller links lock the rotary joint in exact alignment so that no eccentric column buckling exists.

Four types of springs are used on this design: Negator springs as cable guards; compression springs as ice breakers (to provide a short-stroke high-impulse force); torsion springs as main panel resistance springs, auxiliary panel deployment drive springs, overcenter latch springs, and diagonal strut springs; and curved washer springs on the overcenter latch and on the diagonal strut pins.

V. Test Program

Testing of the array in an earth gravity field has been identified as a complex problem. The fully deployed structure, intended exclusively for space operation, hardly supports its own weight in the 1-g environment. Each subpanel must be completely supported independent of the adjacent subpanel and without putting excessive forces on the hinges. The supporting equipment must introduce a minimum resistance to deployment when driven with the panel deployment drive system, to minimize the influence of the equipment on the array characteristics and to avoid masking the attainment of system objectives. Deployment data and hard vacuum operation are obtained using prototype mechanisms mounted to small aluminum frames. Friction, latching, frame deflection, and performance tests are completed before the test article is inserted in a vacuum chamber. Hinge centerlines are positioned vertically to minimize gravity effects.

Full-size main subpanel deployment requires a fixture that fully supports the subpanels and minimizes operating friction (see Fig. 6). The fixture uses an overhead suspension system to support the deployed subpanels, simulating 0-g conditions, while the undeployed subpanels are carried on an air-bearing sled that follows a

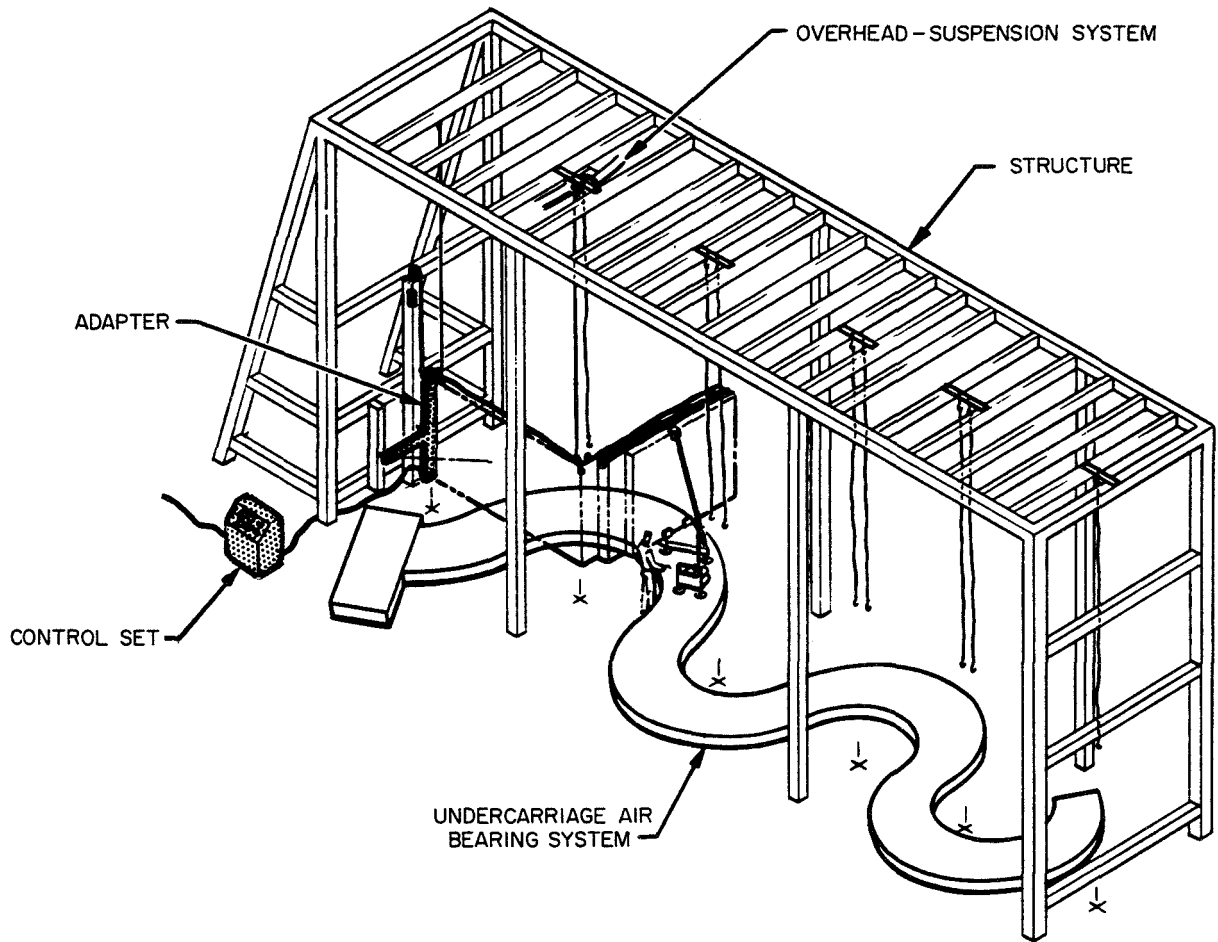


Fig. 6. Artist's drawing of the air-bearing track and overhead support used to provide the 0-g environment for the array during the deployment test. The air-bearing sled and air supply tender are also shown

curved track made of cast aluminum sections. Each section has an epoxy coating and is machined flat to within ± 0.0005 in. in 10 in. On installation, the sections are leveled to ± 0.003 in. The air-bearing gap varies between 0.0008 and 0.0013 in., depending on the load when supplied with 15 to 20 psig air. The sled air is supplied from a tender which contains its own pressure vessel and regulator to eliminate drag, which an air hose from a ground supply would cause. Tests, using mass and balance simulated aluminum main subpanels, have shown that the

solar panel deployment mechanisms are adequate to drive the ground equipment as well as the deploying subpanels.

Auxiliary subpanel tests use a fixture that mounts a main subpanel and its contiguous auxiliaries with the hinge pin centerline vertical. Mechanical bearings rather than air bearings are used to overcome gravity loads. An artist's conception of the subpanel test fixture is shown in Fig. 7.

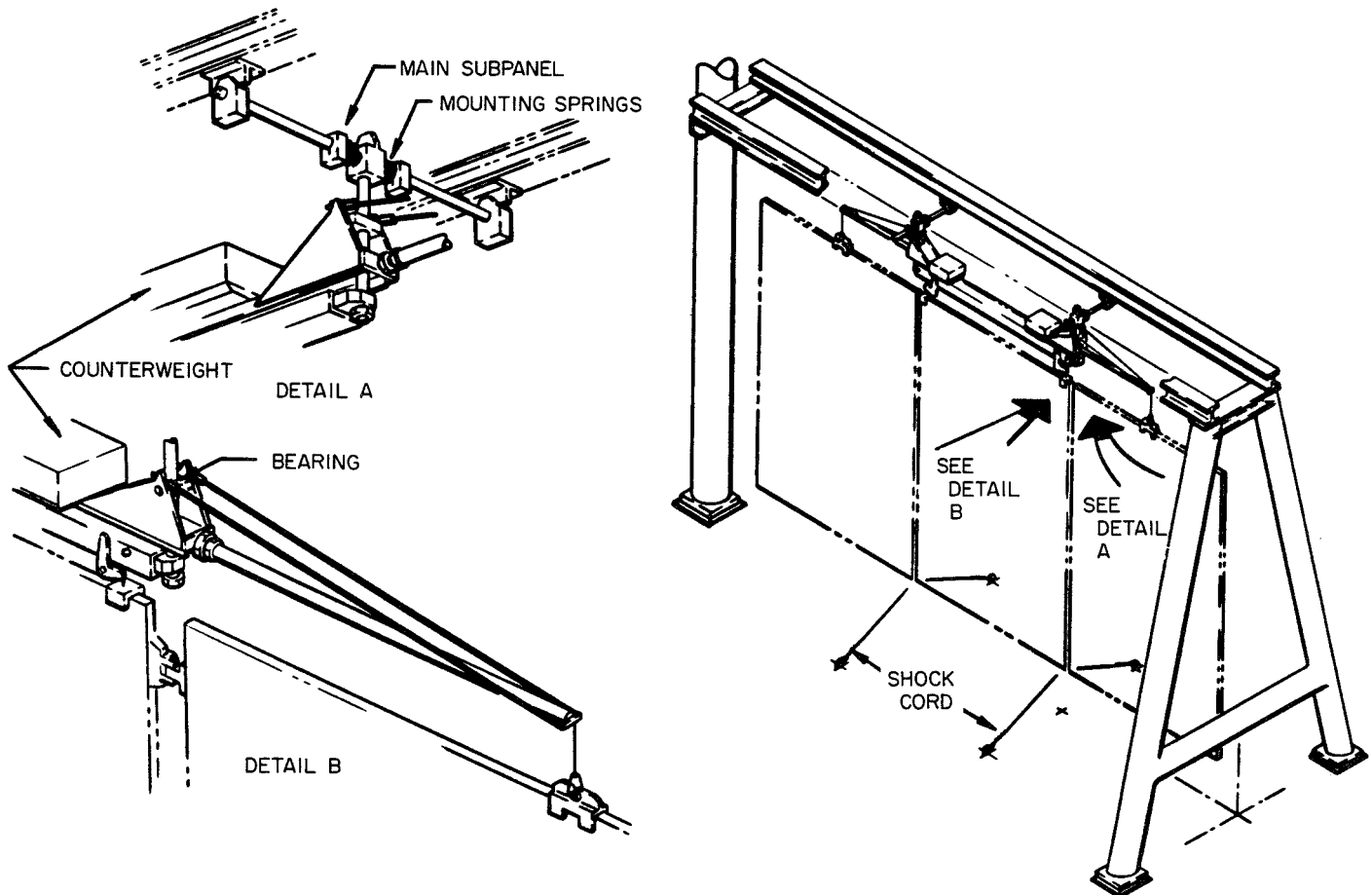


Fig. 7. Artist's drawing of the overhead support system providing for a 0-g auxiliary panel deployment environment

PRECEDING PAGE BLANK NOT FILMED.

N 69-11809

Lubrication of DC Motors, Slip Rings, Bearings, and Gears for Long-Life Space Applications

B. J. Perrin and R. W. Mayer
Ball Brothers Research Corporation
Boulder, Colorado

The Vac Kote lubrication system, which was developed in support of the Orbiting Solar Observatory program, is described. The system involves the use of fluid organic compounds, solid films, and grease formulations. Theoretical principles underlying lubrication in the high vacuum of space are discussed. A summary of flight performance and laboratory test data on Vac Kote-lubricated parts is given; such parts include torque motors, slip ring assemblies, bearings, linkages, solenoids, potentiometers, and gears.

I. Introduction

Lubrication of moving parts, in the high-vacuum environment of space, is one of the special considerations of space technology. Inadequate lubrication of sliding or rolling metallic surfaces exposed to this environment not only results in excessive wear and erratic performance, but usually also in cold welding of surfaces and catastrophic failure. In addition to its customary functions of reducing friction, supporting loads, reducing wear, and transferring heat, the successful space lubricant must also satisfy the unique requirements imposed by ultra-high vacuum, zero gravity, and radiation.

In the atmosphere, surfaces can be lubricated by conventional methods, and a thin oxide layer will often prevent metals from adhering, even when no lubricant is present. Water vapor and organic contaminants in the atmosphere also help lubricate the interfaces. None of these welding inhibitors is normally available in sufficient concentration, in a space environment, to provide adequate lubricant protection. Conventional lubricants are not satisfactory for space application since many evaporate or decompose rapidly. The lubricant material must have a very low vapor pressure in order to prevent premature exposure by evaporation of the contact interface.

In space, zero gravity eliminates the use of gravity feed and some pressurized lubricating systems. Any system must therefore rely upon the surface mobility of the lubricant material (both across the surface and away from it) and unconventional reservoir devices. Two transportation mechanisms can be used in a lubrication system designed for space applications:

- (1) Direct contact of interface with a near-proximity reservoir (a lubricant-saturated bearing retainer, for example).
- (2) Molecular migration of the lubricant to the interface from a remote reservoir (a small, lubricant-saturated, sintered, nylon matrix, for example).

II. Vac Kote Lubrication Process

Both a theoretical model of material characteristics and their interaction, and an engineering model, defining the application, are required to evaluate the ability of lubricants to provide long-life component performance in the space environment. M. M. Fulk, staff scientist, Ball Brothers Research Corporation (BBRC), developed a theoretical model in 1959–1960.¹ This model forms the basis of BBRC's long-life vacuum lubrication processes, collectively known as Vac Kote.

Vac Kote involves the use of fluid organic compounds, containing metallo-organic complexes and long-chain hydrocarbon molecules; solid films (consisting mainly of molybdenum disulfide); and grease formulations. The BBRC models are used to evaluate molecular characteristics of the interface materials, the environment anticipated, and the performance requirements. This evaluation determines the specific combination of materials and techniques to be used. Thin-film coatings are applied by vacuum processing and adhere to metal surfaces through molecular bonding. Solid film coatings are applied mechanically.

All organic materials are adversely affected by radiation. This factor must be considered in the choice of lubricant materials. Primary radiation sources in space are the Van Allen belts, solar radiation, and cosmic radiation. The amount of annual radiation dosage, from these sources, inside a 0.25-in.-thick aluminum housing has been estimated to be approximately 5×10^6 ergs/gram for a synchronous orbit of 22,000-mile altitude. Threshold

¹Fulk, M. M., *Mechanics of Wear and Interaction of Metal Surfaces*, TN65-303. Ball Brothers Research Corporation, Boulder, Colo., Nov. 1965.

damage of Vac Kote lubricant, due to radiation, has been determined to be approximately 5×10^{10} ergs/gram, indicating approximately 10,000 years survival of such radiation exposure.

The Vac Kote lubrication system is designed to provide lubrication during the ground handling and testing required prior to equipment use as well as during space operation. The low vapor pressure of the lubricant permits the use of conventional open configurations in the design of the drive mechanisms, eliminating the need for complex seals of uncertain reliability. Simple mechanical designs, material selection, and extremely low vapor pressure coatings control lubricant outgassing contamination of other spacecraft devices. The very low vapor pressure of Vac Kote lubricant and its replenishment mechanism provide long-term lubricant availability at all contact interfaces.

The basic steps in the Vac Kote lubrication process are:

- (1) Pretreatment inspection and performance testing.
- (2) Vac Kote vacuum application.
- (3) Vacuum chamber run-in.
- (4) Inspection and performance testing after vacuum run-in.

III. Theoretical Principles

BBRC's approach to determining the special properties of a lubricant for high-vacuum space applications is based upon conventional lubrication technology, expanded by applicable fundamental principles of molecular physics, surface physics, and physical chemistry. For most applications, under normal atmospheric conditions, conventional lubrication technology can be used to determine the lubricant characteristics for supporting loads, controlling friction, and transmitting heat. The unique requirements of a high-vacuum space environment require consideration of additional lubricant properties.

BBRC uses two basic models to analyze these additional considerations: (1) a theoretical model that provides the analytical tool for evaluating the interaction of interface materials, and (2) an engineering model for analyzing the performance of hardware components, mechanical geometry, and lubrication system under the conditions of operation, load, and environment peculiar to the specific application.

The theoretical model uses the standard theory of dislocations to account for the mechanics of wear. This theory assumes that adhesive wear accounts for most of the destruction. The model uses the concept of quantum electrodynamic forces to explain surface interaction and holds that the dielectric properties of films can be made to interact with the electrodynamic field to reduce the interaction between surfaces. In general, the critical dielectric properties of the Vac Kote thin film lubricant between surfaces are employed to alter the electrodynamic field and thus shield one surface from another. This shielding is known to prevent the type of component surface destruction commonly referred to as "cold welding."

In practice, BBRC employs several conventional models, used in lubrication technology to determine surface finish, lubrication load carrying characteristics, and heat transfer characteristics, as a part of the complete solution. These models are presented in several lubrication handbooks. This paper presents only the unique model used at BBRC to determine the additional properties of lubricants required for high-vacuum applications.

Wear is the deterioration and/or failure of interacting objects in use. *Wear* and *friction* are generally concurrent, but are not necessarily related in the sense of being simply proportional to one another. The major causes of wear are:

- (1) Corrosive destruction (electrolytic and/or chemical).
- (2) Mechanical destruction (galling, spalling, scoring, scuffing, seizing, abrasion, erosion, fretting, melting, plowing, cracking, etc.).

Mechanical wear occurs in solids but not generally in fluids. Mechanically generated wear is fundamentally a plastic flow on the surface of a solid. It is also a fatigue and fracture problem that occurs both in the body and on the surface of a solid. The relative motion of a dynamic system induces energy in the solids. This energy cannot be simply dissipated as it is in fluids. Instead, it must be dissipated throughout the inhomogeneous crystalline structure of the solid. Propagation of this energy results in plastic flow and/or nucleates cracks and propagates these cracks at stress levels far below their static fracture strength. Basically, this is the result of the effects of dislocations in the crystalline structure of the surface material, their generation, propagation, energy storage, and general accumulation. Dislocations are irregularities in the crystalline structure of materials. Their existence has been demonstrated and is the consequence of an

assembly of atoms or molecules in a quasi-static geometric array (the condition of atoms and molecules in stable solids). Wear is related to the energy pumped into the system minus the heat generated. If all the energy dissipated in the system appears as heat, wear is small. This energy input and resulting wear and heat can be reduced by lowering the interaction between surfaces. Friction is a resisting force that is displayed when relative motion is imposed upon a system, and, as a resistance force, friction acts to oppose the relative motion.

Surfaces of matter show many phenomena. One is the ability to interact with another surface and display a "friction force." Surfaces are not strictly the two-dimensional region that bounds a solid (or liquid). This anisotropy of the surface occurs in the material crystalline structure and energy distribution. This external friction of solids can be a combination of a number of factors that contribute to the resistance of motion between their interacting surfaces.

Some of the factors known to contribute to this surface-to-surface "friction" are:

- (1) Interlocking of surface irregularities.
- (2) Electrical fields.
- (3) Anelasticity.
- (4) Adhesion (solid-to-solid adsorption, "cold welding").

Plastic and/or elastic deformation allows interacting surfaces to get together intimately at "spots." These spots are solid-to-solid adsorption or adhesion and are as strong as the yield strength of the base materials. Static adhesion sometimes appears to drop almost to zero when the load is removed because the accumulated elastic stresses under the spot are released and break these junctions or spots. Shearing of these adherent spots consumes energy and sometimes causes destruction of the interface. It is now generally accepted that this solid-to-solid adsorption, adhesion, or cold welding, as it is often called, is one of the main sources of destructive action between surfaces.

All physical phenomena display four basic physical forces:

- (1) Strong forces in the nucleus.
- (2) Weak forces in the nucleus.
- (3) Gravity.
- (4) Electromagnetic forces.

The forces of greatest concern in technological problems are electromagnetic. As a matter of fact, all the ordinary chemical, mechanical, and biological effects are due to the interaction of electric charges and the fields they produce. These electromagnetic forces include atomic, molecular, and intermolecular binding forces. These forces, which emanate from the surface of solids to cause interaction, are identified by the general term "friction."

Electromagnetic forces appear in many guises. The charge is quantized into (+) or (-). The force can be attractive or repulsive and is velocity-dependent, changing from electrostatic to electromagnetic, depending on the relative velocity of source and observer. The agent of this force is the photon. If two bodies are "separated" by a vacuum, electromagnetic forces are the only interaction between them. If the gap is occupied by some other medium, there is the possibility of a nonelectromagnetic interaction, such as that caused by sound oscillation in the medium.

An electromagnetic field can be modified by adding a dielectric material between the surfaces of interest. For example, two charges, $+e$ and $-e$, separated by a distance r in vacuum, will interact with a force e^2/r^2 . If, however, there is some medium between the two charges, then the interaction force is decreased and becomes

$e^2/\epsilon r^2$, where ϵ is the dielectric permeability (generally greater than 1).

Thus, the dielectric properties of the medium reduce electromagnetic interaction and act as a "shield" for the electric field (photons). Dielectric permeability is a measure of the medium's interaction with the electric field or photons.

If the interaction between solids is caused by the electromagnetic field (photons), then it seems reasonable to use the dielectric properties of a separate layer or film to reduce interaction between surfaces. There is a formal relation between the dielectric permeability ϵ , the index of refraction η , and the absorption coefficient k , as shown in the following equation:

$$\begin{aligned} \epsilon &= \epsilon_1(\eta) + i\epsilon_2(\eta) \\ \text{complex} & \quad \text{real} \quad \text{imaginary} \\ \text{dielectric} & \quad \text{part} \quad \text{part} \\ \text{constant} & \\ &= [(\eta) + ik(\eta)]^2 \\ & \quad \text{index of} \quad \text{absorption} \\ & \quad \text{refraction} \quad \text{coefficient} \end{aligned}$$

This relationship is an expression of the theoretical model for determining the "shielding" properties of materials for use in lubricants.

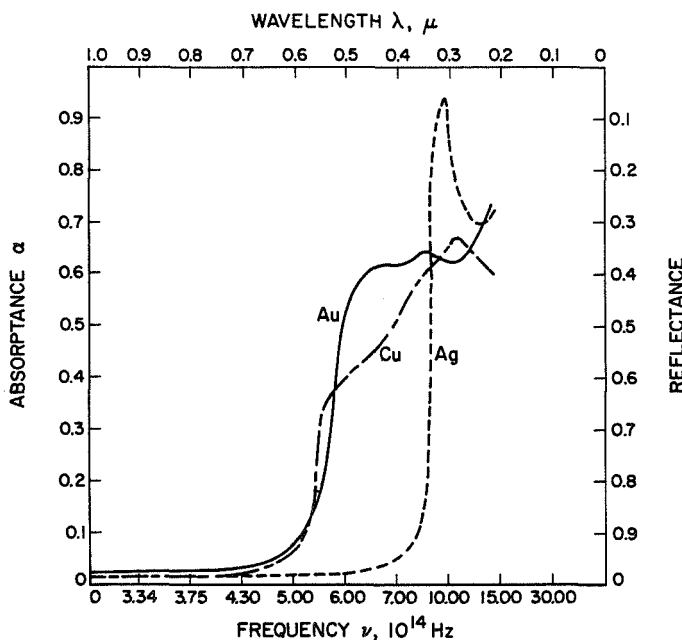


Fig. 1. Absorbance of Au, Ag, and Cu

The index of refraction η and the absorption coefficient k are both measures (albeit of different kinds) of the interaction of a medium with electromagnetic waves (photons). The index η alters the velocity of propagation, and k alters the intensity of the electromagnetic wave. Both are a result of the interaction of electromagnetic waves (photons) with the electron clouds present in the medium.

In general, the main microscopic property of bodies that determines the strength of electromagnetic interaction is the imaginary part of the dielectric constant. Thus, the main frequency of the electromagnetic interaction (photons) between objects is best determined by their absorption spectra. Figure 1 shows the absorption spectra for some metals. The frequencies of the electromagnetic field (or photons) that cause the interaction start at 10^{15} Hz; therefore, this is the frequency in which we are interested in the dielectric properties of films. The film on slip rings and similar equipment must be thin,

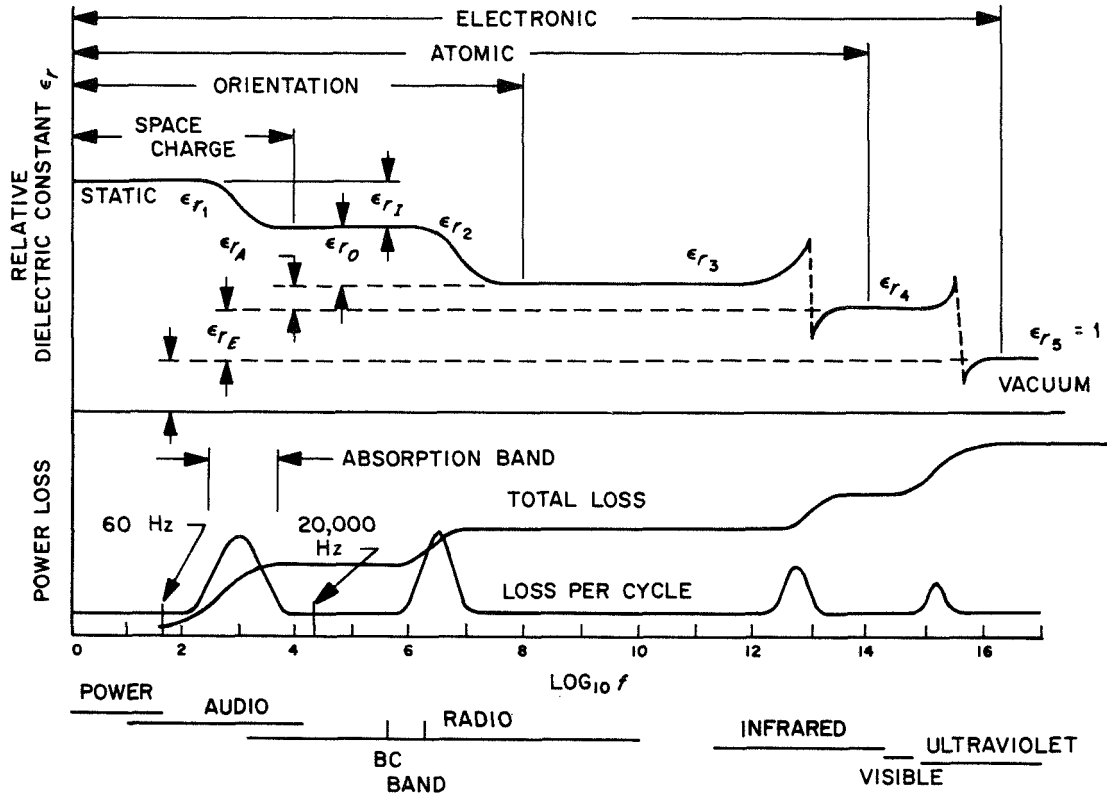


Fig. 2. Frequency dependence of relative dielectric constant and losses

$\ll 100 \text{ \AA}$ thick, because of the need for electrical continuity. In thick films, dielectric permeability at other frequencies is of interest for such uses as ball bearings.

Figure 2 shows roughly the pattern of frequency dependence of dielectric permeability and losses. To reduce the electromagnetic interaction between metals, the electromagnetic field must be reduced by using films with maximum absorption and/or maximum anomalous dispersion and resonant absorption in the regions of interest.

Through the use of characteristic patterns, similar to Figs. 1 and 2, a lubricant is selected for use between interacting surfaces to alter the electromagnetic field.

IV. Applications and Results

A. The OSO Satellite

BBRC's Vac Kote lubrication system was developed in support of the *Orbiting Solar Observatory* (OSO) program. The first use of this lubrication system was in 1959 to lubricate a biaxial drive system on the spinning OSO. With the launch of OSO-I in 1962, Vac Kote became the

first space-demonstrated, long-life lubrication system for moving metal-to-metal surfaces.

The accumulated total OSO satellite operation time in orbit, without measurable deterioration of the electrical and mechanical interfaces, now stands at 56 months. OSO-I was launched on March 7, 1962, and, when last interrogated after 24 months in orbit, showed no measurable deterioration of control and drive systems. Drive systems in OSO-II, launched Feb. 3, 1965, were performing equally well when the spacecraft was powered down after 9 months of continuous operation in orbit. This satellite was reactivated on March 3, 1966 (after 4 months of orbiting totally inactive). The control, drive, and data transmission systems operated normally. In May 1966, OSO-II drive systems were again called upon and operated within normal limits after 16 months in space. The drives of OSO-III, launched in March 1967, and OSO-IV, launched in October 1967, are continuing to function entirely within specifications.

B. Components Lubricated

Over 300 component operating years in vacuum have demonstrated that Vac Kote provides a reliable, long-life

lubrication system for bearings, dc torque motors, slip rings, gears and sliding devices in the space environment. This operating time figure includes OSO orbit operating time and tests in vacuum at BBRC. It does not include the ground test and checkout time accumulated for hardware processed by BBRC for other program contractors. Further, the use of Vac Kote permits conventional open configurations instead of complex seals, resulting in savings in weight and higher reliability. The design life goal of systems which depend on such components is up to 5 years in space. There have been no reported failures of Vac Kote-lubricated flight-qualified hardware to date.

Both radial and thrust ball bearings have been used in most BBRC space applications that require rotating hardware. Sizes of Vac Kote-processed bearings range from 12-in.-OD thin-wall bearings to 0.25-in.-OD precision instrument bearings. Significant bearing performance data for both oscillatory and rotating motions in space have resulted from the OSO program. All OSO bearings have functioned without apparent increase in torque from satellite launch to subsequent shutdown. Any degradation due to increased bearing torque would have been detected by an increase in power consumption by the control system.

BBRC has conducted considerable motor and slip ring lubrication study, analysis, and investigation in vacuum, sponsored by NASA, industry, and BBRC. These studies include current density, contact construction, and interface-radiated noise, commutator/slip ring/brush material evaluation, slip-stick wear phenomena, plasma-generated emf, and high-current phenomena. The Vac Kote lubrication system has been an important factor in the success of drive systems in space to despin payloads and orient antennas, and in attitude-pointing subsystems.

Vac Kote-processed dc torque motors, slip rings, bearings, and gears have been used in the following aerospace programs and applications:

- (1) OSO-I, OSO-II, OSO-III, and OSO-IV (solar array despin mechanism and elevation axis: dc torque motors, slip rings, and bearings, as well as bearings and moving parts of experimental payloads).
- (2) ATS-II, ATS-IV (mechanical antenna despin assembly, camera bearings, and gears).
- (3) OGO (experiment payload bearings).
- (4) LES (experiment payload bearings and slip rings).
- (5) *Apollo* Applications Program (experiment payload bearings and gears).
- (6) ITS-III (mechanical antenna despin assembly: bearings).
- (7) IDCSP/A, United Kingdom satellite (antenna despin assembly: bearings).
- (8) AF-191 (mechanical antenna despin assembly: dc torque motor, slip rings, and bearings).
- (9) Classified military reconnaissance (solar array drive: dc torque motors, slip rings, and bearings).
- (10) Sounding rockets (despin mechanism and experiment pointing mechanism: bearings and gears).
- (11) OAO (star tracker: dc torque motors, bearings, tachometers, sun slide mechanisms, and miscellaneous sliding parts).
- (12) LIDOS (solar array drive: dc motor, bearings, and slip rings).

C. DC Torque Motors

Much of the motor lubrication research and testing activities at BBRC has been directed toward the dc torque motor. This device is ideally suited for space application because of its high torque-to-inertia ratio, light weight, and direct drive (no gearing). Both OSO orientation axes (azimuth and elevation) use dc torque motors. In addition, all rotating components tested at BBRC have been driven in vacuum by dc torque motors. As a result, considerable test data are available on these torque motors; more than 500×10^3 component hours and 200×10^6 component revolutions have accumulated in vacuum operation to date. After 4,800 hr (17.3×10^6 revolutions) operation in vacuum of 10^{-6} torr, these motors showed no signs of wear (see Fig. 3).

The brushes, as shown in Fig. 4, are barely "broken in." The vertical lines on the brush surface are the original surface tooling marks.

D. Slip Rings

BBRC has also conducted more than 6 years of research and testing in the field of lubrication of slip rings for space application. The slip ring lubrication problem is particularly difficult because of varied and stringent electrical and mechanical requirements. Several BBRC slip ring lubrication systems designed for 5-year space

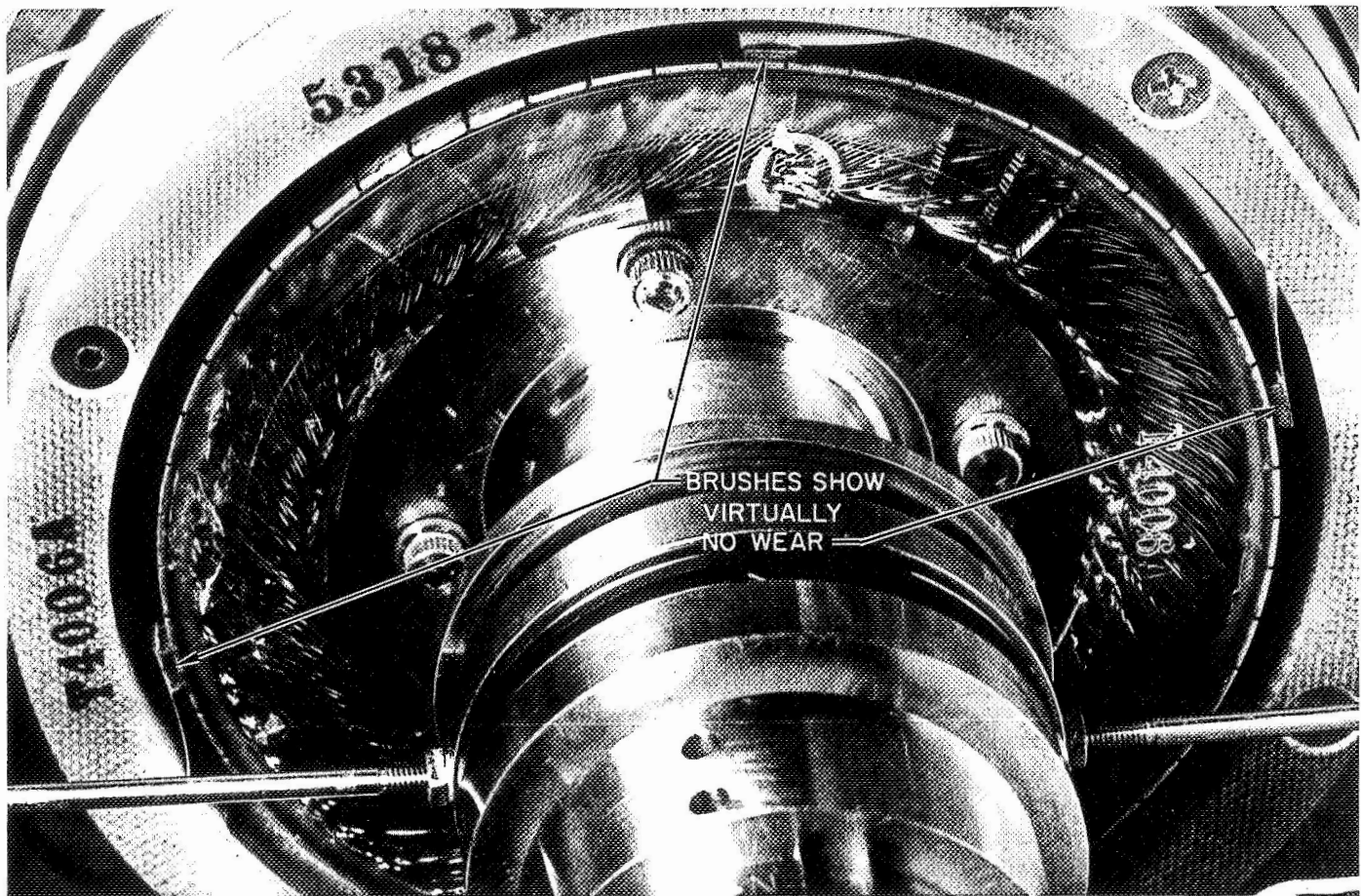


Fig. 3. Vac Kote-treated 1.8-ft-lb torque motor for OSO satellite after 4800 h operation in vacuum of 10^{-6} torr (17.3×10^6 revolutions)

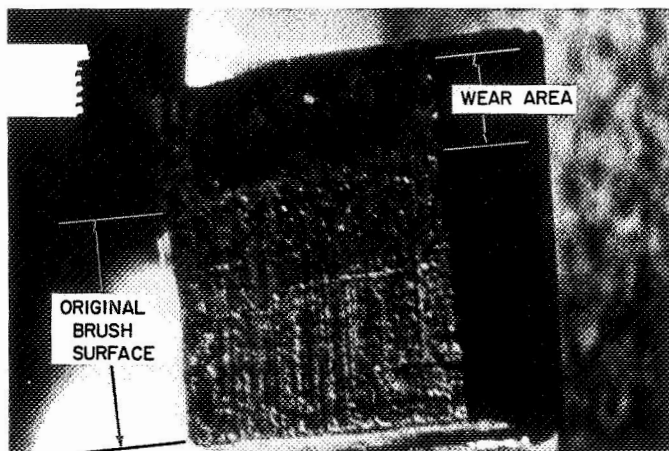


Fig. 4. Closeup of brushes

life have recently been incorporated into satellites. Figures 5 and 6 illustrate typical Vac Kote-treated slip ring brush performance obtained at BBRC.

Total life requirement of this test was 500 h at 10^{-8} torr. The light area on the brushes indicates a lubricant-brush-metal slurry which prevents brush-ring wear while providing electrical contact. Part of this slurry may remain on the ring when the brushes are removed.

E. Ball Bearings

Radial and thrust ball bearings have been used in most BBRC space applications requiring rotating hardware. Sizes of bearings that have been Vac Kote-processed range between 12-in.-OD thin-wall bearings and 0.25-in.-OD precision instrument bearings. To date, Vac Kote-processed bearings have recorded more than 1.9×10^6 component hours and 7.7×10^8 component revolutions of operation in vacuum. Figure 7 shows Vac Kote-treated balls after 8 months of vacuum testing, and Fig. 8 shows a Vac Kote-treated race after 8 months of vacuum testing.

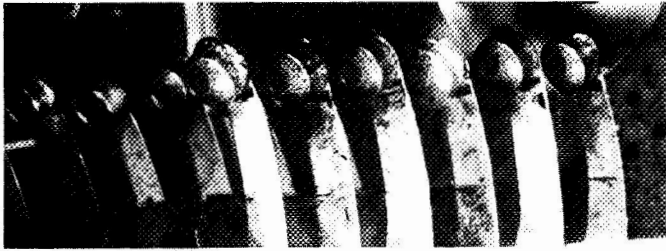


Fig. 5. Vac Kote-processed slip ring brushes before vacuum life test

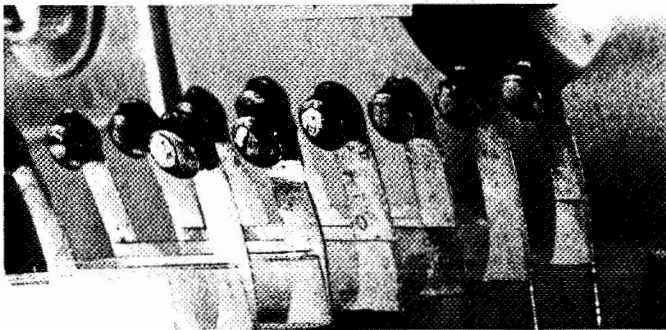


Fig. 6. The same brushes as in Fig. 5, after test

The balls, loosely placed in the bore of the disassembled bearing, are free of blemishes or scratches. No indication of wear or degradation is observed. The rectangular mark on each ball is the camera reflected in the mirror-like surface.

The bearing race illustrates:

- (1) Glossy reflection from undisturbed groove surface.
- (2) Camera reflection.
- (3) No evidence of degradation of ball track.
- (4) Shadow on groove surface.

V. Summary of Flight Performance and Laboratory Test Data

A summary of significant Vac Kote lubrication tests and applications is shown in Table I.

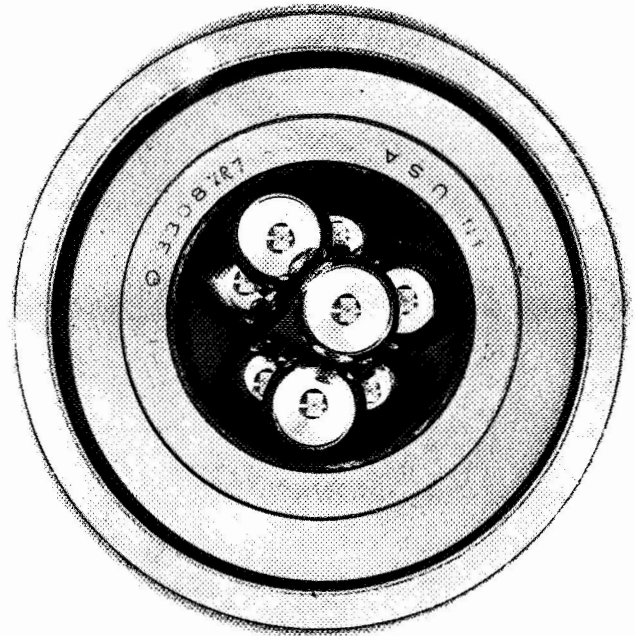


Fig. 7. Vac Kote-processed balls after test

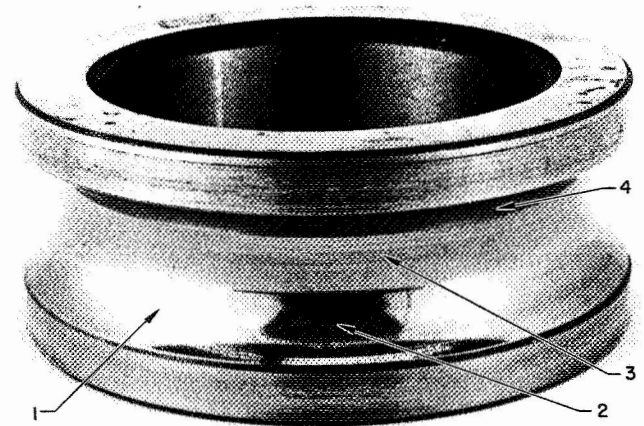


Fig. 8. Vac Kote-processed bearing races after test

Table 1. Vac Kote flight performance and laboratory test data summary^a

Component	Program	Application	Vacuum exposure ^b duration, mo	Component		
				Number	Operating time, 10 ³ h	Operation, 10 ⁶ revolutions
Torque motors	OSO I (S16)	Solar array despin	24.0	2 ^c	10.2	6.1
	OSO II (S17)	↓	16.0	2 ^c	13.1	8.0
	OSO III	↓	12.0 ^d	2 ^c	17.5	10.5
	OSO IV	↓	4.5 ^d	2 ^c	6.6	4.0
				0.1	6	0.3
	OAO	Star tracker	3.5	100	20.0	3.0
				0.8	4	0.8
	Classified			4		11.6
	Classified	Despin mechanism	3.0	1		
	OAO (backup)	Star tracker	3.0	16	411.0	55.5
	Development and qualification	Despin mechanisms	12.0	80		
	OSO second source	Solar array despin	6.0	6	28.5	47.0
	IDCSPA/UK	Antenna despin	0.1	2	0.1	0.3
	AF 191	Antenna despin	0.1	6	0.4	0.6
	Classified	Solar array despin	0.1	16	1.0	1.5
	Total			249	509.5	150.4
	Slip ring assemblies	OSO I (S16)	Signal, instrumentation, and power	24.0	1	5.1
OSO II (S17)		↓	16.0	1	6.5	8.0
OSO III		↓	12.0 ^d	1	8.8	10.5
OSO IV		↓	4.5 ^d	1	3.3	4.0
LIDOS		↓	4.0	1	2.8	0.3
Classified		↓	4.0	1	3.0	5.0
		↓	4.0	1	3.0	5.0
		↓	3.0	1		
		↓	6.0	4	75.0	31.0
OSO Development		↓	6.0	25		
LES		↓		1		0.1
Development		↓		2		0.2
OSO second source		↓	6.0	6	26.5	47.0
AF 191		↓	0.1	5	0.4	0.7
Classified	↓	0.1	3	0.2	0.3	
Total			54	134.6	118.2	
Bearings	OSO I (S16)	Despin mechanism	24.0	4 ^c	20.4	12.2
	OSO II (S17)	↓	16.0	4 ^c	26.2	16.0
	OSO III	↓	12.0 ^d	4 ^c	35.0	21.0
	OSO IV	↓	4.5 ^d	4 ^c	13.2	8.0
	OSO qualification	↓	8.0	44	158.4	312.6
				2.0	12	2.4
	OAO	Star tracker	4.0	12	30.6	0.8
	ATS	Camera and despin mechanism	11.0	22	16.7	100.2
	LIDOS	Despin mechanism	3.8	1	2.8	0.3
	ITS	Despin mechanism	0.1	275	13.7	24.7

^aSignificant tests to March 1, 1968.

^bMaximum continuous time of one or more components.

^cOne motor despins solar array. One motor oscillates elevation control. In this table, revolutions are for 1 motor and 2 bearings on the despin drive. Oscillatory motions of elevation assembly components are not included.

^dOSO III and OSO IV are still operating in space.

Table 1. (contd)

Component	Program	Application	Vacuum exposure ^b duration, mo	Component		
				Number	Operating time, 10 ³ h	Operation, 10 ⁶ revolutions
	OAO	Star tracker	8.0	230		
	Development	Despin mechanism	8.0	622	1504.0	80.0
	OSO second source	↓	6.0	12	53.0	94.0
	IDCSPA/UK		0.1	9	0.1	3.0
	AF 191		0.1	28	1.6	3.2
	Classified		0.1	42	2.2	1.1
	Total			1325	1880.3	679.4
Linkages	OAO °	Star tracker	3.5	30	2.5	>1000 cycles
Solenoids	OAO	Star tracker	3.5	31	5.0	>1000 cycles
Potentiometers	Development	Antenna positioning	2	3		8 × 10 ⁷ cycles
Gears	ATS	Camera and instrumentation		140		
	Development	Instrumentation	4	12	21.4	12.6 × 10 ⁶ rev.



Panel Discussion
Bearings and Suspensions in Space

OVERLEAF: *Members of the panel were, left to right, William J. Kurzeka, Atomics International Division of North American Rockwell Corporation; H. I. Silversher, Lockheed Missiles & Space Company; William J. Schimandle, Jet Propulsion Laboratory, moderator; D. L. Kirkpatrick, General Electric Company; and George G. Herzl, Lockheed Missiles & Space Company*

N 69-11810

Evaluation of Dry Lubricants and Bearings for Spacecraft Applications

D. L. Kirkpatrick and W. C. Young
General Electric Company
Valley Forge Space Technology Center
King of Prussia, Pennsylvania

Instrument-size ball bearings lubricated with bonded dry films or transfer films have been successfully operated for 130 million revolutions during a 9000-h vacuum test at 10^{-9} torr. This test simulated conditions anticipated in unsealed mechanisms of an interplanetary spacecraft. The conditions included prolonged idle periods, as well as extended periods of continuous rotation, with reversals, while the bearings were exposed to hard vacuum. The performance of several bearing-lubricant combinations surpassed that required to complete the projected spacecraft mission. Extensive quality control in the preparation of the bearing-lubricant combinations was necessary to attain the lifetimes achieved. This paper describes the unique test procedures and techniques developed and the test results, which include some new insights into the behavior of transfer film lubricants.

I. Introduction

During preliminary design studies of an interplanetary spacecraft, it became apparent that severe mechanism lubrication problems would have to be overcome to ensure mission success. These included long-term (up to 2 years) exposure of the mechanisms to hard vacuum and intermittent operation interspersed with protracted static dwell periods. Low outgassing would be required both to conserve lubricant during the 2-year mission life and to minimize contamination of optical and thermal control surfaces on the spacecraft. Anticipated temperatures ranged from possible prelaunch thermal sterilization at 250° F (minimum) to extended subzero conditions during interplanetary cruise and subsequent orbital operations. In addition, low and uniform bearing frictional torque

would be needed to minimize mechanism design weight and power consumption and to ensure reliable operation.

These requirements were judged too severe for the liquid lubricants used on a majority of earlier space vehicles, unless all mechanisms were provided with hermetic sealing and active thermal control. In hope of avoiding the penalties of increased mechanism weight, complexity, and power consumption which these measures would entail, attention was turned to the possibility of using dry (solid) lubricants. These lubricants generally exhibit extremely low vapor pressure, their lubrication mechanisms are essentially independent of ambient pressure, and they are only slightly affected by temperatures within the range of interest. In addition, operating life is

predictable since it is primarily a function of the number of operating cycles, rather than time. Because of these desirable properties, the suitability of a group of commercially available dry lubricants was studied.

A detailed literature search identified several potentially suitable lubricants, but the use of conditions and measurement techniques from which the available data derived had varied widely. In addition, performance of a given lubricant sometimes varied significantly in the different applications or tests reported. Besides the variability of use conditions and batch-to-batch variations in the lubricant and substrate, handling and quality control differences were suspected of having a significant effect on previously observed performance. These factors combined to make uniform comparison and determination of relative life expectancy extremely difficult. Therefore, this test program was established to provide comparable performance evaluation of several of the most promising dry lubricants operating under conditions closely simulating those expected in the planetary exploration spacecraft being studied.

The lubricants selected for evaluation are described in Table 1. They fall into two major categories: (1) lubricants bonded or plated onto the surfaces to be lubricated, and (2) lubricants transferred to the balls and races from the retainer surface bearing operation.

Table 1. Lubricants selected for evaluation

Code	Description
Group 1: Bonded or plated lubricants	
A	Molybdenum disulfide and graphite bonded with sodium silicate
B	Molybdenum disulfide and antimony trioxide bonded with polyimide resin
C	Molybdenum disulfide diffused into a soft, multilayered, plated metallic film
D	Molybdenum disulfide applied by an electrophoretic process
E	Molybdenum disulfide applied by an <i>in situ</i> process
F	Tungsten disulfide (modified) applied by a diffusion process
G	Electroplated silver
Group 2: Transfer film lubricants	
X	TFE and molybdenum disulfide, reinforced with glass fibers
Y	TFE reinforced with ceramic filler
Z	TFE coating on metallic retainer

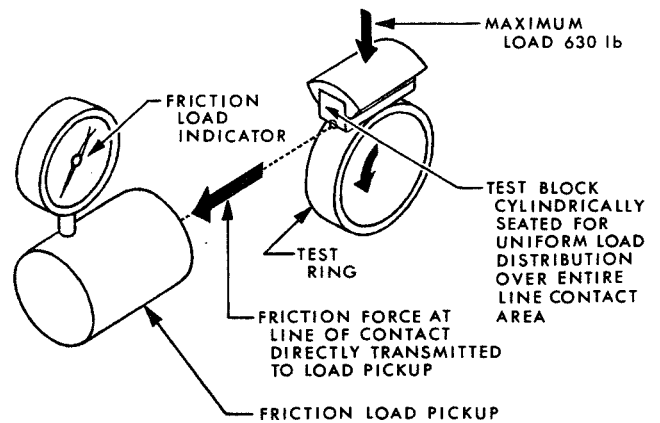
II. Lubricant Analysis Techniques

To ensure future repeatability and usefulness of the lubricant performance data obtained in this test program, techniques for determination of lubricant constituency and uniformity were evaluated. X-ray, emission-spectrographic, electron-probe, and electron and optical microscopic techniques were investigated to determine their usefulness in the quantitative and qualitative evaluation of these lubricants. Such investigations identified areas of usefulness of several techniques. These analytic techniques were supplemented with conventional sliding friction tests in air to determine adhesion and wear resistance of the bonded and plated lubricant films. Results of these tests are shown in Table 2.

Table 2. Sliding wear test results in air using the Alpha Model LFW-1 sliding friction and wear test machine^a

Lubricant	Lifetime ^b , h	
	Range ^c	Average
A	11 to 17	13
B	27 to 35	31
C	13 to 228	77
D	1.4 to 38	18
E	26 to 104	78
F	0.06 to 0.08	0.07

^aFunctional diagrammatic view of the Alpha Model LFW-1 machine is shown below. Friction force sensed by the load cell is shown on the load indicator.



Radial load: 630 lb
 Peak Hertz stress: 110 kpsi
 Rotational speed: 72 rpm
 Ambient conditions: 70°F, 1 atm, 60% RH

^bTests were ended when coefficient of friction exceeded 0.1.

^cFour samples of each lubricant were tested, two from each of two different batches.

X-ray emission techniques have been useful in determining the distribution of molybdenum disulfide by determining the quantity and distribution of sulfur in several of the lubricant coatings. X-ray diffraction techniques have proved relatively ineffective in the determination of the uniformity of lubricant film constituency and consistency, because of the amorphous character of some lubricants and the multilayered nature of others. Emission spectrographic analysis has given useful data for batch constituency determination, but has not proved well-suited to bearing parts.

The electron probe has also shown itself to be an effective tool in quantitative and qualitative determination of the composition and uniformity of solid lubricant coatings. Photographs of each lubricant constituent have been made from the characteristic X-ray spectra generated by scanning the sectioned lubricant sample with a focused high-energy electron beam. This technique has been particularly effective in the examination of multilayered lubricants such as the Code C material.

Electron and optical microscopy were both used in the examination of lubricant coatings. Because of the extremely high magnification ($10,000\times$) of the electron microscope, slight compositional variations in good coatings have widely different appearances and may give the impression of extreme nonuniformity. Fortunately, the ultramicroscopic nonhomogeneity indicated in observed specimens does not necessarily preclude acceptable lubricant performance.

Optical microscopy ($400\times$) proved to be extremely useful in the examination of lubricant coating characteristics. This technique has obvious value for the nondestructive inspection of lubricant coatings to determine surface uniformity and to detect inclusions, porosity, and voids. In addition, it is possible to observe the uniformity and apparent adhesion of fluorocarbon transfer films.

In the inspection of the inner ring of a Code Y bearing, which had previously been run-in in air and disassembled for inspection, evidence was found that significant quantities of gases were entrained within the film. The microscope used had a small vacuum chamber with optical ports surrounding its specimen stage. The lubricant was first examined at atmospheric pressure and room temperature. It had a whitish, translucent, gelatinous appearance. The specimen chamber was then evacuated in preparation for examining the surface with the electron probe. As the pressure was reduced to the 10^{-5} torr level in 3 min, it was noted that the transfer film coating on

the bearing race surface began to craze and flex, although the part was not being subjected to thermal or mechanical disturbances. As the crazing process continued, the coating lifted from contact with the race in several areas and ultimately attained a somewhat shriveled appearance.

Observation of this phenomenon led to the conclusion that the transfer film, which had been established on the bearing during run-in in air, contained a quantity of entrained gases and/or moisture which were desorbed in vacuum causing mechanical damage to the film. This observation may indicate a method for attaining a higher degree of reliability in transfer film-lubricated bearings. It is likely that an initial transfer film of greater mechanical integrity, which would not be subject to vacuum-shock deterioration, could be established through initial run-in of the bearing in vacuum.

III. Test Bearing Preparation

For vacuum performance testing of the selected lubricants, the R-4 instrument bearing was chosen as the standard test specimen. Bearing rings and balls were made of AISI 440C steel; the retainer type and material depended on the lubricant used. The Code X and Y bearings (see Table 1) had one-piece retainers machined from the lubricating material. All other bearings had two-piece stainless steel ribbon retainers. The Code Z bearing lubricant was bonded to the retainers only. The other lubricants were applied to the races and the retainers.

By means of a thorough visual inspection of the lubricated parts with a $40\times$ microscope, we eliminated all parts that had incomplete coverage, nonuniformity of surface texture, and apparent inclusions on some parts.

The accepted parts were returned to the bearing vendor for assembly. Balls were selected to achieve a radial clearance of 0.0008 to 0.0011 in. in each bearing. This relatively large clearance was specified to lessen the danger of bearings being jammed by lubricant wear debris.

Visual inspection of the assembled bearings revealed several defects which could have caused failures if they had not been corrected. On two of the ribbon retainers, a holding tab had not been crimped; consequently, it scraped against the outer race during rotation. Also, on several of the Code X and Y bearings, the retainers were not completely deburred. Either of these conditions could

Table 3. Running torque^a after run-in of dry-lubricated R-4 bearings

Lubricant	Number of samples	Torque, 10 ³ mg-mm			
		Avg torque, range	Peak torque, range	Torque for entire sample, avg	Peak torque, avg
A	5	8 to 14	26 to 36	11	32
B	12	2.5 to 11	10 to 42	6	23
C	5	8 to 16	28 to 48	11	37
D	5	6 to 15	20 to 80	10	44
E	4	10 to 30	38 to 50	16	45
F	10	3 to 16	11 to 50	9	30
G	5	6.5 to 35	25 to 125	17	66
X	10	3 to 13	8 to 25	6.3	19
Y	10	2 to 4	7 to 15	3.2	12
Z	10	6 to 14	25 to 44	8.4	34
None ^b	4	1.5 to 2	5 to 25	1.8	10
Grease ^c	5	50 to 200	80 to 200	144	150

NOTE: Dry- and grease-lubricated bearings shown for comparison only, not run or tested further.
^aMethod: MIL-STD 206, 400-g axial load, 0.5 rpm.
^bSteel ribbon retainer, no lubricant.
^cGE G-300 silicone grease, phenolic retainer, 25% fill.

have resulted in a jammed bearing through generation of excessive debris in operation.

Prior to subsequent testing, all bearings were run-in in a uniform cycle to ensure a smooth ball track in the case of the bonded or plated lubricants and to ensure that a transfer film had been established on the ball and race surfaces in the case of the transfer lubricants. Each bearing was then tested on a MIL Standard 206 torque tester to determine its running torque. The results of these tests, summarized in Table 3, were used both to determine the range of torque levels which might be expected from dry-lubricated bearings with various lubricant types and to provide screening data for the subsequent selection of bearings for vacuum testing.

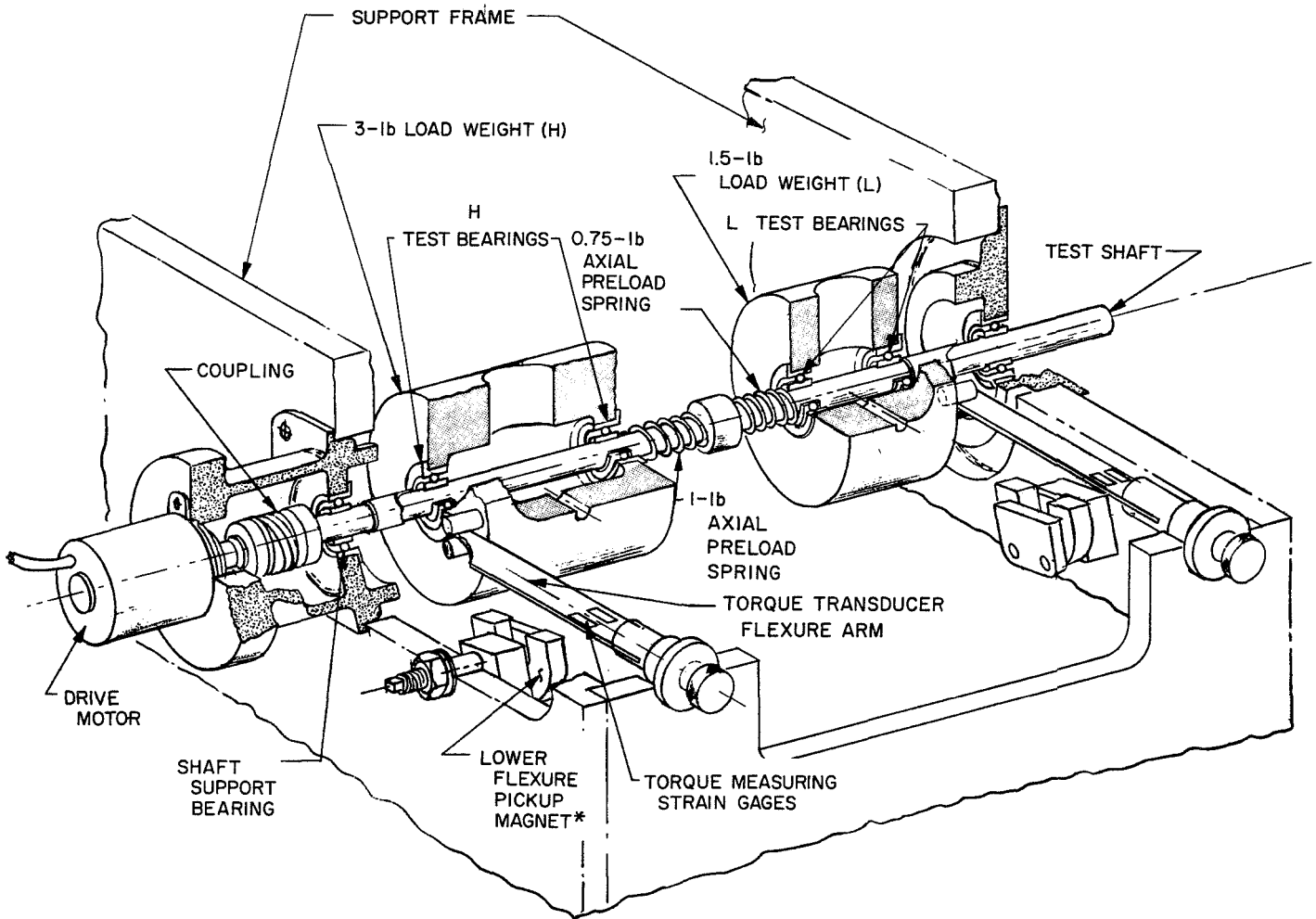
IV. Vacuum Test Fixture Design

A vacuum test fixture was designed for endurance testing of bearings under combined radial and axial loads. There are six identical test shafts in the fixture; a diagram of one test shaft is shown in Fig. 1. On each shaft there are two pairs of test bearings, H and L. These are loaded radially, by rotationally balanced cylindrical weights, and axially, by calibrated compression springs

concentric with the shaft. The H pair of test bearings supports a 3-lb weight, while the L pair supports a 1.5-lb weight. The axial loading is 1.0 lb on the H pair of bearings and 0.75 lb on the L pair.

During test operation, as the motor rotates the shaft, a separate torque transducer arm balances the bearing friction torque on each weight. A strain-gage bridge bonded to the arm provides an electrical output proportional to the resulting deflection of the arm and, therefore, proportional to the running torque of the bearing pair. A pair of test bearings fails, by definition, when its torque exceeds 300,000 mg-mm (30 gm-cm). As this torque is reached, the two pins on the weight that contact the flexure arm rotate to a position where they slip free of the end of the arm. As this occurs, the flexure arm is attracted by one of two magnets on the frame which pulls the arm 0.010 in. clear of the pins, permitting the failed bearing load weight to rotate freely with the shaft. This unique arrangement permits continued operation of either test bearing pair if the other fails.

Other instrumentation includes thermocouples to monitor the operating temperatures of the support bearings and the rear bearing of each motor. A rotation-sensing



*THE UPPER FLEXURE PICKUP MAGNETS ARE NOT SHOWN

Fig. 1. Typical shaft of bearing test fixture

reed switch is provided for each shaft; a magnet rotating with the shaft actuates the switch once each revolution. Electrical impulse counters outside the vacuum chamber count the revolutions of each shaft. Vibration transducers are applied at three points on the end of the test fixture opposite the motors and are monitored during vacuum testing.

Particular care was taken in designing the fixture to minimize or eliminate potential sources of outgassing in hard vacuum. Materials selection was particularly important. Polyimide or TFE insulation was used wherever uncoated woven glass fiber could not be employed. Strain gages were bonded with a sprayed ceramic material (Al_2O_3); a limited amount of special epoxy was used to bond the vibration pickups and ceramic terminal strips.

Most shaft support bearings had the same lubricant as the test bearings on that shaft. The remaining support bearings and all motor bearings are provided with Code X lubricant.

V. Vacuum System

The two vacuum systems used are each equipped with a 500-liter/s ion pump and a 5000-liter/s titanium sublimation pump. Each chamber is equipped with a mass spectrometer monopole detector for use in partial-pressure gas analysis within the chamber during operation. A trigger ion gage reading to 1×10^{-11} torr is used to monitor chamber pressure. The systems are capable of pumping to and holding approximately 1×10^{-11} torr

(if the test fixtures are not operating). Both vacuum systems were purchased new for this test. Therefore, there was no danger of residual contamination from earlier test operations. To produce a hard vacuum in this type of vacuum system, it is first necessary to drive out moisture, entrapped or adhered gases, and organic contaminants from the test fixture and the internal surfaces of the chamber. To accomplish this, each vacuum chamber is equipped with an electrically heated bakeout mantel capable of raising the temperature within the chamber to 750°F. In these tests, a temperature limit of 375°F was established to prevent damage to the soft-soldered electrical connections and the bonding epoxies used in the test equipment. One six-shaft bearing test fixture was installed in each vacuum system.

After a 24-h bakeout at 375°F, each system was pumped to 10^{-11} torr, and test operations were begun. An initial increase in chamber pressure of about three decades was seen when all bearing drive motors were started. After a few hours of operation, chamber pres-

sure decreased to the 10^{-9} torr range and remained in this region throughout subsequent tests. The second chamber has frequently been at approximately 5×10^{-11} torr, although during periods of continued operations the pressure normally rises into the 10^{-9} torr range. The pressure rise during operation can be attributed to two principal causes:

- (1) The major source of outgassing (determined by partial pressure analysis of the chamber contents) is the internal gases from the lubricating materials. In bearing operation, continual exposure of fresh molecular surfaces permits evolution of these entrained or adsorbed gases. Evidence of free fluorine has also been observed, indicating a breakdown of the CF bond in the fluorocarbon lubricating compounds. This probably results from localized generation of temperatures in excess of 350°F (the lowest CF dissociation temperature) in the operating bearings.

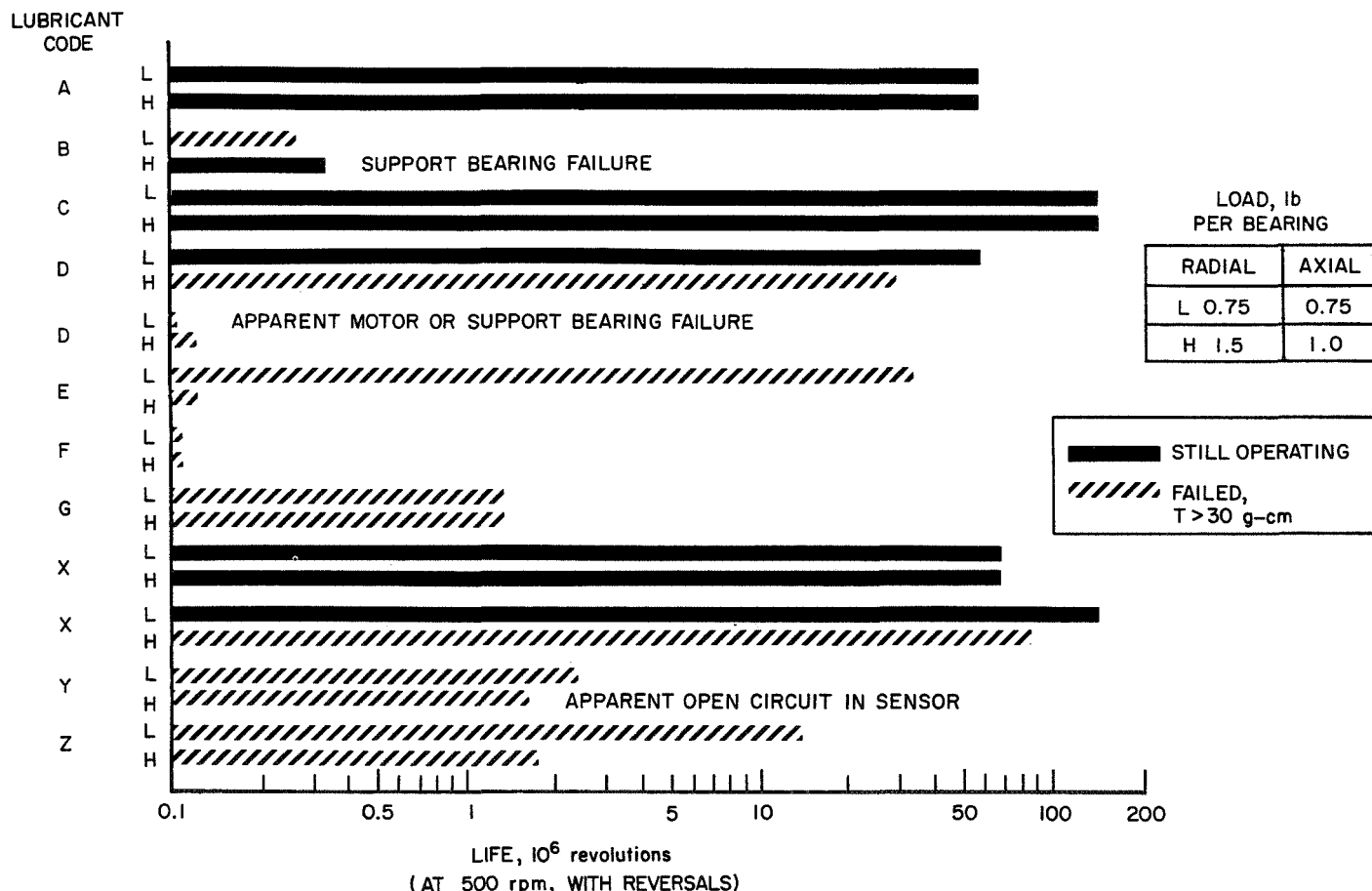


Fig. 2. Vacuum endurance life of dry-lubricated bearings (R4 pairs)

- (2) The second source of outgassing is the polyimide insulation in the motors, which reached temperatures in excess of 200°F in normal operation.

VI. Vacuum Testing: Procedure and Results

Bearing vacuum testing was divided into four phases. The phases included: (A) checkout, (B) space mission simulation, (C) effects of dwell determination, and (D) long-term life testing. Forty-eight bearings – twelve pairs of test bearings, six pairs of support bearings, and six pairs of motor bearings – were operating in each fixture at the beginning of the tests. The cycles attained by the test bearings are shown in Fig. 2; apparent failures of the remaining bearings are also noted.

When operating, all shafts rotated at speeds between 480 and 500 rpm. Bearings were rotated for equal periods clockwise (CW) and counterclockwise (CCW), except in Phase C. Frequency of reversal is noted in the description of each phase, as follows:

A. Phase A

Phase A included a 2-h checkout in air, followed by a 375°F bakeout for 24 h. After pumpdown to 10^{-9} torr, there was a 48-h run, with reversal every 2 h, for a total of 1.5×10^6 total revolutions. All instrumentation and test bearing operation was checked out and carefully monitored during Phase A; several failures occurred during this period.

B. Phase B

Phase B consisted of 2 h of 4-min run, 2-min dwell, with reversal after each dwell, for 0.1×10^6 additional revolutions. Phase B was designed to simulate ten times the total operating cycles in vacuum of R-4 bearings in the motor or gear train of a hypothetical antenna actuator. Although the vacuum exposure of a 2-year space mission was not approached, the total wear of the lubricant was simulated.

C. Phase C

Phase C determined the effects of dwell in vacuum on torque. Dwell durations of 1, 6, 24, 48, and 72 h were employed. Starting and running torque were measured after each of three dwells of each duration. There were 0.1×10^6 additional revolutions.

In Phase C, some of the transfer film lubricants exhibited increased starting torque after periods of dwell, while their running torque level, measured a few seconds after start-up, was not noticeably affected by dwell duration.

As shown in Fig. 3, starting torque of the Code Y(L) bearing pair rose fairly linearly from approximately 10,000 mg-mm for 0 to 1 h dwell to 30,000 mg-mm after 72 h dwell. However, after a few seconds of operation, the running torque decreased and stabilized around 10,000 mg-mm, regardless of prior dwell duration. The

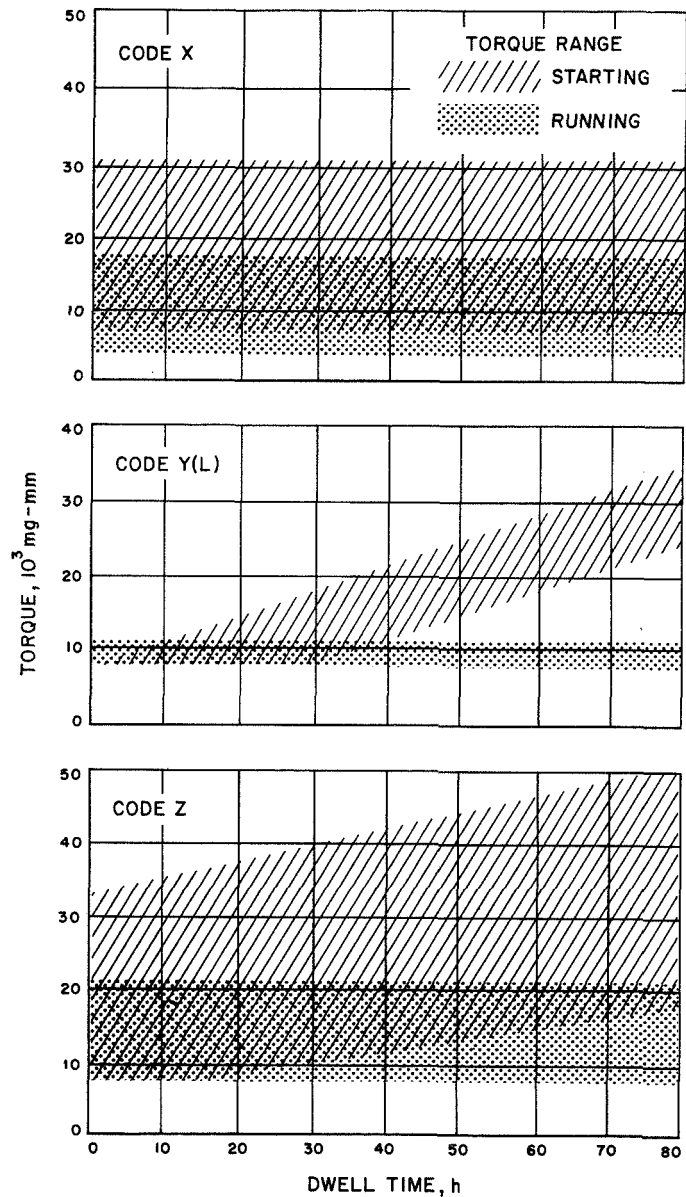


Fig. 3. Effects of dwell on bearing torque

Code Z bearings exhibited a somewhat more pronounced increase in starting torque after dwell. It may be significant that their average starting torque, after even the short duration dwells, was somewhat higher than their average running torque.

If the increase in starting torque with increased dwell duration is attributed to embedment of the bearing balls into the lubricant film under load, this would be expected. The Code Y lubricant, with its glass fiber reinforcement, should have a higher bulk modulus, and hence a higher resistance to indentation, than the Code Z, which is essentially pure TFE.

In contrast to the behavior of the Code Y and Z bearings, dwell appeared to have no significant effect on the Code X bearings. Although both test fixtures contained Code X test bearings, none of the four pairs tested exhibited this phenomenon. In an attempt to determine whether the Code X lubricant would exhibit this behavior after dwells of longer duration, further tests were made (at approximately 45×10^6 revolutions in Phase D). Ultimately, a 10% increase over the starting torque measured after an 80-h dwell was measured after a 240-h dwell. On the basis of the available data, it is not possible to determine whether the Code X lubricant is more resistant to the embedment phenomenon (if this in fact causes this behavior) or whether the MoS_2 present in the Code X lubricant helps to nullify this effect.

D. Phase D

Phase D consists of a sequence of 50 h CW rotation, 50 h CCW rotation, and 68 h dwell, to be repeated until failure occurs, with 3×10^6 additional revolutions each week.

Phase D testing is being continued, to establish relative "life" or cycle capabilities of the lubricants and bearings still operating successfully. Vacuum testing of the second fixture was begun approximately 2 months after the first test series was begun; this is the reason some

of the bearings still operating have completed fewer revolutions than others. (The Code X bearings in the second test had previously been run for an additional 8×10^6 revolutions in vacuum in an initial facilities checkout.)

VII. Conclusions

Useful analytic techniques for dry-film lubricant characterization and quality control have been identified or developed. X-ray emission techniques are effective in determining constituent distribution in nonlayered homogeneous lubricants. The electron probe technique proved particularly effective in the analysis of multilayered lubricant coatings. Optical microscopy was found to be extremely useful in the evaluation of all the coatings tested.

Some lubricants have shown definite increases in starting torque as a function of dwell duration. Codes Y and Z bearings exhibited starting torques two to three times their average running torque after 80 h dwell under load in vacuum. While this torque increase is not excessive, consideration should be given to this phenomenon in applications where low excess torque is available and intermittent operation is expected.

Improved transfer lubricant films may result from initial run-in in vacuum. Evidence of "vacuum shock" crazing and reduced film adhesion was seen in a transfer film established in air at atmospheric pressure.

Performance tests have been designed and conducted which have demonstrated the capability of some dry-film lubricants to operate for extended periods in hard vacuum, while other lubricants failed under the same conditions. Two lubricants, Codes C and X, have performed successfully for over 130×10^6 revolutions in 10^{-9} torr vacuum. In a subsequent test, Codes A, D, and X were operating smoothly after 60×10^6 revolutions, also in hard vacuum.

N 69-11811

Development of Bearings for Nuclear Reactors in Space*

William J. Kurzeka
Atomics International
A Division of North American Rockwell Corporation
Canoga Park, California

Atomics International, under an AEC program, has developed bearings to operate in reactor control components in a space environment at pressures from as low as 10^{-12} torr to as high as 10^{-3} torr at temperature ranges from 950 to 1500°F, with a life requirement of 1 to 5 years.

Three development phases included: (1) a 1000-h sliding friction evaluation at design temperature in ultrahigh vacuum, to screen candidate materials; (2) a compatibility test in vacuum, at and above the design temperatures, with candidate materials in static contact; and (3) testing of prototype bearing assemblies under design loads in the design environment. Test results were used to select material combinations for reactor control drum bearings; these combinations are tabulated for the listed SNAP systems. Information obtained was also used in selecting material combinations for such other components as electric actuators, position sensors, limit switches, and ground test scram mechanisms.

I. Introduction

Over the past 9 years, Atomics International has developed bearings for nuclear reactor operations in space and has directed its efforts into areas where stringent conditions are imposed and where few agencies or companies are actively involved. These conditions are long-term operation (1 to 5 years), high temperature (950 to 1500°F), high radiation levels (10^{20} nvt, 10^{11} rad), and high launch shock and vibration loads.

The bearings used in our SNAP¹ reactor control drum, which is a 15- to 30-lb cylindrical segment, eccentrically mounted between two pivot points (Fig. 1), were the focal point of bearing development. Bearings for other components were designed from the control drum bearing data. The choice of a journal bearing in a self-aligning ball was made early in the program, because of the heavy launch loads, low operating speed, long dwell

*This work was performed under Contracts AT(11-1)-GEN-8 and AT(04-3)-701 for the U.S. Atomic Energy Commission.

¹Systems for Nuclear Auxiliary Power. For more information on the SNAP reactors, see "The Development Philosophy for SNAP Mechanisms," by O. P. Steele III, in these *Proceedings*.

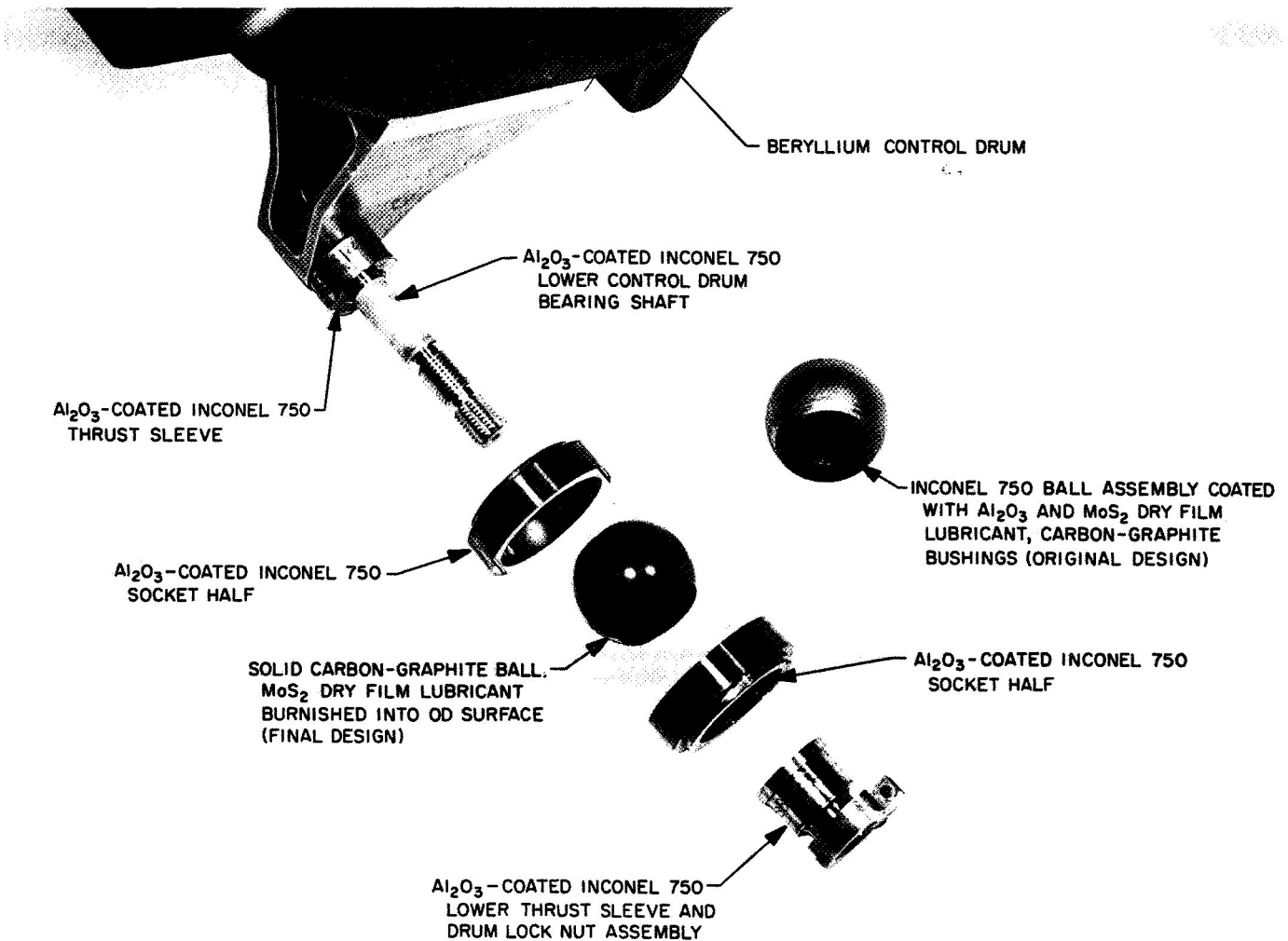


Fig. 1. SNAP 8 control drum thrust bearing assembly

periods, and cost. Table 1 summarizes the results of our bearing program.

II. SNAP 10A and SNAP 2 Reactor Programs

The SNAP 10A, 950°F, 1-year life bearing was our first milestone. Friction tests, to screen material combinations for 1000°F, were conducted in an oil diffusion-pumped, 10⁻⁵-torr vacuum chamber (Ref. 1). As the effects of high vacuum on materials and the effects of diffusion pump oil on bearing couples became known, we added self-weld testing and extended our friction testing to ion-pumped, 10⁻⁸-torr vacuum chambers (Refs. 2 and 3). Several combinations of materials looked promising, but the material couple used was spray-coated Al₂O₃

against sintered TiC. Table 1 shows the testing and operating history.

From friction tests, carbon graphite against Al₂O₃ had been found to be the material combination having the lowest friction, but designing around its low expansion, brittleness, and tricky machining properties was not developed for SNAP 10A. However, the SNAP 2 design used carbon graphite impregnated with a lithium salt as inserts in the self-aligning ball. The backup choice for SNAP 2 was a solid carbon graphite ball with Al₂O₃-spray-coated shaft and socket. Initially, fretting of the carbon ball during vibration was a problem, but the use of bonded MoS₂ on the socket provided damping to overcome the fretting.

Table 1. SNAP reactor control drum bearings (self-aligning ball-socket type)

Reactor	Design conditions	Material combinations		Status
		Shaft to ball	Ball to socket	
SNAP 10A	950°F 1-year life 10 ⁻³ to 10 ⁻¹² torr 20-g shock 7.5-g vibration	Al ₂ O ₃ (spray coat) ^a against TiC	TiC against Al ₂ O ₃ (spray coat) ^a	Operated after 43 days on spacecraft at 600°F. Operated after 10,000 h of nuclear ground test at 600°F, 3.6 × 10 ¹⁸ nvt, and 10 ⁻³ torr. Qualification tested 5000 h at 700°F and 10 ⁻³ torr.
SNAP 2	1000°F 1-year life 10 ⁻⁴ to 10 ⁻¹¹ torr 20-g shock 7.5-g vibration	Al ₂ O ₃ (spray coat) ^a against carbon graphite impregnated)	TiC against Al ₂ O ₃ (spray coat) ^a and MoS ₂	Prototype tested to 1500 h at 850°F and 10 ⁻⁷ torr.
SNAP 8	1150°F 12,000-h life 10 ⁻⁵ to 10 ⁻¹¹ torr 35-g shock 19-g vibration	Al ₂ O ₃ (spray coat) ^b against carbon graphite (no impregnant) and MoS ₂	Carbon graphite (no impregnant) and MoS ₂ against Al ₂ O ₃ (spray coat) ^b	1000-h friction test completed at 1250°F. 5000-h compatibility test completed at 1250 to 1450°F. Design verification tests in progress at 1150 and 1250°F, 10 ⁻⁵ and 10 ⁻⁹ torr.
Advanced ZrH reactor	1500°F 3- to 5-year life 10 ⁻⁶ to 10 ⁻¹² torr 35-g shock 19-g vibration	Al ₂ O ₃ (spray coat) ^c against carbon graphite (no impregnant)	Carbon graphite (no impregnant) against Al ₂ O ₃ (spray coat) ^c	Operational test of prototype in progress at 1500°F and 10 ⁻⁸ torr. Friction and compatibility tests to start in Fiscal Year 1969.

^aTi-6 Al-4V substrate.
^bInconel 750 substrate.
^cTa-10 W substrate.

III. SNAP 8 Reactor Program

Next, we started work on the SNAP 8 reactors, with a 12,000-h life and 1150°F bearing temperature. To provide for the higher temperature requirement, the structural material for the bearings was changed from Ti-6 Al-4V to Inconel 750; to accommodate thermal expansion, the TiC ball was discarded in favor of Al₂O₃-sprayed Inconel 750. Otherwise, SNAP 2 material combinations were used.

The testing of prototype bearing assemblies was proceeding satisfactorily, until they were examined after 10,000 h at 1150°F; it was then discovered that the Al₂O₃ was spalling from the shaft. Spalling occurred only when the Al₂O₃ was in contact with the impregnated carbon graphite. Examination of the Al₂O₃ showed a phase change from γ to α , which represents an 8% density increase. Later, it was shown that the impregnant, and not the carbon graphite, had some catalytic effect on this phase change.

With a year to go before the startup of the reactor was scheduled, a selection of other promising couples was made, and a three-phase approach to the development of a stable shaft coating was implemented as follows:

- (1) Sliding friction tests (Fig. 2) were conducted for 1000 h in ion chambers. Using our 1000°F fixturing with heaters at 1250°F presented problems. The Kanthal A-1 heater wire oxidized and burned up in 100 h, and a switch to platinum wire was necessary. The stainless steel specimen supports also had to be strengthened.
- (2) Concurrently, stacks of candidate material couples were cooked in a vacuum at 1250, 1350, and 1450°F for 500, 1000, 2000, and 5000 h (Fig. 3). This required the design and fabrication of vacuum heaters of tantalum. Temperatures above the design temperature were selected, to accelerate any incompatibilities in order to obtain early results. Couples of Al₂O₃, in contact with both impregnated (the original SNAP 8 combination)

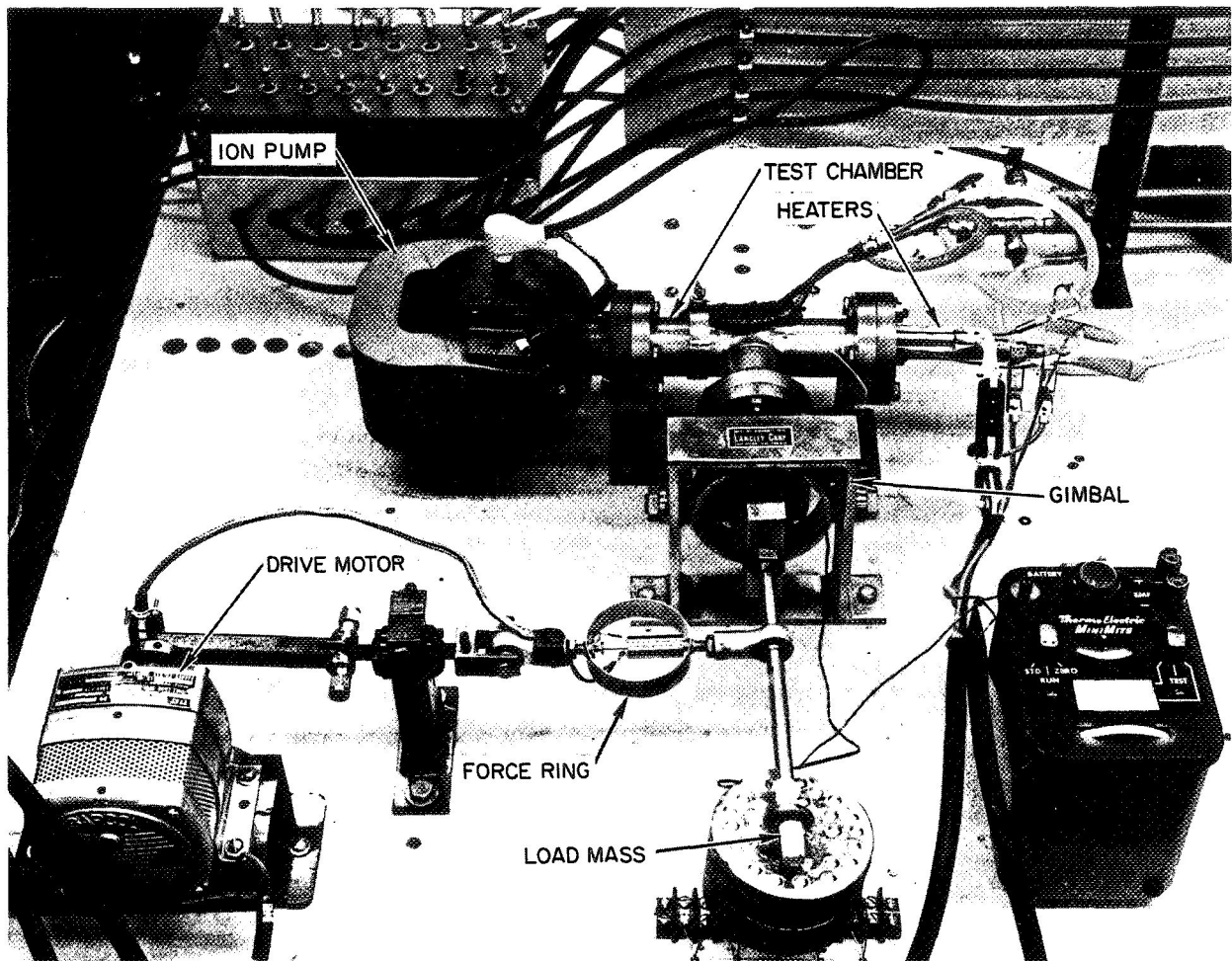


Fig. 2. Sliding friction test facility

and nonimpregnated carbon graphite, were also included.

- (3) Journals, coated with several other candidate materials, were also put on test in the impregnated carbon graphite bearings, under design load, cycling, and temperature conditions (Fig. 4).

The results of this three-phase program are summarized in Table 2. The catastrophic failure of Al_2O_3 against P5N was duplicated, and the stability of Al_2O_3 against the nonimpregnated carbon graphite was demonstrated. Both Cr_3C_2 and WC showed considerable transfer of chrome to the P5N. A choice of P5 against Al_2O_3 was made; and the complex Inconel 750 ball, coated with Al_2O_3 and fitted with P5N inserts, was replaced with a solid, nonimpregnated carbon graphite ball. Design verification testing of this choice, to 12,000 h at 1150 to 1250°F and 10^{-5} to 10^{-8} torr, is underway.

IV. Advanced ZrH Reactor Program

We have started the development of a 1500°F bearing for an advanced reactor and are taking the three-phase approach found so effective for the SNAP 8 program. Upgrading test fixtures for this temperature requirement has been as difficult as testing the candidate combinations.

Tantalum alloys are used for basic high-temperature structure, and high-purity alumina is used for insulators. The handling and cleanliness of all parts that go into the vacuum chamber must be given special attention. Material combinations of P5 against K162B, P5 against Al_2O_3 coated on Ta-10 W, solid Al_2O_3 against LT-2 (a cermet of W, Cr, and Al_2O_3), LT-2 against P5, and LT-2 against LT-2 are to be tested for 1600°F compatibility and friction. In addition, P5 against Al_2O_3 on Ta-10 W is on test as a prototype bearing.

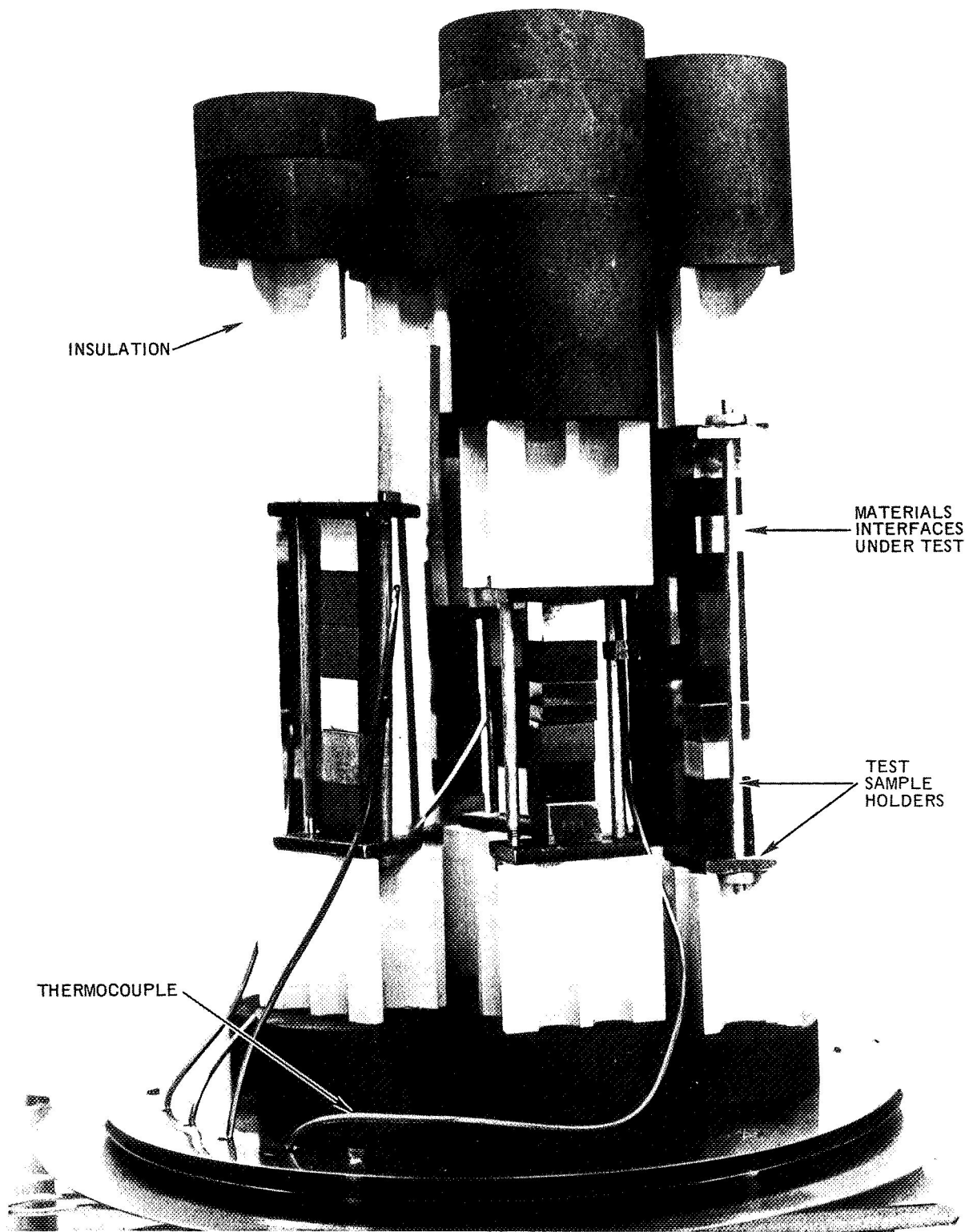


Fig. 3. Compatibility tests of candidate bearing materials

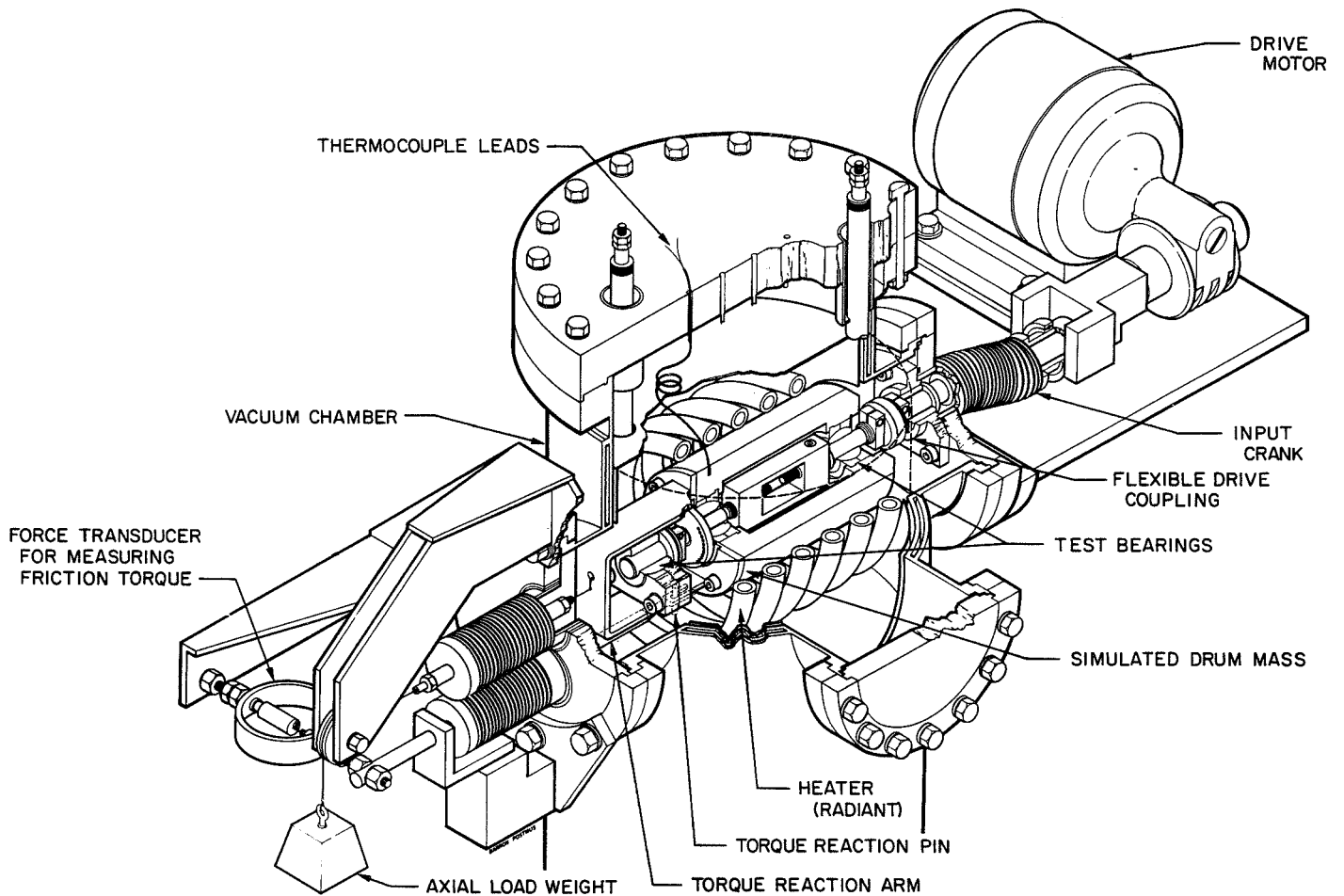


Fig. 4. Bearing development test fixture

Table 2. SNAP 8 bearing redesign program

Bearing couple	Maximum friction coefficient (1000 h, 10^{-7} torr)		Maximum torque, 1250°F shaft tests (700 to 2000 h, 10^{-5} torr), in. -lb	Compatibility tests (1000 h, 10^{-5} torr) (1250, 1350, and 1450°F)
	1250°F	Room temperature		
Al ₂ O ₃ against P5	0.29	0.69	—	Coating showed no significant changes.
Al ₂ O ₃ against P5N	0.28	0.69	2.5	Coating separated from substrate.
TiC against P5N	0.62	0.78	5.7	Generally stable, but showed slight porosity increase.
Cr ₃ C ₂ against P5N	0.85	0.68	4.8	Chrome transfer to the P5N was apparent.
WC against P5N	1.0	2.0	5.5	Chrome transfer to the P5N was apparent.
Cr plate against P5N	0.32	0.64	Heavy chrome transfer to P5N prompted no further testing.	
K162B against P5N	0.35	0.50	Long time for delivery of material precluded use on this program.	

NOTES: P5N and P5 are carbon graphites from Pure Carbon Co., impregnated (Li salts) and unimpregnated, respectively.
 Al₂O₃, TiC, Cr₃C₂, and WC were spray-coated on Inconel 750.
 K162B is a TiC sintered material from Kennametal Corporation.

V. Concluding Remarks

Information obtained in the testing program was used not only to select material combinations for bearings, but also in selecting such other components as electric actuators, position sensors, limit switches, and ground test scram mechanisms.

Some of the problems encountered during our program should be of interest to other developers of high-temperature components. The materials selected for these extreme conditions tend to be exotic, and suppliers tend to give rather poor delivery, especially on small development quantities. Also, they do not always have adequate specifications for the materials, or proprietary processes may be involved, and they resist giving us the details necessary for us to analyze the materials. The machining of such materials can also require considerable effort, on

our part, in locating and working with the fabrication vendors.

Fabricating test fixtures from materials that have not had wide use (e.g., tantalum alloys) has required training in machining practices in our own shop. Heaters for our uses were not available from commercial vendors, and we found ourselves involved in a heater development program. Also, our personnel who were setting up tests had to be trained in clean handling practices.

Where there are long-term design life goals, it pays to devise methods of accelerating the effects, as in our compatibility tests at above-design temperatures. At the same time, the test sequence on prototype assemblies should not be so severe, or have such an excessive margin, that a failure leaves one wondering whether the test might not have been successful with just a modest margin.

References

1. Kurzeka, W. J., *Bearing Materials Compatibility for Auxiliary Power Systems*, NAA-SR-8476. Atomics International, a division of North American Aviation, Inc. (now North American Rockwell Corporation), Canoga Park, Calif., Sept. 1961.
2. Kellogg, L. G., *SNAP Reactor Materials Development – Ultra High Vacuum Friction Studies*, NAA-SR-9644. Atomics International, a division of North American Aviation, Inc. (now North American Rockwell Corporation), Canoga Park, Calif., June 1964.
3. Kellogg, L. G., *SNAP Reactor Materials Development Self-Weld Studies*, NAA-SR-9643. Atomics International, a division of North American Aviation, Inc. (now North American Rockwell Corporation), Canoga Park, Calif., June 1964.

PRECEDING PAGE BLANK NOT FILMED.

N 69 - 11812

Controlled-Leakage Sealing of Bearings for Fluid Lubrication in a Space Vacuum Environment

H. I. Silversher
Lockheed Missiles & Space Company
Sunnyvale, California

This paper analyzes an example of sealing hydrodynamic bearings to the extreme requirements established by the functional mission of space vehicles in synchronous orbit for extended periods of time. The present concept of a synchronous orbit is a constant altitude of between 20,000 and 25,000 miles. The economy of many missions in synchronous orbit will require functional effectiveness for at least 7 years.

The problems imposed by severe environmental conditions for the extended period of time are discussed so that relevant design criteria for hydrodynamic bearing lubrication systems can be established.

I. Introduction

The applicability of synchronous orbiting mechanisms to space technology is manifested in the communications satellite. The *Applications Technology Satellite (ATS)* and *COMSAT* designs represent the state-of-the-art concepts for reception and transmission, forming an important facet of a global communications network. Both designs depend on bearings for stability and orientation. Some designs utilize bearings in power and signal transfer. In all designs, the reliability of bearing function is critical to the success of the mission. A bearing failure is catastrophic.

Valuable information covering the probable failure modes of antifriction bearings and bearing surfaces in the

space vacuum environment is available from such publications as NASA technical reports; proceedings of the annual Aerospace Mechanisms Symposiums; proceedings of meetings conducted by the American Society of Lubrication Engineers and the Aerospace Council; and company research projects funded by government agencies. Such information is obtained, for the most part, from the results of simulated tests in terrestrial laboratories, and, to a lesser degree, from information transmitted by orbiting spacecraft.

II. Constraints

The lubrication of spacecraft systems operating in a synchronous orbit is complicated by (1) ultra-high

vacuum, (2) volatilization, (3) condensation of volatiles, (4) absence of reactive gases, (5) poor thermal conductivity, (6) weightlessness, (7) temperature extremes, and (8) penetrating radiation. When knowledge of constraints is applied to bearing design, the resulting lubrication system should be the product of the proper selection of materials, suitable engineering design, and the careful application of nondestructive testing and check-out procedures.

A. Ultra-high Vacuum

The most important problem in the space environment influencing materials for lubricated systems is ultra-high vacuum. The ambient pressure of the synchronous orbit is about 10^{-13} torr. The detrimental effects on the lubrication system attributed to this low ambient pressure are volatilization, condensation of the volatiles, absence of reactive gases, and poor thermal conductivity.

1. Volatilization. The equilibrium value is a thermodynamic function of the molecular species involved and is established when the rate of molecules returning to a surface equals the rate of leaving. In an absolute vacuum, the mean free path is large enough so that those departing molecules can be permanently lost and equilibrium cannot be attained. Therefore, if a solid or fluid lubricant has a high vapor pressure, it may evaporate appreciably during long-time space orbits, with a contingent loss of lubricative function.

2. Condensation of volatiles. The detrimental effect of volatiles condensing on a cold surface is contamination. Optical and thermal control surfaces are particularly vulnerable and cannot perform satisfactorily with gross changes in diffraction, absorption, and emissivity. Electrical contacts, slip rings, and brushes are detrimentally affected by changes in conductivity due to contaminating films.

3. Absence of reactive gases. Absorbed or chemisorbed gas films, such as oxides, are normally present on even the cleanest metal surfaces in terrestrial atmosphere. Such films prevent bare metal-to-metal contact and the formation of strong welded junctions. However, when these films are removed by frictional phenomena, they are lost to space vacuum, and gross seizure and welding can occur.

4. Poor thermal conductivity. Poor thermal conductivity results from the absence of gases between adjacent or contacting surfaces down to the prominent asperity

level. In the terrestrial atmosphere, the spaces between contacting asperities are filled with air which conducts thermal energy from one substrate surface to another, thereby producing a low gradient. However, in vacuum, the absence of thermal conducting gases restricts the flow of heat to the real areas of contact (asperities), resulting in a high gradient. The poor thermal conductivity, coupled with the absence of convection cooling, establishes higher heat-resistance requirements for lubrication systems.

B. Weightlessness

The only beneficial effect of weightlessness is that, once in orbit, bearings need not support a structural load. The bearing load is reduced to the level required by the initial load associated with acceleration and deceleration, the effect of unbalanced dynamic forces, and the centrifugal force of the bearing against raceways and retaining mechanisms. Reduced bearing load means less wear and friction. However, the detrimental effects have a greater influence on bearing design. The latter effects are:

- (1) The obvious malfunction of gravity-fed systems such as fluid reservoirs and hydraulic system accumulators.
- (2) In combination with ultra-high vacuum, the absence of convection currents for cooling. Therefore, frictional surfaces will operate at higher temperatures than those induced by the same loading conditions in a terrestrial environment.

C. Temperature Extremes

The effect of temperature extremes on spacecraft lubrication is more pronounced on those parts outside of the vehicle skin. The cause is direct radiation from the sun and, to a lesser extent, solar reflection from the earth. Components such as solar array bearings can experience temperatures as low as -280°F when positioned away from the influence of solar radiation. Temperatures within the vehicle are protected from extreme conditions by controlling the absorptivity and emissivity of the outer spacecraft skins so that the only problem is the increased temperature rise on frictional surfaces caused by the lack of convection heat transfer.

D. Penetrating Radiation

The net effect of penetrating radiation on lubrication is the energy supplied for chemical reactions within the

molecular structure of the lubricants and the temperature rise due to the absorption of energy, which can detrimentally affect required chemical and physical lubricant properties. Space environment radiation is not considered a major problem in lubrication. Radiation-resistant lubricants have been developed, newer lubrication system design provides effective shielding through housings and retaining mechanisms, and the oxygen required to accelerate radiation degradation in some lubricant materials is absent in space vacuum environments.

III. Lubrication Systems

There are many bearing surfaces and mechanisms functionally peculiar or common to the communications satellite. These include mechanisms such as motors, gear chains and trains, gyros, or stabilization wheels; mechanical devices such as pull pins, threaded fasteners, closures, and valves; equipment for recording and transmission, relays, and timing devices; electrical contact surfaces such as brushes and slip rings; and critical bearings for positioning antennas and solar arrays or for spinning and despinning the satellite.

The purpose of a lubrication system is two-fold: (1) to maintain a low torque level consistent with part function and available allotted power, and (2) to maintain the required conductivity for contacting electrical surfaces. Increasing the torque of any of the aforementioned mechanisms can render the available power supply inadequate, and a failure mode is established. Increasing torque is the product of friction, wear, and adhesion. Decreased electrical conductivity can render electrical power and signal transfer inoperable.

We must design a lubrication system for mission life. We can discount the problem of environmental radiation where the bearings are housed and shielded unless there is a nuclear power source for the spacecraft. The problem of meteoroids is part of total spacecraft design and not peculiar to the lubrication system. Therefore, we must design for protection against the adverse conditions imposed by the low ambient pressures, weightlessness, and temperature extremes.

The primary consideration is the lubricant itself. The two most widely used generic types are fluid and solid. The fluids (oils and greases) are useful for hydrodynamic systems, and the solids are more applicable where boundary conditions are encountered.

A. Solid Lubricants

We will not dwell on the solid lubricants, although they are more compatible with the space vacuum environment than the fluids. However, they have a tendency toward sacrificial wear, whereby they reduce the wear rate between rubbing surfaces by wearing themselves, until they are removed or the debris formed becomes a contaminant. If a thicker film is employed for longer wear, the wear can become greater than design-allowable dimensional tolerances, or the greater amount of debris can compound the contamination problem. An excellent example is in electrical contacts such as slip rings and brushes, where debris from contacting brushes can create a "short" by depositing a conductive path between adjacent slip rings. Another problem is that the greater the speed of rubbing surfaces, the faster the wear. The failure mode with solid lubricants is usually catastrophic. However, there are applications where only solid lubricants can be used, and a judicious selection should be made.

B. Fluid Lubricants

For the purpose of this session we will discuss the design of hydrodynamic lubrication systems for bearings and flexures in space vacuum environments.

The greatest problem with fluid lubricants is volatility. Vacuum increases the evaporation rate of the material, and any increase in temperature from friction with the lack of convection cooling accelerates volatilization. Therefore, an oil or grease with low volatility and thermal stability should be selected. We have found that lubricating fluids based on chlorophenylmethyl polysiloxane and fluorosilicones impart excellent lubrication to instrument-type bearings in vacuum for rather long periods of time. A test using a fluorosilicone is still in progress after more than 5½ years, in a chamber pressurized at 1×10^{-8} torr. The tests performed on fluid lubricants at 10^{-8} or 10^{-9} torr are valid even though the synchronous orbit ambient pressure is 10^{-13} torr. Effectively designed shielding and sealing of bearings will increase the pressure surrounding the bearing to from 10^{-3} to 10^{-8} torr. Some of the highly refined paraffinic and petroleum oils and greases show promise, but the changes in viscosity are more pronounced than those of the silicones with changes in temperature.

C. Bearing Materials

Another important factor in vacuum bearing technology is the selection of the bearing material. Two metals

often used are 52100 chrome steel and 440C corrosion-resistant steel – both materials heat treated to a Rockwell hardness of C58-63; vacuum melt fabrication stock is preferred to assure freedom from gross imperfections during alloying. We prefer the 440C for the total mission because of its resistance to the prelaunch atmospheric environment.

IV. Controlled-Leakage Sealing

When the type of bearing and the lubricant have been selected, the design of the lubricating system for mission life follows. Design parameters should include calculations assuring an adequate supply of lubricating fluid. Since volatilized fluids are gases in vacuum, the calculations should be derived from the flow behavior of gases at the different pressure levels.

Complete or hermetic sealing of the lubrication system is most effective in vacuum. However, there is a possibility that the optimum seal could be broken by disrupting forces during the 7-year minimum requirement. Therefore, other sealing methods that can function with some exposure to ultra-high vacuum should be investigated. An excellent, flight-proven candidate is controlled-leakage sealing.

The design for controlled-leakage sealing is based on a minimum loss of lubricant by evaporation. M. Knudsen (Ref. 1) states that since on a molecular scale even smooth surfaces appear rough, the direction in which a molecule rebounds after collision with the surface is statistically independent of the angle of incidence. Therefore, the molecular flow resistance of small orifices can be made relatively high.

A. Theoretical Discussion

We relate the controlled-leakage mechanism to the molecular flow of gases rather than to viscous flow because the reduced pressure of space vacuum causes the molecular mean free path to exceed the cross-sectional area of the gas path, and tangential shear between gas layers cannot be effected. An equation developed by M. Knudsen and colleagues modifying the classic kinetic gas theory is useful in designing a fluid lubrication system for functional bearing life by calculating the escape rate of oil from a bearing assembly. The equation is

$$Q = \frac{4}{3} (2\pi)^{1/2} \left[\frac{(R_2^2 - R_1^2)(R_2 - R_1)}{L} \right] \frac{1}{(\rho_1)^{1/2}} (p_1 - p_2) \quad (1)$$

where

- Q = volume flow rate of oil vapor
- R_1, R_2 = inside and outside radii of annulus
- L = length of annulus
- ρ_1 = density of oil vapor at standard conditions
- p_1 = pressure in the housing
- p_2 = ambient pressure

According to M. B. Weinreb (Ref. 2), this equation was employed in designing a radiometer spindle assembly for the *Tiros II* meteorological satellite (Fig. 1). The lubricant used was a MIL-L-6085A diester oil with a vapor pressure of 10^{-4} torr. When the ambient pressure reaches 10^{-2} torr, molecular gas flow occurs around the shaft through the small clearance of 0.0005 in.

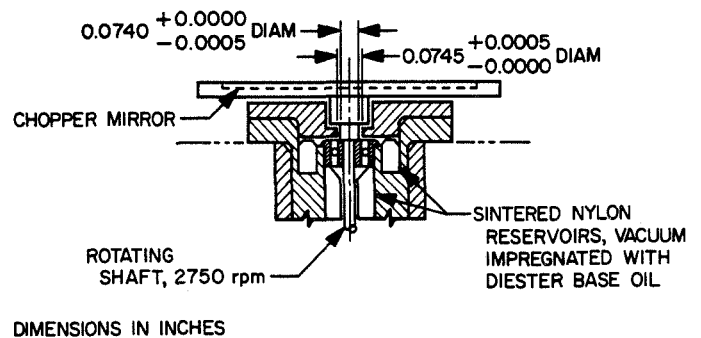


Fig. 1. Radiometer spindle assembly

S. P. Lester (Ref. 3) describes the effect of modifying the kinetic gas theory for a simple aperture (Eq. 2):

$$w = 0.0583 P \left(\frac{M}{T} \right)^{1/2} A \frac{\text{grams}}{\text{second}} \quad (2)$$

where

- w = weight loss in grams/second through simple aperture
- P = vapor pressure of the gas in torr
- M = molecular weight of the gas
- T = temperature of gas in degrees Kelvin
- A = area of the aperture in cm^2

Equation (2) should be further modified by a fraction factor of loss f . Since f is based on gap width a and channel length l in the order of mean free path, it is possible to establish a numerical value of f for escape path configurations other than the simple aperture. The Monte Carlo Technique (Ref. 4) can be used for this calculation if the (l/a) ratio of the path length to width is 16 or greater in the equation $f = \pi(a/l)$. The term f can then be introduced into Eq. (2) as follows:

$$w = \left[0.0583 P \left(\frac{M}{T} \right)^{1/2} A \right] f \frac{\text{grams}}{\text{second}} \quad (3)$$

Several examples of escape paths measurable for f are shown in Fig. 2. These and other possible configurations contribute to the effective design of labyrinth seals. Controlled-leakage sealing is augmented by using fluid lubricants with low vapor pressures. It is sometimes difficult to correlate a high average molecular weight product with a uniform low vapor pressure, since many fluid lubricants contain a wide range of molecular weights. The low molecular weights probably volatilize first so that the loss factor will be somewhat erratic until the system is stabilized. This should be considered when calculating sealing requirements.

B. Results of Tests on Selected Oils

S. P. Lester (Ref. 3) tabulated the vapor pressure and viscosity of oils that were selected for low-vapor properties and that have been evaluated by the Lockheed Missiles & Space Company as lubricants for instrument-size ball bearings (Ref. 5). These are listed by generic chemical type in Table 1. The results of the tests are tabulated in Table 2.

Table 1. Vapor pressure and viscosity of selected oils

Oil (chemical type)	Vapor pressure, torr	Viscosity, cS
Chlorophenyl-methyl polysiloxane	0.1 at 125°F	52 at 100°F
Petroleum base oil	1×10^{-9} at 70°F 1×10^{-3} at 572°F	3535 at 104°F
Paraffinic base petroleum oil with additive	5×10^{-4} at 70°F	440 at 70°F 155 at 100°F 15 at 210°F
Diocetyl sebacate	3×10^{-5} at 70°F 1×10^{-3} at 176°F	23.5 at 70°F 9.37 at 130°F 3.85 at 210°F

Except for the dioctyl sebacate, all the lubricants were operable in vacuum for more than 1 year with impregnated phenolic retainers and without labyrinth seals. A fluorosilicone oil (not listed in the table), with a viscosity of 250 cS, is operating in a pressure of 1×10^{-8} torr after more than 5½ years. A well-designed labyrinth seal should improve the performance of the tested oils.

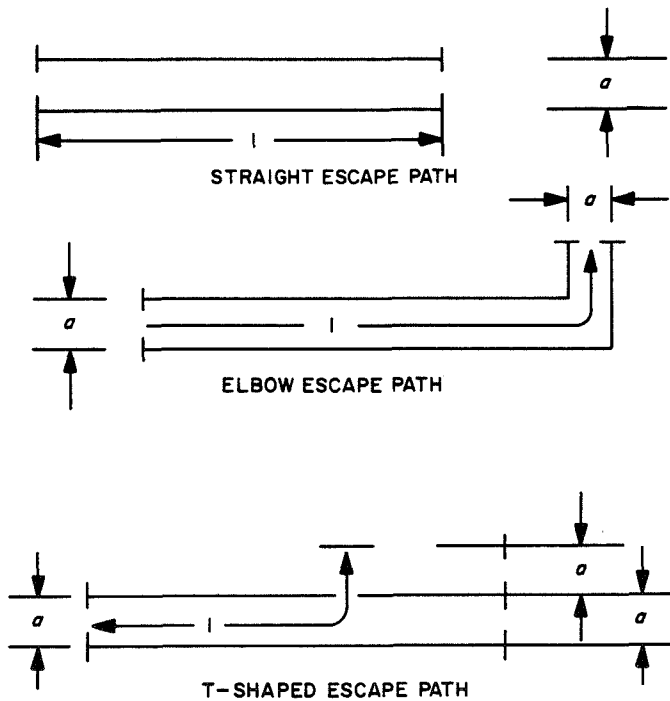


Fig. 2. Measurable escape paths

Table 2. Test results for selected oils (Ref. 5)

Oil (chemical type)	Maximum test pressure, torr	Results (as of Sept. 1967)
Chlorophenyl-methyl polysiloxane	4×10^{-9}	Motor stalled at 23,460 h. Cause of failure being determined.
Petroleum base oil	1×10^{-8}	Test discontinued at 20,019 h. Bearings were satisfactory with oil still present. No change in torque from start to finish.
Paraffinic base petroleum oil with additive	1×10^{-8}	Still running after 18,457 h in an ambient temperature of 250°F.
Diocetyl sebacate	1×10^{-3}	Failed at 3584 h.

V. Specific Recommendations

To optimize the design of a fluid lubrication system for bearings in the space vacuum environment for extended periods of time, the following recommendations are made:

- (1) The bearings should be fabricated from vacuum-melt 440C corrosion-resistant steel, hardened to Rockwell C 58-63.
- (2) Retainers should be porous phenolic laminate, vacuum-impregnated with a low-vapor-pressure fluid lubricant selected from the first three types listed in Tables 1 and 2.
- (3) Controlled-leakage seals should be designed with an adequate supply of low-vapor-pressure fluid

lubricant (for mission life) vacuum-impregnated into sintered nylon reservoirs (18-25% porous).

- (4) The judicious deployment of barrier films will decrease creepage of the lubricant from the bearing surface and the minimized surface area exposed to low pressures will reduce the loss factor.

VI. Conclusions

The vacuum space environment does afford some advantages to the hydrodynamic lubrication systems using fluids. Weightlessness reduces the high bearing loads and the boundary condition resulting from the loss of the fluid film. With controlled-leakage sealing, the reservoirs need not be in direct physical contact with the bearing; as a result, the torque requirement is decreased.

References

1. Knudsen, M., *Kinetic Theory of Gases; Some Modern Aspects*, Third Edition. Methuen and Company, Ltd., London, 1950.
2. Weinreb, M. B., *Results of Tiros II Ball Bearing Operation in Space*. Meteorological Branch, Goddard Space Flight Center, National Aeronautics and Space Administration, Washington 25, D. C., March 1961.
3. Lester, S. P., *Labyrinth Sealing of Bearings for Vacuum Environment*, Engineering File MT 13285. The Bendix Corporation, Eclipse-Pioneer Division, Teterboro, N. J., Aug. 29, 1966.
4. Salmon, W. A., and Apt, C. M., "A Lubrication System for Space Vehicles," presented at the Automotive Engineering Congress, Detroit, Mich., Jan. 1963, SAE 632E, Society of Automotive Engineers.
5. Silversher, H. I., and Drake, S. P., Jr., *Lubrication Evaluation*, MP-1503,01. Lockheed Missiles & Space Company, Sunnyvale, Calif., Sept. 1967.

Selected Bibliography

The author acknowledges the general information about lubrication in space vacuum environment obtained from the following publications:

Bisson, E. E., and Anderson, W. J., *Advanced Bearing Technology*, NASA SP-38. National Aeronautics and Space Administration, Washington 25, D. C., 1964.

Goetzel, C. G., Rittenhouse, J. B., and Singletary, J. B., *Space Materials Handbook*, Second Edition, ML-TDR-64-40. Air Force Materials Laboratory, Research and Technology Division, Air Force Systems Command, Wright-Patterson Air Force Base, O., Jan. 1965.

Rittenhouse, J. B., and Singletary, J. B., *Space Materials Handbook, Supplement 1 to Second Edition*, MIL-TDR-64-40, Supp. 1, NASA SP-3025. National Aeronautics and Space Administration, March 1966.

PRECEDING PAGE BLANK NOT FILMED.

N 69 11813

Mechanical Suspensions for Space Applications

George G. Herzl
Lockheed Missiles & Space Company
Sunnyvale, California

Mechanical suspensions may be preferable to bearings for space applications because of the absence of wear, backlash, lubrication requirements, and other factors. Such factors as temperature changes, magnetic and electric fields, and force fields may cause instability in suspensions and must be considered in design. Major types of suspensions (torsion, filar, flexure, coil, and combinations) are described, with examples of use. Characteristics of mechanical suspensions are summarized in tabular form.

I. Introduction

Designers are increasingly using mechanical suspensions, where they previously used bearings, to support moving components of aerospace mechanisms. Mechanical suspensions have demonstrated a capacity to operate continuously for millions of cycles. Such long life is predictable because of the absence of wear, backlash, lubrication requirements, and other operational variables. As a means of providing long life in the space environment, mechanical suspensions can be preferable to even very-low-friction bearings (of comparable weight, volume, and complexity).

To help the designer choose between bearings and suspensions, their basic characteristics are compared in Table 1.

Table 1. Basic characteristics of bearings and suspensions

Component	Action	Motion	Restoring torque
Bearing	Rolling, sliding	Continuous rotary	Absent
Ball	↓	↓	↓
Roller	↓	↓	↓
Journal	↓	↓	↓
Conical pivot	↓	↓	↓
Suspension	Bending, twisting	Oscillatory	Present
Torsion	↓	↓	↓
Filar	↓	↓	↓
Flexure	↓	↓	↓
Coil	↓	↓	↓
Membrane	↓	↓	↓

One characteristic of mechanical suspensions, namely, restoring torque (due to bending or twisting motion that accommodates rotation of the suspended part), rules them out for continuous-rotation applications. For many other applications, however, they are the best choice. This paper discusses their advantages, as well as some design implications. Table 2, at the end of the paper, gives characteristics of the most common suspensions, along with equations to help the designer select the type best suited to his purpose.

II. Design Advantages of Suspensions

For aerospace applications, including various ground-based simulating devices, the advantages of mechanical suspensions are:

- (1) The absence of contacting surfaces precludes cold welding in the hard vacuum of space.
- (2) Shock mounting can be done fairly easily to protect against the rigors of launch, reentry, and explosive disturbances.
- (3) Components are ordinarily made from radiation-resistant material.
- (4) Lubricants and seals are not required.
- (5) High electrical conductivity can be maintained between stationary and rotating parts of the suspension.
- (6) Break-away torque is low because internal friction of materials replaces sliding or rolling friction encountered in bearings.

III. General Considerations

The most commonly used types of suspension are:

- (1) Torsion.
- (2) Filar.
- (3) Torsion and filar composite.
- (4) Flexure.
- (5) Coil.

- (6) Membrane.
- (7) Combination.

The torsion and filar (and their composite) types are further classified as single and double. Single — a suspension at only one end of the supported part — can be used in stationary devices where gravity can keep the suspension taut, as in orbital simulating devices. Spaceborne mechanisms employ double suspensions, since these can operate satisfactorily in any position and in an environment subject to shock and vibration.

To select an appropriate type of suspension, the designer should consider the following factors:

- (1) Required angle of rotation.
- (2) Type of restoring torque (positive, negative, or neutral; linear or nonlinear).
- (3) Available space.
- (4) Permissible axial motion.
- (5) Constancy of restoring torque.
- (6) Accuracy of null position.

The first four design considerations listed above are covered in Table 2 and in the following discussions of the various types of suspension. The last two, constancy of restoring torque and accuracy of null positioning, determine suspension stability and can be adversely affected by certain environmental factors and material characteristics, as discussed in detail in the following section.

IV. Designing for Maximum Suspension Stability

The designer must be aware of any factors that could cause instability, such as temperature changes, magnetic and electric fields, force fields, and other adverse factors. The geometry of a suspension may also affect its stability.

A. Temperature Changes

The effect of temperature changes on the restoring torque and the null positioning of mechanical suspensions is primarily a function of material characteristics. In designing for maximum stability, therefore, the designer must take into account the material characteristic most vulnerable to temperature-induced degradation in

each type of suspension. The following list shows this relationship:

Type of suspension	Material characteristic most affected by temperature changes
Torsion	Shear modulus
Filar	Thermal expansion
Flexure	Modulus of elasticity
Coil	Modulus of elasticity
Torsion and filar (or other) combination	Combination of characteristics above

Some techniques that minimize the effects of temperature changes on the stability of mechanical suspensions are as follows:

- (1) Subjecting the suspension elements to many cycles of pulsating temperature variations and subsequently annealing them to eliminate stress concentrations and invisible kinks. (For severe thermal operating environments, the pulsation should simulate actual conditions; for example, the abrupt and extreme temperature changes encountered when a satellite passes from the sunlit to the shadowed side of the earth.)
- (2) Using filament materials with low coefficients of expansion.
- (3) Using a different material for each filament, in order to provide a self-compensating feature (typical of early clock pendulums).
- (4) Using bimetallic compensating components to regulate tension in the suspension.

B. External Magnetic and Electric Fields

Torque constancy — a critical factor when a mechanism is involved in the measuring of extremely small forces — can be enhanced by employing materials that are not sensitive to magnetic or electric fields, by ensuring appropriate processing during manufacture of components, and by providing shielding.

C. Force Fields

If the instrument must operate in an unusual force field, such as those encountered during launch, on a

rotating platform, or in the weightlessness of space, the instrument must be dynamically balanced.

D. Other Adverse Factors

Certain material characteristics and certain other phenomena can have deleterious effects upon suspension stability. These include the following:

- (1) Inelastic creep of suspension material.
- (2) Internal friction, particularly of woven filaments.
- (3) Aging of suspension material.
- (4) Protective coatings (multiple coatings in particular).
- (5) Associated functions (for example, damping of oscillations may produce such effects as asymptotic return to zero position).

E. Geometry and Stability

Suspension stability is also related to the geometry of its parts. To improve stability, inherently null-stable geometries may be incorporated. A filar configuration, for example, can be made more null stable by separating the filaments at either end (or both ends) of the suspension. However, the possible effects of such alterations on other design parameters such as spring rate or shock resistance must be considered. The introduction of revised geometries should be subject to results of trade-off studies of the particular design.

V. Suspension Characteristics

The types of suspension discussed below include torsion, filar, flexure, coil, and combination.

A. Torsion Suspension

This type consists of one or more taut wires of an elastic material. Round wire is commonly used because it permits maximum twist for a given material. Other cross sections can be used if there is need for greater resistance to bending in a particular direction. Table 2 shows characteristics for elliptical as well as round torsion wire; for other configurations, see Ref. 1.

The restoring torque of torsion suspensions is always positive (increase in torque corresponds to increase in angle of twist) but can be made extremely small by using thin synthetic strands or woven thread as the suspension

filament. The relation of torque to twist is linear for relatively large angles of twist. Variation in filament tension affects the restoring torque indirectly by producing, under proper design circumstances, only minute changes in filament diameter.

A practical application of torsion-wire suspension is a magnetic hysteresis damper (Fig. 1)¹ used on satellites

¹The Nomenclature section applies to the figures as well as to Table 2.

oriented by gravity-gradient effect to dampen vibrations during orbit (Ref. 2). Typically, such a double torsion suspension uses high-strength steel wire 2 in. long and 0.008 in. in diameter, with a torsional spring rate of 0.36×10^{-3} ft-lb per radian. The damper consists of two units affixed to each other at right angles. Each unit is free to rotate 60 deg in either direction from the null position. Tension adjustments are provided at the ends of the suspensions to keep the wire taut and preclude axial motion of the suspended parts under a wide range of operating temperatures.

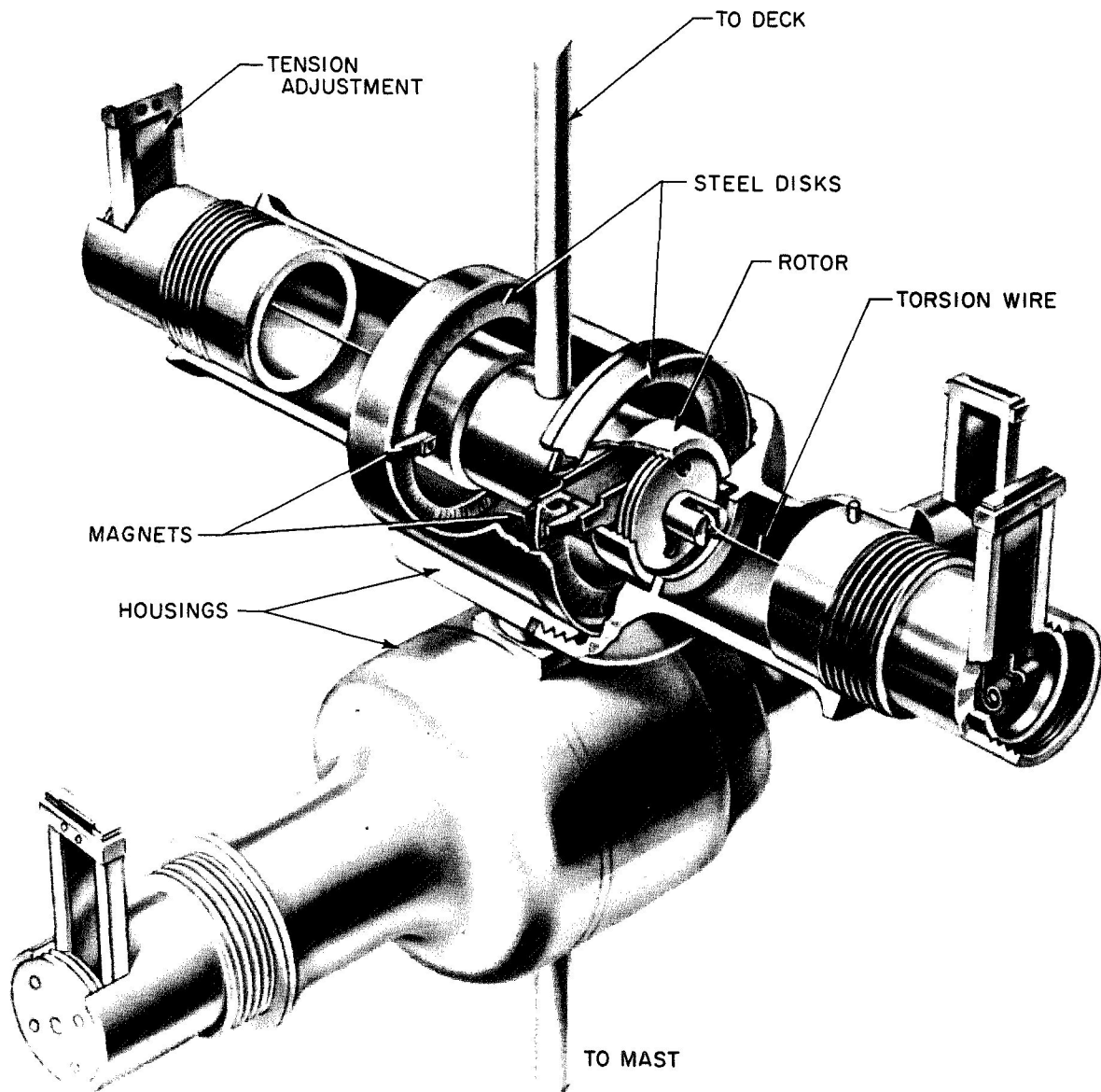


Fig. 1. Torsion-wire suspension used in magnetic hysteresis damper. Each unit contains a double suspension and each is free to rotate 60 deg in either direction from the null position (photograph courtesy of American Telephone and Telegraph Co.)

B. Filar Suspension

Filar suspension employs filament sets consisting of two or more filaments each, the number of sets varying according to design requirements. If parallel motion of the axis of the suspended part is required, a two-set (bifilar) configuration is employed on each side of the part. If parallel motion of the entire configuration is required, a three-set (trifilar) configuration is used on each side. More than three sets are seldom used, except to double as carriers of electricity to a suspended part requiring several connections. Several filar configurations are shown in Fig. 2.

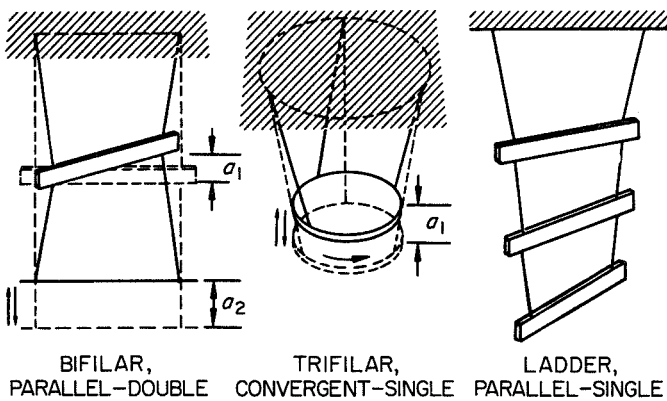


Fig. 2. Typical filar suspension configurations

Accuracy of null positioning and easy adjustment of restoring torque are special advantages of the filar configurations. For a comprehensive discussion of the filar technique, see Ref. 3.

The restoring torque in filar suspensions is derived primarily from tension in the filaments. In filaments of finely woven thread without resistance to torsion and bending, restoring torque is proportional to the sine of the angle of rotation. (The data in Table 2 are based on this assumption.) Fine wire with some elasticity can be used, but the effect of the elasticity on restoring torque must be considered.

Elements of the filar suspension are located along the axis of rotation. Provision must be made for one or both ends to be free to move because of inherent axial motion of the suspension elements. This effect, largest when one end of the suspension is fixed, can magnify motion by converting small axial motion into relatively large rotation.

C. Torsion and Filar Composite Suspension

This type, made up of two or more taut strips side by side, derives its restoring torque from the combined effects of the filar configuration and torsional stress. Composite suspensions can attain better null-positioning accuracy than that provided by torsion suspension alone, while avoiding some of the complexity of the all-filar suspension.

D. Flexure Suspension

This suspension consists of a flat spring supporting a rotating part. The most common configurations are single-strip, two-strip, and three-strip (Fig. 3). They differ mainly in complexity; capability to provide very low, zero, and negative spring rates; and amount of motion of the center of rotation as a function of load and angle of twist.

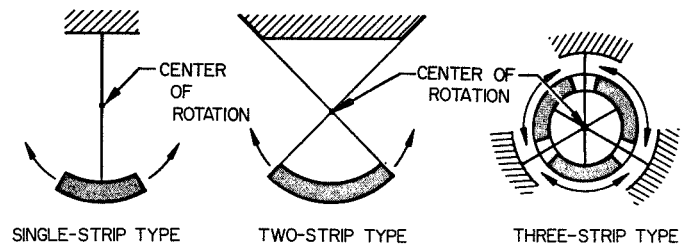


Fig. 3. Flexure suspensions (flat springs that support a rotating part). Three types are shown

1. *Single-strip type.* This configuration has been used for more than a century for suspending pendulums in grandfather clocks. In practice, single-strip flexure suspensions are used only for positive spring rates. The center of rotation changes with angular deflection and load.

2. *Two-strip type.* This type is finding such aerospace applications as suspensions for missile control nozzles and a wide range of ultraprecision spaceborne instruments—from gyroscopes to large telescope assemblies. An external tension load to the strips can produce very low, zero, or negative spring rates; this change of spring rate should be considered in the design of devices that operate in the weightlessness of space but are to be tested on the ground. The location of the center of rotation changes with angular deflection and load by a smaller amount than in single-strip suspension. A two-strip configuration, in which one of the strips has been divided for increased lateral rigidity, is shown in Fig. 4.

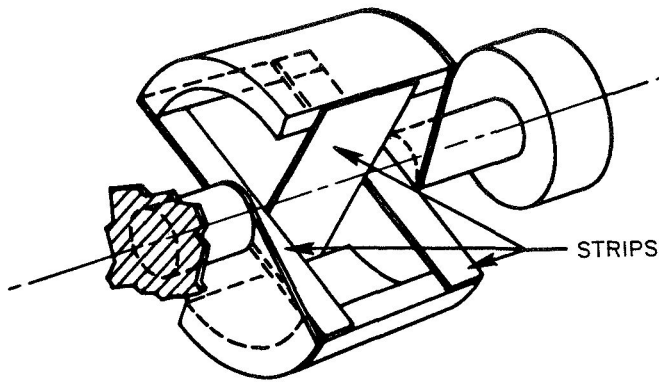


Fig. 4. Two-strip flexure suspension with one strip in one axis and two in the other axis

A recent use of two-strip flexure suspension was one that the author suggested, and NASA adopted, for supporting a telescope mount weighing several tons in an Apollo spacecraft originally scheduled for 1968 launch (Fig. 5). This suspension, employing four flexure pivots, makes possible an extremely precise pointing capability because of its low breakaway torque. It also satisfies the requirement for long service life in a hard-vacuum environment and eliminates the hazard of optical contamination that would be posed by the use of a lubricant on bearings.

3. *Three-strip type.* This complex type is the most versatile of the flexure suspensions. It is adjustable to provide either positive, zero, or negative restoring torques

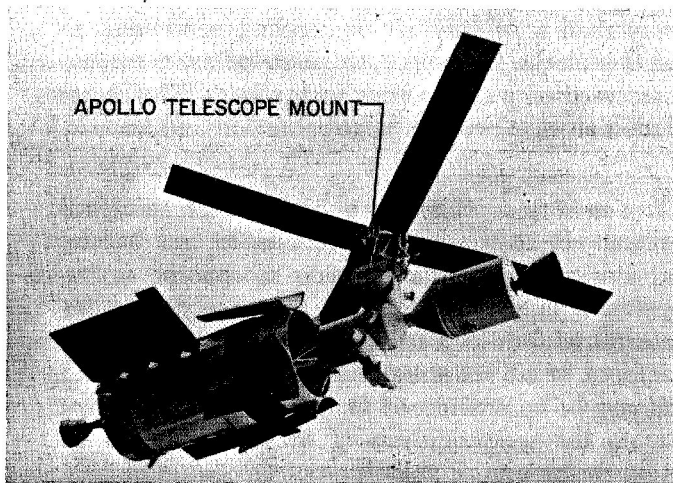


Fig. 5. The Apollo Telescope Mount (ATM) supported on two-strip flexure suspension — a systems concept suggested by the author

even when there is no external load. In theory, deflection of the suspended part does not affect the center of rotation. However, strip misalignment does cause a slight shift of the null position and some motion of the center of rotation when the suspension deflects, and these effects should be taken into account in high-precision designs.

The formulas given in Table 2 for restoring torque assume no axial forces acting on the flexure suspension; for a discussion of other cases, see Ref. 4.

E. Coil Suspension

Coil suspensions may be of the spiral or helical configurations. Spiral springs (Ref. 5), as a sole suspension element, are used only for lightweight parts (Fig. 6). This type is commonly used with very-low-friction bearings, such as conical-pivot bearings (Fig. 7), which limit lateral motion of the suspended part and absorb axial thrust of gravity and shock.

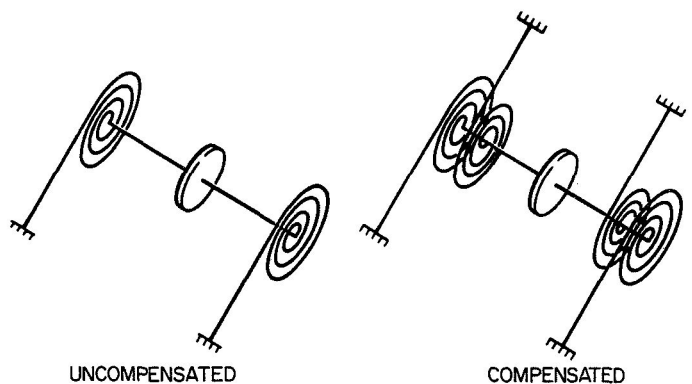


Fig. 6. Spiral spring suspensions

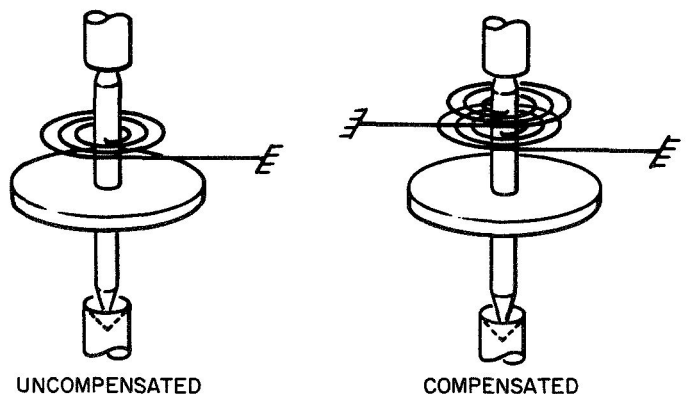


Fig. 7. Spiral spring suspensions with conical bearings

Thermal stability, often the most vital design consideration for aerospace mechanisms, can be improved by the use of pairs of matched, counter-wound, spiral springs; each tends to compensate for the thermal expansion of the other (see Figs. 6 and 7).

Spiral spring data presented in Table 2 apply to springs having many coils that do not touch. Stiffness can be increased by the use of a small number of coils (Ref. 6). Spring rate also increases when coils touch during operation.

Helical spring suspensions employ coiled elastic materials and provide six degrees of freedom to the suspended part (Fig. 8). Typical applications are shock mounts and isolation mounts. Calculation of restoring torques is complicated by the interaction of lateral and longitudinal forces and resulting torques; thus no simple relationships can be developed.

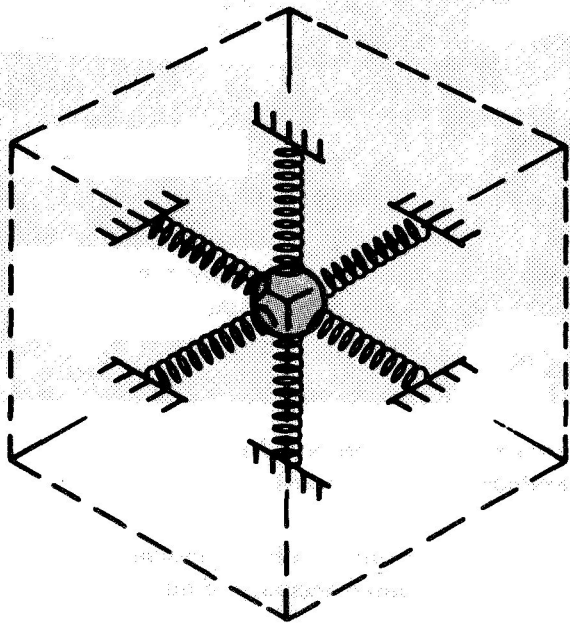


Fig. 8. Helical spring suspension. This type is most often used as a shock isolation mount

F. Combination Suspension

A design can sometimes combine two or more of the principal suspension types. A typical example is a combination of flexure and torsion (or filar) suspension. Such a combination provides a shock mounting for the delicate

wires of low-restoring-torque suspension (Fig. 1). Another example is the use of a bimetallic spring in place of the monometallic flat type to obtain a variable spring rate as a function of temperature. A combination that uses membranes in lieu of flexure suspensions is shown in Fig. 9.

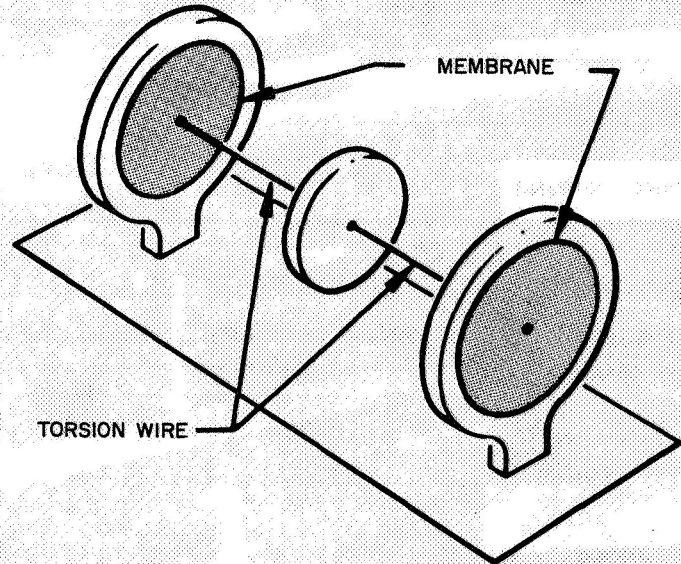


Fig. 9. Combined membrane and torsion-wire suspension

Still another example (Fig. 10) is a device which was designed to simulate quasi-static orbital conditions by providing oscillatory motions with periods of one hour or longer. It is basically a torsional pendulum having large inertia, which is acted upon by a low restoring torque. The restoring torque is provided mainly by the spiral spring, since the spring rate of the torsion wire is much smaller. Very small torques can be applied to the suspended assembly by rotating the end of the spiral spring attached to the rotary table.

VI. Summary

A summary of the characteristics of the most common mechanical suspensions is given in Table 2. Some comments to aid in interpreting the table are listed below.

In the first column of Table 2, "single" and "double" indicate whether the part hangs on a single suspension or is suspended at both ends. Equations for double-suspension types were developed on the assumption that both suspending elements are made of identical material.

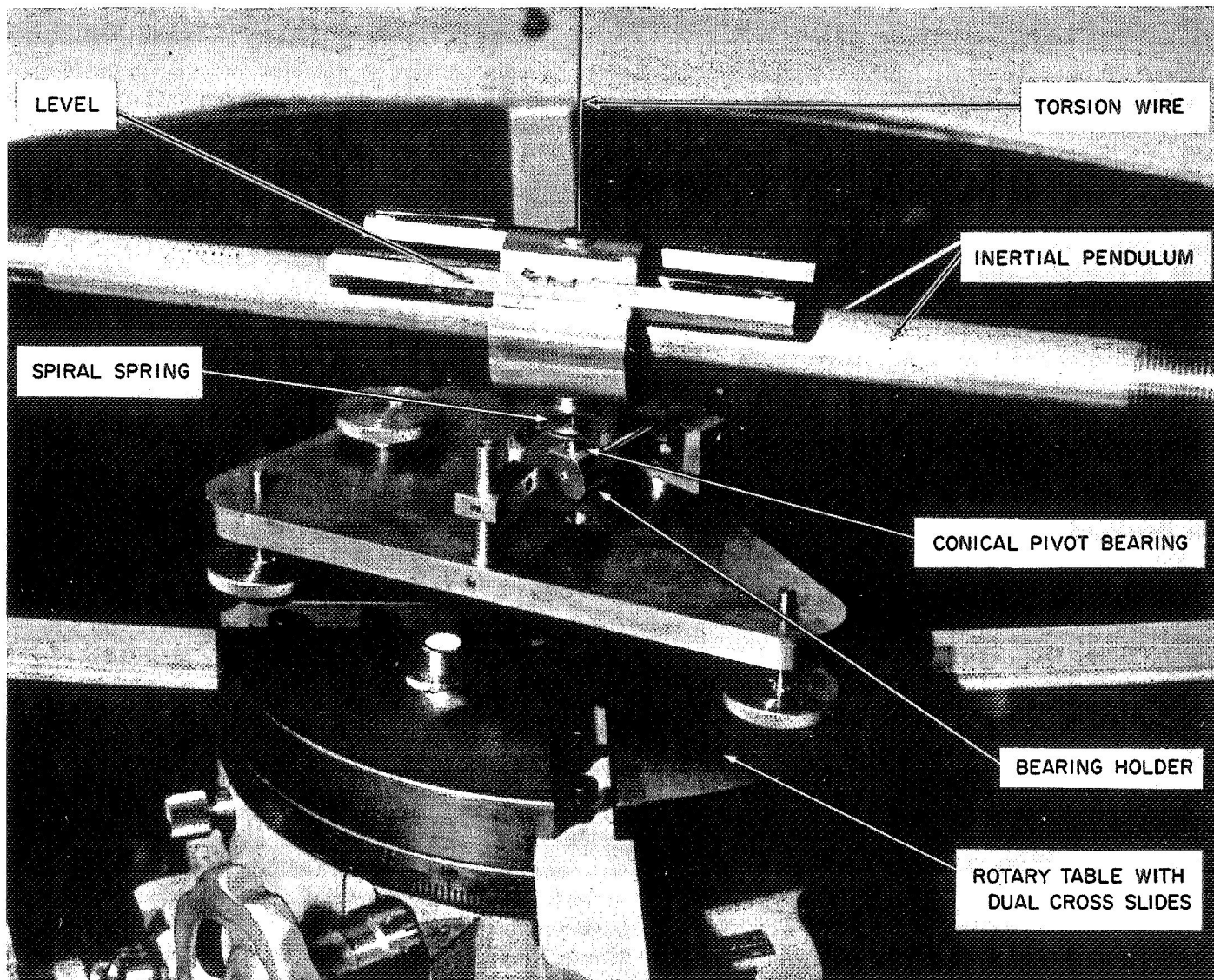


Fig. 10. Torsion wire and spiral-spring suspensions in an orbital simulator designed by the author (photograph courtesy of Philco-Ford Western Development Laboratories)

“Installation configuration” indicates whether the suspension elements are along the axis of rotation or in the radial direction.

“Source of restoring torque” shows only the principal source; the equations disregard secondary sources.

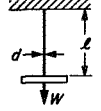
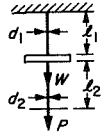
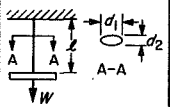
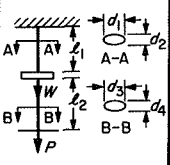
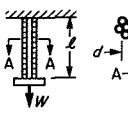
“Approximate permissible twist” values are indicative only of the range in which restoring torque is linearly proportional to deflection, and for which no permanent deformation occurs. These values should be used only for the initial selection of a suspension type, since actual

range can vary significantly with suspension complexity and configuration, required accuracy of null position, and restoring torque.

“Axial motion” refers to motion of the suspended part toward the fixed-suspension end; one end of the suspension is assumed to be fixed and the other able to move axially. (Axial motion of the part can be eliminated by providing for symmetrical motion of both ends of the suspension.)

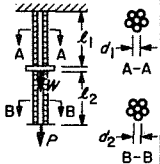
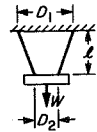
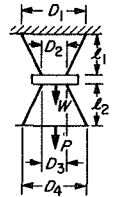
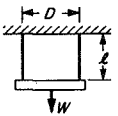
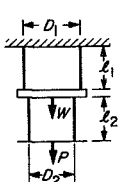
“Null position accuracy” ratings indicate only the relative merit of each type.

Table 2. Characteristics of mechanical suspensions

Type	Sketch	Installation configuration	Source of restoring torque	Restoring torque	Approximate permissible twist	Axial motion ^a		Null positioning accuracy ^b
						Suspended part	Moving end of suspension	
Torsion wire, circular cross section—single		Axial	Shear stress	$\frac{\pi}{32} G \frac{d^4}{l} \theta$	± 1 turn	$\frac{d^2}{16l} \theta^2$	—————	B-C
Torsion wire, circular cross section—double		Axial	Shear stress	$\frac{\pi}{32} G \left(i_1 \frac{d_1^4}{l_1} + i_2 \frac{d_2^4}{l_2} \right) \theta$	± 1 turn	$\frac{d_1^2}{16l_1} \theta^2$	$\frac{1}{16} \left(\frac{d_1^2}{l_1} + \frac{d_2^2}{l_2} \right) \theta^2$	B-C
Torsion wire, elliptical cross section—single		Axial	Shear stress	$\frac{\pi}{16} G \frac{d_1^2 d_2^2}{d_1^2 + d_2^2} \frac{1}{l} \theta$	± 1/2 turn	$\frac{1}{8l} \frac{d_1^2 d_2^2}{d_1^2 + d_2^2} \theta^2$	—————	B
Torsion wire, elliptical cross section—double		Axial	Shear stress	$\frac{\pi}{16} G \left(\frac{d_1^2 d_2^2}{d_1^2 + d_2^2} \frac{1}{l_1} + \frac{d_3^2 d_4^2}{d_3^2 + d_4^2} \frac{1}{l_2} \right) \theta$	± 1/2 turn	$\frac{1}{8l_1} \frac{d_1^2 d_2^2}{d_1^2 + d_2^2} \theta^2$	$\frac{1}{8} \left[\frac{d_1^2 d_2^2}{(d_1^2 + d_2^2) l_1} + \frac{d_3^2 d_4^2}{(d_3^2 + d_4^2) l_2} \right] \theta^2$	B
Torsion filament bundle—single		Axial	Shear stress	$\frac{\pi}{32} i G \frac{d^4}{l} \theta$	± 10 turns	$\frac{k^2}{2l} \theta^2$	—————	C

^aAssuming one suspension-end to be fixed.
^bNull positioning accuracy ratings: C—good, B—very good, A—excellent.

Table 2 (contd)

Type	Sketch	Installation configuration	Source of restoring torque	Restoring torque	Approximate permissible twist	Axial motion ^a		Null positioning accuracy ^b
						Suspended part	Moving end of suspension	
Torsion filament bundle—double		Axial	Shear stress	$\frac{\pi}{32} G \left(i_1 \frac{d_1^4}{l_1} + i_2 \frac{d_2^4}{l_2} \right) \theta$	± 10 turns	$\frac{k_1^2}{2l_1} \theta^2$	$\frac{1}{2} \left(\frac{k_1^2}{l_1} + \frac{k_2^2}{l_2} \right) \theta^2$	C
Bifilar and trifilar, nonparallel—single		Axial	Axial force	$\frac{1}{4} W \frac{D_1 D_2}{l} \sin \theta$	± 90 deg (max)	$l - \left(l^2 - D_1 D_2 \sin^2 \frac{\theta}{2} \right)^{1/2}$	—————	A
Bifilar and trifilar, nonparallel—double		Axial	Axial force	$\frac{1}{4} \left[(W + P) \frac{D_1 D_2}{l_1} + P \frac{D_3 D_4}{l_2} \right] \sin \theta$	± 90 deg (max)	$l_1 - \left(l_1^2 - D_1 D_2 \sin^2 \frac{\theta}{2} \right)^{1/2}$	$l_1^2 + l_2^2 - \left(l_1^2 - D_1 D_2 \sin^2 \frac{\theta}{2} \right)^{1/2} - \left(l_2^2 - D_3 D_4 \sin^2 \frac{\theta}{2} \right)^{1/2}$	A
Bifilar and trifilar, parallel—single		Axial	Axial force	$\frac{1}{4} W \frac{D^2}{l} \sin \theta$	± 90 deg (max)	$l - \left(l^2 - D^2 \sin^2 \frac{\theta}{2} \right)^{1/2}$	—————	A
Bifilar and trifilar, parallel—double		Axial	Axial force	$\frac{1}{4} \left[(W + P) \frac{D_1^2}{l_1} + P \frac{D_2^2}{l_2} \right] \sin \theta$	± 90 deg (max)	$l_1 - \left(l_1^2 - D_1^2 \sin^2 \frac{\theta}{2} \right)^{1/2}$	$l_1^2 + l_2^2 - \left(l_1^2 - D_1^2 \sin^2 \frac{\theta}{2} \right)^{1/2} - \left(l_2^2 - D_2^2 \sin^2 \frac{\theta}{2} \right)^{1/2}$	A

^aAssuming one suspension-end to be fixed.^bNull positioning accuracy ratings: C—good, B—very good, A—excellent.

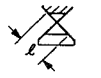
Table 2 (contd)

Type	Sketch	Installation configuration	Source of restoring torque	Restoring torque	Approximate permissible twist	Axial motion ^a		Null positioning accuracy ^b
						Suspended part	Moving end of suspension	
Bifilar and trifilar ladder, parallel—single		Axial	Axial force	$\frac{1}{4} W m \frac{D^2}{l} \sin \frac{\theta}{m}$	± 90 m deg (max)	$l - \left(l^2 - m^2 D^2 \sin^2 \frac{\theta}{2m} \right)^{1/2}$	—	A-B
Bifilar and trifilar ladder, parallel—double		Axial	Axial force	$\frac{1}{4} \left[(W + P) m_1 \frac{D_1^2}{l_1} \sin \frac{\theta}{m_1} + P m_2 \frac{D_2^2}{l_2} \sin \frac{\theta}{m_2} \right]$	Smaller of ± 90 m ₁ and ± 90 m ₂ deg (max)	$l_1 - \left(l_1^2 - m_1^2 D_1^2 \sin^2 \frac{\theta}{2m_1} \right)^{1/2}$ $l_2 - \left(l_2^2 - m_2^2 D_2^2 \sin^2 \frac{\theta}{2m_2} \right)^{1/2}$	$l_1^2 + l_2^2 - \left(l_1^2 - m_1^2 D_1^2 \sin^2 \frac{\theta}{2m_1} \right)^{1/2} - \left(l_2^2 - m_2^2 D_2^2 \sin^2 \frac{\theta}{2m_2} \right)^{1/2}$	A-B
Filar and torsion composite, multistrip—single		Axial	Shear stress and axial force	$\left(\frac{1}{3} G \frac{b^3}{n^2 l} + \frac{1}{12} W \frac{b^3}{l} \right) \theta$	± 30 deg	$\frac{k^2}{2l} \theta^2$	—	A-B
Filar and torsion composite, multistrip—double		Axial	Shear stress and axial force	$\left\{ \frac{1}{3} \left(\frac{b_1^3}{n_1^2 l_1} + \frac{b_2^3}{n_2^2 l_2} \right) G + \frac{1}{12} \left[(W + P) \frac{b_1^3}{l_1} + P \frac{b_2^3}{l_2} \right] \right\} \theta$	± 30 deg	$\frac{k_1}{2l_1} \theta^2$	$\frac{1}{2} \left(\frac{k_1}{l_1} + \frac{k_2}{l_2} \right) \theta^2$	A-B

^aAssuming one suspension-end to be fixed.

^bNull positioning accuracy ratings: C—good, B—very good, A—excellent.

Table 2 (contd)

Type	Sketch	Installation configuration	Source of restoring torque	Restoring torque	Approximate permissible twist	Axial motion ^a		Null positioning accuracy ^b
						Suspended part	Moving end of suspension	
Flexure, one strip		Radial	Bending stress	$E \frac{bt^3}{12l} \theta$	± 20 to 30 deg	≈ 0	_____	A-B
Flexure, two strip		Radial	Bending stress	$E \frac{bt^3}{6l} \theta$	± 20 to 30 deg	≈ 0	_____	A
Flexure, three strip		Radial	Bending stress	$E \frac{bt^3}{4l} \theta$	± 20 to 30 deg	≈ 0	_____	A
Coil, spiral spring		Radial	Bending stress	$E_i \frac{bt^3}{12l} \theta$	± 1 turn	≈ 0	_____	A-B

^aAssuming one suspension-end to be fixed.
^bNull positioning accuracy ratings: C—good, B—very good, A—excellent.

Nomenclature

<i>a</i>	axial motion, in.	<i>l</i>	length, in.
<i>b</i>	width of strip or coil, in.	<i>m</i>	number of steps of ladder suspension
<i>c</i>	diameter of wire or filament, in.	<i>n</i>	number of strips in multistrip suspension
<i>D</i>	diameter of suspension attachment, in.	<i>P</i>	external load, lb
<i>E</i>	modulus of elasticity, psi	<i>t</i>	total thickness of strip or of composite strip, in.
<i>G</i>	modulus of rigidity, psi	<i>W</i>	weight, lb
<i>i</i>	number of wires in strand	θ	angle of deflection, deg
<i>j</i>	number of spiral springs in suspension		
<i>k</i>	radius of gyration, in.		

Subscripts 1, 2, 3, 4 refer to parts of suspensions.

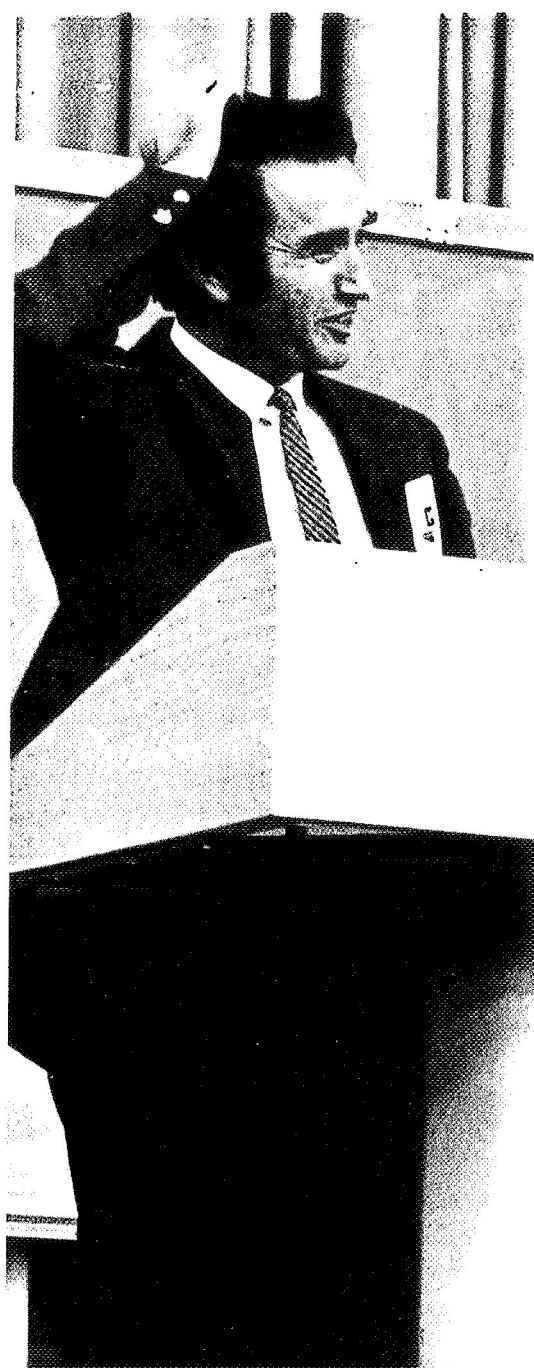
References

1. Chironis, N. P., *Spring Design and Application*, p. 141, McGraw-Hill Book Co., Inc., New York, 1961.
2. Paul, B., West, J. W., and Yu, E. Y., "A Passive Gravitational Attitude Control System for Satellites," *Bell Syst. Tech. J.*, Vol. 42, No. 5, p. 2204, Sept. 1963.
3. Geary, P. J., *Torsion Devices*, British Scientific Instrument Research Association, 1954. (Extensive bibliography lists other references.)
4. Weinstein, W. D., "Flexure-Pivot Bearings, Part 1," *Machine Des.*, Vol. 37, No. 13, June 10, 1965; "Part 2," Vol. 37, No. 16, July 8, 1965.
5. Wahl, A. M., *Mechanical Springs*, Second Edition. McGraw-Hill Book Co., Inc., New York, 1963.
6. Kroon, R. P., and Davenport, C. C., "Spiral Springs With Small Number of Turns," *J. Franklin Inst.*, Vol. 225, p. 171, 1938.

Selected Bibliography

- Herzl, G. G., "How to Design for Minimum Torque in Pivot Bearings," *Machine Des.*, Vol. 37, No. 28, pp. 146-152, Dec. 9, 1965.
- Herzl, G. G., "Conical Pivot Bearings for Space Applications," *Proceedings of the First Aerospace Mechanisms Symposium*, University of Santa Clara, Santa Clara, Calif., May 1966.
- Herzl, G. G., "Instrument Suspensions," *Machine Des.*, Vol. 39, No. 2, pp. 182-191, Jan. 19, 1967.
- Herzl, G. G., "Theory of Flexure Pivot With Displaced Center of Rotation," to be published in *Machine Des.*

PRECEDING PAGE BLANK NOT FILMED.



Session III

Preceding page blank

OVERLEAF: *Bernard Roth, Stanford University, Session Chairman*

N 69-11814

Mechanical Design of the Spin-Scan Cloud Camera

D. T. Upton

Santa Barbara Research Center
A Subsidiary of Hughes Aircraft Company
Goleta, California

The development and design of two Spin-Scan Cloud Cameras, successfully operating at a 23,000-statute-mile synchronous altitude, are described. The first, a single-color camera (black and white pictures), was launched from Cape Kennedy on December 6, 1966. This camera is still in daily use and has provided many thousands of high-resolution pictures. The second, a multicolor camera, was launched on November 6, 1967. Use of the satellite spin, combined with a precision step mechanism to obtain pictures of the earth's cloud cover, is described in detail.

I. Introduction

Early in 1965, personnel from the University of Wisconsin, Hughes Aircraft's Space Systems Division, and the Santa Barbara Research Center investigated concepts to provide high-resolution pictures of the earth's cloud cover from synchronous altitude. The result was the Spin-Scan Cloud Cameras, which are carried on *Applications Technology Satellites* (ATS) and have provided thousands of such pictures (Fig. 1).

The *Application Technology Satellites* B and C, designed and built by Hughes Aircraft's Space Systems Division for the NASA Goddard Space Flight Center, are spin-stabilized spacecraft which rotate with their spin axes parallel to the earth's rotational axis. The con-

cept was to capitalize on this feature and use the 100-rpm spin of the spacecraft to provide the horizontal, or longitudinal, sweep as one component of a scan raster. The second component, the vertical step, would be incorporated in the camera mechanism. By utilizing the spinning spacecraft and a stepping camera, a picture would be generated much in the same manner as a television picture.

II. Functional Description

The black and white camera, Fig. 2, consists of a high-resolution telescope and a light detector or detectors coupled with a step mechanism. The latitudinal, or vertical, step mechanism advances one step for each spacecraft revolution. When the step mechanism has completed

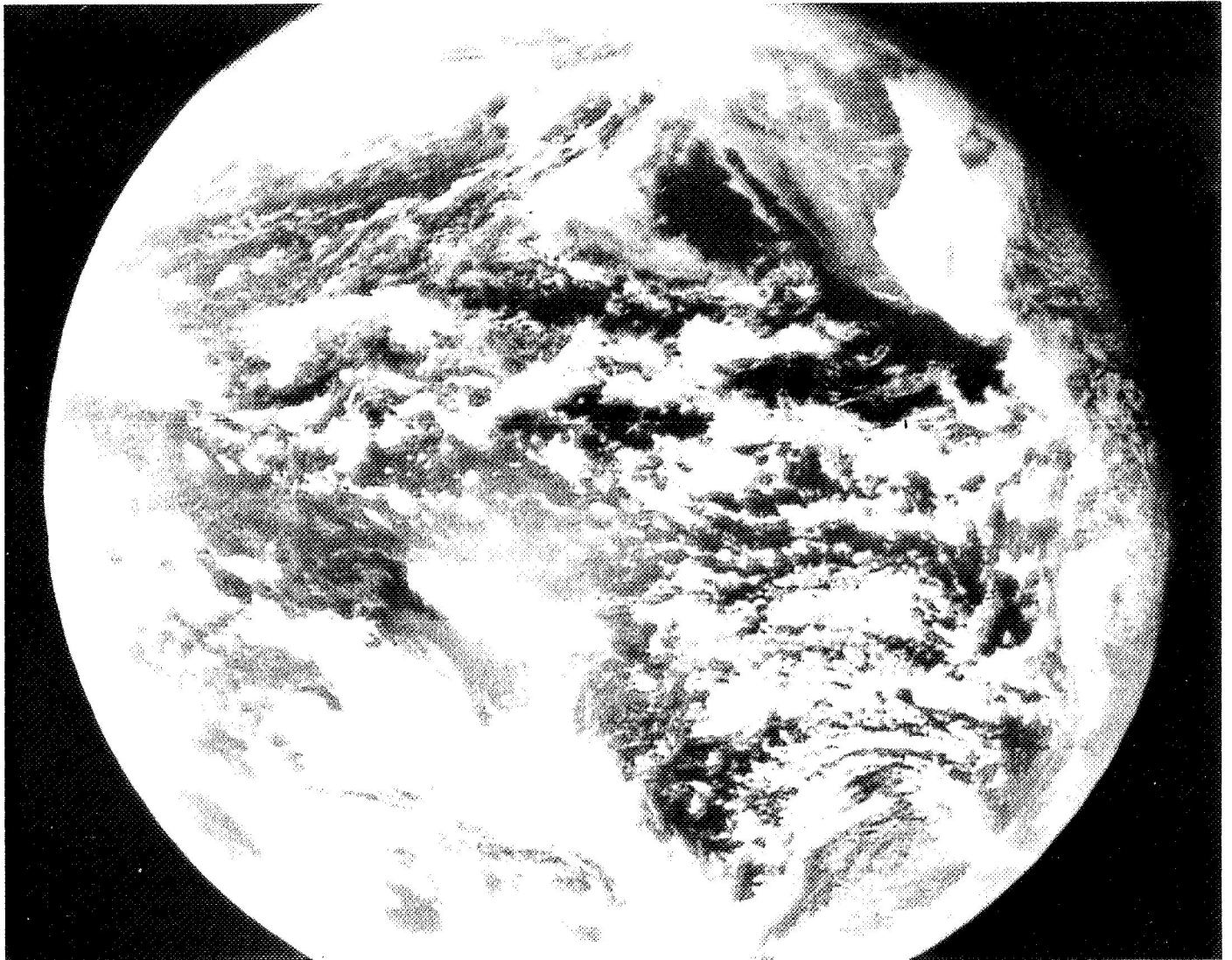


Fig. 1. View of the earth taken from ATS-1 spacecraft in a synchronous equatorial orbit, 19,300 nautical miles altitude

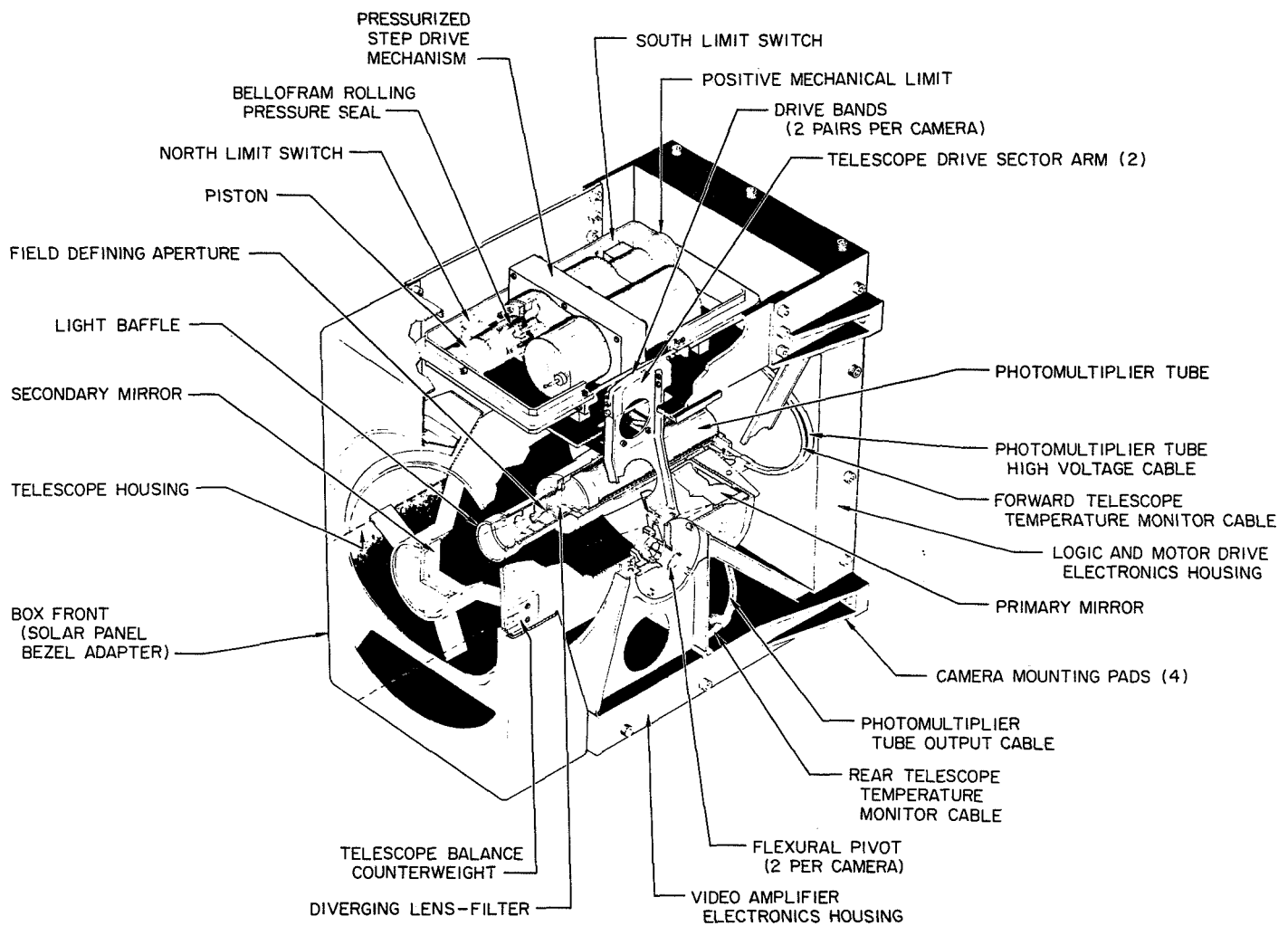


Fig. 2. Cutaway drawing of the single-color Spin-Scan Cloud Camera (SSCC)

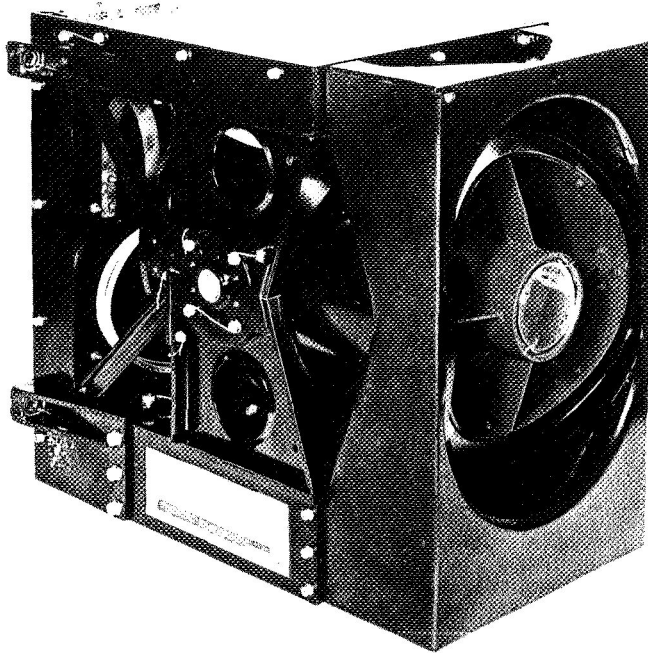


Fig. 3. Single-color Spin-Scan Cloud Camera

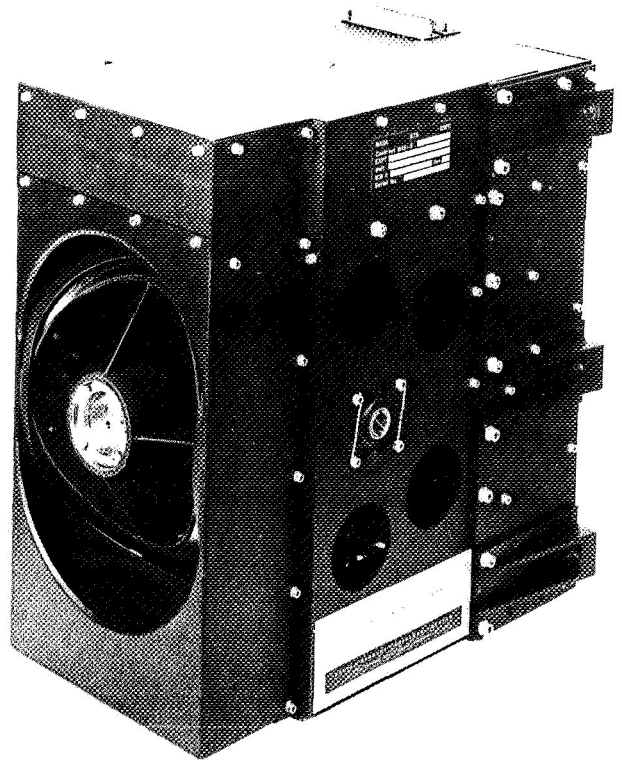


Fig. 4. Multicolor Spin-Scan Cloud Camera (MSSCC)

2000 steps in approximately 20 min, a limit switch initiates retrace and the telescope returns to the top or north latitude position. At this point, another limit switch starts the normal north-south stepping in synchronism with spacecraft rotation. Figure 3 shows the assembled black and white camera. The multicolor camera, Fig. 4, scans the full earth disk and requires 2400 steps, approximately 24 min, to complete one picture.

III. Mechanical Description

The mechanical design requires a high degree of precision in only two areas: (1) the spacing and mounting of the optical elements into the telescope housing and (2) certain parts of the precision step mechanism.

The two cameras are identical in every major respect except in the number of photomultiplier tubes required. Figure 5 shows the relationship between the telescope and the single photomultiplier tube required for the black and white camera, and Fig. 6 shows the photomultiplier tube housing, located aft of the telescope, supporting the three photomultipliers required on the color camera. Figure 6 also shows the block closing the end of

the tube housing and forming one end of the fiber optics bundle which relays the energy to each photomultiplier tube. The fiber optics bundle (Fig. 7) consists of three 0.005-in.-diameter glass fibers. These are terminated in the telescope behind an aperture plate (Fig. 8) containing three 0.0015-in.-diameter holes spaced 0.010 in. apart. The apertures lie in a plane normal to the spacecraft's spin axis. The fiber optics permit relative motion between telescope and photomultiplier tubes.

A. Telescope

The telescope is the only component in each camera that is sensitive to the temperature extremes likely to be encountered in the hostile environment of space. To maintain the 0.1-mrad optical resolution, the telescope housing assembly is fabricated from Invar 36 steel alloy. The longitudinal shift permitted is on the order of 0.0003 in. The thermal characteristics of this material closely match those of the quartz optical elements. The telescope assembly consists of a tube, a secondary mirror housing with support legs brazed into the forward end of the telescope tube, and a primary mirror support plate bolted to the aft end.

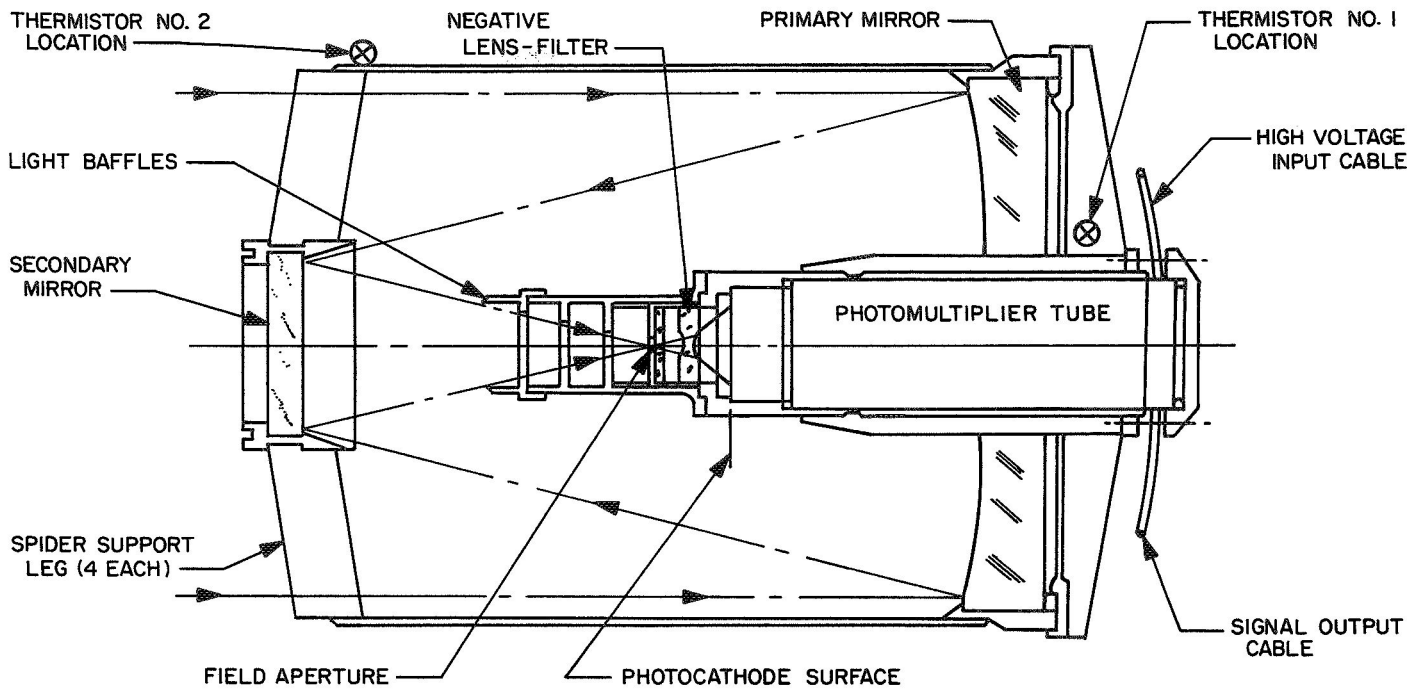


Fig. 5. Cross section of telescope assembly, SSCC

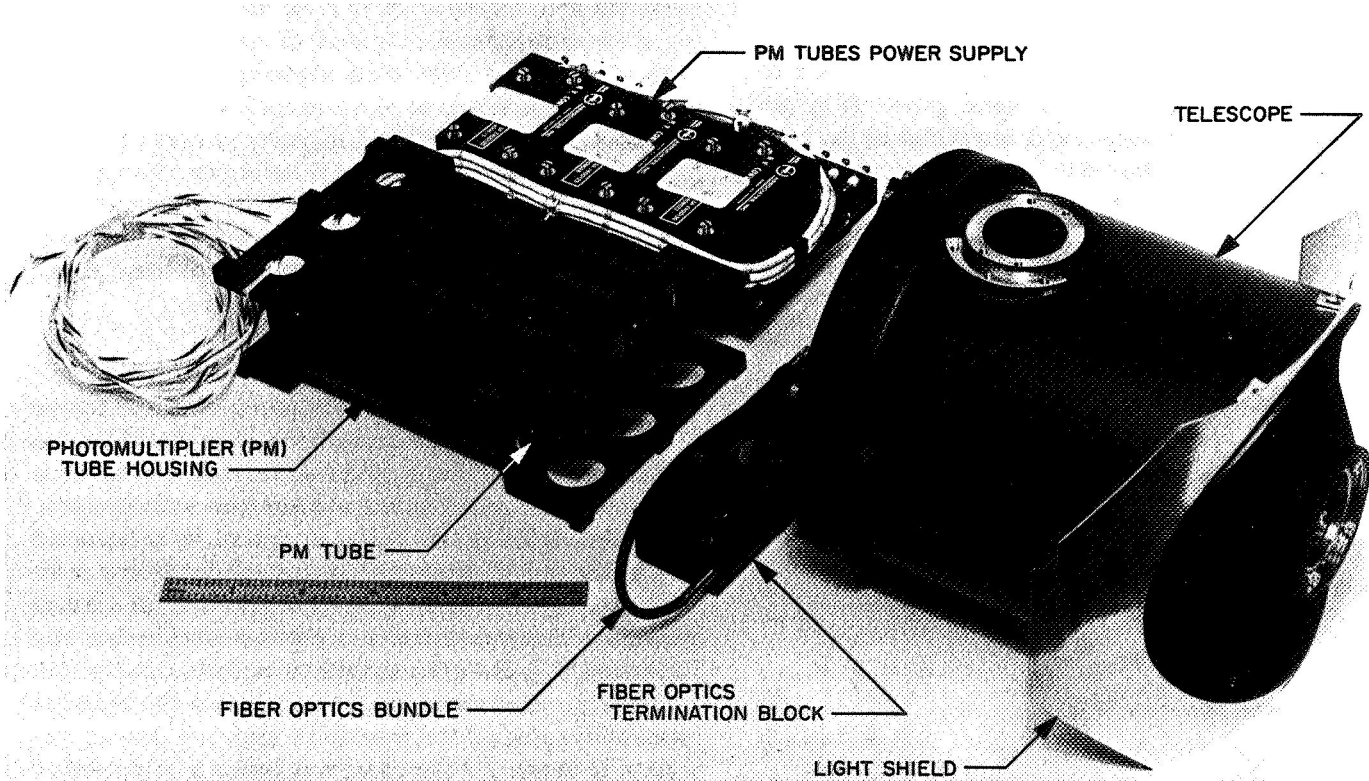


Fig. 6. Multicolor camera telescope and photomultiplier tube housing

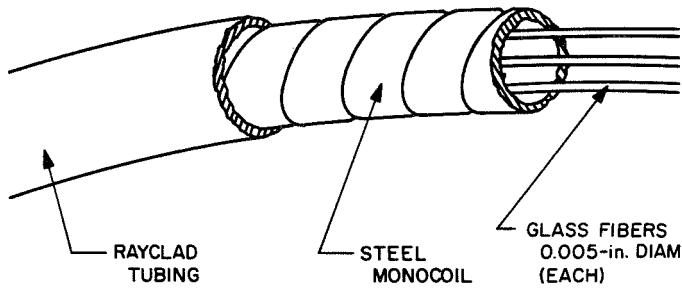


Fig. 7. Fiber optics housing, MSSCC

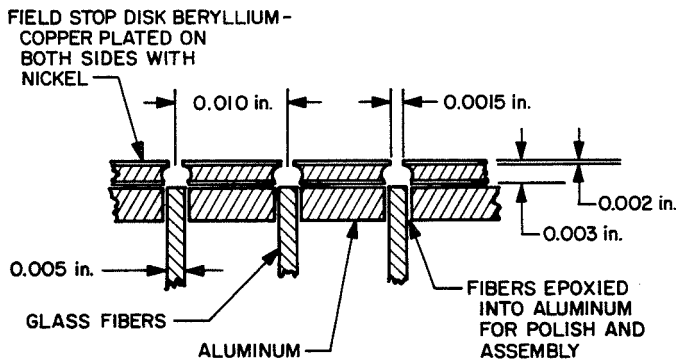


Fig. 8. Field stop, MSSCC

The telescope assembly is supported at its center of gravity by two double-ended, flexural pivots (Fig. 9). Two sector arms are attached and registered to the telescope at these pivot points. The sector arms roll on the drive frame, which is part of the step mechanism, and are attached to the drive frame by drive bands. These

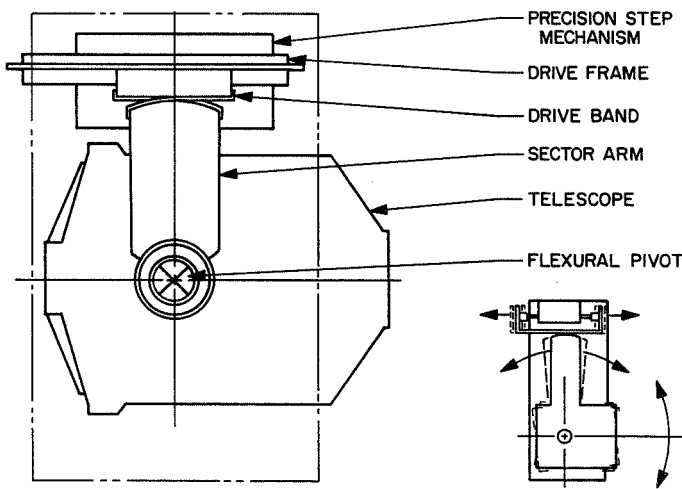


Fig. 9. Schematic showing sector arms, drive bands, and flexural pivots, MSSCC

bands, two on each sector arm, permit roll action but are pulled tight to eliminate backlash. The radius of the sector arms is governed in part by the large reduction ratio required in the step mechanism and in part by the physical clearance needed between telescope and drive.

In synchronous orbit, the camera is constantly subjected to a centrifugal force approximately six times gravity due to the 100-rpm spin of the spacecraft. To obtain full earth coverage, the telescope requires ± 9 deg of angular motion. Flexural pivots, properly oriented, are ideal for this application. They permit the required angular motion and yet provide adequate radial support with no radial play. Any radial play in the telescope pivot bearings would introduce error in the step linearity and step position repeatability. The flexural pivots and the drive bands are ideally suited to the hostile environment of space.

B. Precision Step Mechanism

The basic step drive consists of a stepper motor, 90 deg per step, 2000 steps required, coupled to a precision rotating nut through a 10.1:1 gear reduction. The rotating nut drives a precision lead screw having 40 threads/in. To obtain a complete earth scan by the multicolor camera, these values were extended to ratios of 10:1, with 50 threads/in. and 2400 steps required. The lead screw causes the drive frame to move linearly 0.0006 in. (black and white camera) and 0.0005 in. (color camera) per step. This linear travel, coupled to the telescope through the sector arms, translates this straight-line motion into rotary motion to provide the required 27 seconds of arc per step at the telescope. The average repeatability of the drive is better than one step in 2000 steps.

The overall reduction from the 90 deg/step of the motor to the 27 seconds of arc required at the telescope is 12,000:1. To obtain maximum life from the precision lead screw, nut, bearings, gears and motor, the drive is lubricated, pressurized to two atmospheres with nitrogen, and sealed. To allow the linear motion to be transmitted from the sealed drive, two rolling diaphragms are used. To each end of the lead screw is attached an aluminum piston which travels inside a stainless steel cylinder. The diaphragm rolls between these two surfaces. The piston supports the diaphragm on the inside and the cylinder provides support on the outside so that only the curved portion between the piston and cylinder is subjected to the pressure differential. The calculated leak rate of the diaphragms is 4×10^{-6} cm³/s, or an operating life of approximately 3 years.

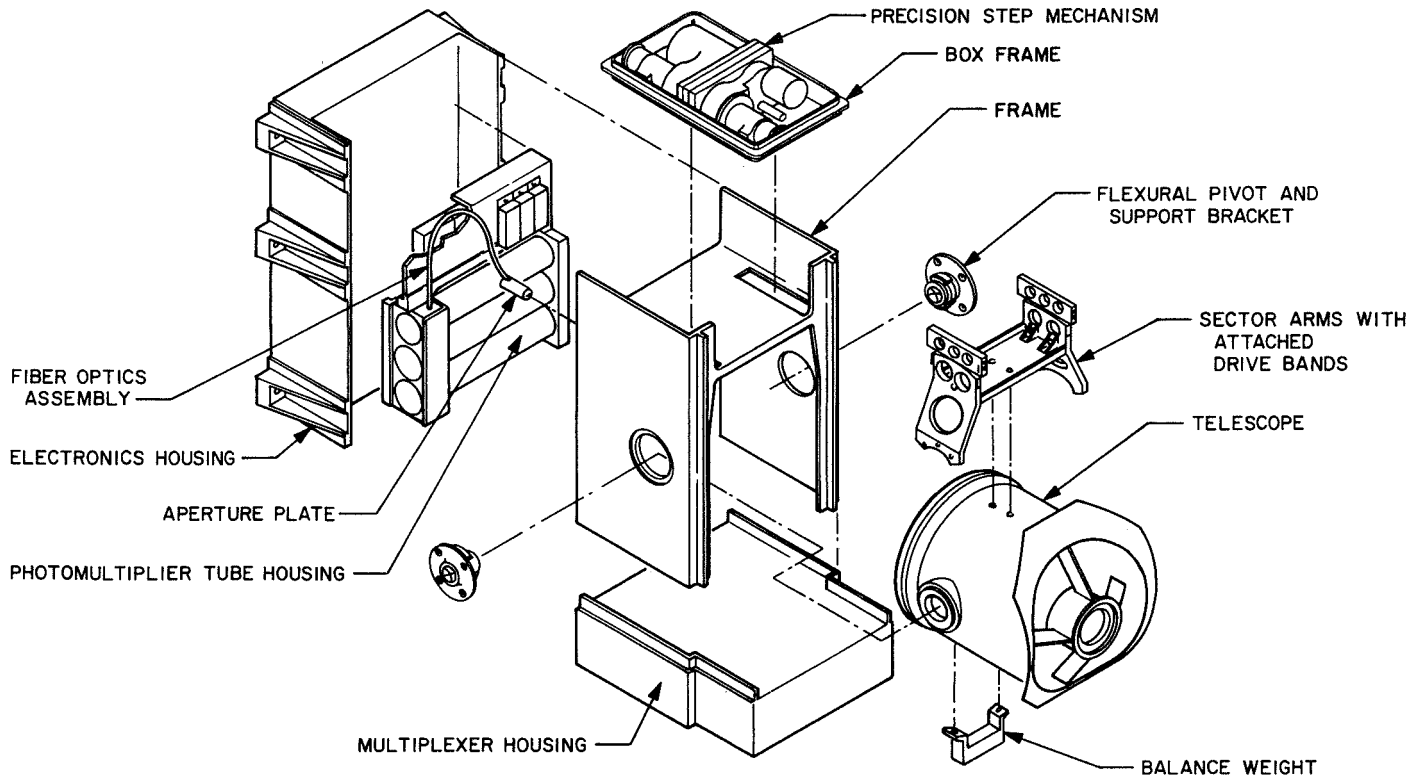


Fig. 10. Exploded view, major mechanical components, MSSCC

C. Frame and Electronics Housing of Color Camera

Figure 10 shows the major components of the color camera. The outside dimensions are 12 in. in height, 7 in. in width and 11 in. in depth. The camera weighs 23.5 lb. (The black and white camera is only 10 in. high and weighs 20 lb.)

Aluminum plates, dip brazed to form a structure, support the step drive mechanism and provide a housing for the electronics.

IV. Conclusion

Simplicity was the keynote of the total program. A straightforward design approach, standard fabricating techniques, high precision only where required, and reasonable tolerances wherever possible produced an excellent instrument of high reliability. More than a year's operation for the black and white camera, which is still operating, proves the adequacy of the lubrication sealing technique. Examination of both color and black and white pictures indicates that focus was indeed held.

PRECEDING PAGE BLANK NOT FILMED.

N 69-11815

A Passive Solar Panel Orientation Servomechanism

R. L. Samuels
TRW Systems Group
Redondo Beach, California

This study presents the design of a servomechanism containing only passive elements designed to orient a solar power panel and maintain sun "lock" without the use of electronic or electromechanical devices or wiring. No expenditure of spacecraft power is required, while torques in the order of 30 in.-lb are readily obtainable with reasonable tracking resolution and pointing accuracy.

This proposed mechanism consists of two basic components: a thermal power piston and housing and a bimetallic sun sensor. These components are linked together to provide a unique closed-loop thermomechanical servomechanism.

I. Introduction

The trend of the modern spacecraft must be towards passive systems. Complex, sophisticated electromechanical systems, while they gladden the heart of the mechanical design engineer, suffer seriously when confronted with the reality of a reliability study parts count and failure mode analysis.

In an effort to find a unique solution to a problem usually solved by electromechanical subsystems requiring relatively heavy power drains, a servomechanism (Fig. 1) utilizing the direct conversion of solar thermal energy to mechanical effort was derived.

II. Mechanism Description

This mechanism¹ consists of two basic components:

- (1) Thermal power piston and housing.
- (2) Thermomechanical sun aspect sensor.

These components (see Fig. 2), linked together, provide a unique closed-loop thermomechanical servomechanism capable of the moderate positioning accuracies quite suitable for solar panel operation (typically within ± 5 deg of sun normality).

¹Subject of a TRW patent application.

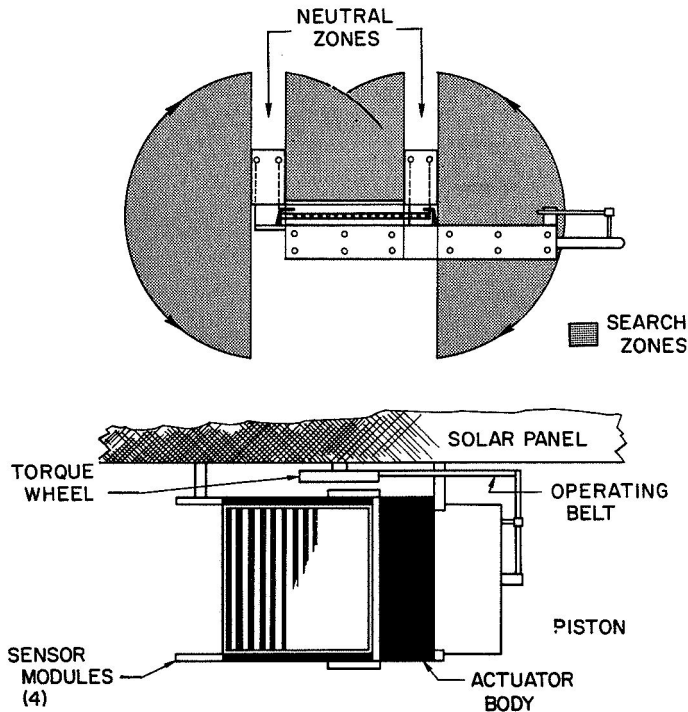


Fig. 1. Operational configuration of passive solar panel orientation system

A. Power Piston Assembly

The basic power piston operates in a cylinder machined in the center web of an H-section slab of aluminum alloy (Fig. 2, No. 1). The cylinder cavity is filled with a suitable fluid such that an increase in fluid temperature results in piston (No. 2) extension in a linear relationship to temperature rise. Similarly, a cooling of the fluid allows retraction of the piston by a torque spring (No. 13) with hysteresis errors of less than 0.5%.

The aluminum body is coated with a high-absorptivity finish on the upper surface and a highly emissive coating on the lower face. The cavities between the upper and lower fins (No. 21) are filled with a sandwich baffle of superinsulation to prevent radiation between surfaces X and Y. Thus any heat flow must take place through the central web containing the piston assembly and operating fluid. Attached to the piston rod is the cross-link (No. 17), which is connected to the torque pulley (No. 16) via a metal operating belt (No. 11).

Therefore, any extension of the power piston results in an increase in belt tension, thereby rotating the solar panel (to which the body assembly is rigidly attached)

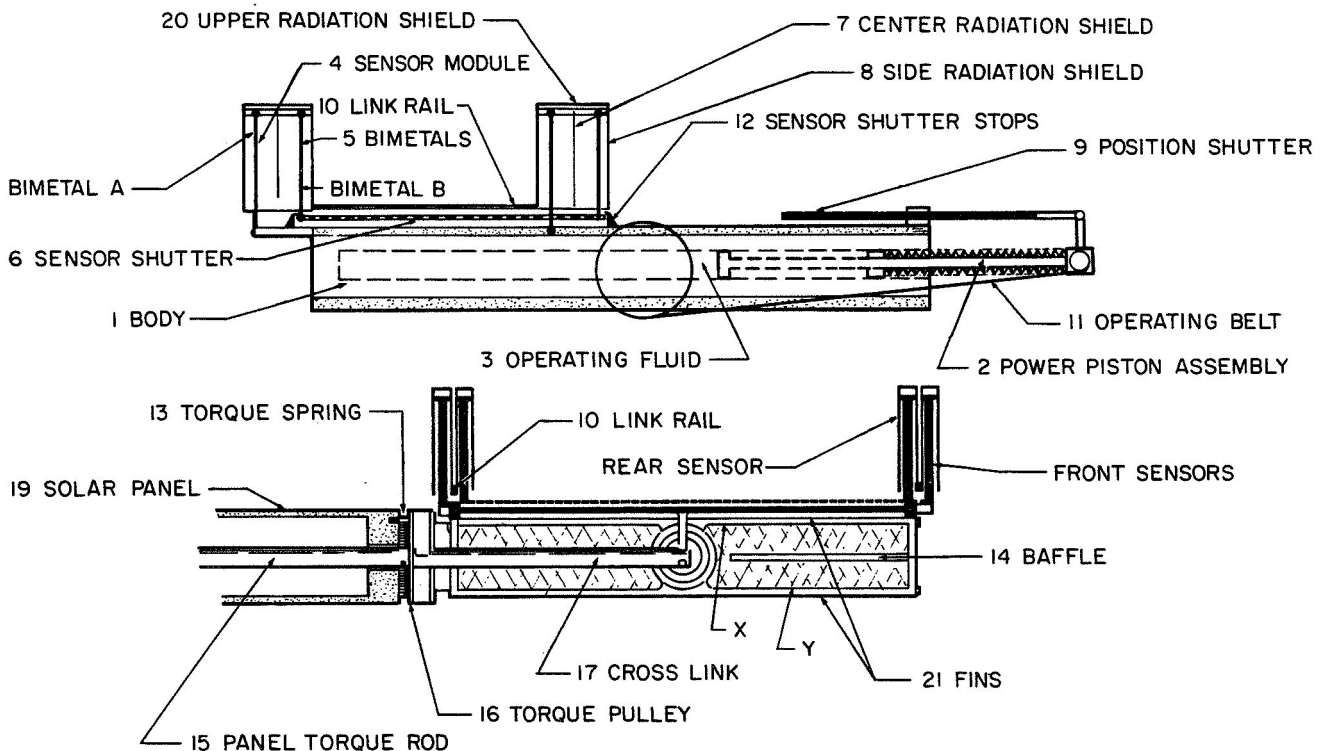


Fig. 2. Passive solar panel orientation servomechanism

around the panel torque rod, which is in turn bolted to the spacecraft structure.

Attached to the piston assembly (No. 2) is the position shutter, which rides in Teflon bushes on the upper surface of the aluminum body. Movement of the piston (following body heat-up or cool-down due to sensor action) will correct body heat balance to retain the new position by covering or uncovering the correct amount of absorptive upper surface. The sensor will of course return to neutral on sensing normal sunlight.

B. Sensor Assembly and Operation

The sensor assemblies control a shutter (No. 6) which, with "normal" sun radiation, covers a portion of the area of the absorptive body surface allotted to directional control of the system. Each sensor module consists of two bimetal strip elements A and B and radiation baffles (Nos. 7, 8, and 20). Bimetals A are attached solidly at their lower end to the body block but are thermally insulated from it, and the upper ends are pin-jointed to the two link rails (No. 10).

Bimetals B are rigidly attached to the sensor shutter (No. 6) at their lower extremities and pin-jointed to the link rails (No. 10).

Thus the sensor shutter (No. 6) is flexure-mounted above the body and restrained from excessive movement (during launch vibration, etc.) by the shutter stops (No. 12).

Solar radiation, when moving off normality towards the left of Fig. 2, will illuminate A bimetals, which will bow their tops towards the right of Fig. 2, thus carrying the link rails (No. 10), the unaffected B bimetals, and the sensor shutter to a position shutting off some solar radiation to the body. The resultant cooling of the body due to radiative heat loss will cause rotation of the whole assembly in a counterclockwise direction due to retraction of the piston assembly (No. 2). Since the piston assembly carries the position shutter (No. 9) to a position covering some of the absorptive upper surface of the body (No. 1), the cooler steady-state temperature will be retained when the sensor shutter returns to its neutral position due to a now "normal" sun (the upper radiation shields (No. 20) shadowing both bimetals at sun normality).

Illumination of the B bimetals by solar radiation from the right in Fig. 2 will cause them to attempt to bow

to the right; however, the link rails, attached as they are via the A bimetals to the body, will enforce displacement of the sensor shutter (No. 6) to the left, thus uncovering some of the absorptive upper surface of the body, which will therefore heat up and extend the piston. Piston extension will rotate the whole assembly clockwise and also uncover some of the absorptive upper surface due to movement of the position shutter to the right in Fig. 1. This repositioning of the shutter (No. 9) will cause retention of the new piston/body position and allow return of the sensor shutter assembly to neutral.

III. Design Considerations

A. Power Piston and Body

The initial concept is based fundamentally on the Pyrodyne² actuator. This device consists of a fluid-filled cylinder and a piston that extends linearly with increase or decrease in fluid temperature.

These components have been qualified for use in space and, in fact, form part of the *Apollo* life-support control system.

Typically, extension ratios of 0.020 in./°F can be readily achieved with no theoretical limit on extension. In practice, however, the long heat-up time enforced by a large mass of fluid and very wide temperature extremes necessary for long extensions causes practical difficulties with sealing and heat-transfer arrangements.

In order to provide useful design criteria, an extension of 4.0 in. was selected, giving a total temperature excursion of 200°F.

Pyrodyne representatives indicated that such a device was practical and could be expected to deliver a 30-lb force over its range, utilizing a specially configured cylinder bore (to aid heat transfer) and a bellows hermetic seal to ensure that no fluid could be lost in space due to vacuum-enforced evaporation.

It was soon apparent that to assist in the all-important rapid heat transfer on which the time response of the device depended, the cylinder should become an integral part of the absorber/radiator system. From these considerations, the H section body was evolved.

²Pyrodyne Division, William Wahl Corporation, Santa Monica, California.

This configuration (see Fig. 2), was arrived at by the requirement to prevent any direct radiated heat flux from passing between the two fins and bypassing the piston assembly. As explained earlier, the volume between the two pairs of fins is filled with metallized Mylar. Aluminized fiber glass panels are used to prevent influx of radiant energy into the edges of the baffle matrix.

B. Orbital Considerations

The one constant necessary for good repeatability of panel position is a relatively consistent solar radiation flux. Variations in flux within earth orbits are unlikely to cause position errors of a magnitude to be measurable within normal operation. However, missions involving planetary flybys, etc., could cause variations in solar flux of sufficient magnitude as to require compensation to ensure maintenance of panel orientation. One method of obtaining adequate compensation is by the use of a "black body" sensor.

This sensor would take the form of a suitably coated spherical shell containing either a fluid thermal-type actuator or a bimetallic element linked to the position shutter so as to apply a bias relating to variations in thermal flux. Obviously, any variations in thermal flux would cause a variation in the steady-state temperature of the spherical housing, thus operating the enclosed actuator. This actuator could also operate a small separate trim shutter on the radiator or absorber surface of the main piston body, thereby producing the biasing action necessary for solar flux compensation. This type of bias would also help to compensate for any surface degradation that might occur in orbit.

It is worth noting that in the case of a spacecraft engaged on a mission involving relatively close sun proximity, this variation in solar flux could be arranged to deliberately allow the misorientation necessary to maintain solar panel temperatures at a reasonable level.

C. Earth Albedo and Thermal Input

Earth albedo and thermal radiation form significant inputs to this type of system at near-earth orbits (see Fig. 3); however, in view of the relatively rapid heat-up rates required at low altitudes, some assistance in response time can be gained from these inputs.

For operation at higher earth orbits, albedo and thermal radiations become insignificant within normal operating tolerances.

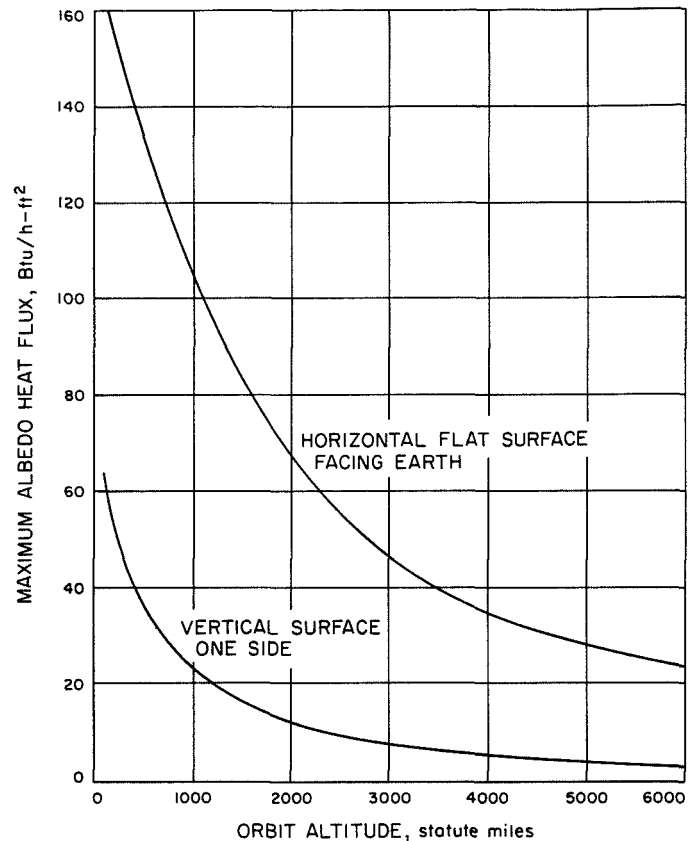


Fig. 3. Maximum albedo heat flux on one side of a flat surface

D. Actuator Slew Rate

About the fastest slew rate that the actuator will have to provide will be during a 90-min ecliptic orbit. Here the panel slew rates amount to about 4.0 deg/min.

Since the orbital height will be about 140 nmi, the time the spacecraft will be in eclipse is approximately 36 min (145 deg), assuming a simple ecliptic orbit.

Now if the solar panel drive system is arranged such that when the spacecraft is coming out of eclipse the actuator body is at its coldest position but with the panel oriented ready to receive "normal" sunlight, no rotation of the spacecraft will be necessary to "capture" the sun (see Fig. 4). It follows that the mechanism must be designed, therefore, for one of the two possible sets of conditions:

- (1) When the spacecraft is in eclipse, the actuator plate cool-down rate must be such that when eclipse is completed the actuator body is at the

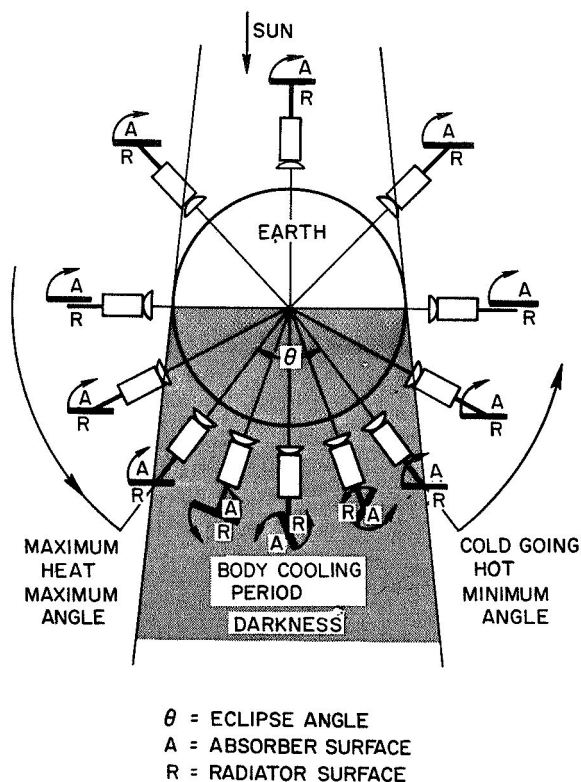


Fig. 4. Actuator body orientation cycle due to eclipse

temperature corresponding to correct sun normality, or

- (2) When leaving eclipse, the actuator plate temperature is such that the sensor is so positioned as to acquire the sun within a very short time.

Since the plate is always heating up during operation, the sensor (for this particular orbit) is always demanding heat until eclipse is reached. At this point, the plate will commence cool-down. It can be seen, therefore, that no secondary systems need be applied for sun acquisition, so long as the spacecraft is three-axis stabilized.

It should be noted that the sensor described earlier has a nearly hemispherical view angle when misoriented (see Fig. 1), removing the necessity for wide and narrow angle sensors in order to achieve acquisition after maneuvering or when on a mission demanding this capability.

This effect is useful when the spacecraft is operated in orbits other than ecliptic (admittedly an ideal case), and, therefore, efficient orientation throughout the seasonal variations of orbital planes usually encountered in normal operation may be maintained.

E. Materials and Coatings

1. *Piston and body.* Aluminum alloy appears to be the logical choice of material for the body. Thermal conductivity is high for a relatively light weight coupled with straightforward producibility. For example, alloy 6101T6 gives very good machinability with a conductivity of 100 Btu h/ft²/°F/ft (at 70°F) and quite adequate strength. The coating of absorber surface for maximum α/E ratio has been provisionally selected as copper plate oxidized in an Ebanol C solution, giving an α/E ratio of 14.0 (0.84/0.06).

This coating is, of course, compatible with an aluminum base by using electroless plating or copper cladding.

The radiative surface of the block is vacuum-deposited silver or silver plate having reflectances higher than 95%. However, in practice, protection of the surface from sulphide spoilage (tarnishing) is very difficult except by adding a fused silica coating. This combination yields an α/E ratio of 0.09 and an emissivity of 0.80 ($\alpha = 0.07$).

F. Thermodynamic Considerations

We require a rod extension of 4 in., and, at 0.020 in./°F, a ΔT of 200°F becomes necessary. Selecting T_{max} as 700°R and T_{min} as 500°R and a fixed radiator area of 1 ft², the exposed maximum and minimum absorber areas can be computed assuming negligible temperature drop throughout the system and become approximately 0.3 ft² at 500°R and 0.9 ft² at 700°R. The linear position shutter travel can be arranged to deal with nonlinear heat input programs due, for example, to cosine law conditions of earth thermal radiation at low orbital altitudes, by arranging a suitable reflective pattern on the absorber surface, uncovered by the position shutter during its stroke.

These figures represent the area ratio based on a 1-ft² radiator; however, actual areas are really a function of desired time response and thermal mass.

Having reached the eclipse point in the ideal ecliptic orbit, the plate will be in the fully heated condition, that is, at 700°R. On entering eclipse, the plate will be exposed only to earth's thermal radiation.

However, the effect of earth's thermal radiation is negligible since the absorber surface emittance is only 0.06; thus, maximum absorbed energy at earth and plate coincidence (this radiation is subject to the cosine law) is 3.9 Btu/h/ft².

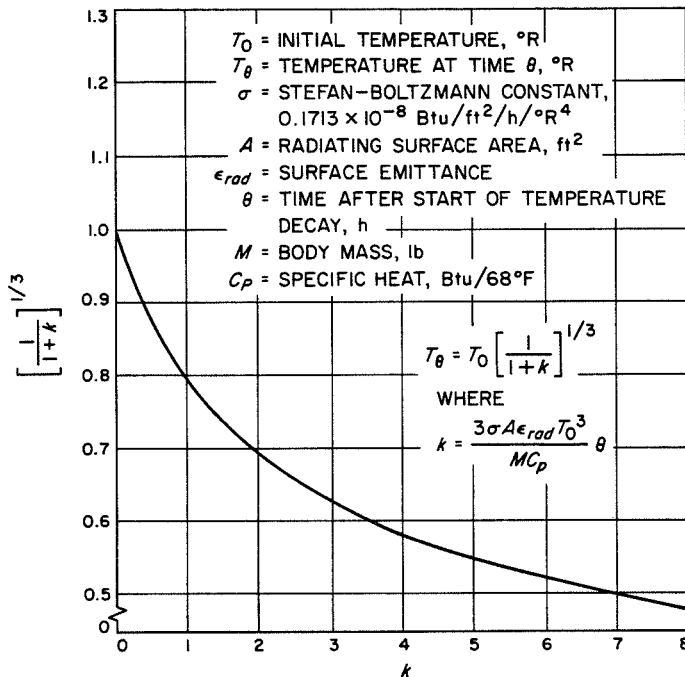


Fig. 5. Temperature decay of body with no internal or external heat input

The temperature decay (see Fig. 5) of a flat surface body with negligible heat input is expressed by

$$T_{\theta} = T_0 \left(\frac{1}{1+k} \right)^{1/3} \quad (1)$$

where

$$k = \frac{3\sigma A \epsilon_{rad} T_0^3}{MC_p} \theta \quad (2)$$

and where

$T_0 = 700^{\circ}\text{R} =$ initial temperature

$T_{\theta} =$ unknown = temperature at time θ

$\sigma =$ Stefan-Boltzmann constant,
 0.1713×10^{-8} Btu/ft²/h/°R⁴

$A = 1.0$ ft² = radiating area

$\epsilon_{rad} = 0.8 =$ surface emittance

$\theta = 0.58$ (time in eclipse) = time decay, h

$M =$ mass of body } $MC_p = 0.445$ (composite)
 $C_p =$ specific heat }

The term MC_p is a composite of the mass of heat expansive fluid and 2 lb of aluminum alloy and the appropriate specific heat constants.

Substituting the values noted above into Eqs. (1) and (2), T_{θ} becomes 495°R , which is very close to the 500°R design point of the mechanism; that is, the fully cold position.

G. Shutter Operation and Response

In order for the mechanism to operate correctly, a part of the front face (absorber) area should be sensory surface. Figure 6 shows a convenient sensor shutter configuration.

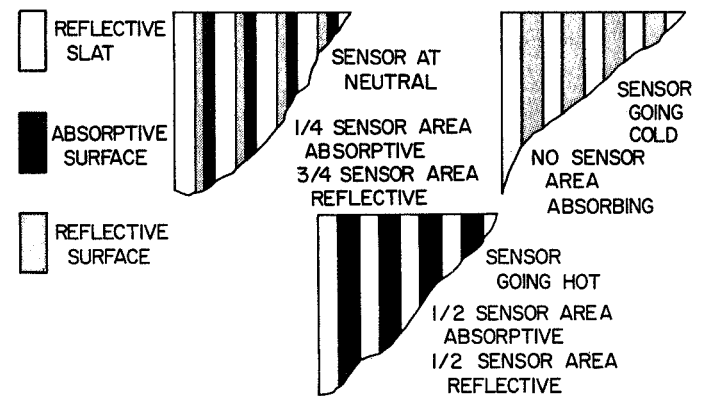


Fig. 6. Sensor area variations

This arrangement with $\frac{1}{4}$ -in. spaces and $\frac{1}{4}$ -in. slats adds or subtracts 93 Btu/h, depending on direction of misorientation, within 2–5 seconds of demand. This is sufficient energy to move the actuator and panel about 1 deg in about 30–40 seconds.

Obviously, to decrease this response time, more sensor area can be arranged by redesigning the absorber surface.

IV. Applications

The device discussed in this study appears to be quite practical for the worst-case orbit used as a model. Obviously, orbits requiring lower slew rates and requiring operation in both “going hot” and “going cold” modes are relatively easy to design for and will cause fewer albedo and reradiation problems than the near-earth orbits.

It is anticipated the device will weigh 4-5 lb and cover an area of 16 × 12 in. It is easily protected from launch shock and vibration by means of the overtravel stops shown in Fig. 2.

The power limitations at this time appear to be based on the 30-lb force actuator used, a trade-off between light weight, response time, stroke, and temperature range requirements. Practical limitations on the feasible maximum and minimum temperatures include such factors as surface treatment damage, excessive material evaporation, seal damage, and thermal distortion effects.

Utilization of a 1.0-in.-radius torque wheel and a 6.0-in. stroke will yield plate rotations of nearly 360 deg at a torque capability of 30 in.-lb.

Reduction of output force requirements would allow lower strokes, faster response, lower hysteresis, and more conservative operating temperatures.

These trade-off suggestions are offered in order to demonstrate the great flexibility of this design and should serve to stimulate persons engaged in the specifying of solar panel orientation systems to consider the possibility of passive thermomechanical operation.

N 69-11816

Mechanical Aspects of the Lunar Surface Magnetometer*

William Schwartz and William L. Nelms
Philco-Ford Corporation
Space & Re-entry Systems Division
Palo Alto, California

Measurement of the weak magnetic fields on the moon requires an instrument of unique capabilities. Combined with the constraints imposed by integration into the Apollo Program, this imposed a complex and rigorous set of problems. This paper surveys the mechanical design of the Lunar Surface Magnetometer, the mission and environmental requirements which determined it, and the rationale whereby some of the problems were solved. Included are some intermediate phases of development.

I. Introduction

The Lunar Surface Magnetometer (LSM), Fig. 1, is one of the experiments comprised in the Apollo Lunar Surface Experiments Package (ALSEP). The package will be deployed on the lunar surface by astronauts during an Apollo landing mission and left in operating condition on the surface of the moon. The experiments are powered by a single radioisotope-thermionic generator, and all transmit data and receive commands through a common communications system.

Scientific objectives dictate the need for a three-axis magnetometer with sensitivity of ± 0.2 gamma, a range of zero to ± 400 gamma, frequency response dc, to 0.27 Hz, and initial positioning within ± 3 deg in level and ± 1 deg in solar azimuth. Capabilities include site

survey of local magnetic field gradients, scientific measurements in three orthogonal axes, internal calibration, and engineering readouts of temperature, voltage, geometry, and status.

II. Mission Objectives

Observations by American and Russian spacecraft have confirmed that the moon has no significant internally generated magnetic field. Therefore, why build the LSM?

The LSM provides the means for obtaining several results that are not only of great scientific value but are impossible to achieve by other means. By examination of the topology of the interplanetary magnetic field as it diffuses through the moon, bounds will be set upon the lunar magnetic diffusivity, and its electromagnetic propagation characteristics will be examined, leading to conclusions as to its gross internal composition. The site

*The LSM was developed for NASA Ames Research Center under Contract NAS 2-3554.

survey, performed early in the mission, will investigate the existence of magnetically retentive materials in a sample of the lunar surface. Readings for a period of one year will provide data including (1) magnetic radiation density when the site is pointing toward or away from the sun, and (2) the lunar response to shock waves and discontinuities associated with the solar wind (which generates interplanetary magnetic fields).

Another important set of results will be measurements of the earth's magnetic field. As the moon intercepts the earth's magnetospheric tail each month, sets of readings will determine its intensity, shape, and direction. Electrical currents in the magnetic plasma will also be detected by determination of the vertical component of the curl of the magnetic field; a nonzero curl will indicate the presence of currents according to Maxwell's equations.

III. Design Constraints

The LSM has three ranges of magnetic measurement: zero to ± 100 , ± 200 , and ± 400 gammas. For compari-

son, a typical midlatitude surface reading of the earth's magnetic field would be 50,000 gammas. Sensitivity requirements imposed on mechanical design a magnetic cleanliness level of less than ± 0.2 gamma at the sensor heads. Combined with a weight limitation of 18 lb, including some 2600 electronic parts, magnetic requirements necessitated careful materials selection as well as design configuration.

The lunar surface temperature ranges from -173 to $+133^\circ\text{C}$. However, because the electronics dictated an operating range of -30 to $+65^\circ\text{C}$, a sophisticated thermal system was required. (The sensor heads, for example, need 2-W heaters, but even these were a magnetic problem; they were made up of two coils each, wound to opposite hand so that their magnetic fields cancel.)

Because the LSM was allotted only $10 \times 15 \times 26$ in. in the ALSEP storage bin on the lunar module, the sensor arms had to be double-hinged and folded. The resulting configuration complicated the transmission of forces to flip and gimbal the fluxgate sensors as well as

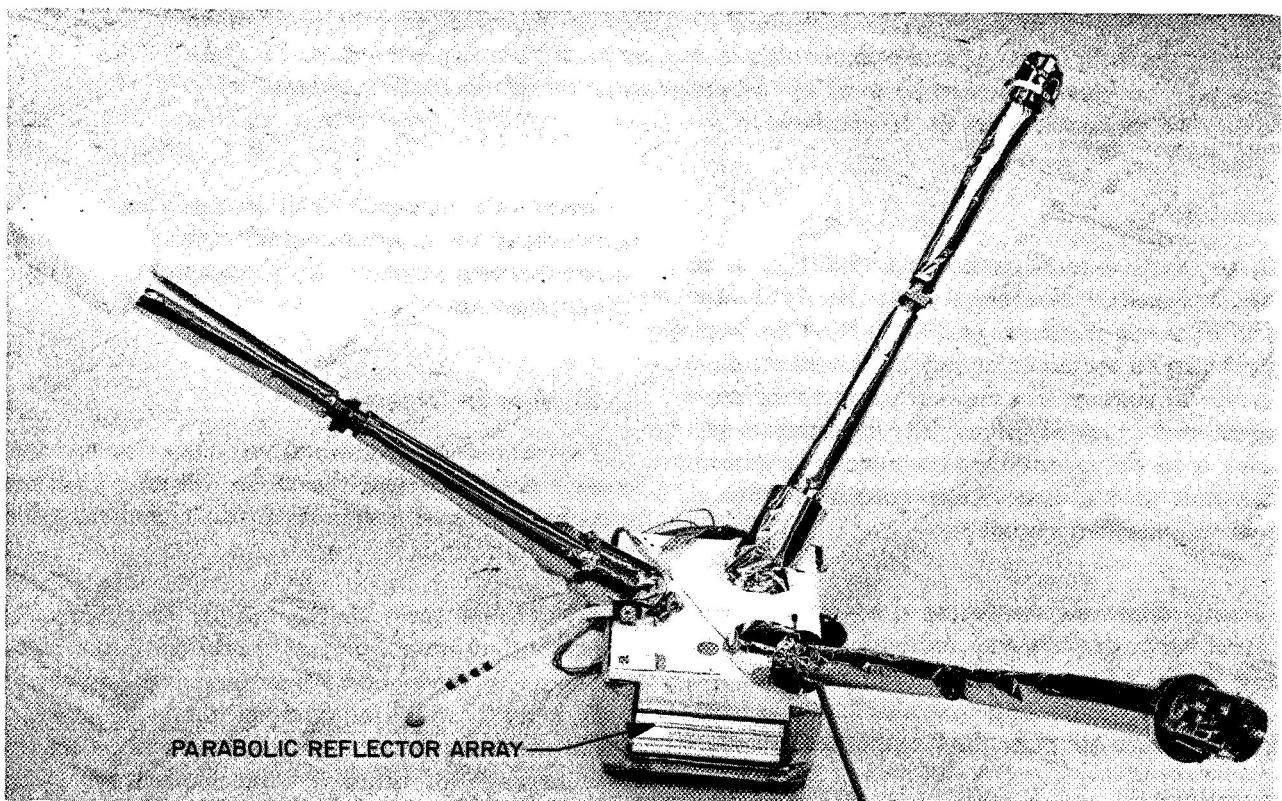


Fig. 1. LSM deployed

the transmission of electrical signals. These requirements also dictated a weak structure in terms of withstanding the stresses accompanying launch of the *Apollo* vehicle.

The three-arm configuration shown in Fig. 1 was dictated by the necessity for the sensors to comprise an orthogonal three-axis system. The three-foot arm length provides sensor/sensor separation sufficient to permit magnetic field detection among the surrounding lunar

debris and also maintains the magnetic bias of the LSM electronics and motors within limits. The support legs provide magnetic and thermal isolation from the lunar surface.

Figure 2 shows the resultant electromechanical system, called the gimbal flip unit (GFU), which includes the three sensor head arms, the sensor heads (not shown), and the drive and mechanical programming assemblies

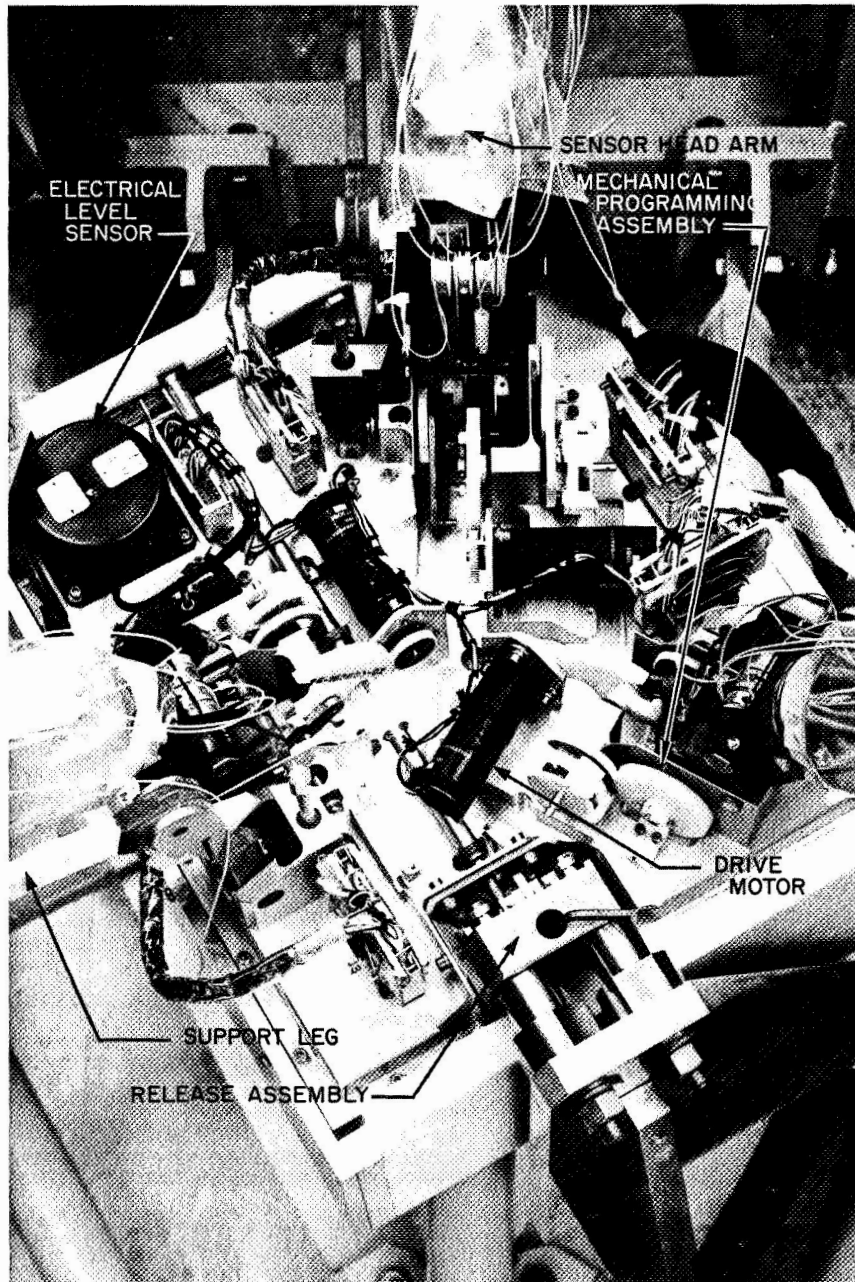


Fig. 2. LSM gimbal flip unit

which operate the drive cables actuating the fluxgate sensors and gimbal mechanisms. Also included in the GFU are the electrical level sensor, support legs, temperature detectors, and (not shown because they are located above the thermal coverings), a solar shadowgraph for azimuth orientation and a visual bubble level.

IV. Operation

A description of the operations can be followed by means of Fig. 3. The motor gearhead (1), which powers the drive cables, is a conventional-looking size 7 instrument motor gearhead, but it had to be specially developed because of magnetic cleanliness requirements, sealing for lubrication retention through the year-long mission in the lunar vacuum, power constraints, and reversing and torque-limiting requirements.

In the science operating mode, readings are alternated every 12 h with short flip-calibrate sequences. An internal LSM program schedules the activity, alternately reversing the motor each cycle. The motor run is timed so

that the primary arm driver (7) moves the primary toggle arm (8) to apply tension to the double toggle spring (11) until it reaches a state of tension which overcomes the restraining forces on the secondary toggle arm (10). The secondary toggle arm then snaps away from one limiting stop (stops not shown) to the other. Rotational motion is transmitted through the output shaft (9) to the two independent (end-tied) cables (22), which flip the sensor (18) against the appropriate 0- or 180-deg stop (stops not shown). Several other designs were considered, but fail-safety was paramount; with this configuration, failure of almost any single part cannot leave the sensor at a position other than against the 0- or 180-deg stop. The LSM can still make valuable readings if it is limited to only one of these positions.

A special mechanical program is needed for the site survey operating mode early in the mission. The LSM starts its mission with each of the three sensor heads gimballed to a "wrist" movement 90 deg from its later position in order to perform the site survey, which requires each arm in turn to assume the 0-deg flip position

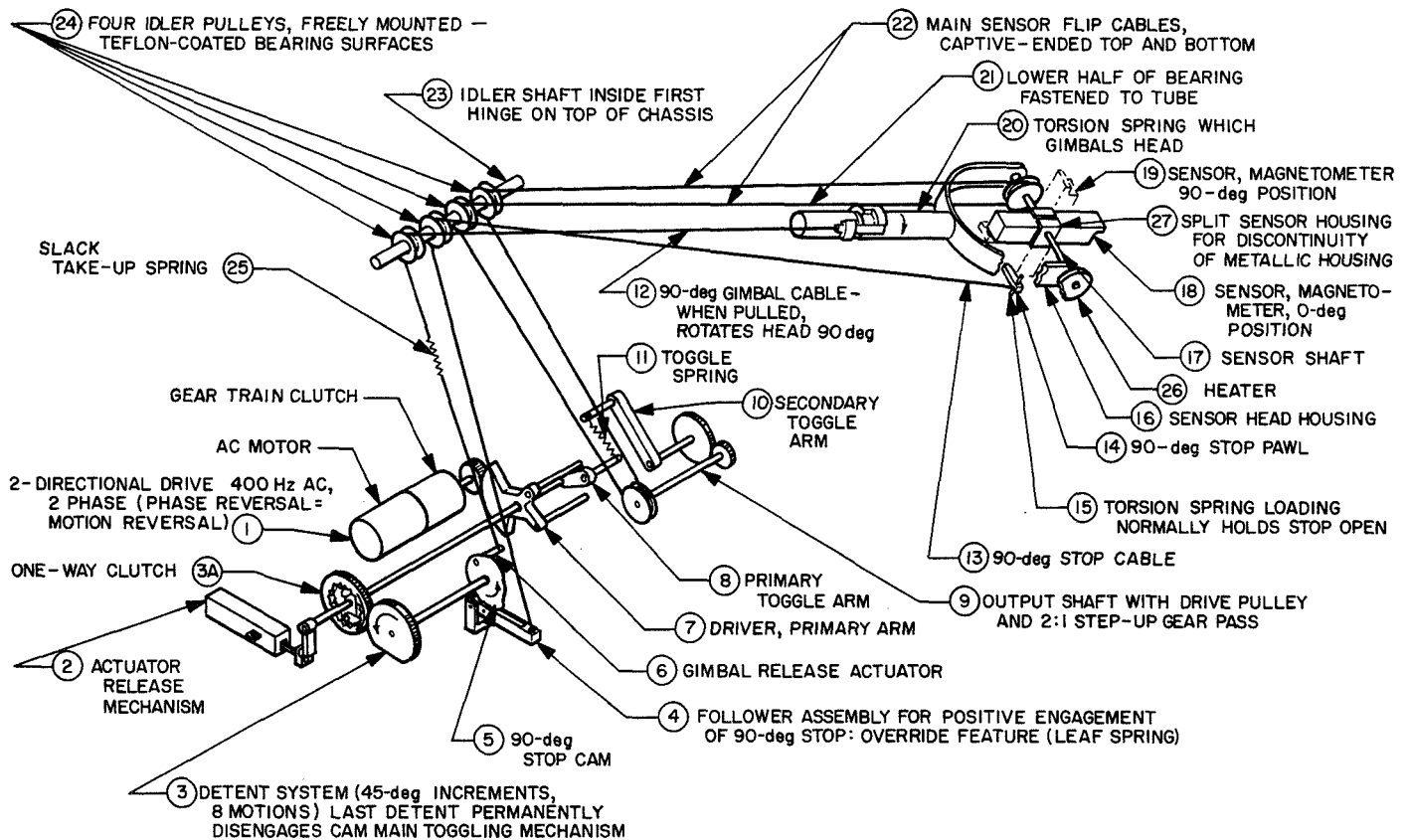


Fig. 3. Schematic of the gimbal flip unit

while the other two arms have their sensors in a position parallel to the arm being surveyed. Flip-calibrate operations precede the site survey, but during half of these movements the primary toggle arm (8) is not turning the detent system drive gear (3), because the electrical program is reversing the motor at each actuation, and the one-way clutch (3A) is slipping. However, at intermediate actuations, the one-way clutch is turning 3, and the gear ratios are such that this movement is 45 deg of the 90-deg stop cam (5).

The shapes and initial positions of these cams, one on each arm, are such that, after the initial flip operations, the lobes of the cams program the site survey event sequence. First, arm X is flipped to 0 deg, and arms Y and Z are at 90 deg. This is accomplished by cam rotation at arm X without tripping the follower assembly (4), whereas cams Y and Z depress 4, pulling the 90-deg stop cable (13) against the torsion spring (15), and placing the 90-deg stop (14) in the path of the fluxgate sensor. The survey about arm Y requires Y to be at 0 deg, but, in order for the X and Z sensors to be parallel to arm Y, they must be at 90 deg and Z must gimbal. To survey the Z arm plane, Z is at 0 deg, X is gimballed and at 90 deg, and Y is at 90 deg and gimballed. Gimbaling is powered by torsion springs under each sensor head, and the energy is released by the gimbal release actuator (6), through the gimbal cable (12). The gimbal movement is restrained by a stop which also maintains proper sensor head position.

When the site survey operation is completed, the detent gear (3) has been turned so that the driver (3A) no longer engages it. Thus the 90-deg stop and gimbal are permanently disabled. After completion of site survey, the LSM alternates between the science and flip-calibrate modes, which consist of sequences of 0- to 180-deg flipping, through the year-long mission.

V. Typical Intermediate Phases of Development

The LSM went through design iterations of almost every critical assembly. For example, prior to receipt of *Surveyor* data, it was thought that launch of the *Apollo* Lunar Module from the lunar surface would result in clouds of particulate matter which would coat all horizontal surfaces of the LSM, changing their thermal characteristics. The first set of thermal controls therefore consisted of shades deployed several inches above the LSM components. Because results from the *Surveyor* program showed that substantial LSM surface contami-

nation with particulate matter is extremely unlikely, the thermal design was redirected toward the parabolic reflector array (PRA) as shown in Fig. 1. Each of the two PRAs consists of three thermal control surfaces and associated parabolic reflectors. The thermal control surfaces emit heat during the day, but, in conjunction with the reflectors and sun-shades, prevent overheating. Together with the insulation, they also prevent excessive heat loss at night.

VI. Testing

Several test programs were conducted at various levels. Assemblies were operated in thermal-vacuum chambers, and other components required evaluation for magnetic cleanliness, which was done in Mu metal flux tanks. Five materials were tested in thermal-vacuum environments to determine the best cable material. The visual bubble level was an unknown quantity; no manufacturer either knew or cared about their performance in vacuum or extreme temperatures. It was necessary to buy the test samples, go through qualification test cycles, dictate modifications, and then retest the production lot.

LSM system level tests were followed by ALSEP interface and integration tests at Ann Arbor, Michigan, by the Bendix Corporation, the ALSEP prime contractor. The test sequence was successfully completed in December 1967.

VII. Lunar Deployment Simulation

Astronaut deployment of the LSM also had to be integrated into the design with deployment activities maintained within the limitations of the suited astronaut. To release the LSM from its attach points, a simple handle was developed, with linkages and cables to quick-release mechanisms, so that a single pull also releases the stowage bracketry and foam padding shown in Fig. 4. The LSM is hand-carried to its operating site, which, dictated by magnetic considerations and local topography, will be within 50 ft of the communications system. As it is carried, a flat communications cable, permanently connected at both ends, is unreeled. After locating a suitable site, the astronaut unfolds the legs, which are positioned by detents. The LSM is positioned in azimuth by means of the solar shadowgraph, and then the legs are levelled by application of a tool to the shafts of worm screws/gear segments controlling each leg. The arms are unfolded, the hinges being detent-controlled.

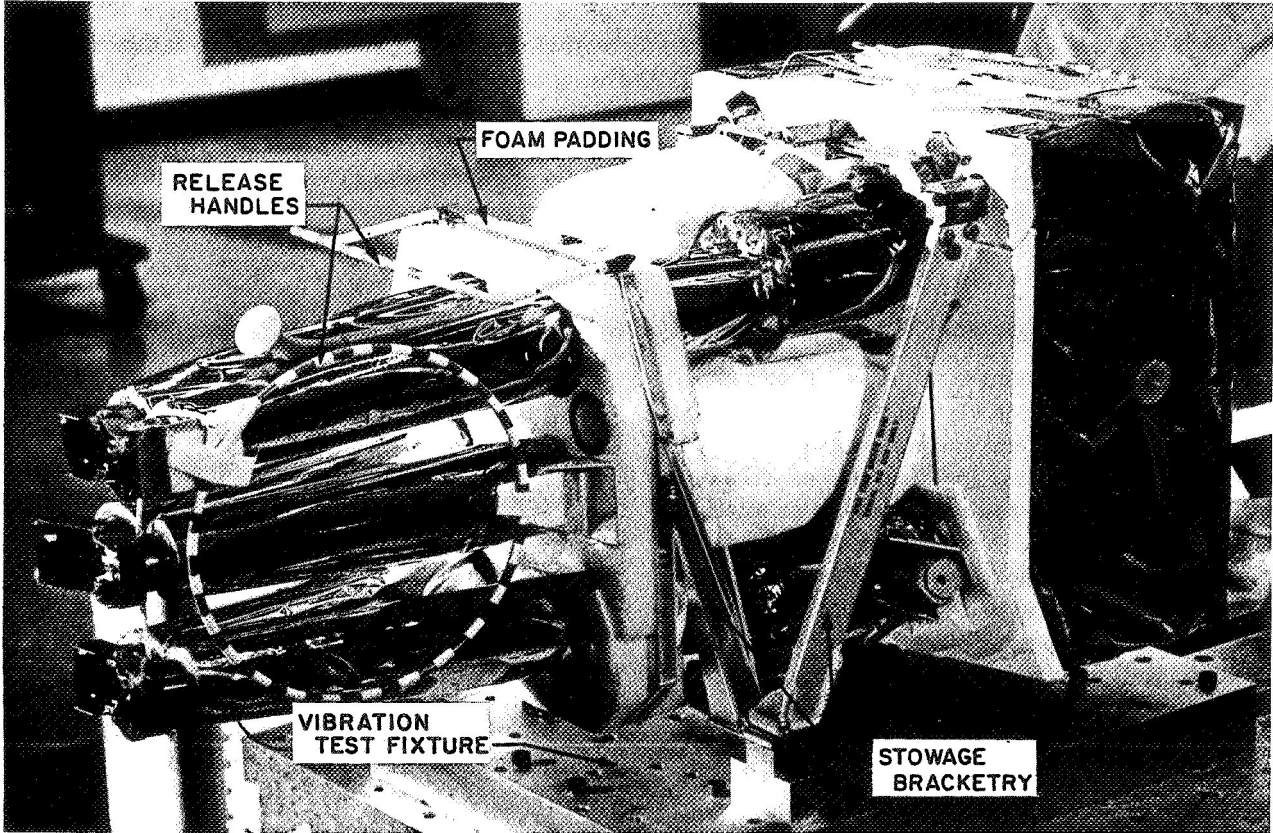


Fig. 4. LSM in stowed configuration

A series of astronaut deployment tests was conducted by the Bendix Corporation at Ann Arbor, Michigan, and by the National Aeronautics and Space Administration at the Manned Spacecraft Center at Houston, Texas, in facilities simulating the lunar surface. These tests identified the requirements for several design and operational changes.

VIII. Conclusion

The LSM program reached state-of-the-art levels in magnetometer design, materials applications, and in mechanical and thermal analyses. Many specialists contributed their expertise, and a close correlation between analytical and test results was achieved.

N 69-11817

Torsionally Rigid and Thermally Stable Boom*

F. C. Rushing, A. B. Simon, and C. I. Denton
Westinghouse Defense and Space Center
Aerospace Division
Baltimore, Maryland

The Torsionally Rigid and Thermally Stable boom uses a unique pattern of windows or perforations, in combination with selected thermal coatings on both inside and outside surfaces, to produce equal thermal distortions on opposite sides of the boom in sunlight and therefore eliminate thermal bending. A typical boom is made of 0.002-in.-thick beryllium copper and is 1/2 in. in diameter. An interlocked seam maximizes torsional and bending rigidities and makes them more predictable. A special deployer has been developed for the boom. Production facilities have been set up, and the boom is now in the flight qualification state.

I. Introduction

Long erectable tubular members (booms) for space applications are required to be immune to sunlight influences on thermal bending, while possessing a maximum of bending and torsional rigidity. Such erectable members are commonly stored in a cylindrical roll and are deployed and retracted on command.

The erectable boom has been particularly applicable in space, where small stored volume and light weight are desirable. Furthermore, in gravity-free space flight, a low-strength, low-rigidity (by earth standards) boom has

filled a need for antennas and gravity-gradient attitude control systems. However, thermal bending and rigidity characteristics have presented serious limitations. In an effort to overcome these limitations, the torsionally rigid and thermally stable boom has been developed by the Westinghouse Defense and Space Center for the NASA Goddard Space Flight Center.

II. Design Principles

A. Thermal Design

The geometric and thermal configuration of this boom controls the rate of absorption of heat on opposite sides of the boom, thus producing equal thermal expansions on opposite walls and avoiding thermal bending. This

*Information for this paper was developed on NASA contracts NAS 5-9598 (Westinghouse G. O. 51340) and NAS 5-10130 (Westinghouse G. O. 51360).

condition is required for all incident angles of the sun. Although the amount of heat absorption changes with the sun's angle, it produces no adverse effects as long as the relationship from side to side is maintained constant. The required thermal stability is achieved by (1) a pattern of windows or perforations in the boom and (2) coatings of different absorptivities on the inside and outside surfaces.

1. Window pattern. A unique window pattern (Fig. 1) is used to produce the same proportionality of inside to outside exposure for all incident angles of the sun. The pattern consists of small circular holes arranged in a double helix pattern. One helix is a left-hand "thread" with a very large lead angle, and the other (intersecting) helix is a right-hand thread with a small lead angle. The holes are kept small to minimize stress concentrations and thermal resistance and maximize bending strength. With this pattern, the incremental lengths which experience the equal exposure ratio can be controlled by the helix angles. Increments less than 1 in. long have been found to be practicable. The window pattern is disrupted by the seam, since there is an overlap of about 30 deg, but the disruption is minimized by having holes in the overlapping tabs and by having the tabs bear hard against adjacent sides of the seam.

2. Coatings. Regardless of the amount of material removed by the holes, the side of the boom nearest the

sun (the front side) is completely exposed to the sun, whereas the back side is always partially shadowed by the front side. In order to absorb the same amount of heat on the back side, the inside surface is given a higher absorptivity than the outside surface.

Moreover, to minimize the cut-out area of the tube wall, the absorptivities inside and outside need to be as widely different as feasible. If the outside is covered with a low-absorptivity coating, the amount of heat involved for either side can be reduced, and thus only small perforations are required to allow sunlight to fall on a high-absorptivity surface inside. As a rough rule of thumb, the ratio of absorptivities outside to inside is equal to the fractional area of wall cut out for windows. Practically, it can be as low as 8 to 15%. By using window areas on the high side of this range, or even higher, the use of extreme and difficult-to-maintain surface absorptivities can be avoided.

To meet the requirements described above, a beryllium copper alloy with an aluminum coating vacuum-deposited on the outside and a dark oxide coating on the inside is used for the boom and gives attractive results. Solar absorptivities of these coatings are approximately 0.12 and 0.85 respectively. The reflection from the outer surface is predominantly specular, and that from the inner surface is diffuse. The proportion of holes to solid wall is adjusted to be compatible with these coatings.

B. Seam Design

The edges of the strips from which the boom is formed have V-shaped notches, and the tabs between the notches of each edge alternately go inside and outside of tabs on the opposite edge. The tabs that go inside are given a slightly inward curvature in advance. Thus, as the seam comes together, the curved tab passes under its mating uncurved tab (Fig. 1).

The shapes and spacings of the V notches can be controlled to predetermine the amount of backlash in the seam under the longitudinal shearing action which accompanies torsion. The backlash can be varied from 0 deg up to 20 deg or more per foot.

The number of Vs per unit length affects the torsional rigidity and strength of the boom. A spacing of $\frac{3}{4}$ in. has been found feasible for a $\frac{1}{2}$ -in.-diameter gravity gradient boom.

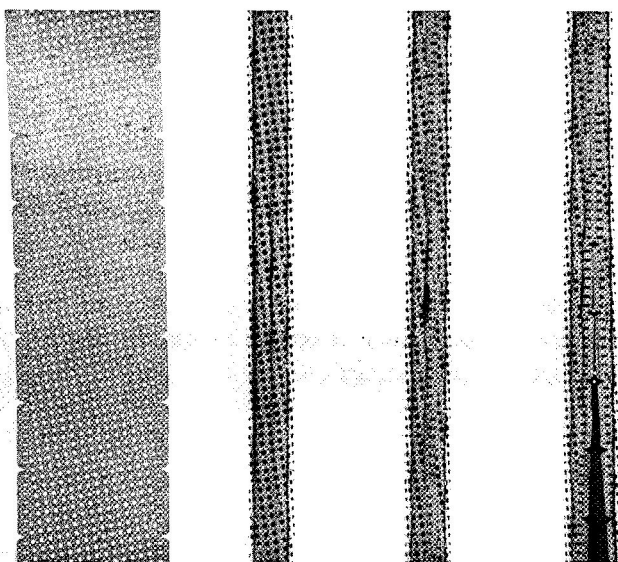


Fig. 1. From left to right: chemically milled strip; boom with double helix window pattern; boom showing joined seam; and detail of seam joining

The seam can be circumferentially preloaded. By forming the boom to a smaller diameter than its working diameter, the seam is held together by elastic strain in the boom. For a 1/2-in.-diameter boom, a formed diameter of 0.4 in. produces an attractively tight seam.

Because of the seam tightness and the hard bearing of the tabs against the opposite edges, coulomb friction is produced for any torsional backlash that is built into the boom. Friction torques in the range of 2 to 3 oz-in. have been measured under laboratory ambient conditions.

III. Thermal Bending Analysis

While elimination of thermal bending is the sole purpose of the hole pattern and thermal coatings, the achievement of exact relationships is required for optimum results. If the optimum is not achieved, the radius of curvature can be analytically computed using the following assumptions:

- (1) The window pattern distributes the radiation to the back side uniformly regardless of boom orientation.
- (2) The temperature variations along the boom's surface at any instant are small (say 10°F) so that every element radiates about the same amount of energy.
- (3) The inside surface coating reflects diffusely (according to Lambert's cosine law).
- (4) The conductivity across the seam is the same as elsewhere.

The first three assumptions have been easily justified. In the case of the fourth, the actual conductivity across the joint is relatively good because of the elastic forces pressing the interlocking tabs of the seam together; furthermore, analysis has shown that the effect of even zero conduction across the seam is relatively small.

The equation for the curvature of the boom due to thermal bending is derived as follows:

- (1) The heat balance for a differential strip running the length of the boom is obtained. This includes radiation from the sun, radiation to space, and internal reradiation and reflections.
- (2) Step 1 leads to an equation giving the temperature distribution around the boom.

- (3) The strain energy due to the thermal gradients is minimized when the boom is allowed to bend. Therefore, the curvature is found by writing an expression for the strain energy due to bending and thermal gradients and finding the curvature required to make it a minimum.

The curvature thus found is given by

$$\frac{1}{R_s} = \frac{erJ_s}{2k't} (1 - A_w) (\alpha_o - A_w\alpha_i) \sin \theta_s \quad (1)$$

where

R_s = radius of curvature due to solar irradiation

e = coefficient of thermal expansion of boom material

r = radius of boom

J_s = solar radiation flux

k' = effective conductivity of boom material considering effect of hole pattern

A_w = fractional window area of holes

α_o = solar absorptivity of outer surface

α_i = solar absorptivity of inner surface

θ_s = angle between boom axis and solar flux

t = constant wall thickness

Thermal bending can then be eliminated, in theory, by choosing the window area so that

$$A_w = \frac{\alpha_o}{\alpha_i} \quad (2)$$

In case α_o , α_i , and A_w are not related according to Eq. (2), Eq. (1) can be used to predict the curvature of the boom.

For near-earth orbits, the infrared radiation from the earth can also cause bending, although this energy is an order of magnitude less than the sun's. Equation (1) is still applicable for predicting this curvature, except that the terms J_s , α_o , α_i , and θ_s must be changed to similar terms for earth radiation instead of solar radiation.

The principles described in this paper are applicable to a wide range of boom diameters such as are required for space applications. Theoretically, Eqs. (1) and (2)

apply, and where Eq. (2) is not satisfied, there will be thermally induced bending. The curvature will be proportional to r/t , which is approximately independent of size. The result is that for larger-diameter booms the practical length will still be limited to that of existing small-diameter booms if it is based on the criterion of straightness.

IV. Strength and Rigidity Analysis

A. Bending

Tests have been conducted on existing patterns with window areas ranging from 15 to 50%, and an empirical relationship that closely predicts the average bending strength is

$$M_{cr} = \left(\frac{S - D}{S} \right) M_{scr} \quad (3)$$

where

M_{cr} = bending strength of boom with hole pattern

S = hole spacing

D = hole diameter

M_{scr} = buckling moment for a solid-wall tube

The bending strength for the Westinghouse 1/2-in.-diameter beryllium copper boom with 15% window pattern is about 8 in.-lb. Equation (3) is shown plotted in Fig. 2.

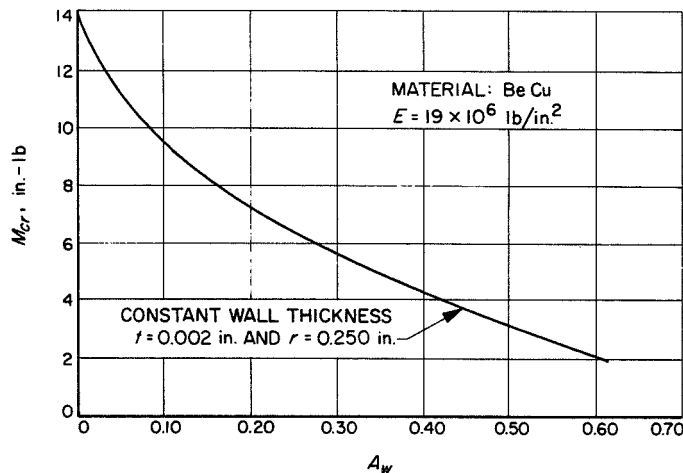


Fig. 2. Bending strength of booms as a function of A_w

B. Torsion

The shear strength of the seam determines the torsional strength for most applications. The shear strength of the seam is dependent on the number of interlocking tabs per unit length because the torsional mode of failure begins with compressive buckling at a tab. By increasing the number of tabs per unit length of boom, the tab is strengthened by being shortened and the shear load is distributed along more tabs.

For a current Westinghouse design of a 1/2-in.-diameter boom with a tab length of 3/4 in., the specified torsional strength requirement was that it exceed 16 in.-oz. This requirement was exceeded by booms with window areas ranging from 15 to 50%. The boom with a 15% window area successfully carried over 50 in.-oz of torsional load.

V. Deployer

The deployer, shown in Fig. 3, provides positive drive both for extension and retraction and contains a simple mechanism for joining the seam. The model shown was made for a special application of a 150-ft-long, 1/2-in.-diameter boom. The end connection was provided for an 8-lb tip mass. It is a compact, rugged design which has successfully withstood vibration testing at space qualification levels.

VI. Production

Production facilities available for the booms are specifically adapted to 1/2-in. beryllium copper booms up to 200 ft long and can be modified for greater lengths and diameters. The window pattern and the edge Vs are produced by chemical milling. Figure 1 shows a chemically milled strip.

VII. Conclusions

A method of minimizing the thermal bending of long tubular members has been developed and applied in the development of the torsionally rigid and thermally stable 1/2-in.-diameter beryllium copper extendible boom for NASA Goddard Space Flight Center. This boom employs an interlocked seam to yield improved torsional rigidity and strength. A flight model deployer has been built and tested. This deployer and boom development can lead to new space applications where longer booms with improved strength and straightness are needed.

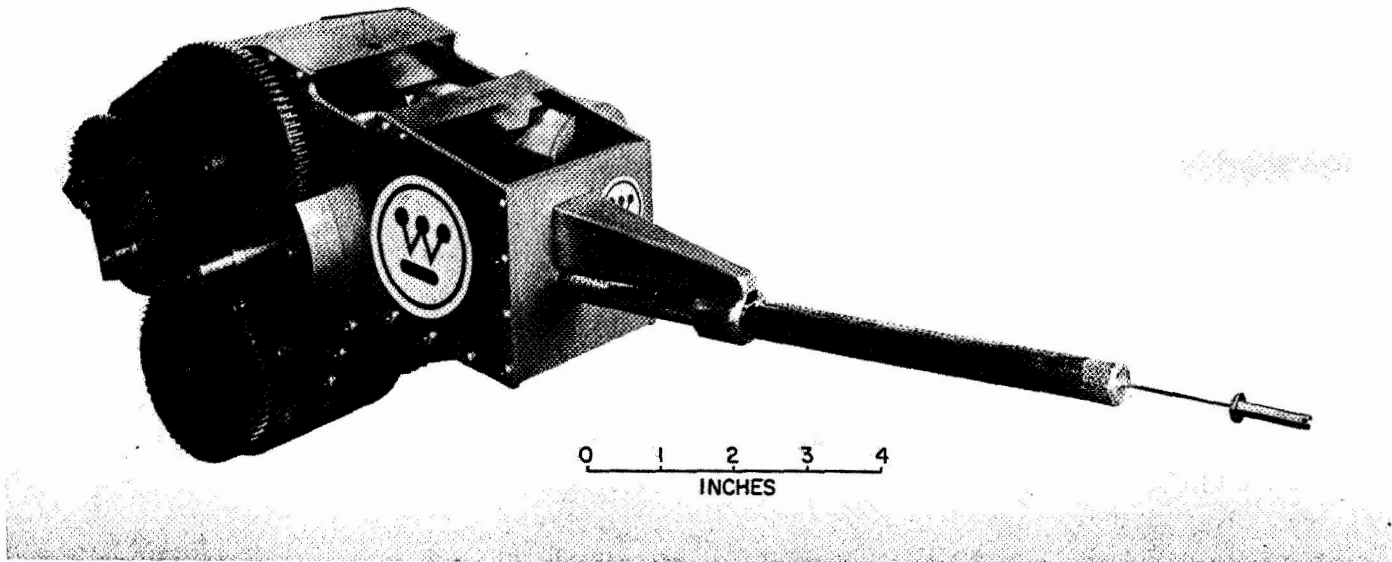


Fig. 3. Deployer for 150-ft-long boom, with provision for tip mass

N 69-11818

A Torsion Wire Damping System for the DODGE Satellite*

Darnley M. Howard
The Johns Hopkins University
Applied Physics Laboratory
Silver Spring, Maryland

The torsion wire damper developed for the Department of Defense Gravity Experiment satellite is described. The damper, which was designed by the Applied Physics Laboratory of The Johns Hopkins University, incorporates two separate damping devices: an eddy current damper and a hysteresis damper. The torsion wire suspension system and caging mechanisms used are described in detail. The damper has operated in space since July 1, 1967.

I. Introduction

The *Department of Defense Gravity Experiment* satellite (DODGE) was launched on July 1, 1967. The primary objective of the satellite was to demonstrate that gravity-gradient stabilization is achievable at near-synchronous altitudes. It was designed to investigate 2- and 3-axis gravity-gradient stabilization using a variety of libration damping techniques in determining correlation between theory and experiment. The torsion wire damper is a component of one of these systems.

The torsion wire damper provides a suspension system of variable moment of inertia, coupled to the spacecraft body by a weak spring. The natural frequency of this system is such that maximum coupling between modes is achieved. Two separate experimental passive magnetic

devices are used to dissipate the energy of the system. The dampers are adjustable in space, upon command from earth.

References 1, 2, and 3 describe theoretical analyses of torsion wire damping systems. Reference 4 analyzes gravity-gradient stabilization at synchronous altitudes and Ref. 5 describes the DODGE satellite. The overall design and performance of the torsion wire damper are described in this paper.

II. Design

A. General

The torsion wire damper is mounted in a mast that protrudes from the main body of the DODGE satellite (Fig. 1). The damper consists of the torsion wire suspension system with two extendible boom mechanisms (with

*This work was performed for the Department of Defense under U.S. Navy Contract N0w62-0604-C.

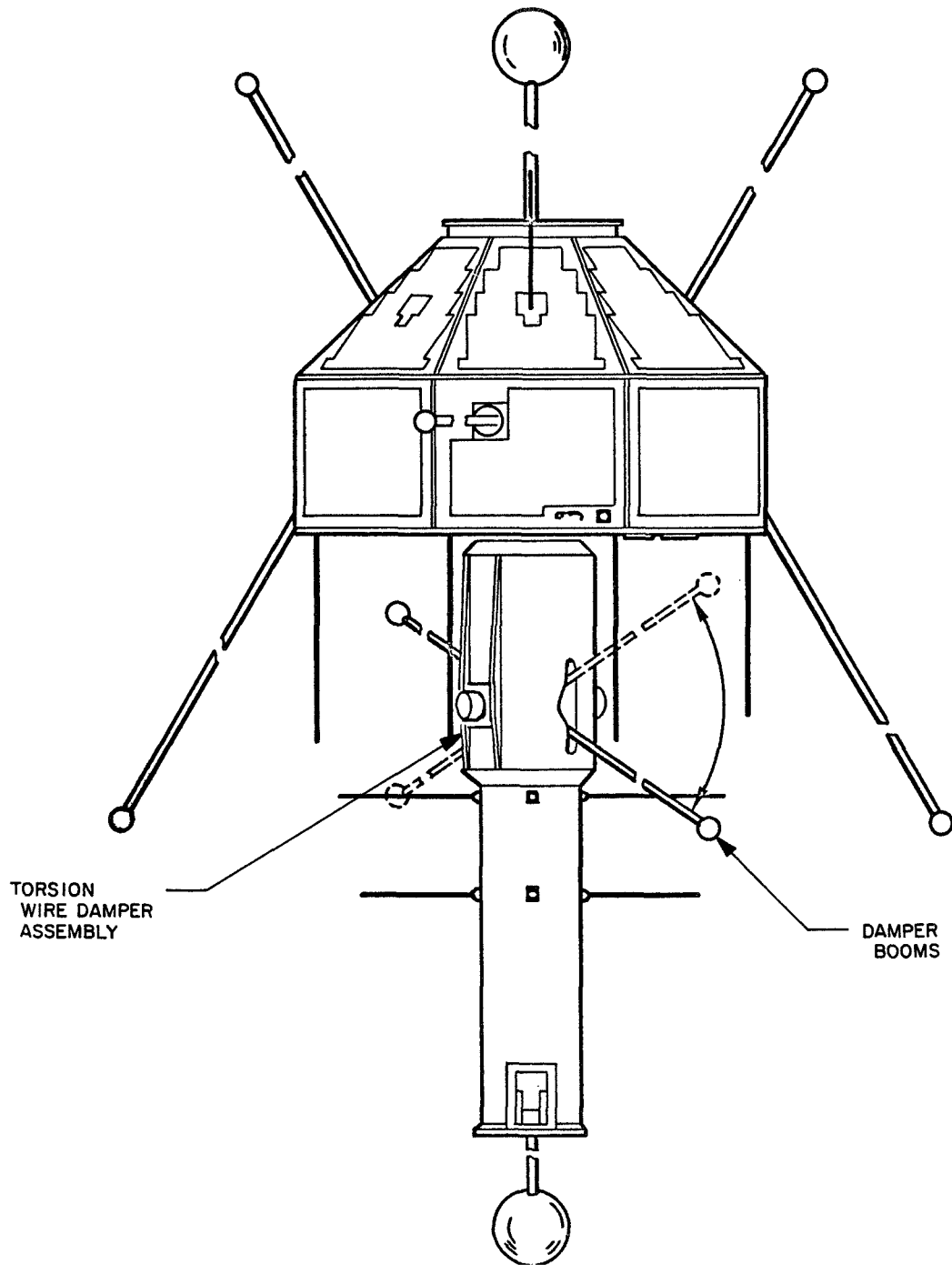


Fig. 1. The DODGE satellite, showing the damper assembly and booms

end masses attached), each of which is mounted at 180 deg with respect to the other and extends through slots cut in the mast. The delicate (0.003-in.-diameter) torsion wire provides an essentially frictionless suspension as well as a restoring torque that causes the damper booms to seek a rest position when the satellite is at rest under gravity-gradient stabilization. The spring constant of the wire is 85 dyn-cm/rad.

The boom mechanisms on DODGE are DeHavilland Model 5489F1-11 Motorized STEM units, with 1/2-in.-

diameter, 2-mil-thick beryllium copper boom tape, silver plated on the outer surface with a reflectivity of about 0.90. A boom mechanism with end mass in the launch position is shown in Fig. 2. Maximum extension capability of the damper booms is 50 ft. Other booms on DODGE have a maximum length of 150 ft.

B. Torsion Wire Suspension System

The torsion wire suspension system consists of two extendible booms suspended between two fine wires

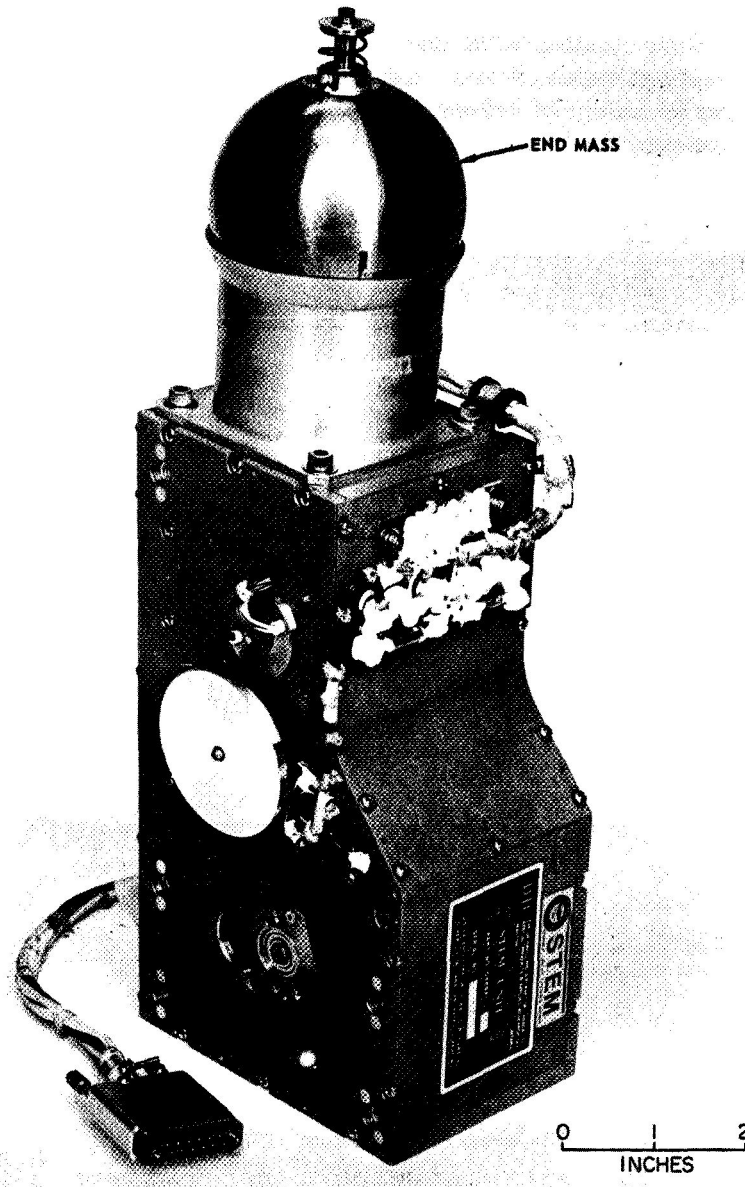


Fig. 2. Boom mechanism with end mass

which act as a torsion spring. The boom mechanisms are mounted side by side in a single housing so that the booms deploy in opposite directions. The entire damper system, including the suspension system, is shown in Fig. 3.

The torsion wires are steel music wire, 0.003 in. in diameter. The ends of the wire are held in tapered chuck grips machined from soft brass. Considerable care was given to the design of the grips to minimize stress concentrations which could result in fatigue failure of the wire during launch. These grips react all of the bending moment and all of the torsion load from the wire and most of the tensile load. The wires are secured to the rear of the grip with solder and are attached to the spacecraft body through soft leaf springs which allow a small axial movement of the damper assembly without damage to the wire. Limit stops are provided so that the damper

assembly will strike a stop when moved in translation $1/16$ in. in any direction from its center position. By the use of two nuts which lock the grip on the leaf spring, a wire tension of about $1/2$ lb was obtained.

The rest position of each wire was determined by aligning each end in a special fixture as the wire hung free. The grips were marked so that this alignment could be maintained when the wires were installed in the damper assembly.

C. Caging Mechanisms

There are two separate caging mechanisms. The first, which provides protection to the entire torsion wire damper during the launch environment, is called the launch lock. The second, called the orbit lock, was designed to prevent oscillation of the torsion wire system

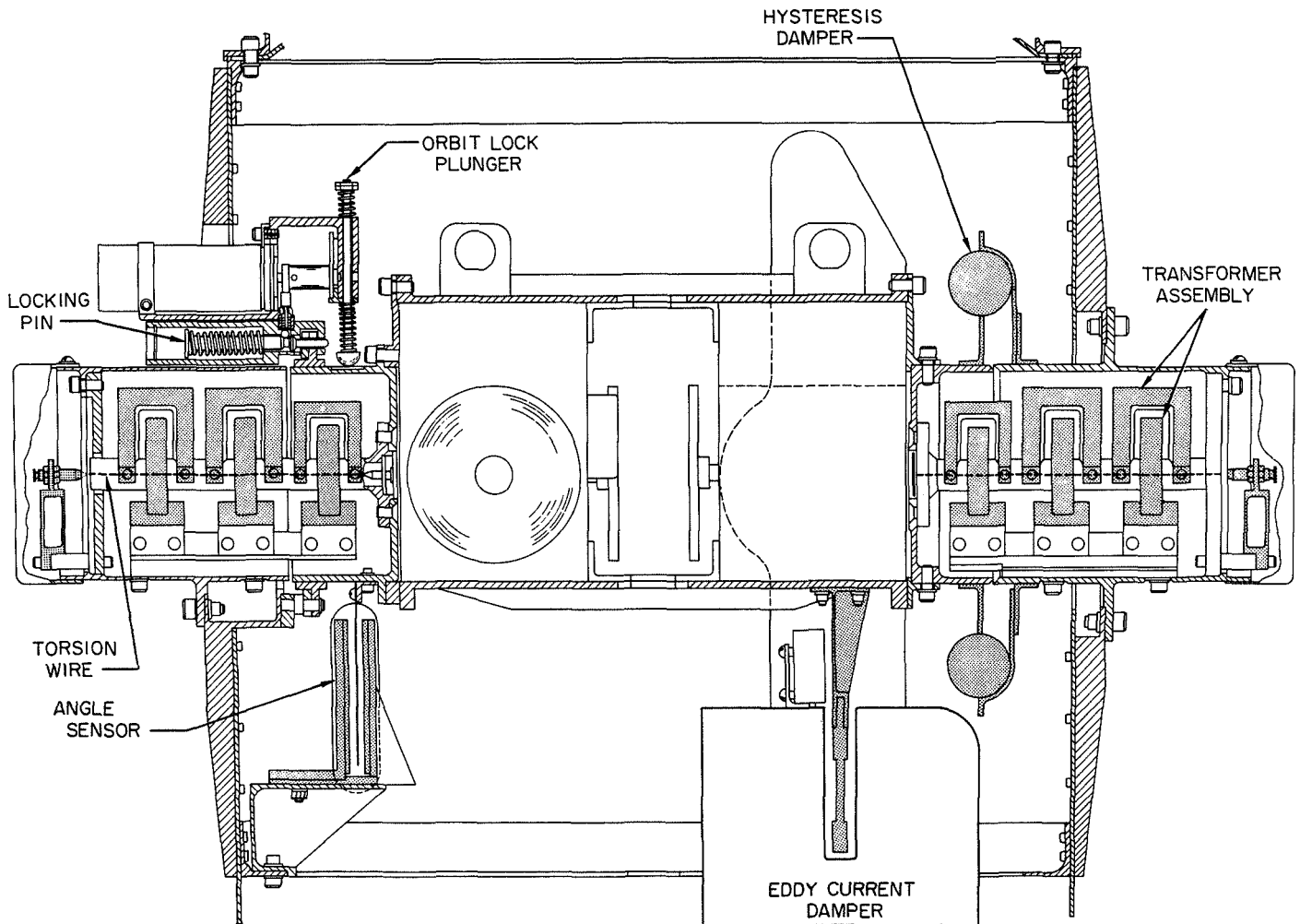


Fig. 3. Drawing of the torsion wire damper assembly

in orbit on command. Both locking systems are operated from a common shaft driven by a hysteresis synchronous motor with a gearhead whose output shaft turns at 1 rpm.

The launch lock operates from one end of the suspension system. The other end is captured by moving the suspension system off center and seating it in a tapered seat. The launch lock itself consists of two semicircular clamp halves hinged at one end (Fig. 4). These clamp halves secure a cylinder which is an integral part of the damper boom housing. In the locked position, the clamp halves are closed and held with a pin. Two flats on the clamp halves and the cylinder prevent rotation of the system, and two cleats mounted on the cylinder bear upon the clamp halves when locked to prevent the assembly from backing away from the tapered seat.

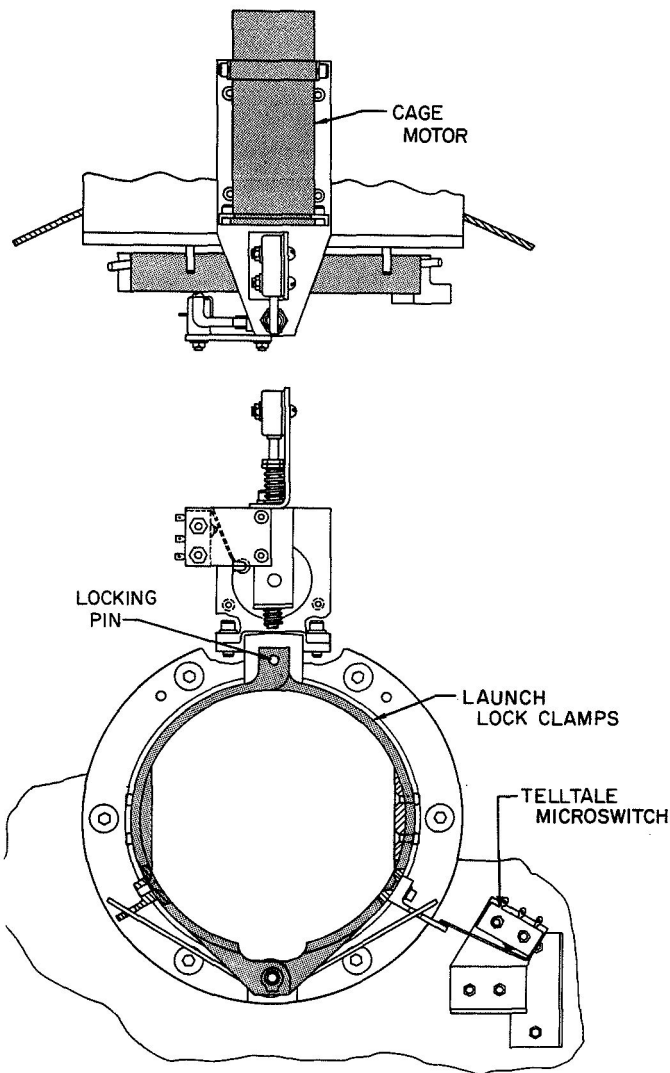


Fig. 4. Launch lock clamping system

The release mechanism is essentially a spring-powered pin puller (Fig. 3). When the pin is in place, i.e., holding the clamp halves in the clamped position, the spring is fully compressed and held in place by a check ball which in turn is restrained by a cam. When the cage motor is started, the cam rotates, releasing the ball, which is then forced out of its seat by the spring. The release mechanism is thus triggered and the spring withdraws the pin. Another spring on the clamp halves forces them apart once the pin is removed and the unlocked condition is achieved.

The launch lock was designed as a single-function device. The lock is set manually before launch or test. Once released, it serves no further function and can only be reset manually.

The orbit lock consists of a plunger which, upon actuation, applies a lateral load to the torsion damper assembly, pushing it against the limit stop. The plunger is actuated toward the lock position with a cam. A return spring allows the plunger to follow the cam away from the lock position. The cam is mounted to the output shaft of the same motor gearhead combination described above. The head of the orbit lock has a hemispherical tip which is designed to seat in a hole in the torsion damper assembly. The seat enables the lock to cage the damper at an angle of 0 deg. The seat is tapered so that the lock will cage at 0 deg from a position of ± 3 deg. The cam actuates the plunger through a spring which is designed to prevent jamming, to allow the cam to complete its rotation, and to permit the lock to operate whether or not the plunger is in the zero-position hole. The orbit lock can be used repeatedly.

D. Electrical System

All the motors on the DODGE spacecraft are hysteresis synchronous motors with appropriate gearheads to preclude the necessity of commutator brushes or hermetic sealing. The motor and gearhead bearings use dry lubricant for long life in the space environment. The power source is 31-V, 400-Hz square wave, and all boom mechanisms and the caging mechanism are powered in this manner.

Electrical connections to the damper booms had to be made in such a manner that no friction would be introduced to the suspension system. This was accomplished by transformer coupling (Fig. 3). The primary winding and core of the transformers are mounted rigidly to the satellite structure, whereas the secondary winding is

mounted on the suspension system and rotates with it. There is no mechanical contact between the primary and secondary. There is an additional transformer for the telemetry signal which monitors boom length. Using this system, the booms may be operated with the suspension system at any angle, and with the suspension system locked or unlocked.

E. Angle Sensor

The suspension system is provided with an angle-sensing device which continuously reads the angle of the suspension system relative to the spacecraft axes. A thin fan-shaped member is attached to the suspension system. Slots etched in the fan form a binary gray code. The sensor, which is rigidly attached to the spacecraft, is a digital device made up of a row of six photo-emitters with photo-transistors as detectors. The detectors sense light which passes through the slots in the moving fan. The output of each detector provides angular position data with a resolution of 1.2 deg.

III. Damping Systems

The torsion wire damper assembly incorporates two separate damping devices: an eddy-current damper and a hysteresis damper.

A. Eddy-Current Damper

The eddy-current damper consists of a copper vane that moves through the field of a chargeable horseshoe magnet. While the satellite is in orbit, this magnet can

be magnetized between zero and full magnetization by discharging a condenser through an electrical winding about the magnet. A Hall-effect detector determines the flux level of the field and is calibrated as an indicator of damping constant. By varying the level of magnetization, the damping constant can be varied from zero to the limit of the system.

B. Hysteresis Damper

A second damper in the assembly uses magnetic hysteresis as a means of damping. An electric coil surrounding a strip of high-hysteresis-loss magnetic material creates, by command from earth, different magnetic field levels, including zero. The energy of motion of the damper is dissipated by hysteresis loss in the magnetic material.

IV. Flight Experience

The torsion wire damper assembly is shown in Fig. 5. The launch caging system performed its function, which was to protect the damper during launch, and upon command was successfully released. The booms have been used many times and, as of this writing, all portions of the torsion wire system are operating as designed. The one aspect of the damper that did not function as designed was the torsion wire alignment. The rest position of the suspension system is not zero but is biased toward one side. All the causes of this bias are not known, but mechanical misalignment may be a contributing factor. On future spacecraft using this system, a more precise method of alignment will be employed.

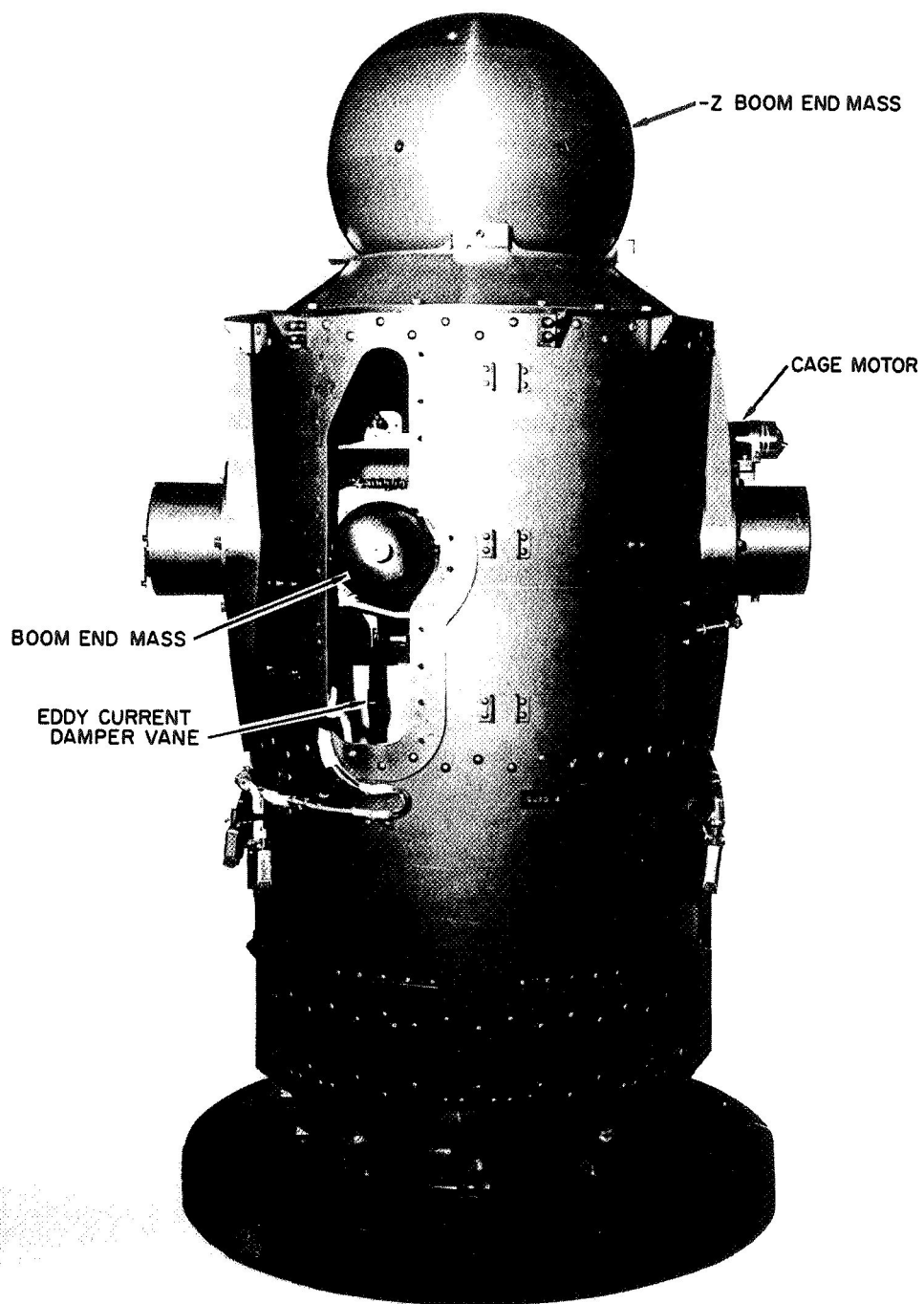


Fig. 5. Photograph of the torsion wire damper assembly

References

1. Tinling, B. E., and Merrick, V. K., "The Exploitation of Inertial Coupling in Passive Gravity-Gradient Stabilized Satellites," *J. Spacecraft Rockets*, Vol. 1, No. 4, July-Aug. 1964.
2. Tinling, B. E., Merrick, V. K., and Watson, D. M., "A Split-Damper Inertially Coupled Passive Gravity-Gradient Attitude Control System," *J. Spacecraft Rockets*, Vol. 4, No. 11, Nov. 1967.
3. Bainum, P. M., *On the Motion and Stability of a Multiple Connected Gravity-Gradient Satellite with Passive Damping*, TG8762. The Johns Hopkins University Applied Physics Laboratory, Silver Spring, Md., Jan. 1967.
4. Bainum, P. M., and Mackison, D. M., "Gravity-Gradient Stabilization of Synchronous Orbiting Satellites," presented at the British Interplanetary Society Spring Meeting, Loughborough University, Loughborough, England, Apr. 1967.
5. Fischell, R. E., *Proceedings of the DODGE Satellite AIAA/JACC Guidance and Control Conference*, Seattle, Wash., Aug. 1966.

N 69-11819

Introduction to Rolamite

J. P. Ford
Sandia Corporation
Albuquerque, New Mexico

Rolamite is a recently invented low-friction suspension system which appears to have applicability to many military and aerospace devices. This paper elaborates on some of the features of rolamite and its probable applications.

I. Introduction

Rolamite was invented early in 1967 by Donald Wilkes, a Sandia Corporation engineer, while he was investigating suspension systems for microminiature components.¹ It was announced publicly in October 1967.

II. Principle of Operation

A. Components

Rolamite is basically a low-friction suspension system which appears to have great applicability. In its most basic form, rolamite consists of two rollers which, for the time being, we will say are cylindrical and whose surfaces are fairly smooth (Fig. 1a). A flat metal band is intertwined in an S-shaped loop around the rollers — and,

for now, we will say that the band is of even width and thickness and is resilient enough to prefer to stay flat if it could (Fig. 1b).

We add a guideway which, for the present, we will assume has smooth, parallel inner surfaces. The guideway serves to position the rollers with respect to each other, provides something to anchor the band to, and provides surfaces for rolling (Fig. 1c). Without the ends of the band anchored, the elements would appear as they do in the top of Fig. 1d. When we apply tension to the band and fasten its ends, the rollers assume the typical rolamite configuration.

B. Cluster Movement

In this configuration, the roller cluster can move freely back and forth in the guideway, as shown in Fig. 2a. And, for reasons which we will soon see, it moves with remarkable ease.

¹Wilkes, D. F., *Rolamite: A New Mechanical Design Concept*, SC-RR-67-656. Sandia Laboratories, Albuquerque, N. Mex., Oct. 1967.

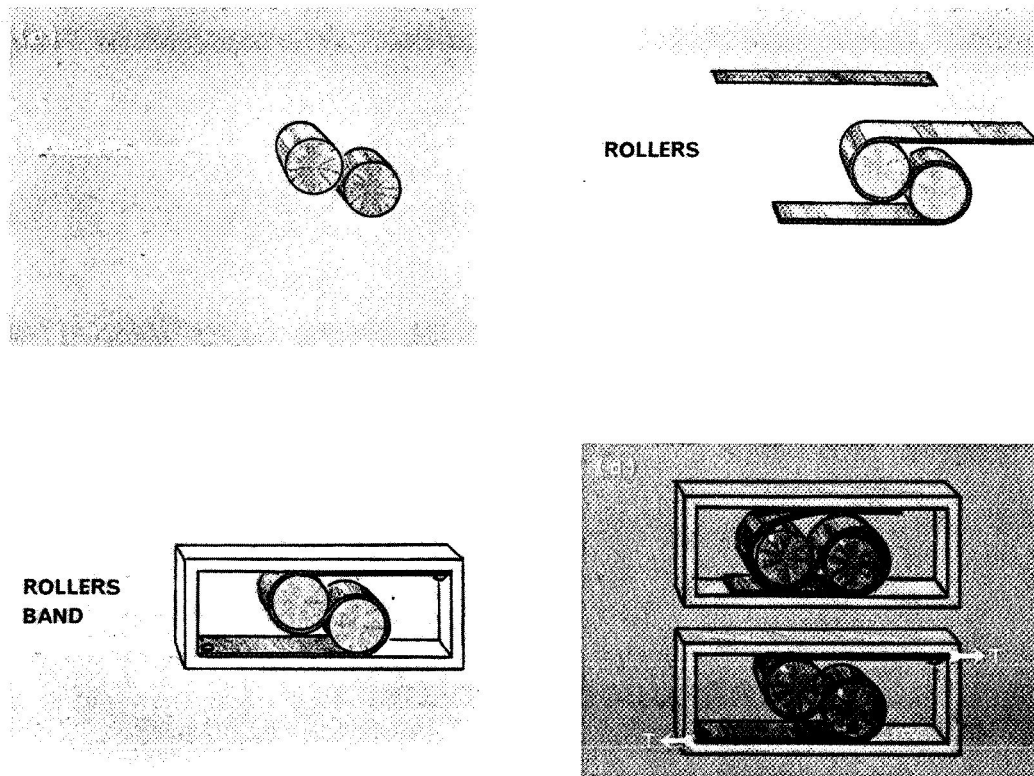


Fig. 1. Basic components of rolamite: rollers, band, and guideway

As the cluster moves between the parallel guide surfaces, the rollers maintain the same angle of repose as when we first tensioned the band (Fig. 2b). Also, as the cluster moves, the rollers counter-rotate. Moving from left to right, the upper roller is "reeling in" band as it moves, and passing it to the lower roller where the two meet, while the lower roller is simultaneously "reeling out" band at the bottom (Fig. 2c).

If we look more closely at this action, we see that all mating surfaces are moving in unison (Fig. 2d). Around the top roller, from A to B, roller and band have the same velocity. Both rollers and band are at equal velocities at B, and so on from B to C. The flat portions of the band, of course, are against the guide surfaces and are not moving. There is no sliding of surfaces in the system, hence no sliding friction. The only friction present is rolling friction, and it is very slight. Tests have shown that coefficients of friction an order of magnitude better than the best ball or roller bearings are possible with the rolamite geometry and are on the order of 0.0005.

Curiously enough, even this small amount of friction improves with the use of rolamite, because all parts re-

mate precisely in use, including the surface imperfections which wear down or are accommodated. Figure 2e shows this feature – as the cluster moves from left to right, the black points on the rollers and white A on the band will move, while white C remains stationary. If we rolled the cluster back to the left, all points would realign exactly as they were at the start.

Because the rollers have both rotation and linear movement, points on the rollers and band follow a cycloidal path in moving (Fig. 2f). This feature is important to an understanding of the rolamite movement, and it forms the basis for some useful functions. For instance, a dial indicator or speedometer could make use of this inherent rolamite feature because of the long cycloidal motion obtainable with a small movement of the roller cluster.

Because there is no sliding friction, most rolamites do not need to be lubricated. And because of surface remating, as we have just seen, they improve with use while operating entirely dry. They are especially valuable in low-pressure applications. Tests have shown, however, that the application of dry film lubricants will lower the coefficient of friction even further.

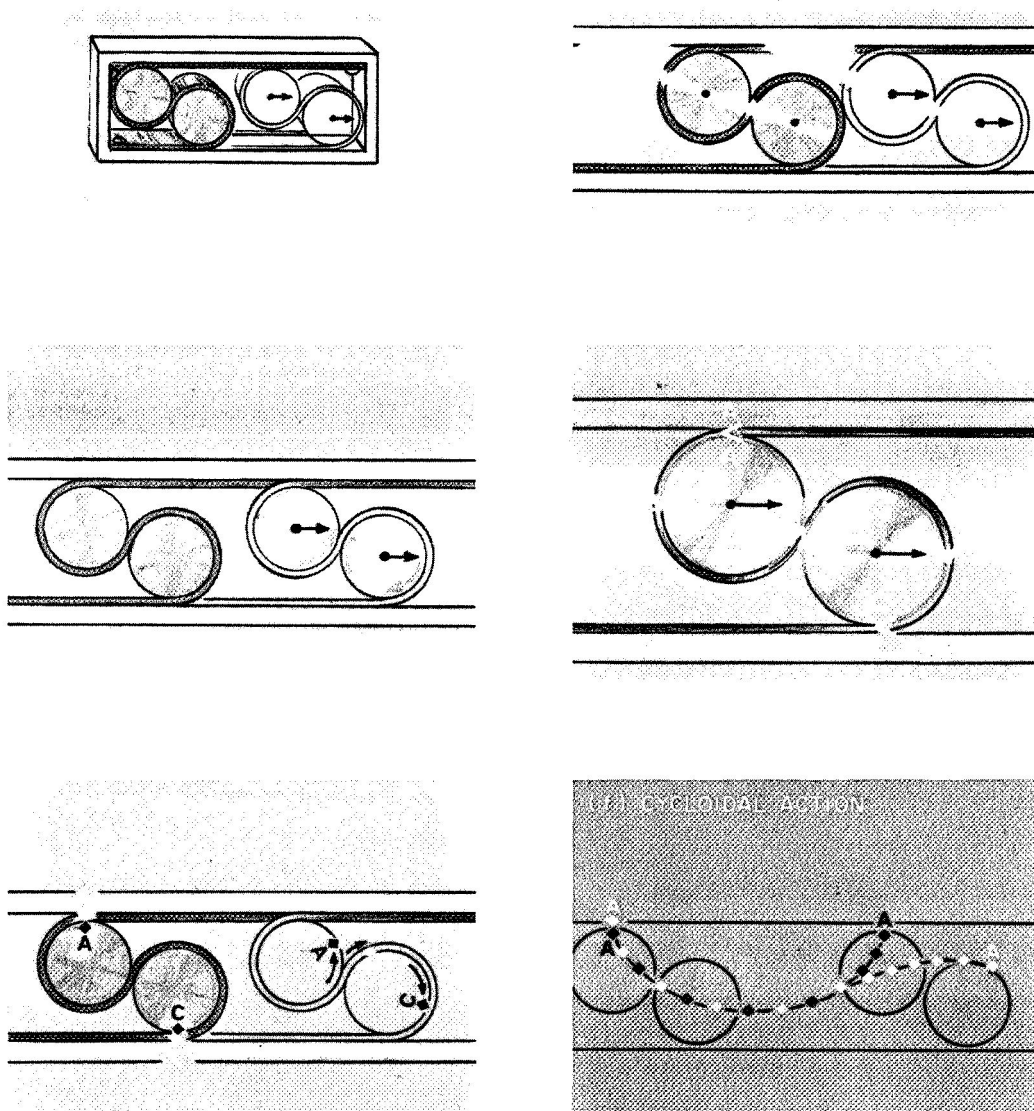


Fig. 2. Cluster movement and cycloidal action of rolamite

III. Force Generation

A. Force Exerted by the Band

Figures 1 and 2 illustrate how the basic parts of rolamite go together and how this achieves virtually frictionless rolling and other inherent features. Other features that can make rolamite versatile for the designer include its built-in capability to produce mechanical forces.

Let's look for a moment at the band (Fig. 3a). Remember that the band is resilient; it prefers to stay flat. If we loop such a band, the bending causes some elastic energy

to be stored in it. In this shape the S can be made to move freely along the distance between the bands, much as the rolamite cluster does in a guideway. The band does not prefer any one position over another.

However, if we weaken the band, as we have done by narrowing it at the arrow in Fig. 3b, the movement is no longer free. As shown, the stronger lower portion will flatten out and try to draw the weakened point into the loop of the S. When this happens, a force is exerted toward the right hand, and an opposite force would be required to move the S back toward the left hand.

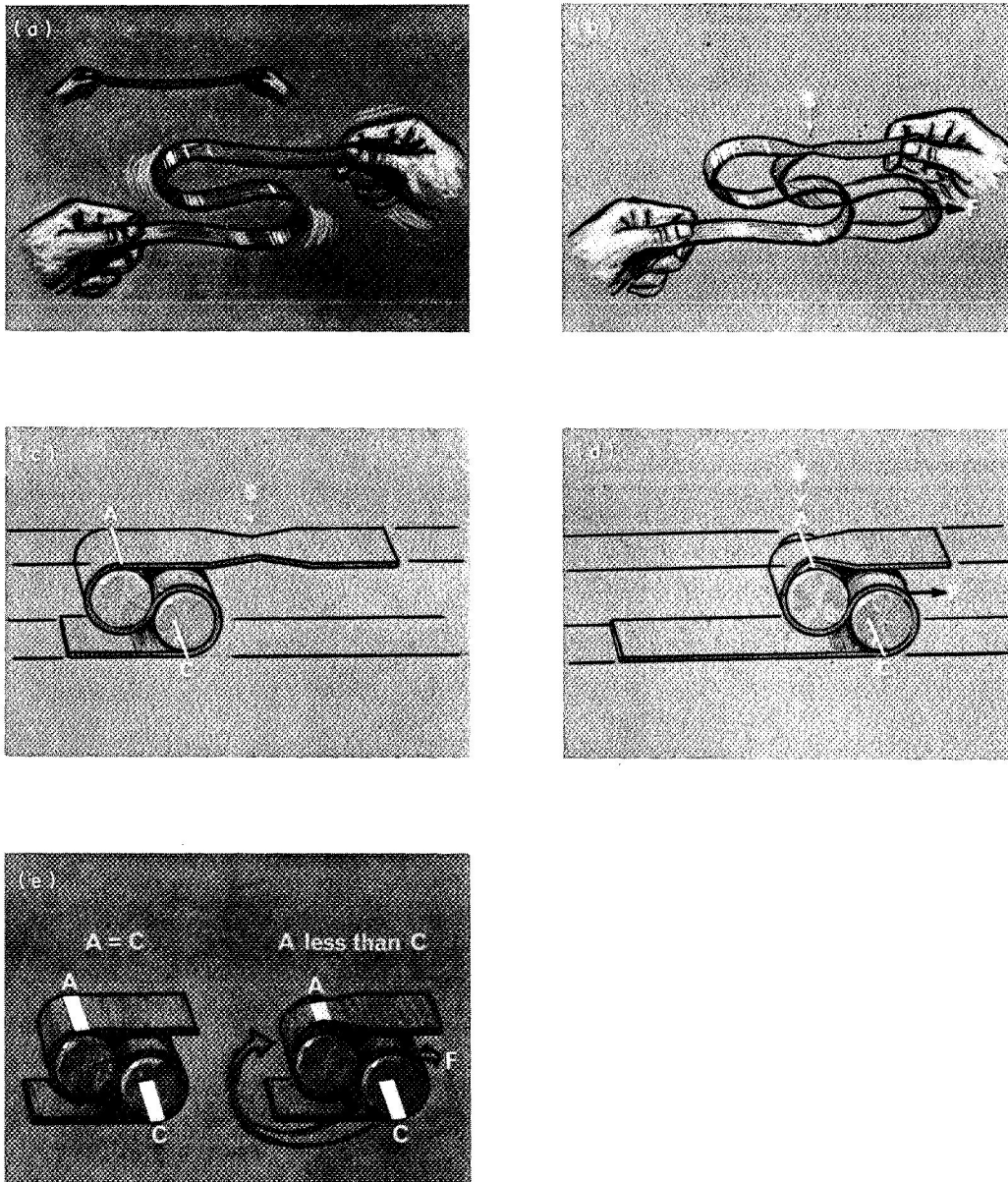


Fig. 3. Force generation by means of the rolamite band

Rolamite operates in much the same way, except that we have the rollers and guideway to consider. Because of them, the only pertinent energy is what is stored in the curved band between A and C. In the position shown in Fig. 3c, the weakened area at the arrow, being outside the area between A and C, would not exert a force to influence cluster motion.

However, if we move the cluster to the right far enough to bring any part of the weakened band portion into contact with line A, the band will exert a force which will move the cluster to the right until the weakened portion has passed A and is wound around the top roller (Fig. 3d). Conversely, if the weakened portion of the band were at C, a force would be generated to the left.

This is true because of the elastic strain energy in the band between points A and C. The energy is introduced in the band at C when the flat band is forced to assume the curvature of the roller. The amount of strain energy developed in the band is a function of the stiffness of the band material, the diameter of the roller, and the thickness and width of the band.

When the band is the same width at points C and A, the strain energy developed in the band at point C is released within the band at point A; hence there is equilibrium and no forces are generated. By narrowing the band at point A, this equilibrium is destroyed. The excess energy may be considered as a force acting at the roller centers, causing the cluster to move to the right, or accelerate motion to the right if the rollers are already moving in that direction. Equilibrium is again reached when the width of the bands at A and C are equal (Fig. 3e).

The force generated may be expressed as follows:

$$F = \frac{Et^3}{24} \frac{(c - a)}{r}$$

where

F = force generated

E = modulus of elasticity of band material

t = thickness of band

c = width of band at C

a = width of band at A

r = radius of roller

B. Alteration of Forces

There are several ways we can alter the band to create forces (Fig. 4a). What we have shown in Fig. 3 is the edge cut. We prefer the cutout method where the outside width is constant and the band is weakened internally. The tapered band is an excellent method of producing constant force deflection curves. The preformed band can be used to produce forces when band width cannot be reduced; for example, when it is desirable to carry electrical conductors in the band.

Figure 4b shows the force-deflection curve produced by a diamond-shaped cutout in the band. If the lead of the diamond were under point A, a force and motion would be produced to the right, and the maximum force would be attained when the widest part of the diamond was at point A. The force deflection curve for a diamond configuration is shown.

Change the shape of the cutout (Fig. 4c) and you change the shape of the force deflection curve. The possible shapes are endless—we show three here: a constant level, a negative spring constant, and a declining step function.

Figures 4a–c have shown how we can produce a force deflection curve with cutouts at one roller. Figure 4d shows a band with two cutouts, arranged so that as A completes passing through the top roller cutout, C begins to pass through the lower roller cutout. With the same direction of motion as before, the A cutout would accelerate the cluster, while the C cutout would decelerate it. Basically, what we are doing with these forces is tailoring the inertial behavior of the cluster mass without adding parts. This is an extremely useful property in many mechanical and electromechanical devices, particularly those that must be very small, yet sensitive and simple.

IV. Special Configurations

Aside from force generation, the band can be useful in many other ways—for instance, in carrying electrical conductors, as shown in Fig. 5a. Using conductive and nonconductive layers, this band works with the rollers to provide two normally open and two normally closed circuits, as in an inertially actuated switching device.

The rollers can also be varied in many ways useful to the designer. The first five shown in Fig. 5b are just a few; each will provide distinctive rolling properties in

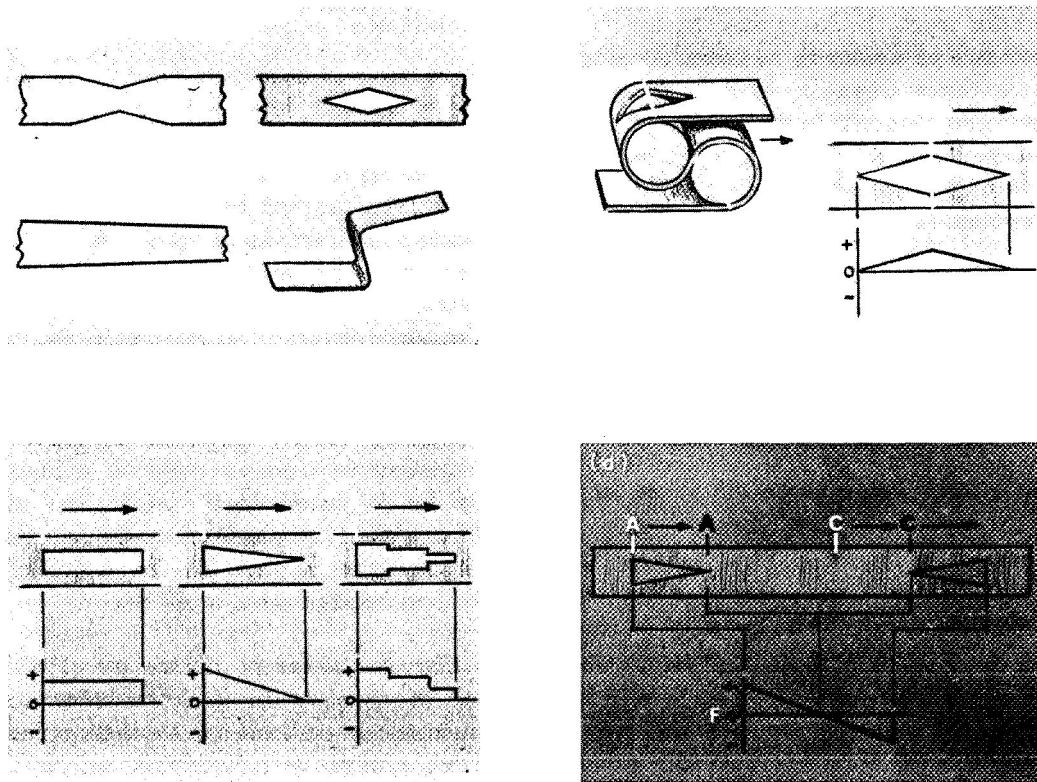


Fig. 4. Types of force generated by band alterations

any given band and guideway configuration. The sixth is an illustration that will not roll properly.

The guideway can also be modified to provide certain design features such as a recess in the surface or a wedge for detenting actions (Fig. 5c). Expanded and curved cross sections may also be used for specific design functions.

We can also alter and add parts in other ways. We can add springs and actuators in various places; cut tabs and tongues in the band for braking and rubbing; and add more sets of rollers and bands, or just more rollers, as shown in Fig. 5d.

Finally, we believe it is possible to develop rotary bearings which would operate with much less friction loss than conventional bearings, by applying the rolamite principles in a circular guideway (Fig. 5e). However, band fatigue is of great concern in high-speed, long-life rotary applications.

V. Capabilities

Basically, rolamite is a suspension system—a technique for suspending and guiding a moving mass with very

little friction loss. From this and its inherent properties, our engineers have developed a list of some 54 subcapabilities, as listed in Table 1.

Table 1. Some functional capabilities of rolamite

1. Force	19. Seal	37. Generate motion
2. Detent	20. Lock	38. Release energy
3. Latch	21. Set	39. Amplify force
4. Align	22. Wind	40. Change speed
5. Disrupt	23. Breakaway	41. Change torque
6. Squeeze	24. Sequence	42. Commutating
7. Insert	25. Record	43. Solenoiding
8. Pump	26. Limit	44. Thermostating
9. Damp	27. Fuse	45. Combined sensing
10. Clutch	28. Counterbalance	46. Potentiometric
11. Decouple	29. Trigger	47. Direct double integrating
12. Brake	30. Sear	48. Fluid resistor regulating
13. Readout	31. Calibrate	49. Programmed fluid resistance
14. Display	32. Switch	50. Tensile changing (such as straining)
15. Animate	33. Actuate pressure	51. Normal force variation
16. Contact	34. Regulate pressure	52. Sliding friction dissipation
17. Cut	35. Regulate fluid flow	53. Viscoelastic restraining
18. Adjust	36. Regulate speed	54. Escapement action

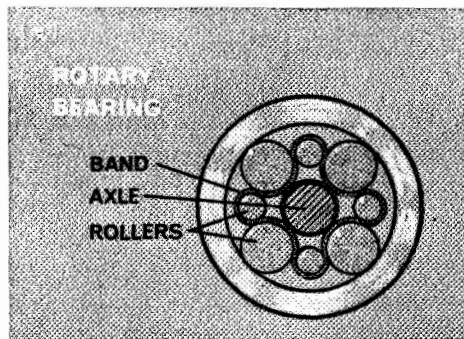
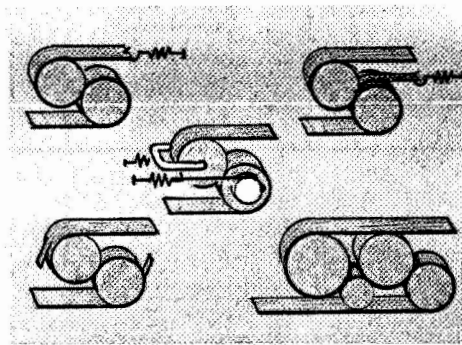
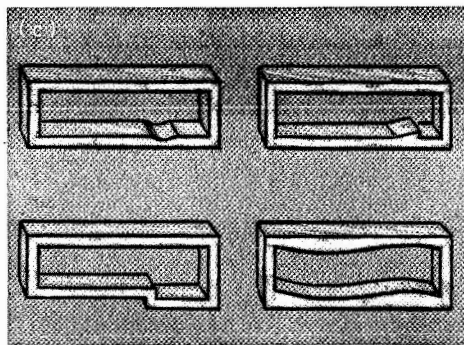
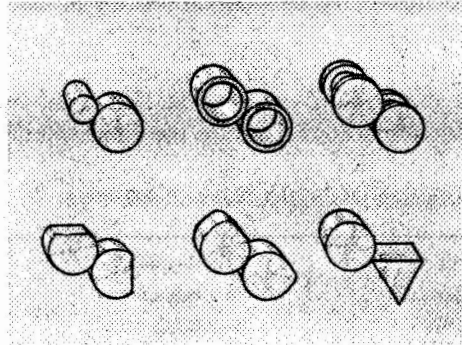
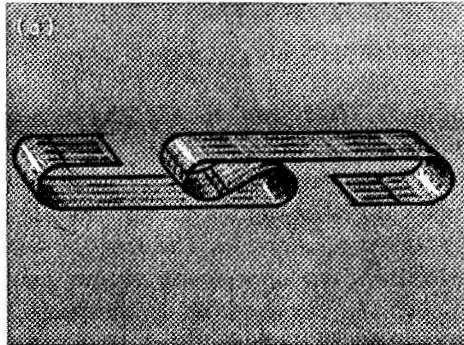


Fig. 5. Special configurations of band, rollers, and guideway

VI. Applications

Some potential uses for rolamite in aerospace applications are shown in Table 2.

To help translate some of these inherent features and capabilities into operating devices, three examples are shown in Fig. 6.

The first is a sheet metal cutter (Fig. 6a). This cutter uses a tight, high-angle configuration for mechanical ad-

Table 2. Potential space applications of rolamite

G-Switches	Commutators
Accelerometers	Actuators
Velocimeters	Firing pins
Sensors	Transducers for:
Odometers	pressure
Antitampers	velocity
Pullouts	distance
Time delays	referencing
Fuzes	recording
Sequencers	force

vantage and a direct stepup in roller diameters to amplify the force of the driver. The material is fed in at the top (A), a blade (B) cuts the material against a crossbar (C) when the cluster is driven forward by the downward pulling of the hydraulic driver (D). A spring attached to the rolamite band would return the cluster after cutting. The absence of gearing and journals would make the device inexpensive.

Figure 6b shows an accelerometer for defense and aerospace applications. Two variable-resistor elements (A) are shorted together by the upper roller (B) as the cluster moves in an insulated housing (C) when the entire unit is accelerated. The force of acceleration is counterbalanced by an opposing force created by the band cutout (D). Acceleration is measured as a function of differences in voltage drop across the two resistors as the upper roller changes their effective length.

In Fig. 6c is shown a thermostat using rolamite. In this device, a conductive bimetal band would have a high-expansion metal (A) and a low-expansion material (B). As temperature increased, the cluster would move to the right and out of contact with the end of the temperature

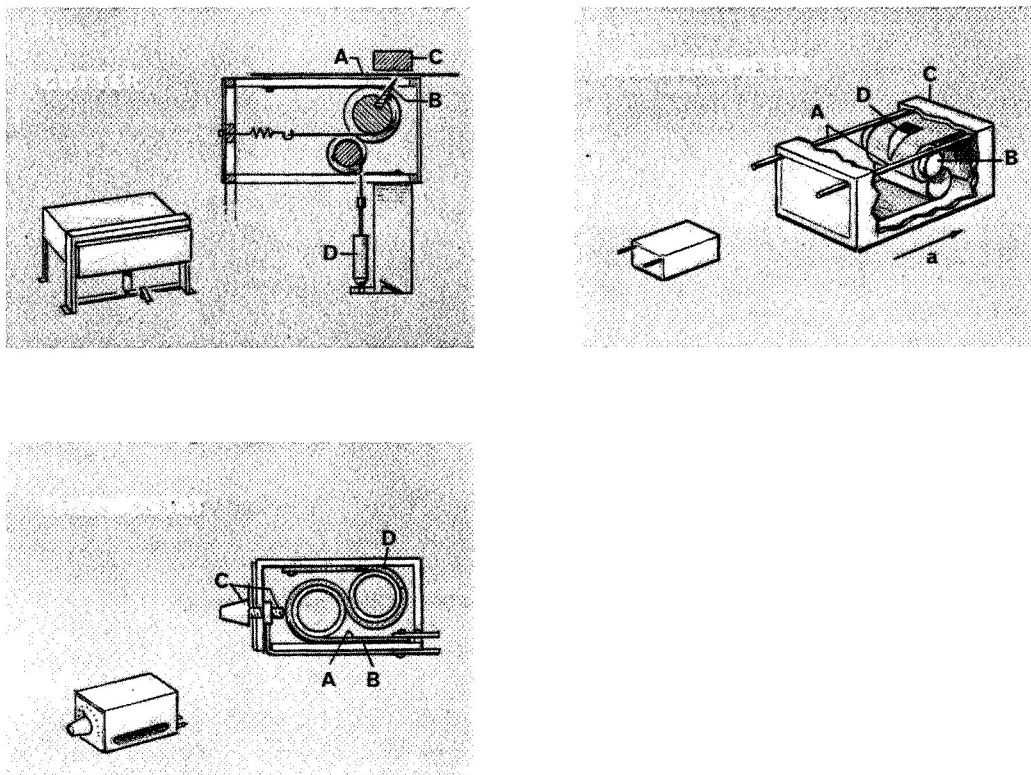


Fig. 6. Some representative applications of rolamite

selector screw (C) to open the circuit and shut off the furnace. As the room temperature cooled, the band cut-out (D) would return the cluster to the contact at C and turn the furnace on again.

Regarding the patent status of rolamite, pioneer patents on the basics of the device and on several applications have been applied for by the Atomic Energy Commission. On written request, the AEC grants non-

exclusive royalty-free unrevokable licenses on the U.S. patents on which it has the right to grant licenses for manufacture, sales, and use. Patents may be applied for on a specific application or design of rolamite on which a patent has not already been applied for. More specific information on the patent status of rolamite may be obtained by writing Mr. Roland A. Anderson, Assistant General Council for Patents, US AEC, Washington, D.C., 20545.

PRECEDING PAGE BLANK NOT FILMED.

N 69-11820

Nonmagnetic, Lightweight Oscillating Actuator

Dennis K. McCarthy
NASA Goddard Space Flight Center
Greenbelt, Maryland

The mechanism described provides a means of multiple indexing of a sensor to 90 deg \pm 15 min. The resulting permanent magnetic field, the power consumption, and the weight of the device are very low. The problems that were encountered in development and the results of the successful operation of the device in three spacecraft are presented.

I. Introduction

An essentially nonmagnetic indexing device was required for in-flight calibration of three orthogonal fluxgate sensors of the magnetometer experiment on *Explorers* 33, 34, and 35. The calibration, which determines the inherent drift in the sensors, is performed by periodically rotating the magnetometer sensors by 90 deg.

The magnetometer was designed to measure the interplanetary magnetic field in earth and lunar orbits. The intensity of the magnetic field in these regions is below 10γ ; thus, it was essential to minimize the permanent field of the mechanism in order to measure the drift in the magnetometer.

The novelty of the mechanism resides in the use of a nonmagnetic thermal actuator to provide oscillatory mo-

tion operable under varying environmental temperatures (-35 to $+70^{\circ}\text{C}$) in a vacuum for a long period with a high mechanical output-to-weight ratio for low power consumption. This paper describes the mechanical and electrical functions of the design which evolved, as well as the problems encountered. It concludes with an evaluation of the objectives achieved and suggests other applications for this device.

II. Objective

The objective was to develop a device which would

- (1) Have a permanent magnetic field (when power was not being applied to the heater) less than 0.25γ at 3 in.
- (2) Rotate 90 deg \pm 15 min of arc.

- (3) Have a minimum capability of 500 cycles.
- (4) Rotate the sensors within 10 min (the *on* time allocated for calibration of the sensors).
- (5) Require less than 3.75 W (2,250 W-s) during actuation.
- (6) Have a weight less than 0.5 lb.
- (7) Fail-safe, i.e., the magnetometers must not stop in any position other than 0 or 90 deg.
- (8) Operate within the temperature range of -35 to $+65^{\circ}\text{C}$.
- (9) Operate in a vacuum for at least 1 year.

III. Design

In selecting a design approach, other methods were considered: conventional indexing devices such as electrical stepping motors and solenoids were eliminated because of their inherent magnetic fields; a spring-powered, explosive-actuated, bistable escapement device is feasible but affords a limited number of actuations; and a bimetallic mechanism is entirely feasible and workable but it did not produce enough force to rotate three sensors as configured.

The oscillating mechanism employing a thermal actuator was adopted because the device could be made entirely of essentially nonmagnetic materials and it afforded a high ratio of mechanical output to electrical power at low weight and volume.

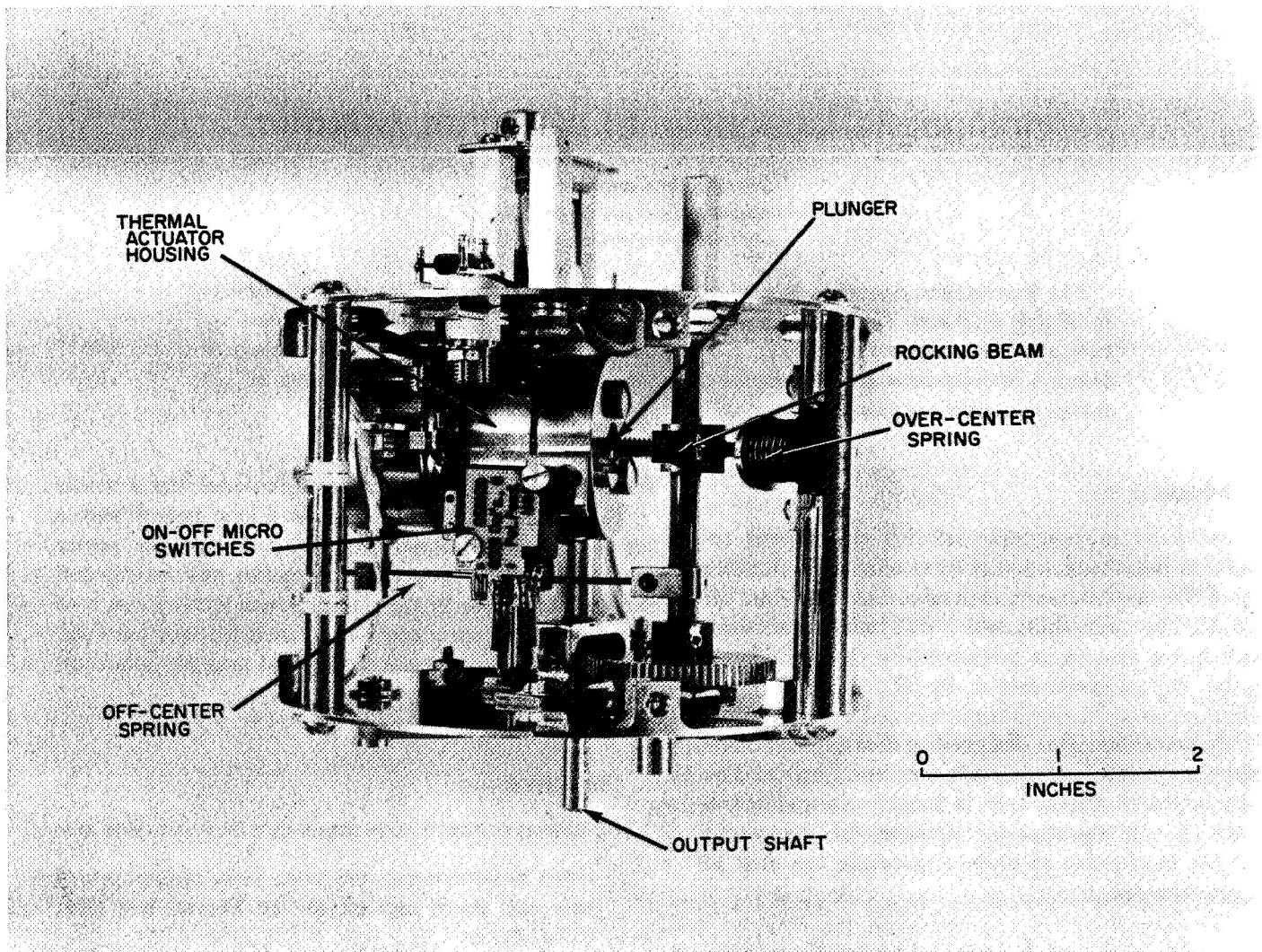


Fig. 1. Oscillating actuator assembly

IV. Mechanical Operation

The mechanism is shown in Fig. 1, and Fig. 2 is a sectional view showing the basic components. The mechanical operation is as follows: Electrical power is applied to a resistance heater plated on the thermal actuator (pellet), which is a paraffin-filled housing with a rubber boot and piston. The heater melts the solid paraffin, causing a volumetric increase of 10% which raises the internal pressure to 2,000 psi. This pressure on the rubber boot causes it to push on the conical tip of the piston, forcing it outward. The piston pushes against a rocking beam attached to a series of gears which rotates the sensors. The over-center spring provides a fail-safe

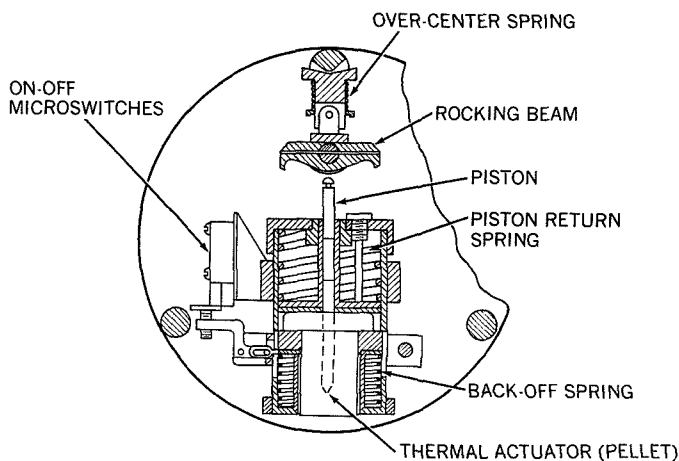


Fig. 2. Basic components of the actuator

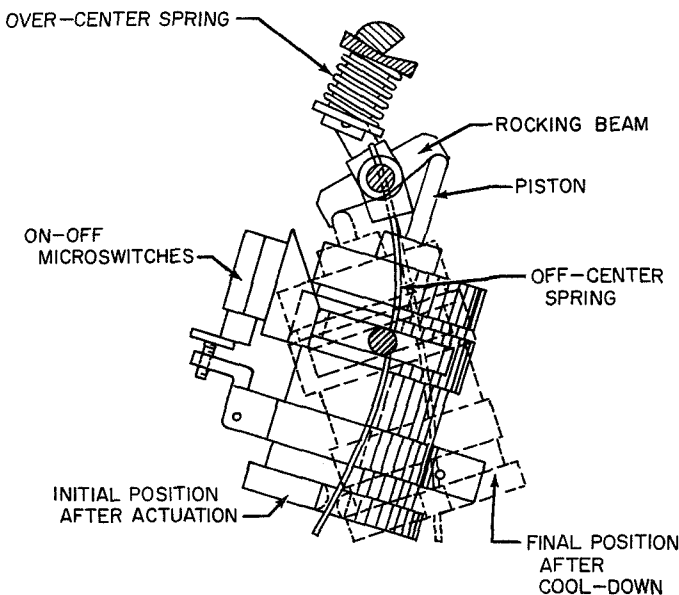


Fig. 3. Basic operation of the actuator

operation, in that it allows the sensors to be only in either of the two desired positions when the electrical power is terminated, as shown in Fig. 3.

Once the mechanism has rotated the sensors within the allowable 10-min time duration, the remaining electrical power input and mechanical power output is dealt with by allowing the pellet to float between compression springs. After the piston has rotated the sensors, it continues to push with increasing force against the rocking beam until it overcomes the force of the back-off spring, whereupon the actuator moves away from the rocking beam and closes microswitches which turn off the power. This allows the pellet to cool and reduce its force until it moves back again, opening the microswitches and allowing heat to be reapplied. This cycling or floating action continues until the 10-min timer terminates the electrical power. This motion prevents any mechanical damage. If the sensors cannot rotate because of mechanical binding, the pellet is allowed to produce a maximum force before it is backed off.

At the end of the 10 min, a compression spring pushes the piston back into the pellet as it cools and the pressure decreases. An off-center spring, preloaded as the sensors rotated, swings the entire actuator over to the other side of the rocking beam to prepare for rotation in the opposite direction during the next cycle.

V. Wax Pellet Actuator

The wax pellet is a standard production line component¹ consisting of a copper case with a rubber boot, a paraffin material, and a piston. The material, which expands on melting, pressing the rubber boot against the conical tip of the piston and forcing it outward, is a mixture of Epolene and a paraffin wax, yielding the desired melting point. A fine copper powder is added to increase conductivity and provide for a more uniform temperature throughout the material. During the solid-to-liquid transition, a volumetric increase of 10% increases the internal pressure to 2,000 psi. Above the operating temperature of 71°C, allowance in piston overtravel must be 0.002 in. for each degree, because the internal pressure could reach 4,000 to 6,000 psi if overtravel were not allowed. The case is designed for 3,500 psi and will deform at higher pressures. After 500 cycles, the piston will

¹Part No. 3005031 from the Harrison Radiator Division, General Motors Corporation.

index with a compression spring to within 0.010 in. of the original position, and the initial operating temperature will rise 1 to 3°C. The pellet weighs 26 g with approximately 750 mg of wax and has a maximum force of 35 lb (15,900 g) with a maximum stroke of 0.375 in.

VI. Materials

The prime considerations in the selection of materials for this device were low magnetic permeability and weight and adequate strength. All springs were made from Elgiloy, the bushings from Delrin, and the canister from fiber glass. The main structure was fabricated from aluminum, with critical wear surfaces hard-coated, to enhance the passive thermal design by polishing the surfaces. (Magnesium surfaces were not used because the need for plating them would have presented a handling problem.)

VII. Thermal Design

Passive thermal coatings controlled the temperature of the mechanism and sensors, which were encased by a fiber glass canister. The canister was coated on the inside with conductive silver paint to provide an RF shield and then scribed to reduce eddy currents. Thermal analysis indicated an interior and exterior coating of vapor-deposited aluminum with three circumferential stripes of white paint on the outside to maintain the sensor temperature between +10 and +50°C. Most of the components were highly polished aluminum in order to obtain a device which would contain most of the available heat by reducing emissivity. The pellet itself had a white paint outer layer to reduce its absorptance and was insulated with nylon bushings.

After the mechanism was optimized for power consumption, it was very sensitive to heat losses. As a result, it was important to isolate the mechanism from conduction and convection losses to ensure proper operation. Proper operating characteristics were obtained when the unit was tested in a vacuum environment.

VIII. Development Problems

The extreme magnetic cleanliness requirement demanded special consideration. Careful selection of mate-

rials and continual monitoring of fabricated pieces and procured items to determine that they had not been magnetically contaminated during manufacture were very successful. All the parts fabricated and finished at the Goddard Space Flight Center met the magnetic cleanliness requirement, as did all but two purchased items.

In one instance, the Elgiloy springs had oxidized during a heat treatment and the oxide coating was magnetic. The original microswitch cases were made of a glass-filled plastic resin that was found to be magnetic. Investigation revealed this to be a function of the fiber length. Lengthening the glass fibers corrected the condition.

Assembly of the mechanism was a very difficult problem. The mechanism appeared functional and accessible on the drawings but it became necessary to build assembly jigs in order to put the various components together.

The initial design utilized a bellows instead of the paraffin-filled pellet. A mathematical model of the mechanism, developed to determine the relationship of the various parameters in order to optimize the design for available power, identified the bellows working fluid combination that could provide the maximum force output for a given electrical power input. The results indicated that an isoamyl alcohol working in a beryllium copper bellows yielded the optimum design for this specific application. However, utilization of the bellows presented several problems:

- (1) Centrifugal force and the fact that the bellows could not be oriented to bring the alcohol in intimate contact with the heater required more power to conduct heat along the bellows to the fluid.
- (2) Since the thermodynamic characteristics of the bellows were a function of the vapor mixture contained in the bellows, it was required that the bellows be filled with only isoamyl alcohol liquid or vapor and sealed at a pressure less than atmospheric at room temperature—a difficult but attainable filling procedure.

The thermal actuator was very attractive for this design because of its high ratio of power output to weight; however, its adoption was strongly dependent upon the ability to provide a reliable nonmagnetic heater in intimate contact with the case. A method was developed for vapor-depositing a gold heater directly to the case in a

pattern that minimized magnetic fields. Its measured magnetic field in the operating condition was less than 1γ at 2 in. The heater was $9\frac{3}{8}$ in. long and 460 \AA ($1.84 \mu\text{in.}$) thick, thus providing a resistance from one heater to another of 80 ± 5 ohms.

IX. Alternative Uses

This mechanism is currently planned for many more satellites which require in-flight calibration of fluxgate-magnetometer sensors. The device can also be employed to actuate shutters or covers or to operate in remote areas where solar heat could be used as the heat input to operate the mechanism.

The metal bellows could be employed instead of the paraffin-filled element if it were not feasible to expose

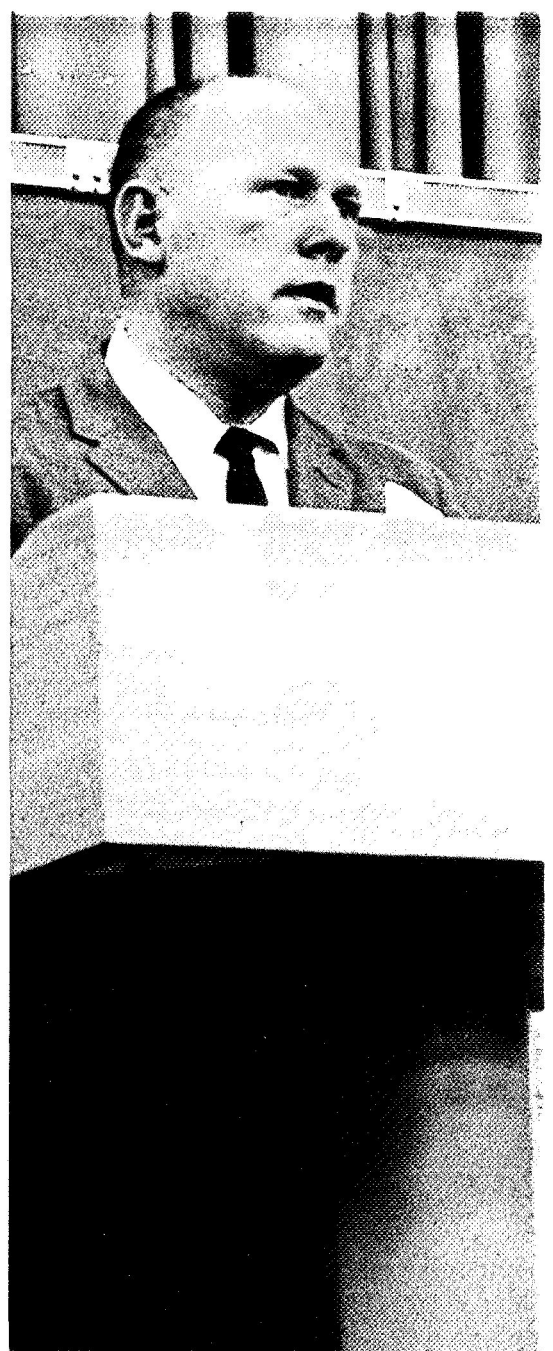
the rubber boot to an environment. Also, different gear combinations allow variable angular oscillatory motion.

X. Conclusion

The mechanism described in this paper provides positive, repetitive indexing, with the sensor rotating $90 \text{ deg} \pm 15 \text{ min}$, the permanent magnetic field less than the required 0.25γ , the power consumed less than 4 W, and the weight less than 0.5 lb.

Three mechanisms have been utilized on spacecraft, with the one employed on *Explorer 33* having the longest duration in the space environment. As of May 1968, this mechanism has operated once per day for 670 consecutive days where temperatures have ranged from $+50$ to -120°C (during a long earth shadow). All three mechanisms continue to operate with no sign of degradation.

PRECEDING PAGE BLANK NOT FILMED.



Session IV

Preceding page blank

OVERLEAF: Francis J. Carroll, NASA Electronics Research Center, Session Chairman

N 69-11821

The Surveyor Shock Absorber*

F. B. Sperling

Jet Propulsion Laboratory
Pasadena, California

The landing shock absorbers used on the Surveyor spacecraft are described. A hydraulic cylinder and piston arrangement was found to be capable of providing both the required damping and spring action. A digital computer program, simulating the landing process, was used to assess performance and spacecraft landing stability. The shock absorbers performed very satisfactorily throughout the Surveyor program.

I. Introduction

The landing gear of the *Surveyor* spacecraft (Fig. 1) consists of three inverted tripod-type landing legs with crushable aluminum honeycomb footpads and three crush blocks (cylindrical pieces of aluminum honeycomb material) mounted on the underside of the spaceframe.

The upper of the three tubular leg members contains a shock absorber spring assembly. The two lower leg members, which are rigid and cross-braced to each other, are hinged to the spacecraft frame (see Fig. 1); at touchdown, they rotate upward, thereby compressing the shock absorber column.

The function of the shock absorbers was to cushion the spacecraft landing impact and to dissipate the residual kinetic energy of the spacecraft at the time of first ground contact. In addition, parallel springs were required to reextend the legs after impact in order to obtain a defined position of the frame relative to the lunar surface. This was necessary in order to perform the planned lunar surface experiments properly.

While the footpads and the crush blocks were also capable of energy dissipation, this was not intended to be their principal function. The footpads (the lower parts of which consist of aluminum honeycomb with a crushing strength of 10 psi) were designed with the objective of protecting the shock absorber columns from excessive lateral loads during impact. The body blocks, with a crushing strength of 40 psi, were incorporated to secure a ground clearance of at least 4 in. between the frame

*This paper presents the results of one phase of research carried out at the Jet Propulsion Laboratory, California Institute of Technology, under Contract No. NAS 7-100, sponsored by the National Aeronautics and Space Administration.

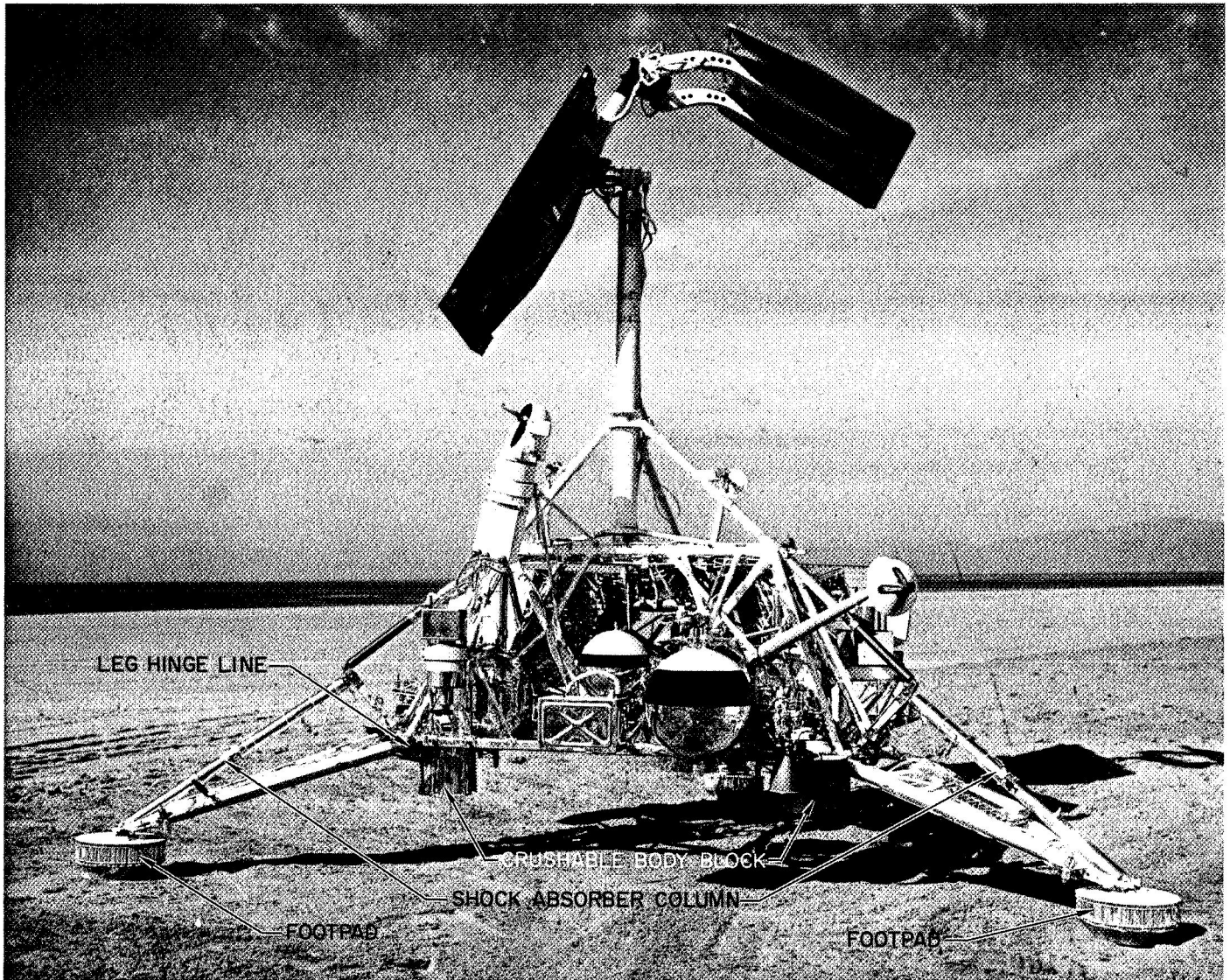


Fig. 1. Surveyor spacecraft model in landed configuration

and a planar landing surface, throughout the touchdown phase.

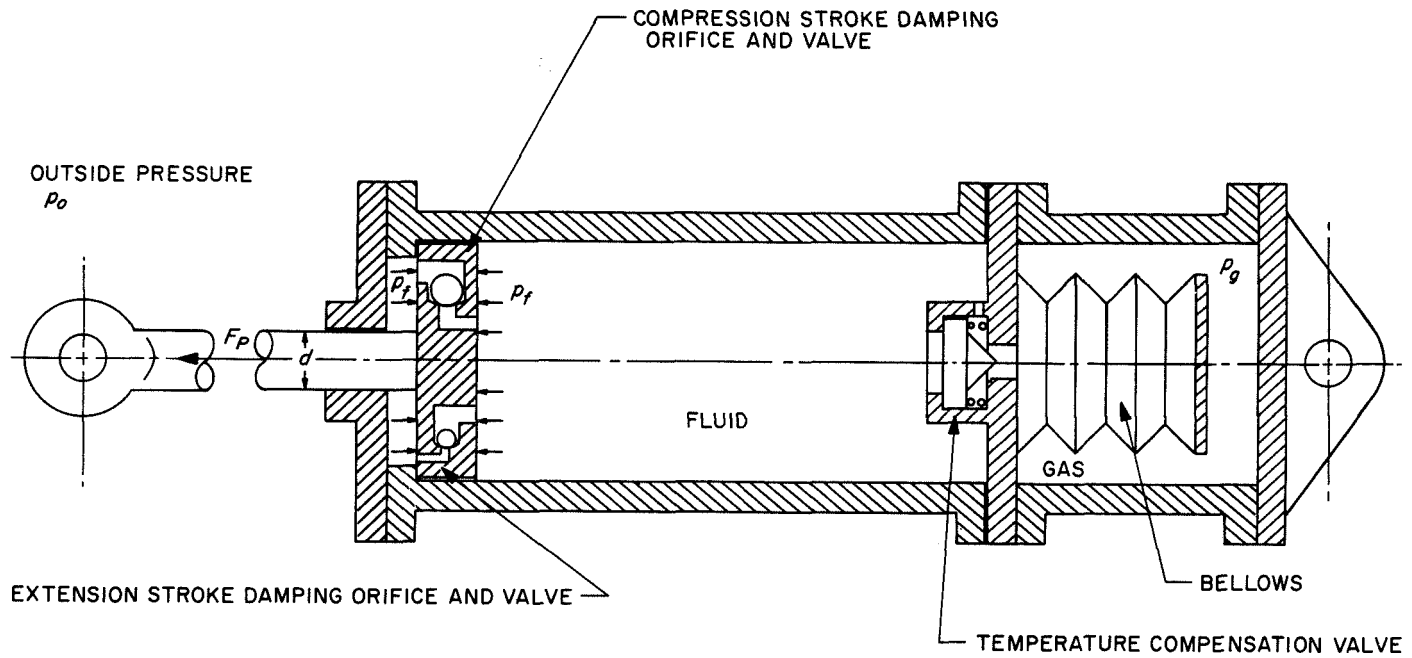
Hence, the shock absorbers had to have the capability of dissipating essentially the entire landing energy. As we now know, this indeed was required of them and was accomplished in all five successful *Surveyor* landings, since practically no footpad or body block crushing took place in any of the landings because of the relative softness of the upper lunar surface layer.

II. Working Principle

While there was no difficulty in satisfying the functional requirement of a combined spring and damping

action with a variety of conventional concepts, the additional requirement of highest possible weight economy could not be met with any type of metallic spring. For the damping action, the dashpot principle, i.e., the forcing of a damping fluid through an orifice, seemed acceptable, and after it was found that the required cylinder and piston arrangement could be utilized to provide the desired spring action at the same time, this concept was adopted.

The working principle is explained in Fig. 2. It is based on the fact that no fluid is absolutely incompressible. Consequently, when a perforated piston (shown schematically in Fig. 2) is pushed into a cylinder entirely filled with fluid and the fluid volume is increasingly



IN EXTENDED POSITION $\left\{ \begin{array}{l} \text{FLUID PRESSURE} = p_f = \text{GAS PRESSURE} = p_g \\ \text{SPRING FORCE (PRELOAD)} F_P = (p_f - p_o) \frac{d^2}{4} \pi \end{array} \right.$

IN STROKED POSITION, THE TEMPERATURE COMPENSATION VALVE IS CLOSED AND THE SPRING FORCE IS INCREASED, BECAUSE OF COMPRESSION OF THE FLUID (ENTERING OF PISTON ROD). A DAMPING RESISTANCE IS ALSO ENCOUNTERED, DEPENDING ON THE FLUID AND ORIFICE CHARACTERISTICS AND LINEARLY PROPORTIONAL TO THE SQUARE OF THE STROKING VELOCITY.

Fig. 2. Working principle of the Surveyor shock absorber spring assembly

reduced by the entering piston rod, the fluid is compressed, resulting in a steep increase in pressure. A restoring force equal to the pressure difference between fluid pressure and outside pressure times the cross section area of the piston rod results.

By pressurizing the fluid above the outside pressure, with the piston in the extended position, a preload can be obtained on the same principle. Since a preload was required to support the weight of the *Surveyor* spacecraft after landing, a provision for fluid pressurization was made by connecting the fluid chamber to metal bellows (Fig. 2) surrounded by a sealed gas chamber. Pressurizing the gas automatically pressurized the fluid to the same level, because of the elasticity of the bellows. However, upon actuation of the piston, the connection to the bellows had to be closed, else the volume reduced by the entering piston rod would have been made up by an extension of the bellows. For this purpose, the spring-loaded temperature compensation valve was incorporated, closing the fluid chamber upon a rapid pressure increase. For a slow pressure rise, however, this valve

stayed open, thus allowing the fluid to expand and contract with changing temperature without significantly affecting its pressure and, consequently, the preload.

III. First Design

Before implementation of the working principle into a design, the specification of such parameters as maximum load, piston travel, and spring and damping characteristics was necessary. It appeared desirable to design a maximum-efficiency shock absorber that would dissipate a certain amount of energy within a certain stroke with the lowest axial peak load, ideally requiring a constant force-vs-stroke characteristic. Since the damping force in an orifice damper varies proportionally with the square of the stroking velocity, the desired characteristic required a variable damping coefficient (i.e., a stroke-dependent variable orifice).

While, theoretically, the loading could have been held to any desired level by allowance of the corresponding

stroke length, the latter was limited by considerations of stability and ground clearance during the landing process to a maximum of 4.5 in. Thus, the constant force in the force-vs-stroke characteristic was determined by the condition that no "bottoming" of the shock absorber was to be encountered for the highest specified landing velocities (20 ft/s vertical and 7 ft/s horizontal).

Many factors were considered in determining how this constant force was to be distributed between the spring force and the damping force and whether or not it was desirable, or even possible, to design for the constant-force characteristic. One consideration unfavorable to the latter was that of the fluid chamber design for pressure. At the beginning of the stroke, the opposing force is almost entirely due to the damping effect — i.e., to the difference of pressures acting on the piston face from the left to the right of the piston. At the end of the stroke, however, the force is a pure spring force, dependent upon the absolute fluid pressure (assuming an outside pressure of zero), acting only on the piston rod cross section. To equalize these forces would have required a considerably higher fluid pressure at the end of the stroke than at the start.

Compromising between these conflicting requirements led to an optimized damping profile (a change of damping coefficient vs stroke) to be implemented by a cylinder-fixed metering pin protruding through the damping orifice and thereby changing its size as the piston moved in.

This compression-stroke damping was found to be totally inadequate for the extension stroke; it would have resulted in a high springback of the spacecraft after the initial landing. Consequently, a separate orifice had to be provided for the extension stroke, and two valves (schematically indicated in Fig. 2) were added, to appropriately open or close the two damping orifices.

The extension damping was designed to provide critical damping for the leg extension stroke. Because the characteristic of the fluid spring was not linear, this could be only approximated for one landing condition with one initial velocity. The selected conditions were for a landing on a level surface with the three legs touching simultaneously and with the nominal vertical spacecraft landing velocity of 12.6 ft/s. In this case, after impact and deflection of the legs, the spacecraft was to rise to its prelanding configuration without overshooting.

A titanium alloy containing 13% vanadium, 11% chromium, and 3% aluminum was chosen for the main body, including the fluid cylinder, because of its high strength/weight ratio. Properly heat-treated tensile coupons showed an ultimate tensile strength of 194,000 to 207,000 psi. For the damping fluid, a silicone compound (Dow Corning F-4029) was selected for its high compressibility and its ability to perform without excessive change in viscosity within the specified temperature range from 0 to 120°F.

A lock-finger arrangement was implemented to prevent spacecraft sagging as a result of possible fluid or gas leakage after landing. Two spring-loaded lock-fingers were mounted on the upper stationary part of the assembly and engaged in a collar on the lower telescoping part. These were shaped so that they would break loose if an axial load of the order of the spring preload were applied. Hence, the intended shock absorber operation was not constrained. After reextension of the legs, the lock-fingers reengaged and would not break loose under the loading imposed by the spacecraft weight.

A redundant locking system was provided by pyrotechnically operated pin drivers. Also located on the stationary part of the shock absorber column, this locking device had the capability of being commanded from the earth to drive a pin into a strip of soft aluminum attached to the telescoping part of the assembly.

Unit dimensions are 2 in. outside diameter and 37.53 in. between connection points in the extended position; the weight is approximately 3.9 lb.

IV. Second Design

During manufacturing and checkout of prototype units, several problem areas became apparent. The selected titanium alloy proved to be hard to machine and particularly difficult to weld. Since the material is brittle and notch-sensitive, each unit became a potential hazard when pressurized to the required room temperature pressure of 1700 psi. It was necessary to impose special shipping and handling procedures to protect the assemblies from even slight scratches or bumps, as well as to protect personnel. Another problem arose in the manufacture of the metering pin. Even though the metering pins were machined to extremely close tolerances, a checkout of assembled units showed a considerable scatter in the damping around the design profile, which specified

a damping coefficient that increased considerably more strongly than linearly with increasing stroke.

A reevaluation led to a second design which conformed to the same principle and basic configuration but which deviated significantly from the first in the two areas described below.

First, the material of the basic structure was changed to a titanium alloy with 4% vanadium and 6% aluminum. Although weaker in tensile strength by approximately 20% compared with the original alloy (13% V, 11% Cr, 3% Al), the latter alloy is far less brittle and less notch sensitive and is easier to machine and to weld. The metering pin was eliminated, and an optimum constant orifice size was determined. Although this resulted in a less desirable force-vs-stroke characteristic, the peak force could be kept below the maximum design load of 10,000 lb. It was found that the damping coefficient, even for a constant orifice, is not constant; rather, it increases approximately linearly with the stroke when a constant compression force is applied. This effect results from the increase in fluid pressure with stroke, and it is, in this application, very desirable because it retains, in part, the advantages of a varying damping profile, which had originally led to the metering-pin concept. A further compensation of the force falloff was accomplished by increasing the spring rate.

Second, the lock-finger arrangement was eliminated. Since its break-loose threshold had proved to be difficult to control, it was decided that the backup locking device (the pyrotechnic pin-drivers) would be sufficient. Unit weight of the second design was approximately 4.4 lb.

This second shock absorber design was used with *Surveyors III* through *VII*; *Surveyors I* and *II* utilized the first design. *Surveyor I* performed a successful landing, and *Surveyor II* suffered a propulsion system failure during the midcourse correction maneuver. Of the remaining *Surveyors*, all but *Surveyor IV* landed successfully. Telecommunication with *Surveyor IV* was lost 2.5 min before predicted touchdown.

V. Analytical Representation

During the conceptual study and design phases of the shock absorber, the most helpful tool for evaluating performance and assessing landing stability and ground clearance was a digital computer program that mathematically simulates the landing process. In this program,

the spacecraft structure above the landing gear connection points is represented as a rigid body with adjustable mass and inertia properties. The landing gear, however, is geometrically and dynamically modeled in detail. For any desired initial landing velocities, spacecraft tilt, and ground slope of a rigid planar surface, analytical landings could be performed by means of this program to indicate spacecraft motion, acceleration, landing gear deflections and loadings, and other performance parameters throughout the landing process. In the program, the shock absorber assembly is represented by the following equation:

$$F_s = \frac{\dot{l}}{|\dot{l}|} \dot{l}^2 R_C S_D + K_D S_K (l - l_0) - F_P + 0.05 \frac{\dot{l}}{|\dot{l}|} [K_D S_K (l - l_0) - F_P]$$

where

F_s = axial shock absorber column force

l_0 = length of column in extended position

l = length of column

\dot{l} = change of column length with time

R_C = damping coefficient

S_D = damping coefficient versus stroke profile

K_D = spring rate at zero stroke

S_K = spring rate vs stroke profile

F_P = spring preload

The first term represents the damping force proportional to the square of the velocity; because of the fractioned factor, its sign automatically reverses with each change in velocity direction, which is also used to select the proper damping coefficient and profile for compression and extension, respectively. The second term represents the increase in spring force with stroke; together with the constant preload, represented by the third term, the entire spring force of the fluid spring is expressed. The last term, in magnitude equal to 5% of the spring force, represents an estimated friction force, again reversed in sign as appropriate by the fractioned velocity factor.

In the step-by-step integration, the first delta stroke (Δl) after ground contact is determined by assuming that no forces are acting on the spacecraft — i.e., that the spacecraft is continuing in its path as though the ground

had not been encountered, for a preselected time increment Δt . For the next step, Δl and Δt are used to define the stroking velocity, while, from the spring and damping profile, the values corresponding to the incremental stroke Δl are selected. From this, the shock absorber force is determined and regarded as acting on the spacecraft throughout the next Δt . As dictated by the spacecraft's equations of motion, this results in a new incremental stroke Δl , which is used again, as above, for the next Δt , and so on.

The quality of this analytical shock absorber force representation could be checked directly by comparison with telemetry data from the *Surveyor* landings, as discussed in the performance section of this report (Fig. 3).

VI. Testing

A very extensive test program was carried out on both type-approval and flight-acceptance levels. The first category included burst tests, vibration tests, leak tests, functional tests, and verification tests for the damping and spring characteristics at room temperature and at the specified temperature extremes. Also conducted were dynamic loading tests, including impact tests, performed in a drop test fixture and increased to the point of unit destruction. Finally, several units were tested in full-size

vehicle drop tests with maximum design conditions in respect to landing velocities, vehicle tilt, and ground slope.

The flight-acceptance test series included functional tests, vibration tests, leak tests, preload tests at various temperatures, and verification of spring and damping characteristics at room temperature.

In addition, preload tests were performed on every flight unit before shipment to the launch site and again immediately before installation on the spacecraft. In these tests, each unit was slowly stroked to $\frac{1}{4}$ in.; the force necessary to initiate and maintain movement was measured. Then, the load was slowly decreased and the unit allowed to extend; again, the force necessary to maintain movement was measured. By this procedure, a check of the preload as well as of the internal friction of the unit was made. For the first design type, this test was conducted with disengaged lock-fingers. If preload and friction were found within acceptable limits, the unit was accepted as fully charged and operational.

VII. Temperature Control

Although the shock absorbers were required to survive temperature extremes of -300 and $+300^{\circ}\text{F}$, the temperature range within which they were to be operational

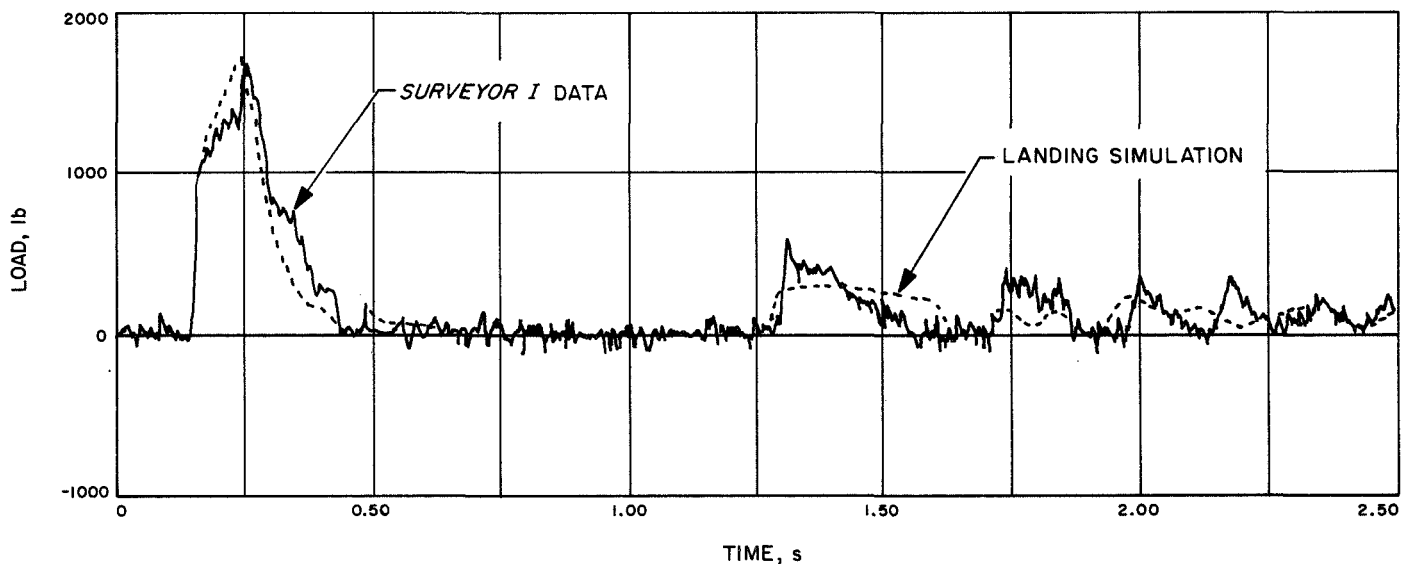


Fig. 3. History of axial loading of the leg 2 shock absorber column during the lunar landing of *Surveyor I*. (The dashed line represents the same data derived from an analytical landing simulation under identical landing conditions.)

could be narrowed to between 0 and 120°F. This was achieved by passive temperature control, from application of thermal paint patterns and aluminized Teflon strips.

VIII. Performance

Each shock absorber unit was equipped with a temperature-compensated strain-gage bridge consisting of four gages attached to the gas-filled cylinder. These were arranged to measure only axial loads. The strain gages, as a part of the engineering instrumentation, were intended to enable assessment of the spacecraft performance during touchdown. The output of the three bridges was transmitted in the form of frequency-modulated, continuous analog data. Within limits, these data could also be used to assess the dynamic behavior of the surface material at the landing site, allowing estimates of lunar surface mechanical properties. Figure 3 shows one of the *Surveyor I* landing shock absorber force histories, together with an analytical simulation. It shows that the compression stroke, building up to a peak force of approximately 1600 lb, lasted about 0.1 s, followed by a 0.2-s extension, at which time the axial force returned to zero, indicating spacecraft rebound. At 1.1 to 1.2 s after first contact, footpad reimpact was registered; this was followed by a ringout oscillation, after which (beyond the time covered in Fig. 2) the force settled at approximately 120 lb, because of the spacecraft's weight. While, in general, a very satisfactory performance of the shock absorber units was found, the rebound was more pronounced than had been expected for a landing with a slightly lower-than-nominal vertical landing velocity. *Surveyor I* landed with 11.6 ft/s vertical velocity (nominal was 12.6 ft/s) on a surface that was within 2 deg of level.

Records very similar to Fig. 3 were obtained from all shock absorbers in each of the successful *Surveyor* landings. Spacecraft rebounding was experienced in all

Surveyor landings; it was slightly higher with the second design type of shock absorber units because of the increased spring rate of the fluid spring. Although this constituted a deviation from the design specification, the spring-back was not detrimental to the landing or to other performances of the spacecraft. It was even found to be advantageous, since, in some cases, it exposed the first footpad imprints to the spacecraft camera, facilitating scientific soil studies.

The leg locking devices appeared to have worked satisfactorily on *Surveyor I*. In the later missions, however, two instances were observed in which a leg did deflect after the command to actuate the lock-pin drivers had been sent. In both cases, this occurred at the beginning of lunar night and did not affect lunar surface operations.

Acknowledgment

Under the technical direction of the Jet Propulsion Laboratory, California Institute of Technology, Pasadena, California, the *Surveyor* shock absorber assemblies were developed, manufactured, and tested by three contracting firms.

Conceptual development and design specification were accomplished by R. E. Deitrick and R. H. Jones of Hughes Aircraft Company, El Segundo, California.

Manufacturing and testing were performed by O. W. Scheflow, T. Scarff, and W. Fruehauf of the National Water Lift Company, a Division of Pneumo Dynamics Corporation, Kalamazoo, Michigan, under subcontract to the Hughes Aircraft Company, and were monitored by R. E. Deitrick and A. L. Peterson of Hughes.

The fluid spring concept was suggested by the Cadillac Gage Company, Monterey, California.

PRECEDING PAGE BLANK NOT FILMED.

N 69 11822

Unique Mechanism Features of ATS Stabilization Boom Packages*

R. A. Lohnes and D. N. Matteo
General Electric Company
Valley Forge Space Technology Center
King of Prussia, Pennsylvania

E. R. Grimshaw
SPAR Aerospace Products, Ltd.
Toronto, Canada

This paper describes the unique mechanism of the motorized primary boom packages and the damper-borne self-erecting secondary boom package utilized on the Applications Technology Satellite (ATS) gravity-gradient experiment. The spacecraft failed to achieve the required orbit, but the mechanism performed as planned.

I. Introduction

In April 1967, NASA placed in orbit the ATS-2, a gravity-gradient-stabilized satellite that was the second of a series of spacecraft known as *Applications Technology Satellites*. A primary purpose of the ATS series is to evaluate the characteristics of gravity-gradient stabilization as a means of satellite attitude control.

Gravity-gradient satellite attitude control makes use of the differences in gravitational forces acting on the distributed masses of the primary stabilization booms to maintain a constant attitude with respect to earth. Gravity-gradient stabilization is possible only if existing

oscillatory motions of a spacecraft can be damped out by some form of energy dissipation.

The ATS-2 (Fig. 1) medium-altitude spacecraft attained a highly elliptical orbit, instead of the planned circular orbit. Accordingly, gravity-gradient stabilization was precluded. Nevertheless, the mechanisms described in this paper functioned successfully in orbit.

The General Electric Company (GE) designed the gravity-gradient stabilization systems for this series of experimental satellites. Each system utilizes four 132-ft primary gravity-gradient booms (deployed in the form of an X) rigidly attached to the satellite, as well as a secondary, or damping, boom (consisting of two 45-ft collinear rods) coupled to a damping mechanism and a torsional spring.

*This work was performed by the General Electric Company for the NASA Goddard Space Flight Center under Contract No. NAS5-9042.

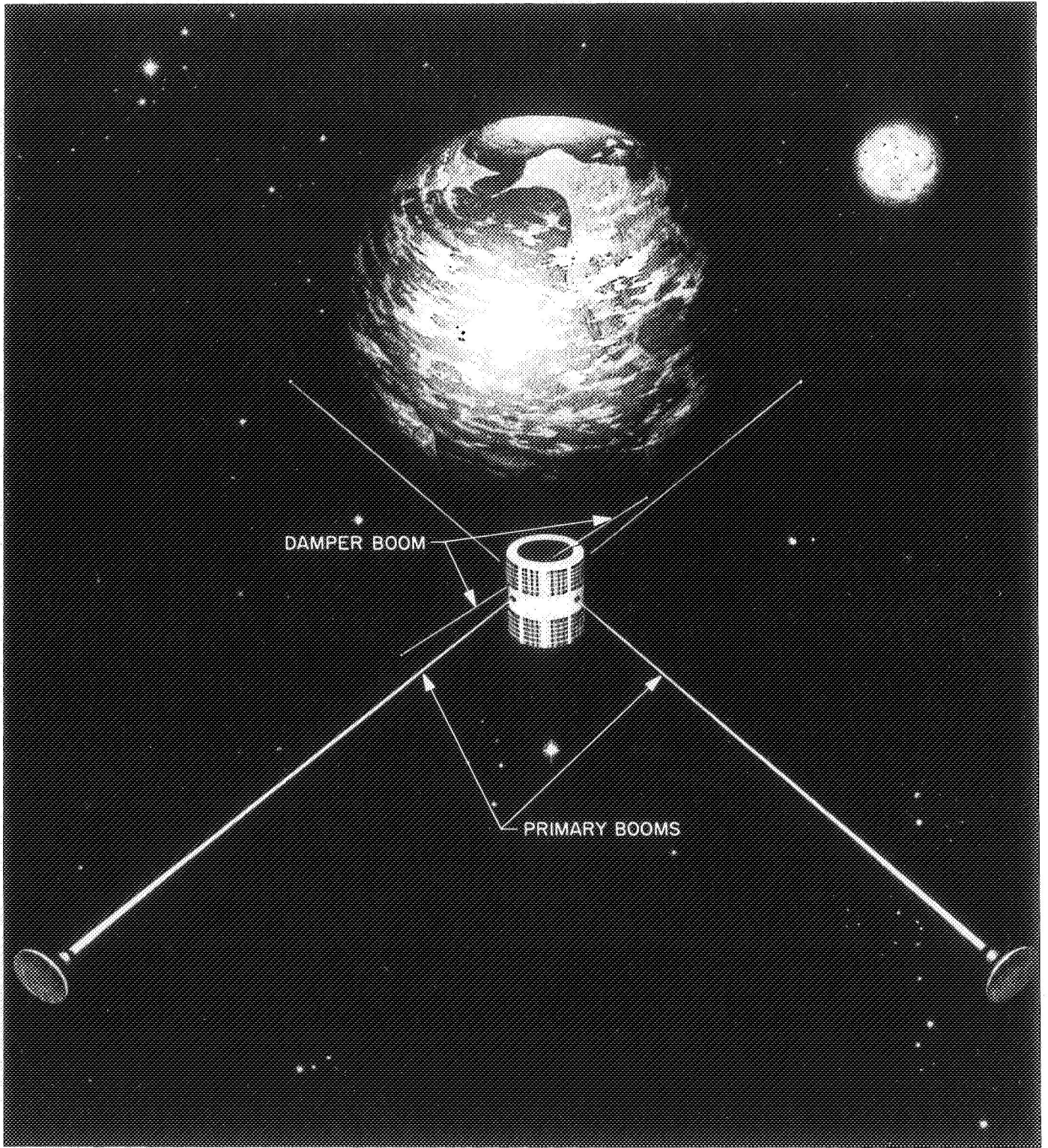


Fig. 1. Artist's conception of the gravity-gradient-stabilized ATS, with booms deployed

The components that deploy both the primary and damper booms were provided by deHavilland Aircraft of Canada, Ltd., Special Products & Applied Research (SPAR) Division (now SPAR Aerospace Products, Ltd.) under a subcontract to the General Electric Company. The basic extendible boom selected for this mission is the storable tubular extendible member (STEM).¹ The STEM technique involves the formation of a tubular section from a flat metal strip which is formed and heat-treated in the tubular form, then flattened under stress and wound onto a storage drum. Subsequent erection in orbit is accomplished by paying out the stowed strip through a set of guides that allow the boom to form into its natural tubular shape. The edges of the metal strip overlap each other to render stiffness to the deployed section.

II. Primary Boom Packages

Each gravity-gradient experiment contains two primary boom half-systems (Fig. 2). To provide boom ex-

¹STEM is a trade name for these deployable booms (see Ref. 1).

tension, retraction, and angular variation capability after injection into orbit, each half-system employs two separate motors: one to drive the storage drums and one to scissor the erection units that contain the storage drums.

In addition to storing, guiding, and electrically isolating the booms, the erection units provide a means of caging the tip masses, which are installed at the boom tips, to achieve a prescribed set of inertias about the principal axes of the spacecraft. The pair of erection units in each half-system, their associated drive train, motors, and scissoring linkage are all mounted within the single framework shown in Fig. 2. The erection units are pivoted to this framework. Motion between the two half-systems is coordinated electrically.

A. Torque Transmission

Each half-system is equipped with one transmission unit, which provides the torque required by the scissors bell-crank and the deployment gear train. Each transmission unit contains two brush-type dc motors, one for boom extension drive (via gear train) and one for scissors

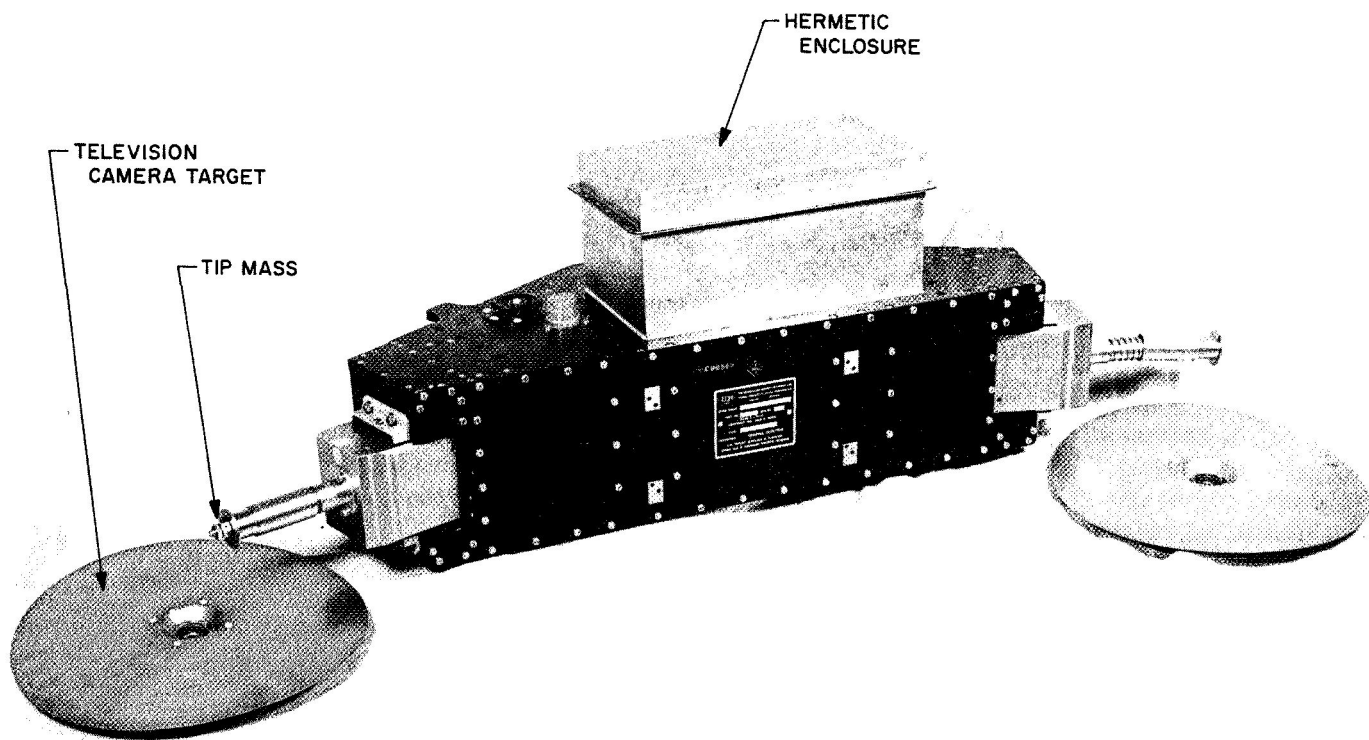


Fig. 2. Primary boom package. The television camera targets, also shown on the deployed booms in Fig. 1, were provided to allow a camera in the satellite to record the boom deployment configuration

drive (via bell-crank linkage). The scissors drive motor is equipped with an integral gear reducer to reduce the speed to that required for a proper scissoring rate.

The transmission unit enclosure confines the motors and drive trains in a vacuum-tight envelope to preserve their useful life in space and uses beryllium copper bellows-type couplings to deliver both the extension and scissor torques through the pressure-tight shell. Two drive shafts protrude from the enclosure: one for the deployment gear train and one for the scissors bell-crank.

The output drive shaft for the deployment gear train is collinear with the input shaft that is within the hermetic enclosure. The rotary motion of the eccentric input shaft within the "wobble" bellows (Fig. 3) provides the necessary external torque for primary boom deployment.

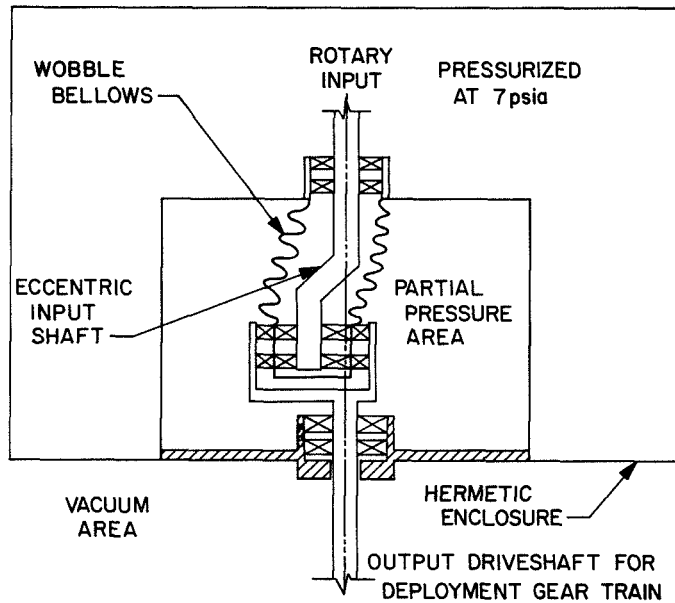


Fig. 3. Bellows drive mechanism

The scissoring output drive shaft is connected to the scissors bell-crank, which transmits linear push-pull motion through a pair of compression bellows (Fig. 4) to provide the required torques to the scissor plates attached to each erection unit.

B. Drum Synchronization

The primary boom erection units require externally applied torque at the boom storage drums for deployment. This torque is provided by a train of four gears in each half-system. One of the center gears of this train is

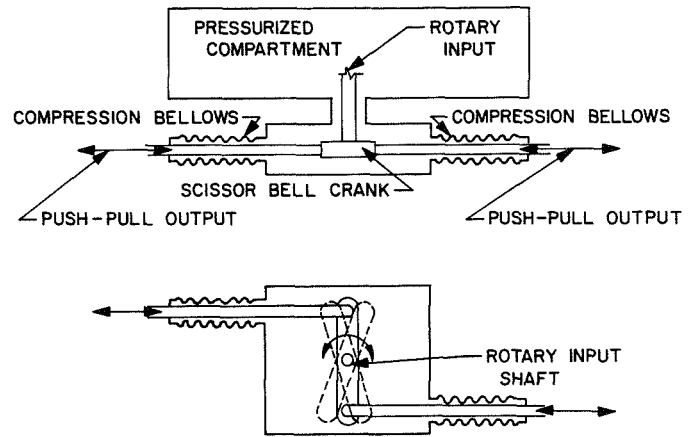


Fig. 4. Scissor drive mechanism

driven by the output drive shaft from the transmission unit. This gear, in turn, drives the boom storage drum of one erection unit directly and drives the boom storage drum of the second erection unit by means of an idler gear. Thus both erection units are driven by a single motor, and their drum rotations are mechanically synchronized by the gear train.

The center of the erection unit drive gear is concentric with the axes about which the erection units are pivoted, to allow the gear train to remain engaged during scissoring motion.

C. Electrical Isolation

An ATS spacecraft experiment required dc electrical isolation of the primary booms from the spacecraft and required that the capacitance between the boom and the spacecraft be reduced to a minimum. The following parts were made of polycarbonate materials to accomplish the required electrical isolation:

- (1) Drive gears internal to the erection units connecting to the storage drum.
- (2) Drive gears external to the hermetic enclosure connecting with the erection unit.
- (3) Support standoff rings between the scissor plates and each associated erection unit.
- (4) Support housings for the erection unit flexure pivots.

III. Secondary Boom Package

Each gravity-gradient-stabilized spacecraft incorporates one self-erecting secondary boom package. This

unit is different from the primary boom system in that it uses the strain energy in the stowed metal strip to rotate the storage drums contained in the boom tip masses and, thus, erect the booms. The tip masses (required to provide prescribed inertias for spacecraft damping) on this package are, in actuality, the erection units; they store and guide the booms and they can be caged to a center body section. The center section is mounted on the damper portion of the GE-constructed combination passive damper (CPD) (Ref. 2).

The two damper-borne secondary booms extend along the same straight line in opposite directions, and their tip masses provide the proper inertia for the operation of the damper. In addition to the main assembly containing the booms, the secondary package includes a sepa-

rate housing that contains the explosive portion of the tip mass release system (Fig. 5).

A. Tip Mass Caging

A ball-lock mechanism, lever arm, electroexplosive cartridge, and mechanical linear actuator combination are used for the damper-boom tip-mass release system. The linear actuator and lever arm are mounted in a separate actuator assembly on the base plate of the CPD.

The receptacles at the ends of the ball-lock mechanism (Fig. 6) provide the coupling between the tip mass and the center body when the damper boom is in the stowed position. The plunger movement is initiated by either or both of the electroexplosive squib-linear actuator devices,

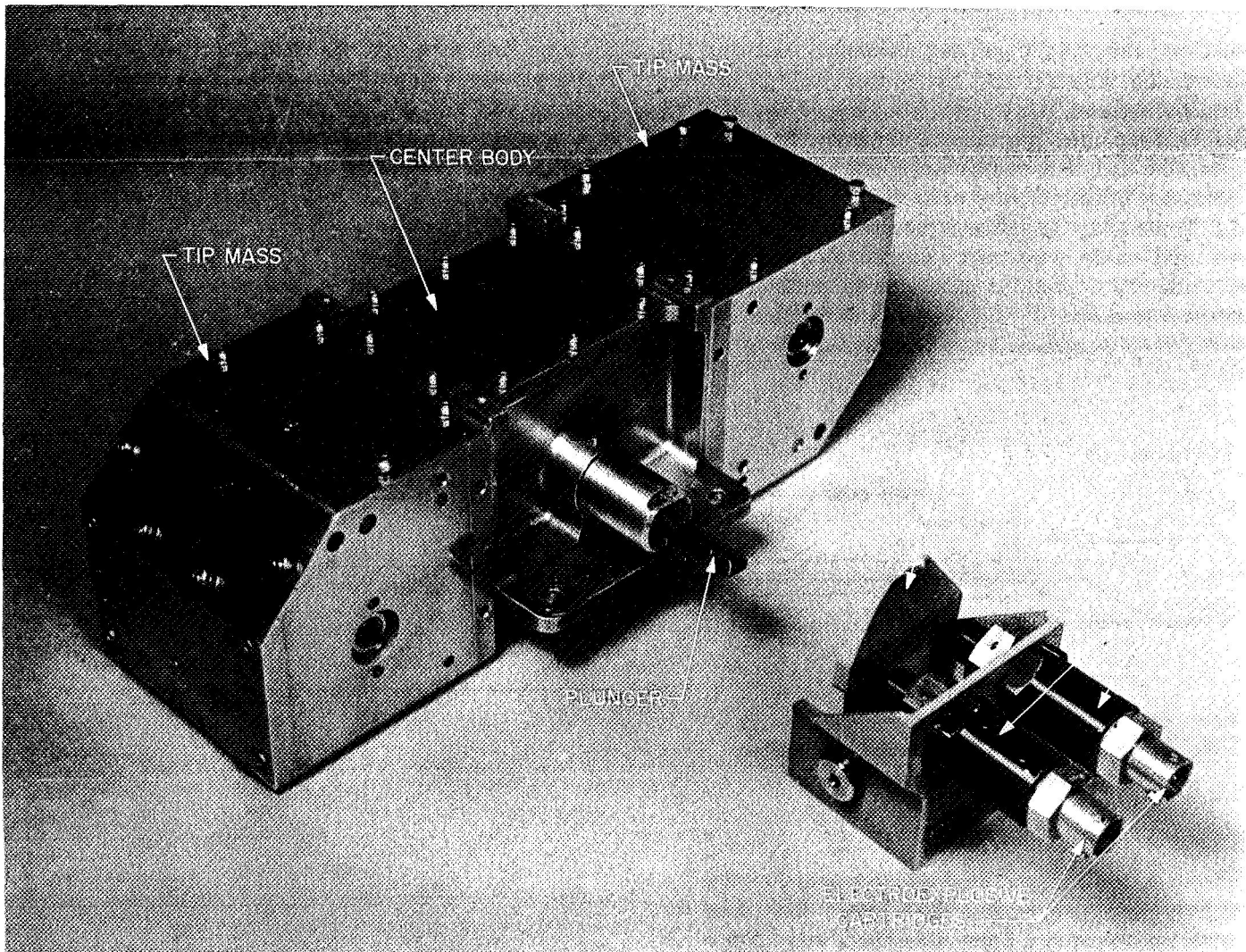


Fig. 5. Damper boom package

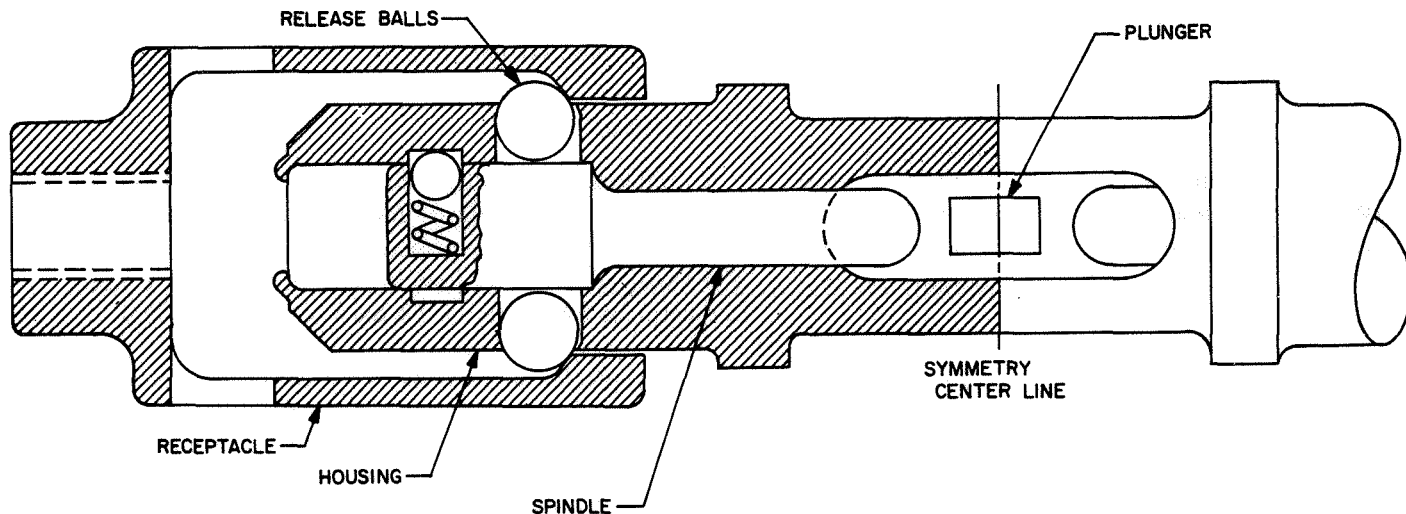


Fig. 6. Ball-lock mechanism

thus depressing the plunger and making contact with the two spindles which permit the release balls to depress inside the housing and release the receptacles. The tip mass then separates from the center body. In the actual system, the end of each boom element is secured to the center body. A liftoff spring at the end of the center body (Fig. 7) provides the initial separation force for the tip mass, and guide pins ensure coaxial separation. Then, the elastically wound boom begins to erect itself and continues to propel the tip assembly to full length. The tip assembly is restrained at the end of the fully erected boom.

2.6 ft/s. Failure due to the stopping of the tip mass at full deployment would occur at speeds above 4 ft/s.) It has been shown (Ref. 3) that the deployment rate of ungoverned self-erecting booms of this type will continue to increase as a function of deployed length, and the maximum length is, therefore, limited by boom strength and mass at the tip.

The governor consists of two diametrically opposed brake shoes, as sketched in Fig. 8, mounted in the tip mass assembly. The brake pivot points are fixed to the boom storage drum. Each of two brake shoes is hinged

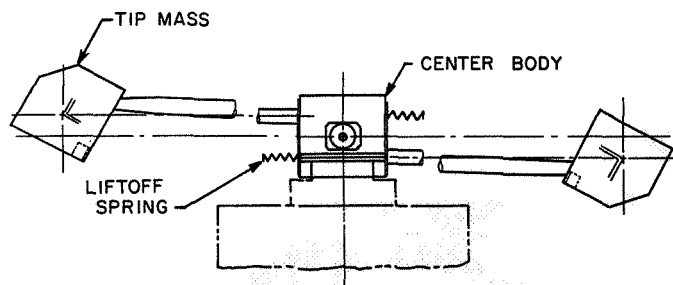


Fig. 7. Damper boom coaxial separation, showing deployment of booms

B. Centrifugal Governor

A governor is used to limit the maximum speed of the self-energized deployment to a speed less than that which would cause failure upon the abrupt stop of the tip mass at the end of deployment. (The specified deployment speed is 1.8 ± 0.8 ft/s, or a maximum of

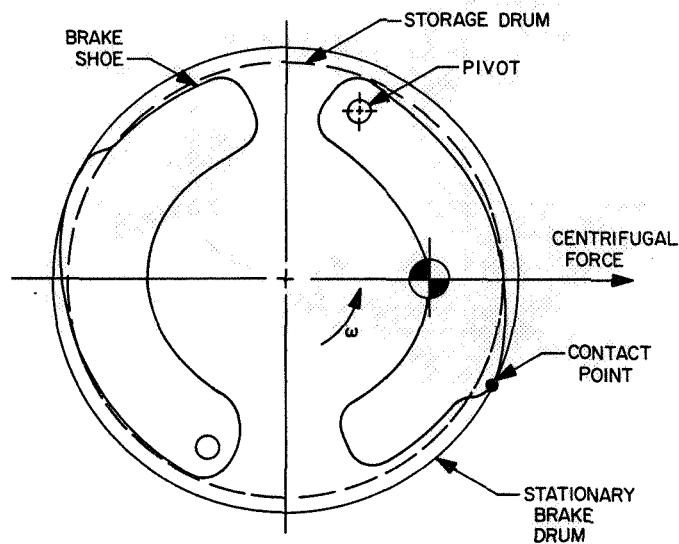


Fig. 8. Damper boom centrifugal governor ($\omega =$ angular change)

at the pivot and rotates into contact with the stationary brake drum under the influence of centrifugal force. Upon tip mass release, the drums are free to rotate, and they are propelled by the self-erecting tendency of the strain energy in the booms. The frictional torques developed by the brake and transmitted to the drum via the pivot pins is a function of drum rotation rate. Equilibrium will be established when the brake torque and losses are equal to the torque produced by release of strain energy.

Because the brake is symmetrical, the net frictional torque developed by the brake is the same as that which would be developed in the absence of the 1-g environment. The effect of earth's gravity during testing is a sinusoidal variation from +1 to -1 g on each brake shoe, about a mean value of 1.8 g. The two brake shoes of each tip mass assembly experience this sinusoidal variation exactly 180 deg out of phase with each other, and the net effect of gravity cancels out. At no time during the drum rotation (at constant speed) does either brake shoe experience a negative acceleration with respect to the brake drum (i.e., either centripetal or gravitational acceleration).

IV. Preparation for Space Operation

A. Gear and Bearing Lubrication

The boom subsystem design involves certain gears and bearings which will be at least partially exposed to the space vacuum and will be expected to operate after a long period of such exposure to the hard vacuum in orbit. In the primary boom half-systems, the bearings that are directly exposed to the space vacuum contain Duroid 5813 retainers.² The secondary package bearings exposed to the space vacuum contain GE F50 oil but are required to operate only once while in the space vacuum. Primary package transmission unit bearings, which are in the partial pressure area, contain a combination of GE Versilube G300 grease and F50 oil. Bearings inside the hermetic enclosure of the primary boom half-systems contain a combination of G300 grease and F50 oil.

The gears outside the primary package hermetic enclosure, as mentioned previously, are of polycarbonate materials and no lubrication is added. The gears inside the hermetic enclosure are lubricated with G300 grease. The high-speed spiroid in the extension drive train has an MoS₂ dry lubricant mixed with the G300 grease for

²An MoS₂-impregnated material, 60% Teflon and 40% glass fibers.

adherence purposes. The secondary boom package contains no gears.

B. Deployment Tests

The gravity-gradient booms are designed for weightless deployment in space. Accordingly, deploying the booms in the 1-g terrestrial environment requires certain special test equipment to avoid damage to the booms resulting from their own weight. Full-length deployment of the stored boom element necessitates either a full-length test track or a coordinated takeup mechanism.

The self-erecting nature of the secondary boom package precluded use of a takeup mechanism for its deployment. The configuration of the primary boom half-system coordinated pair of erected booms and their extended lengths precluded utilization of two full-length test tracks for their deployment. The resultant facility for deployment tests (Fig. 9) consists of a fixed, 150-ft-long, channel-shaped track and a movable, 10-ft channel-shaped track, angularly positioned about a support pedestal for compatibility with the half-system configuration and its scissoring requirement.

Testing of the primary boom package is accomplished by mounting the unit on the support pedestal and aligning the booms to lie in the center of the test tracks. The end of the boom lying in the long test track is attached to its tip mass, which, in turn, is supported by a deployment trolley on wheels. The end of the boom lying in the short test track is attached to a takeup mechanism on wheels. To minimize friction and boom plating damage during the motorized deployment testing of the primary boom units, the bottom of the channel test track is lined with Teflon. All trolley and takeup mechanism wheels are mounted on ball bearings to reduce friction.

Testing of the secondary boom package is accomplished by mounting the unit in the center of the long test track with deployment trolleys on wheels attached to each tip mass.

Unlocking the ball-lock assembly results in release and launch of the tip mass erection units. As soon as the tip mass kickoff is initiated, the offset tip mass centers of gravity cause rotation of the tip mass about the storage drum support axis (Fig. 7). This oscillation and its resultant boom damage is minimized by incorporating hydraulic oscillation dampers attached to tip mass counterbalance arms on the outboard ends of the tip masses.

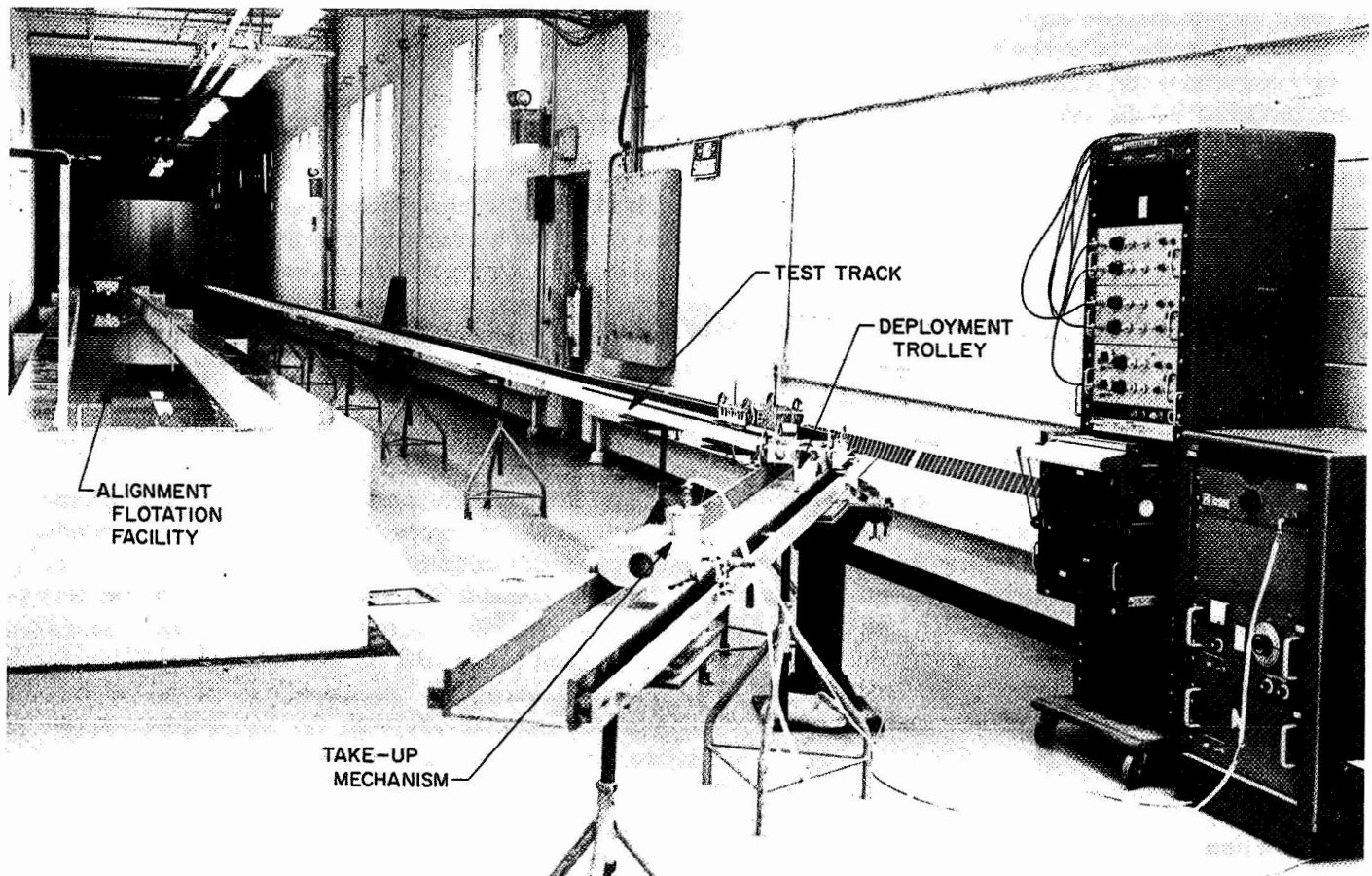


Fig. 9. Boom deployment test track. The alignment flotation facility was not used in the tests described in this paper

V. Flight Performance and Current Status

Although ATS-2 attained a highly elliptical orbit, instead of the planned, medium-altitude circular orbit, all the primary and secondary booms uncaged and extended to full length upon command. Subsequent scissor operations of the primary booms to both extreme limits were accomplished successfully — one 4 months after launch, the other 6 months after launch.

During October 1967, ATS-2 spacecraft power was reduced to a minimum and monitoring was halted for the time, since the ground equipment was needed to cover the ATS-3 launch. Concentration on spin-stabilized ATS-3 has precluded further monitoring to date on ATS-2. Just prior to power reduction, telemetry data indicated no significant degradation in initial hermetic enclosure

pressure, primary boom package electrical isolation, or secondary boom package mechanical isolation.

Both the primary and secondary boom packages have passed qualification test programs in both the medium and synchronous altitude configurations, and vibration levels greater than 18 g were sustained by these configurations during qualification. The next gravity-gradient ATS spacecraft to be launched will be designed for synchronous altitude. The main difference in the two configurations is the weight of the tip masses; the synchronous weight is approximately three times that of the medium-altitude weight. Thus the tip mass weight for the primary booms at medium altitude configuration is 2.5 lb each, and, at synchronous altitude configuration, 8 lb each. Comparable tip mass weights for the damper booms are 1.6 and 4.06 lb each.

References

1. MacNaughton, J. D., Weyman, H. N., and Groskopfs, E., "The BI-STEM – A New Technique in Unfurlable Structures," in *Proceedings of the 2nd Aerospace Mechanisms Symposium, Held at the University of Santa Clara, Santa Clara, California, May 4–5, 1967*, Technical Memorandum 33-355, pp. 139–145. Edited by G. G. Herzl. Jet Propulsion Laboratory, Pasadena, California, Aug. 15, 1967.
2. Buerger, E. J., "Development of a Passive Damper for a Gravity Gradient Stabilized Spacecraft," in *Proceedings of the First Aerospace Mechanisms Symposium, Held at the University of Santa Clara, Santa Clara, California, May 19–20, 1966*, AD 638 916, pp. 297–309. Edited by G. G. Herzl. Defense Documentation Center, 1966.
3. Rimrott, F. P. J., "Storable Tubular Extendible Member – A Unique Machine Element," *Machine Des.*, Dec. 9, 1965.

PRECEDING PAGE BLANK NOT FILMED.

N 69-11823

Mechanism Design—A Test Laboratory Viewpoint

J. M. Haley

Lockheed Missiles & Space Company
Sunnyvale, California

The test laboratory can be a valuable resource for the mechanism designer, especially in determining environmental requirements, cost estimates for test phases, clues to design pitfalls, and data references for tests of similar mechanisms. The designer should carefully define in writing the functional and environmental requirements for the item he is designing. He should also be aware of the "personality problems" (binding, galling, and fusing) of moving parts.

I. Introduction

The service test laboratory has a unique vantage point for viewing company operations. First of all, it participates in almost all contractual activity which involves hardware, and, secondly, it usually is not predisposed to the goals or philosophies of any one program or group. This second factor is important, since the test laboratory must function as an unbiased agent in providing support to engineering, manufacturing, and product assurance.

In this service capacity, the laboratory is afforded a broad and uncluttered view of what is happening. It frequently is in a position to provide constructive comments concerning both hardware and nonhardware factors. However, the basic function of the test laboratory is simply to subject the hardware to prescribed functional/environmental requirements and present the results.

Seldom is this organization asked to evaluate or draw conclusions concerning the quality of the design or manufacturing process. Despite this operational mode, the laboratory does become exposed to quality factors. It sees the successes and failures, the good and bad designs, and the good and bad manufactured products. The purpose of this paper is to present laboratory observations gained from this vantage point as they concern the design process and offer a set of suggestions to the mechanisms designer.

II. Two Sets of Requirements

Before the designer of an aerospace mechanism can proceed with his work in depth, two sets of requirements must be established. One set is general and the other set specific. The general set presents the mission objectives

and the controlling overall environmental specifications, whereas the specific set identifies the functional purpose and use habitat of a particular part or assembly. In theory, both of these guidelines should exist well in advance of full-blown efforts to design the hardware. Normally this condition is true for the general set; however, advanced availability for the specific set is the exception rather than the rule.

III. The Stability of General Requirements

General requirements of the program are essentially based upon mission objectives which are fixed by the customer after many months and sometimes years of research, engineering studies, and conceptual designs. Once defined and released to the contractor, the mission objectives remain relatively stable. Major changes in their scope or timing are uncommon, since these events have an impact on the national budget, and, therefore, may involve congressional approval.

An important part of the general requirements is a specification which prescribes overall environments. The content of this document is determined by the characteristics of the launch booster and the use habitat. Here, again, the decisions of long-range planning will apply, since they set forth the launch vehicle, the "on station" mode, and the reentry phase if there is one. Major changes in these areas, after contract award, are indeed rare and, if they occur, generally constitute grounds for schedule and cost redirection.

For the most part, the booster is selected from an available inventory of proven vehicles for which performance/environmental characteristics are well known. It is infrequent that a new booster and payload evolve simultaneously with the resultant necessity to predict system characteristics based upon wind tunnel and other tests. For space vehicles and ballistic missiles, the launch booster dictates environments of the ascent profile, with particular attention to dynamics of vibration, acceleration, pressure and thermal exposure. Usually, the ascent phase constitutes the greatest challenge for payload survival, particularly in areas of mechanical environments. However, certain reentry payloads are an exception, since the mechanical conditions are sometimes more severe during that phase.

It is accepted that environmental requirements will vary considerably between space vehicles and ballistic

missiles. Examples of the variations are the long-term exposure to the unfriendly conditions of deep space experienced by an orbiting vehicle or space probe as compared with the defensive measures exercised against a missile warhead. However, regardless of the program type, the general environmental requirements are broad and concern the common needs of the total vehicle rather than specifics.

IV. The Dynamic Character of Specific Requirements

The specific requirements for each identifiable assembly, subassembly, and even, sometimes, each part, are normally enumerated by the design control document. For future reference, I will call this document the Design Control Specification (DCS). The intent of the DCS is to prescribe the functional/environmental requirements of proposed hardware for the purpose of guiding the individual designer. It seldom achieves this objective, since it usually does not exist in a released and approved state at the time that the designer needs the information to begin his work. Even if an early release is achieved, the first publication rarely establishes the final requirements. There is a practical reason for this condition, which is recognized by the individual designer: the requirements for aerospace vehicles, in total or in part, seldom are static during the design phase, particularly during the conceptual period. As a consequence, the DCS will be revised throughout the life of the program. The number of revisions is higher in the early stages, and the paperwork system often falls behind in documenting this reality of evolving requirements. During the preliminary and conceptual phases, many changes are not even introduced into the documentation network, but are left to accumulate for a later group updating.

As a test laboratory, we have experienced instances where the prototype specimen is fabricated and available, the design is in blueprint form, and yet the DCS has not been released. In some cases, the best document that is available is a red-lined mark-up of a comparable document from another program, or an unreleased final draft. This condition does not reflect a disregard for configuration control. Nor is it peculiar to any one company. It is an industry-wide problem that is inherent in the nature of the programs undertaken. The underlying causes can be traced to factors such as the first-time aspect of the mission; the complexity of the project, encompassing both hardware and software; the need to

perform concurrent development and sometimes invention; schedule squeeze; and the inertia of the contractual paperwork system.

In view of these realities, it is essential that the mechanism designer exercise a good deal of judgment and communication with his many interfaces when attempting to interpret and apply the DCS. This includes other designers responsible for mating hardware and utilities, and support engineering agencies such as those concerned with stress, thermal conditions, and weights, to mention a few.

V. The Unpublished Guideline

The ultimate objective of any mechanism design is to provide a device that will balance technical, cost, and schedule factors with the mission objective. To do this, it must supply the needed function, perform adequately under exposure to the use habitat, satisfy the life requirements, incorporate simplicity, and achieve an economic balance considering its own cost to produce and its impact upon associated hardware and systems.

Indeed, this is a worthwhile objective and an oversimplification of a real challenge. Considering this difficult goal and the generally unavailable state of the DCS, the first thing that the designer should do is to carefully evaluate and define in writing the functional and environmental requirements of the hardware for which he is responsible. The scope of this action will vary, depending upon each situation; however, it is recommended that this be an unpublished document prepared in outline form. It should record the current and realistic requirements as recognized by the prime parties concerned. An early-release DCS is a starting point, but a designer should not rely completely on this source, since it often may prescribe needs that are outdated by the inability of the paperwork to keep pace with a fast-moving program. It is especially recommended that the designer go beyond those boiler plate functional/environmental callouts of the DCS to specify intimate factors that are peculiar to the individual mechanism.

Each part to be designed has a personality all its own as dictated by its particular functional requirement and use habitat. For this reason, it is often dangerous to accept the total vehicle or even subsystem parameters as all-encompassing. In contrast to black boxes, most mechanisms have special needs to be considered: namely,

the inherent features of displacement and motion. These features introduce new dimensions to interpretations of environmental and functional specifications. They place added emphasis upon evaluating hardware performance under conditions such as zero gravity, mechanical vibration, high vacuum, and temperature extremes. Many designers have learned from experience that moving parts of mechanisms, in contrast to fixed assemblies, have "personality problems" that are often exhibited by the binding, galling, and fusing of moving parts. These unique personality problems of mechanisms must be recognized early in the design and integrated into the development plan. If the DCS is inadequate, then the working guideline must specify these factors as appropriate to the particular device in question.

Now another comment from the laboratory viewpoint. At an early point in establishing the design plan, the designer would do well to contact the test laboratory and obtain leads concerning like mechanisms that have undergone development and qualification testing. He can then be directed to test reports that record in detail the experiences of similar hardware. These documents describe the test specimen, the environmental exposures, the functional requirements, and the results.

However, this screening process should not be restricted to in-house operations. Sometimes it is advantageous to undertake a literature search of similar mechanisms designed and tested by others in the industry. The government data bank of the Defense Documentation Center can be of value in this regard. The individual technical libraries are aware of these sources and know how to interrogate the data banks. Results of these contacts and discussions will frequently supply valuable information concerning the successes and failures of others, as well as furnish reliable cost data for testing. Also, these contacts will help to compensate for the natural tendency of designers to be optimistic concerning the ability of their creations to pass the testing phase. It is expected that the content of the working guideline will be influenced by the findings of this communication.

Once the working guideline and plan have been established, the individual designer has at least the latest basis upon which to proceed. Furthermore, he personally can keep this requirements paper up to date by his own editing, since it does not constitute part of the formal documentation process. This work sheet will also provide a good foundation for eventual updating and final release of the DCS. A written trail will exist from first conception through to the last configuration.

VI. Conceptual Work

Now, with latest requirements documented and coordinated, the designer can direct his full attention to the hardware. He can, with reduced risk, proceed to resolve the geometry and the selection of materials and parts. Certainly, downstream changes will occur, but at least action has been taken to avoid those major surprises that arise from lack of adequate preparation and coordination.

As the design starts to take final form, the designer should contact the test laboratory again for an informal critique, at a point where the design is well conceived but not yet frozen. There is a definite logic to this proposed second communication with the testing personnel. Generally, the assigned engineer has not been responsible for the design and testing of all similar mechanisms for a variety of projects within the company. Furthermore, in a large company, he seldom has personal access to the multiplicity of designers who have engaged in such endeavors. However, the laboratories in the company usually have been exposed to all these mechanisms and the testing personnel have first-hand knowledge concerning some do's and don'ts.

Generally, only one contact of this type is necessary, since most companies do not duplicate the laboratory function, because of the expense for equipment and special facilities. Personnel who staff these laboratories have had painful experiences that will be most helpful to the individual designer in an objective critique of the conceived approach. At the very minimum, such a critique can assure the designer that he does not expose himself to the known pitfalls of others.

VII. Development of the Hardware

After the design comes the testing of the hardware, both prototype and end-item configuration. Two phases of testing normally occur — the first concerned with evolution of the design and the second with formal proofing of the final product. Both of these phases should encompass functional and environmental aspects. Again, from a laboratory viewpoint, it is our experience that the maximum emphasis of the designer in the development phase tends to focus on the functional requirement. Environmental factors are considered in catalog selection of the parts that go into the assembly, but actual environmental confirmation of these parts and prototypes of subassemblies is, for the most part, deferred until the qualification phase. Herein lie the seeds of disaster. As

design problems are encountered in the qualification test program, two factors work against implementation of the best solution. One is time, and the other is the packaged state of the configuration.

Speaking from experience, I cannot emphasize too strongly that all unproven parts and subassemblies should be thoroughly evaluated under the use environment before final incorporation into the mechanism design. For outside-purchased parts, the responsible designer should be careful of interpreting or extending vendor performance data. Remember that the vendor's fact sheet is primarily marketing-oriented. Sometimes the performance data may be optimistic and not fully supported by test exposure. To protect himself, the designer should not hesitate to ask the vendor for the results of his test program. Even here, caution must be exercised, since the test data might not consider the effects of combined environments, life expectancy, or mounting orientation. If possible, as the design is evolved, prototype subassemblies and assemblies should be subjected to selected environmental conditions of the use habitat. Breadboard and bench evaluations of the mechanism from a functional viewpoint are only part of the assignment. Neglect of the complementing environmental exposure constitutes a gamble.

This expansion of environmental testing in the development phase costs money, but it certainly has economic and other advantages over incorporating a fix under conditions of a schedule panic, or loss of a multimillion dollar vehicle at launch, or loss of data from "on station" due to malfunction of an "insignificant" part or mechanism. This recommendation is not a make-work program for the test laboratory. It is a recommendation born of experience. Let me cite one example of a qualification failure that could have been avoided by an adequate test program in the development phase.

Figure 1 depicts a payout cable mechanism used in one of the *Agena* configurations. Its function is to supply an extended electrical connection between the booster and *Agena* vehicles during the separation sequence. As the *Agena* moves away from the booster on a rail system inside the booster adapter, the stowed cable is fed out at a rate of 5.5 ft/s. When the cable is fully extended and the *Agena* has cleared the booster adapter, then the force from the displacing masses is applied through the cable to the mating connectors. This pull force engages a mechanism in the *Agena* mating connector which causes disengagement of male and female segments and

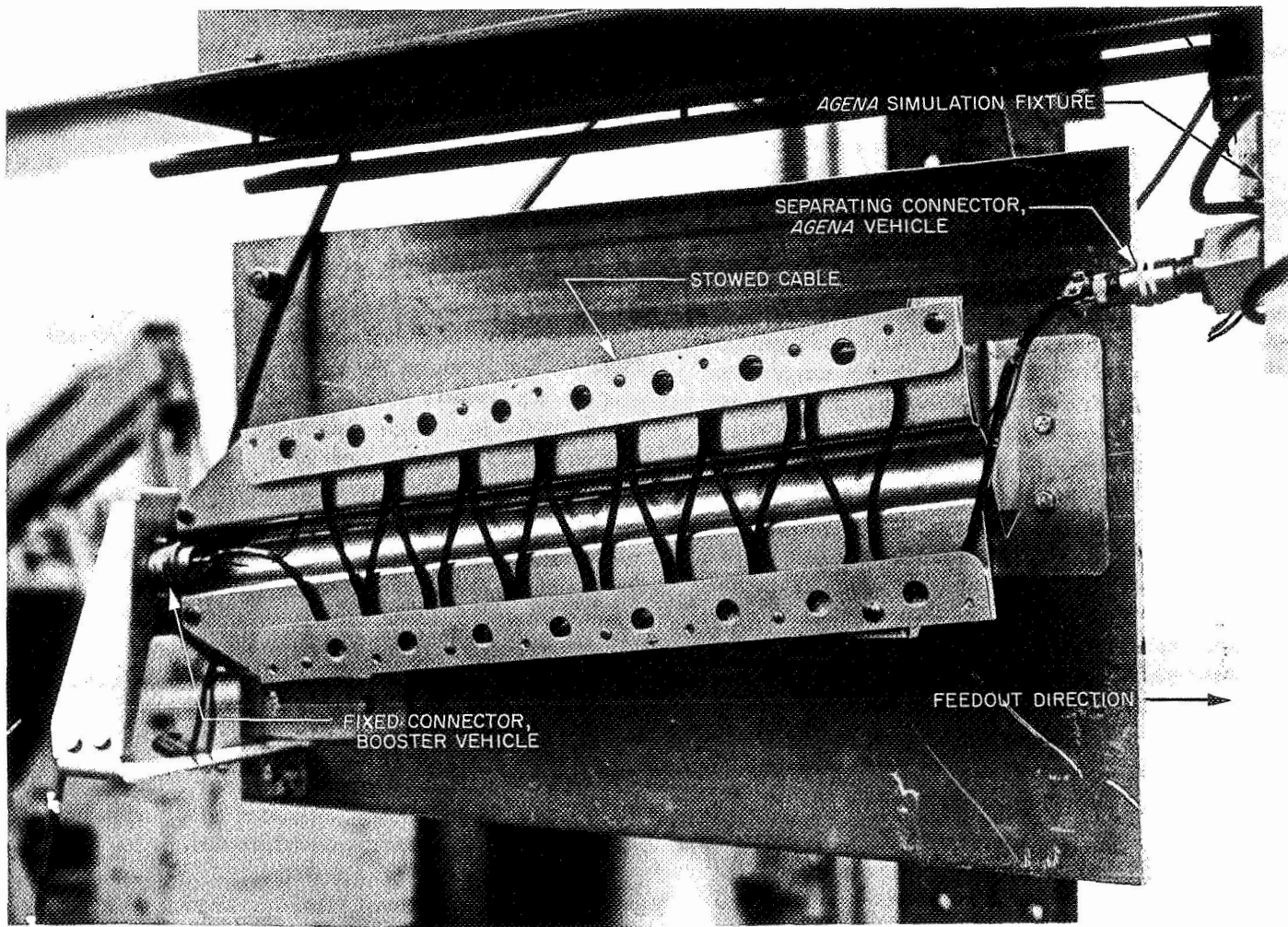


Fig. 1. Payout cable installed in functional test fixture (top cover off)

release of the two vehicles. Magnitude of the load necessary to activate the separation device was established at 15 lb maximum. The amount of pull required was considered important because of the unwanted effect of a higher load requirement upon the orbit path. This assembly ensures that if a hang-up occurs in the slide-out phase, then the extended electrical connection will permit destruction of the total complex if necessary. Two mechanisms are involved, one for stowing and guiding the cable, and a second for disengaging the *Agena* mating connector.

The assembled specimen was submitted for qualification without the benefit of a prior development test. The specification called for exposure to mechanical environments of acceleration, shock, and vibration, with functional tests before and after each environmental condition. The delivered specimen was installed in a test fixture

that simulated the exit motion of the *Agena* from the booster assembly. This fixture was designed to duplicate the mounting orientation of the payout assembly and supply the prescribed motion rate and force load to the *Agena* end connector as the cable was deployed.

In the first functional evaluation, the cable jammed in the housing. It did not extend even when a pull force in excess of 100 lb was applied. To correct this situation, several design changes were made in the housing. These changes provided greater clearance in the relationship of the stowed cable and the feed-out guides. The reworked specimen then passed the pre-environmental functional test in accord with the specified feed-out rate and pull force.

As the first environmental exposure, the specimen was subjected to several levels of steady-state acceleration.

While the specimen was under acceleration load, electrical continuity was uninterrupted and the cable retained a packaged position. A post-environmental functional test was performed, and the system worked as required. The next environmental exposure was a shock condition. All proceeded well during this environmental condition, and the subsequent functional test was satisfactory.

Finally, the assembly moved to the vibration environment. The vibration fixture and specimen mounting were designed in a manner that simulated the vehicle configuration. With this setup, the specimen was exposed to the prescribed vibration loads. Here, again, electrical continuity was satisfactorily maintained during the environmental exposure. Afterward, the specimen was removed from the shaker and installed in the simulated vehicle fixture to perform a post-vibration functional test. The cable fed out as required, but the *Agena* connector failed to disengage at the fully extended cable position and the prescribed pull load. A visual inspection of the connector revealed galling and pitting of the race and ball mechanism which activated the male-to-female release. Further testing established that a force of 121 lb was necessary to achieve disengagement, as compared with the design requirement of 15 lb maximum.

Since time did not permit the search for a new separating connector, action was taken to decrease the vibration level experienced by the component. After several changes in the mounting arrangement, an improvement was made. As a result, the galling and pitting problem was minimized, and separation of the connector was obtained at a pull force of 21 lb. These corrections were made after a series of vibration exposures in different mounting configurations.

The improved performance of the connector still was considered marginal and, therefore, a backup separation approach was begun. The backup system was based upon a failure of the conductor strands at the point of attachment to the connector housing. This safety arrangement was to take over only if the connector failed to disengage. A series of destruct tests was run to determine the load requirements for break-away of the conductors from the plug attachments. Findings indicated that with a multistrand cable of equal conductor lengths, the force was well in excess of 100 lb. A load of this size was not acceptable because of the effect upon the orbit path. To correct this situation, the electrical conductors were assembled in varying lengths so that the pull force

would be applied to each strand, one at a time. This change lowered the force requirements to within acceptable limits. In actual flight, the modified system functioned well, and a clean separation was obtained.

Although, on the surface, the payout cable mechanism appears to be relatively simple, the qualification test program ultimately involved three development efforts. These included a first effort for functional payout of the cable, a second for mounting orientation of the connector, and a third for establishment of a backup release system. In addition to the specimen requirements, a moderate development program was necessary to de-bug the test fixture which simulated speed and pull force of the deploying *Agena* vehicle.

This qualification test was originally estimated at 1215 manhours and was expected to be complete in 3 weeks. In the final process, the test effort required an expenditure of 3076 manhours, and a time period of 6 weeks. Compounding the situation were extreme pressures for resolution, since the flight schedule was rapidly approaching.

The purpose of this example is to demonstrate that even in the simplest devices, there can exist unexpected complications. These complications are magnified when they are encountered for the first time in a qualification test program. A development test program encompassing both functional and environmental factors is a sound investment in the long run: it minimizes the chance of a major failure during the formal qualification demonstration, and it protects against those unplanned expenses that occur when a major redesign must be developed and incorporated as the flight date rapidly approaches. I am sure that all of us have experienced the disappointments of a last-minute test failure and recognize the problems that result in cost, strained customer relationships, internal organizational conflict, and personal pressures. To minimize these prospects, a good design plan must be prepared early, and it must contain an adequate test program.

VIII. Summary

In summary, I would like to offer the following suggestions:

- (1) Establish design requirements for the individual mechanism in writing before proceeding with

conceptual work. Consider both functional and environmental factors. Do not depend upon the availability of a DCS document. If a DCS is available, do not accept its content as the current requirement without checking.

- (2) Take steps to identify those highly personal needs of each mechanism. Thoroughly sort out potential problems introduced by the factors of motion or displacement peculiar to your mechanism.
- (3) Don't be reluctant to turn to the test laboratory for assistance in determining the environmental requirements, cost estimates for test phases, clues in design pitfalls, and data references for tests of similar mechanisms.

- (4) Place maximum emphasis upon functional and environmental testing during the development phase in order to avoid cost disadvantages and embarrassment associated with a failure during qualification.

In conclusion, the test laboratory organization is a source of knowledge and experience which can be valuable to the individual designer. Unfortunately, these talents are rarely tapped in the planning, design conception, or development test phases. As a consequence, in many companies the test laboratory functions almost exclusively as a qualification shop rather than an arm of engineering and design. I urge the mechanism designer to take advantage of this available knowledge and make the laboratory a contributing partner in the design.

PRECEDING PAGE BLANK NOT FILMED.

N 69-11824

Ball-Lock-Bolt Separation System

J. I. Moulton

Peltec Division of Quantic Industries
San Carlos, California

This paper describes the ball-lock-bolt separation system, which was developed for aerospace applications that require a low-shock, controlled-release, nonfrag-menting fastener. Different versions of the system are discussed, including mani-folded arrangements and single-point release types, both of which have been successfully flown in space.

I. Introduction

The total system requirements for the ball-lock-bolt separation system may include any or all of the following constraints:

- (1) The separation function must be "soft," imparting no impulse to the separating vehicle.
- (2) The system must completely contain all pyrotechnic gases, particles, and contamination.
- (3) The system must have high strength in tension and shear for structural load requirements.
- (4) Actuation must be manual for ease of assembly and handling.
- (5) The flight system must be capable of being tested for function during ground handling operations.
- (6) Flight safety must be maintained by providing an inert system until final installation of the pyrotechnics.

II. Principle of Operation

The ball-lock-bolt separation concept provides a basic mechanism of simple design with a proven history of satisfactory performance. Figure 1 depicts the basic elements of the mechanism. These are the bolt body, the actuation spool, the restraining collar, and the release balls. The collar and the bolt disengage when the actuation spool is displaced such that its reduced diameter allows the ball to retract below the outer diameter of the bolt. The only energy released as a result of the separation action is the strain energy involved in pre-loading or torquing the bolt on installation.

A kinematic study of the release action of a ball-lock-bolt is shown in Fig. 2. This study presents four loading conditions encountered during the release action.

A. Static Loads

Figure 2a depicts the condition of the system under a static tensile load F . All forces through the ball act

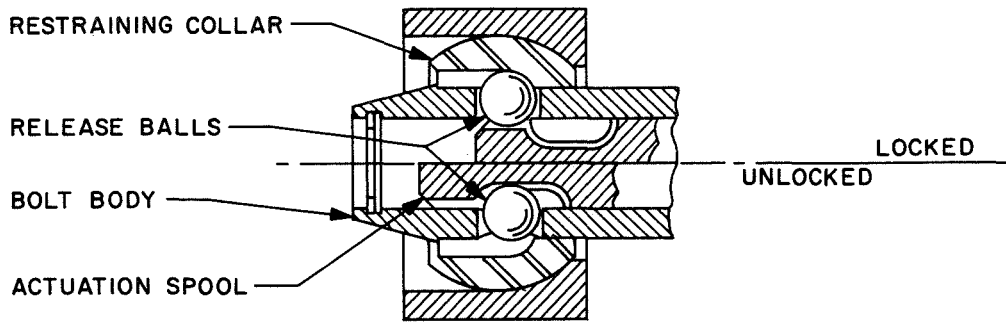


Fig. 1. Basic elements of the ball-lock-bolt mechanism

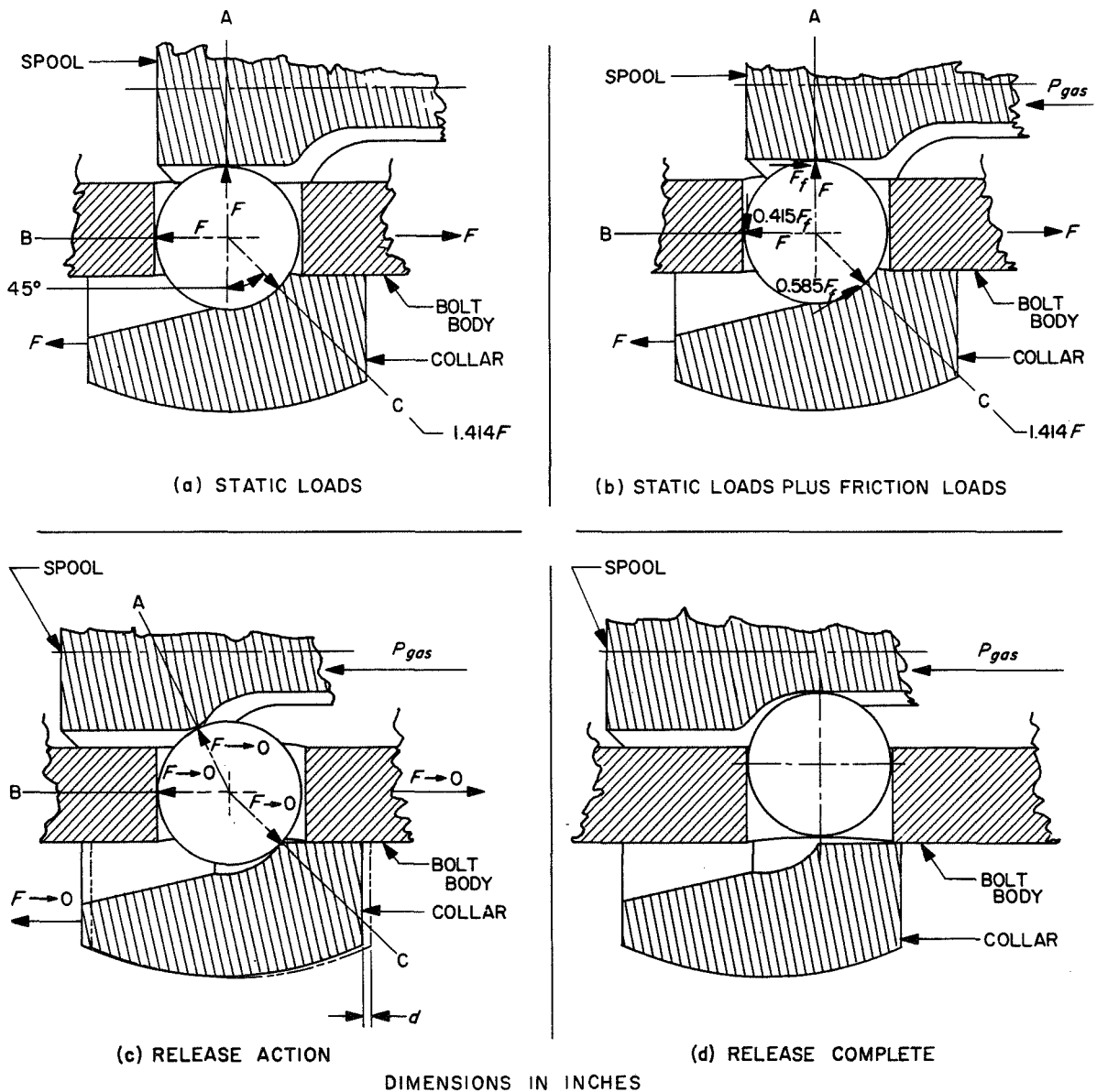


Fig. 2. Kinematic study of the ball-lock-bolt release action, showing four loading conditions

normal to the surface of the ball. Assuming a 45-deg contact angle with the collar, the reactions at points A and B are equal to the applied force F , and the reaction at C equals $1.414 \times F$. This loading condition may be maintained indefinitely at levels below the proof loads shown on Fig. 3.

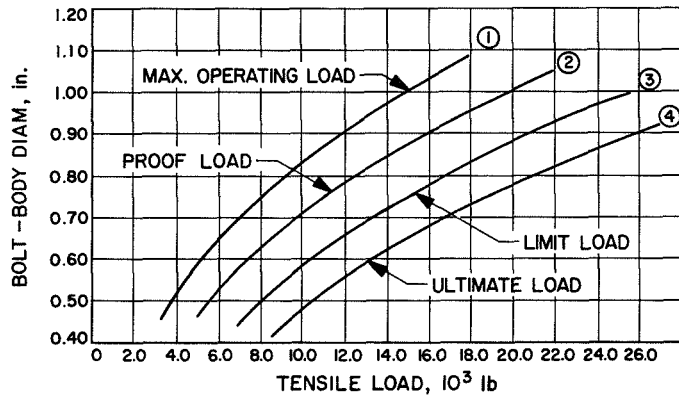


Fig. 3. Load capacity of a properly proportioned ball-lock-bolt mechanism

B. Static Loads Plus Friction Loads

Figure 2b depicts the condition of the preloaded system at the instant of first pool motion under gas pressure P_{gas} . The full breakaway static friction force F_f is developed only at point A. This sliding friction force tends to produce rotation of the ball, which is counteracted by static friction forces at B and C. It is noted that the friction reaction at C is in the direction to oppose motion of the collar.

C. Release Action

Figure 2c depicts the condition of the system as the ball has started to retract within the bolt body and the system preload has dropped to zero. The system preload is represented by the distance denoted as d , which is equal to the total elastic strain of the system under preload. At this point, no forces are acting on the ball. It is noted that the motion of the collar at this point is due to the elastic spring-back of the restrained system, not to any release action attributable to the bolt.

1. Release Complete

Figure 2d depicts the final condition of the system as the spool has moved sufficiently to permit the ball to drop below the outer diameter of the bolt. The collar is now completely free to disengage and separate from the parent vehicle.

III. Tensile Strength

The tensile strength of a ball-lock-bolt mechanism is a function of the number of balls utilized and their geometric arrangement. The load capacity of a properly proportioned ball-lock bolt is depicted in Fig. 3. The four curves represent the various loading conditions as a function of bolt-body diameter versus tensile load. These curves represent the results of actual tests and may be considered typical for a well-proportioned bolt.

Curve 1 represents the maximum operating load, defined as the maximum load at which the device may be released without degradation. It is recommended that the bolt be operated at as low a tensile load as the application will allow.

Curve 2 is the proof load or maximum structural working load. This load is applied to each bolt as an individual acceptance test. Any subsequent loading within this limit may be applied repeatedly without plastic deformation taking place.

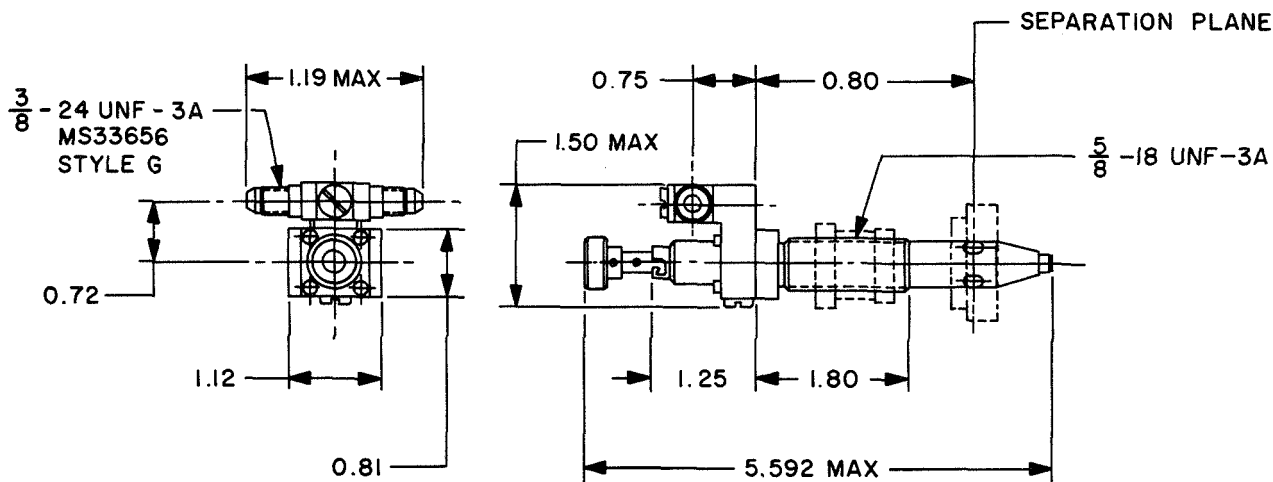
Curve 3 represents the limit load, defined as the load which will cause a minimum deformation and which, after being removed, would have produced sufficient yield to reduce the initial preload to zero. However, the bolt will still maintain that applied load, after which successful release can be accomplished.

Curve 4 represents the ultimate load, defined as the load at which sufficient deformation has taken place to prevent clean separation. The bolt, however, will be structurally intact. The point at which tensile failure or fracture will occur is somewhat above this curve; for example, the 0.550-in. diameter bolt shown in Fig. 1 has been loaded to destruction in the 14,000- to 15,000-lb range.

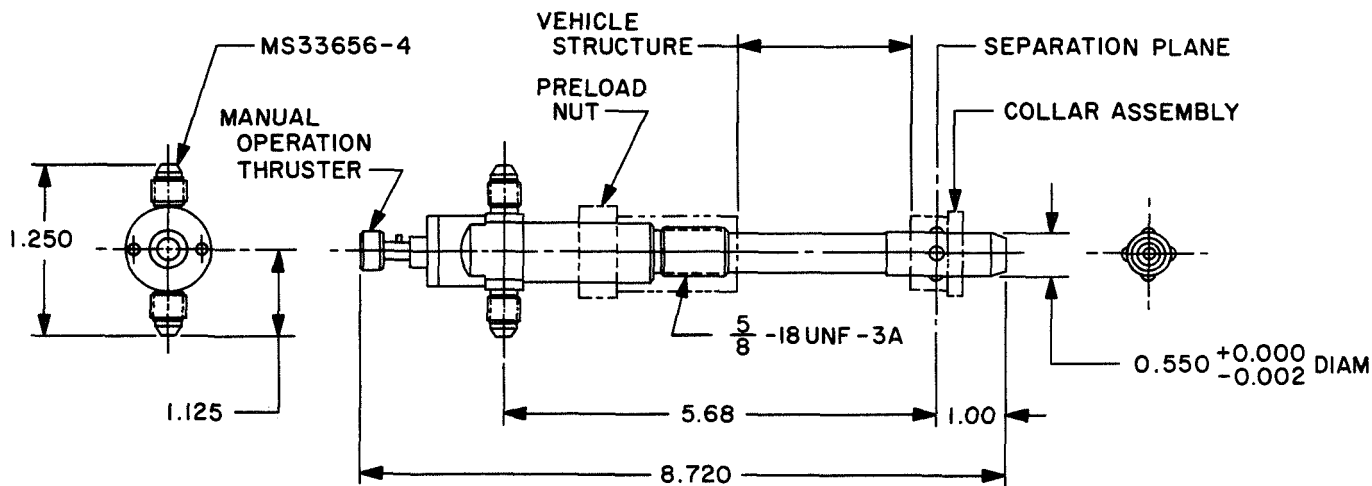
IV. Applications

Figure 4 depicts typical separation-system bolts, which were flown on the MK11, 11A, and 12 reentry vehicles, and Fig. 5 shows several general arrangements for the associated gas generator and tubing manifold systems. The manifolding may take the form of pneumatic tubing, a confined detonating fuse, or an electrical network distribution.

The pneumatic-tubing arrangements shown in Fig. 5 are usually applied either when insufficient electrical



(a) MK II AND MK IIA REENTRY VEHICLES



(b) MK 12 REENTRY VEHICLE

DIMENSIONS IN INCHES

Fig. 4. Typical separation-system bolts

power is available or the number of circuits is at a minimum. Two electrically initiated gas generators, either of which will operate the separation system, with the appropriate tubing manifold, constitute the usual arrangement, as shown in Fig. 5a and b.

For manifolded systems requiring release under high preload conditions or high active-load conditions, the recommended arrangement is that shown in Fig. 5c, in which three gas generators are available but any two will successfully operate the release system. This scheme would reduce the peak pressure required of the full

operating system. Another possible source of manifold pressure is a cold-gas storage bottle with a single- or dual-cartridge valve. In cases where electrical energy is abundant, each separation bolt can incorporate dual cartridges.

Should higher load levels than those depicted in Fig. 3 be required, a second row of balls may be added rather than increase the bolt-body diameter. The capacity of a tandem-row ball-lock bolt will be approximately 190% of the curves shown. However, Curve 1, representing the maximum operating load, would remain essentially unchanged.

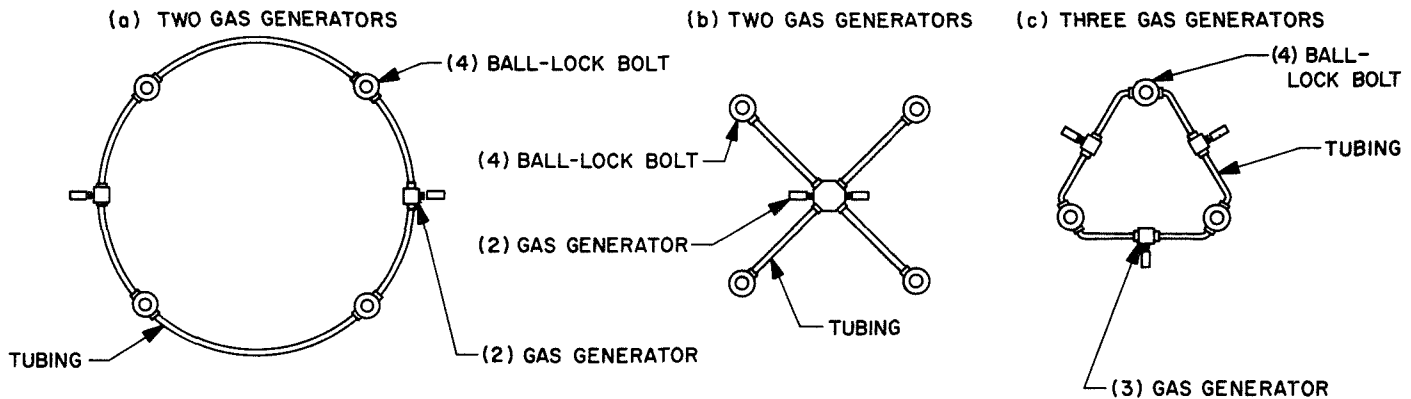


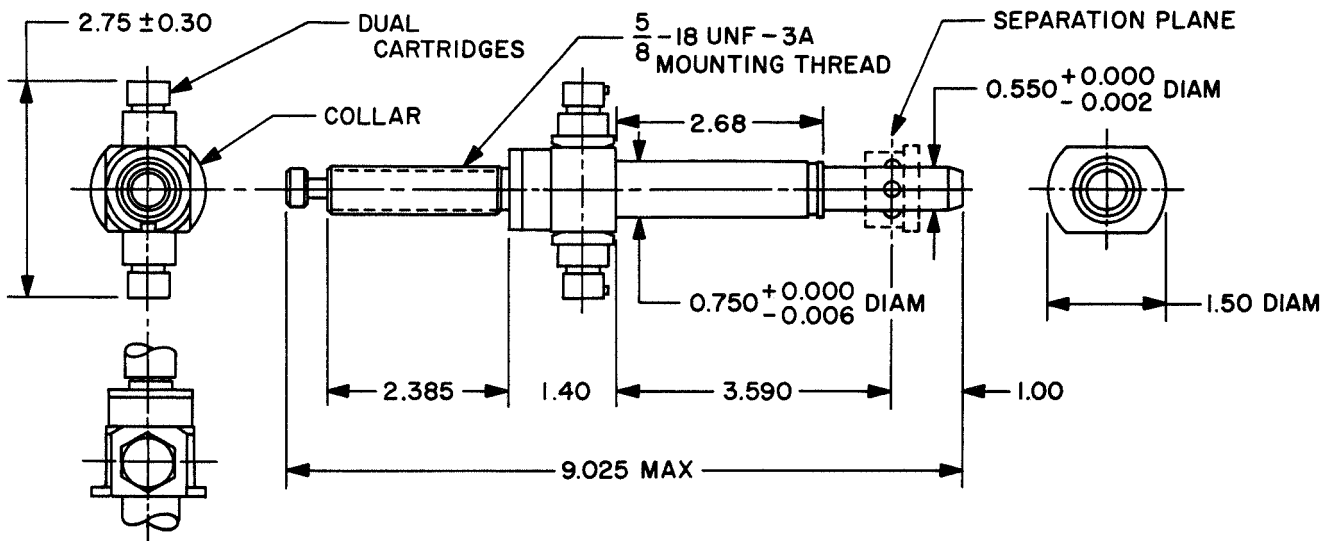
Fig. 5. Three general arrangements for gas generator and tubing manifold systems

V. Single-Point Release Applications

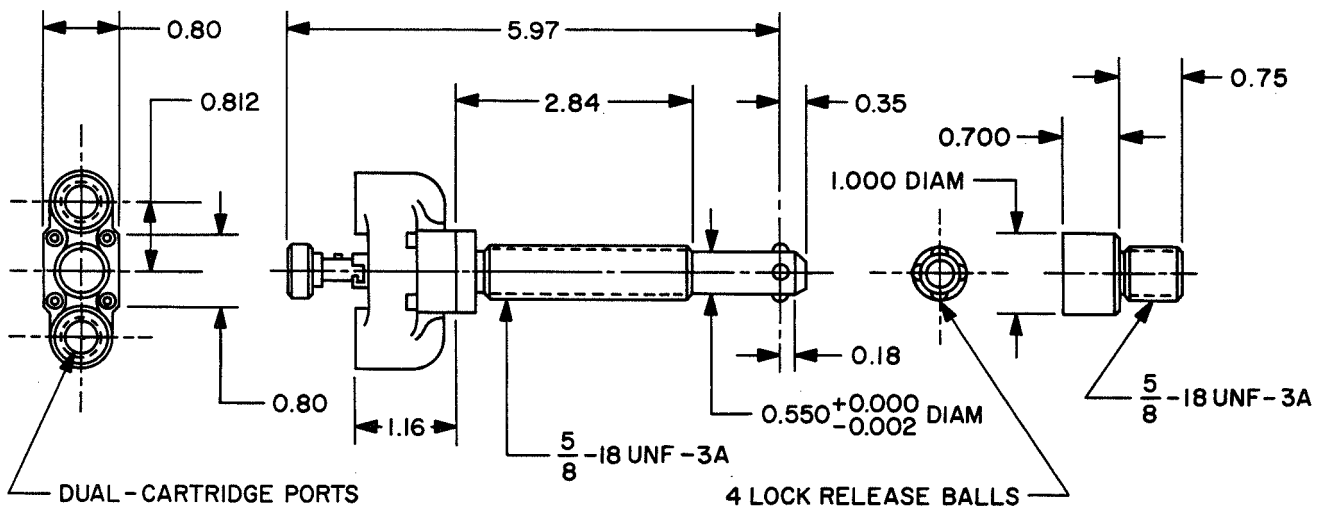
A number of versions of the ball-lock bolt have used single-point restraint. Figure 6 depicts two typical single-point release bolts, both of which have performed successfully in space. In these applications, multiple nuts are used in the long threaded portion to retain the bolt after separation, and the attitude-control-package release bolt doubles as an ejection-spring guide. This arrangement, in which the bolts are released by direct-fired dual cartridges, has proved very satisfactory. However, for systems requiring very high preloads, the peak energy of the dual cartridges produces an excess-energy problem. For high preloads, in the range of 5,000 lb, repeated tests may be conducted on a single bolt only at the single-cartridge pressure level. Reuse after dual-cartridge operation is not recommended.

VI. Conclusion

The ball-lock-bolt separation system offers the designer a wide range of potential applications for soft separation functions. Its application for quick-release systems is limited only by the ingenuity and imagination of the systems designer. For example, a ball-lock bolt could both release and retract with the pyrotechnic energy of the gas generator system, providing a clean separation plane. Conversely, separation thrust could be provided by continuing the stroke of the actuation spool, thus utilizing the manifold energy for separation force. It is possible to hydraulically interconnect a system of bolts whereby simultaneous release and thrust are guaranteed. Since the test hardware for any new system could be used repeatedly, these systems could be developed in a minimum time with a minimum cost.



(a) ATTITUDE CONTROL PACKAGE RELEASE BOLT



(b) BIOSATELLITE RELEASE BOLT

DIMENSIONS IN INCHES

Fig. 6. Two typical single-point release bolts

N 69-11825

Fluid Thermal Actuator*

B. A. Shepherd and K. R. Johnson
Radio Corporation of America
Astro-Electronics Division
Princeton, New Jersey

The purpose of this investigation was to design, develop, and build a thermal actuator for use as the sensor and prime mover of a spacecraft active thermal control system for use on NASA's ITOS (Improved TIROS Operational System) meteorological satellite. Specific thermal requirements of the spacecraft imposed certain design constraints on the actuator, among which were: a predictable operating temperature range, flexibility of range adjustment, over-temperature relief, and a comparatively large force output. Additional requirements were minimum weight and high reliability. Investigation indicated that a design based on the thermal expansion characteristics of a confined fluid was the best means of meeting the requirements. Design philosophy and the implementation are reviewed, and a series of design equations from which predicted performance curves can be derived is given. A comprehensive test program, developed and performed on a breadboard model and on flight-configured units of this actuator, is described, and the results are presented in relation to the specified design goals and the predicted characteristics of the device. The operating parameters of the actuator, as designed for the ITOS satellite, are summarized, and the degree of flexibility of the basic design concept and its adaptation to other systems of spacecraft active thermal control is discussed.

I. Introduction

In the design of any space vehicle, thermal control of the environment is of prime importance in maintaining the operational reliability of the onboard equipment. There are reliable passive techniques of control, such as control of surfaces, location of equipment, and orbit configurations; however, in many cases, they become

burdensome and unpredictable, and an active thermal control system is required.

Typically, active thermal control systems vary the effective area of a radiative surface with a louver, or series of louvers, opening and closing in response to temperature. The thermal actuator described in this report (Fig. 1) provides the sensing and prime motion in such a system. The actuator operates on the principle of controlled thermal expansion of a confined fluid; its

*The work described in this paper was performed for the NASA Goddard Space Flight Center under Contract NAS 5-10306.

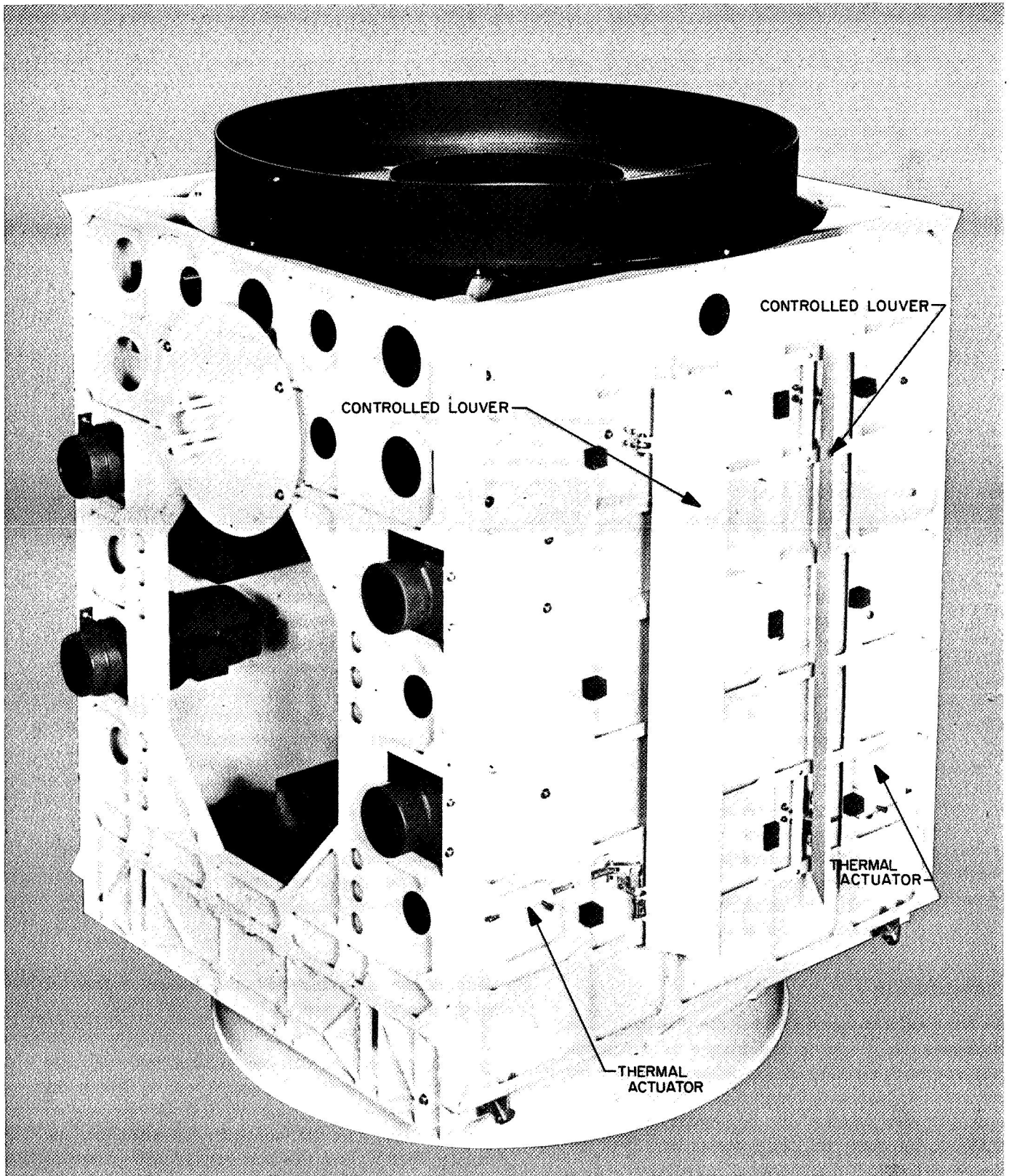


Fig. 1. Thermal actuators and controlled louvers on the ITOS satellite

output is linear motion as a function of the sensed temperature.

The consideration for an active thermal controller on NASA's ITOS meteorological spacecraft stimulated the development of this thermal actuator, which culminated in an actuating device that senses the spacecraft temperature and controls a single 35- × 5-in. louver. Four of these systems in different locations on the spacecraft provide the required thermal environment.

II. Design and Development

A. Constraints for ITOS Actuator

The ITOS active thermal control system had need for a thermal actuator that would meet the following requirements:

- (1) Operating temperature range, 20 ± 1.5 centigrade degrees.
- (2) Range selection from -10 to $+10^\circ\text{C}$ and up to $+35$ to $+55^\circ\text{C}$.
- (3) Over-temperature relief, regardless of selected range, of $+60$ centigrade degrees.
- (4) Minimum weight.
- (5) Reliable operation in space for 1 year (equivalent to 5000 cycles).
- (6) Linearity of the driven louver stroke temperature gain within $\pm 10\%$ of full stroke for any point in the range.

The size of the controlling louver and the resultant bearing design dictated that the actuator have a relatively high force output compared with that of other actuators of a similar function. A further restriction prevented this device from consuming any of the available power from the solar array.

B. Preliminary Study

Actuator selection necessarily had to be fitted to overall system requirements of a particular application. A survey was made of existing actuating devices to determine which was most applicable for the ITOS requirements. The designs investigated included use of the following: (1) bimetallic springs, (2) *on-off* and proportional heater controls, (3) stepper motors and solenoids, and (4) gaseous expansion actuators. None of the schemes reviewed could satisfy the ITOS requirement of high

force output without supplementary power drain on the spacecraft power supply. Therefore, it was decided to proceed with a design that had not previously been used for this purpose, one that utilized the controlled thermal expansion of a confined fluid. There were several advantages to this method that was selected for development: (1) such a design would provide local temperature sensing at the actuator, (2) it would not require an external power source, and (3) a large force output could be extracted from the thermal energy imparted to the fluid due to temperature changes.

C. Fundamental Design Equations

The equation describing the volumetric characteristics of a compressible fluid at rest is derived as follows:

$$v = f(T, p, m)$$

$$dv = \frac{\partial v}{\partial T} dT + \frac{\partial v}{\partial p} dp + \frac{\partial v}{\partial m} dm \quad (1)$$

where

v = volume

T = temperature

p = pressure

m = mass

For a closed system, dm is zero. If we define thermal expansion coefficient β_T as

$$\beta_T = \frac{1}{v} \frac{\partial v}{\partial T}$$

and fluid bulk modulus β_p as

$$\beta_p = -v \frac{\partial p}{\partial v}$$

then Eq. (1) becomes

$$dv = \beta_T v dT - \frac{v dp}{\beta_p} \quad (2)$$

Rearrangement and integration of Eq. (2) give

$$\Delta v = v_0 \left[\exp(\beta_T \Delta T - \frac{\Delta p}{\beta_p}) - 1 \right] \quad (3)$$

Let

$$x = \beta_T \Delta T - \frac{\Delta p}{\beta_p}$$

then, from the Fourier expansion of e^x and Eq. (3),

$$v = v_0 \left[\left(1 + \frac{x}{1!} + \frac{x^2}{2!} + \cdots + \frac{x^n}{n!} \right) - 1 \right] \quad (4)$$

By an order-of-magnitude analysis,

$$O(x) = 10^{-2}$$

$$O(x^2) = 10^{-4}$$

Therefore, the terms of $n = 2$ and higher in Eq. (3) can be neglected, and the reduced form of the equation becomes

$$v = v_0 \beta_T \Delta T - v_0 \frac{\Delta p}{\beta_p} \quad (5)$$

To implement this equation, it is necessary to select a fluid with predictable β_T and β_p , define pressure as a function of temperature, and provide a means of converting Δv into linear motion.

The thermal expansion and bulk modulus coefficients of most fluids are clearly defined and are available as a function of such other parameters as temperature and viscosity. For the actuator of this report, silicone oil is used — primarily for its constancy of expansion coefficient with temperature, its low vapor pressure, and the expansion coefficient selectivity permitted over the range of available viscosities.

Conversion of volumetric expansion into linear stroke is conveniently accomplished with an expandable chamber — namely, a bellows of sufficient stroke and pressure capability. Using a bellows, the relationship between stroke and volumetric change required in Eq. (5) is given by the following:

$$\delta = \frac{\Delta v}{A_M} \quad (6)$$

where A_M is the mean area of the bellows. This design uses two bellows, one for the driving function and the other to provide adjustment of range and over-temperature relief. The inherent spring rates of these bellows provide the energy necessary for motion as the fluid contracts with decreasing temperature.

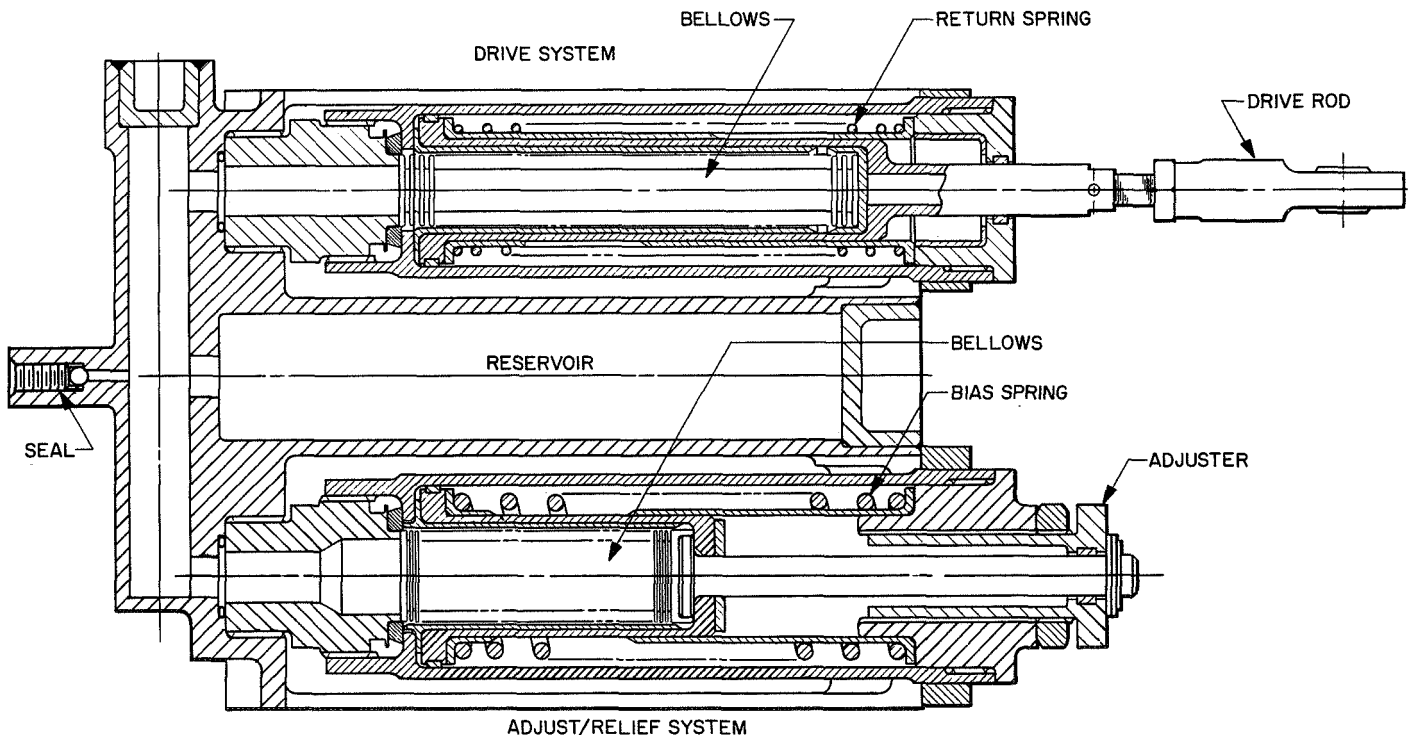


Fig. 2. Cross section of the thermal actuator

Each bellows operates in concert with a drive spring. These springs supplement the bellows spring rate and raise the force level of the system. The bellows/spring combinations are the sole determinants of the pressure buildup in the actuator.

D. Configuration and Operational Description

A cross section of the actuator is shown in Fig. 2. Basically, the actuator can be considered in two parts, referred to as the drive system and adjust/relief system. These two systems are hydraulically coupled to each other and to the reservoir. The fundamental components of the drive system are the drive bellows, drive spring, and drive piston.

The drive piston moves linearly on two piston-ring Teflon bearings. Not being rigidly attached to any fixed part, the piston is free to rotate; this provision allows linear adjustment of the external rod when it is locked on a shaft. The drive bellows is made of nickel and is accurately fabricated by electrodeposition for predictable spring rate, stroke, and pressure capability. To provide a usable stroke in a minimum package, the bellows is used in compression and extension, with the drive spring accomplishing the compression of the bellows.

As the fluid in the actuator expands with temperature, the drive bellows moves linearly to accommodate the expansion, working against the drive spring and moving the drive piston in an outward direction. In a cooling mode, with the fluid contracting, the drive spring provides the necessary force levels.

The drive spring is preloaded so that the minimum force level of the drive spring-drive bellows combination with the drive piston full in ($\delta = 0$) is not less than 4 lb. This available return force increases linearly as the drive spring is compressed with the piston moving out. The calculation of this force reflects the combined spring rates of the spring and bellows. Figure 3 shows the relationship between drive position and available return force.

At first glance, it would seem that the available force in the outward direction during heating would be extremely large and limited only by any compressibility of the fluid. However, the force is limited to the threshold force or internal pressure at which the relief system picks up.

The adjust/relief system consists of a bellows, spring, and piston arrangement similar to the drive system and,

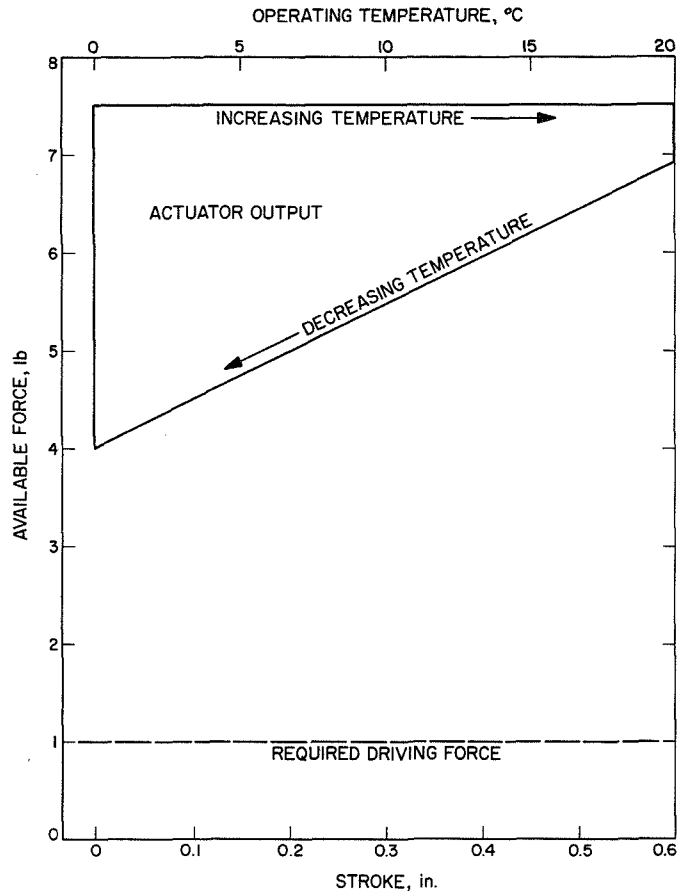


Fig. 3. Available force diagram, thermal actuator

also, an adjuster with a locking nut. This combination of components performs the two supplementary functions of the thermal actuator: adjustment of the operating range and over-temperature relief. The spring and bellows spring rates of this system are sized to be compatible with the drive system. That is, the relief system is preloaded such that the minimum pressure required to move it is greater than the maximum pressure developed in the drive side. A typical pressure/temperature plot for the actuator is shown in Fig. 4.

This adjust/relief system also incorporates the adjustment feature that permits the nominal 20 C° temperature range to be selected anywhere between -10°C and $+55^{\circ}\text{C}$. Adjustment in all cases means adjusting to the temperature at the low end of the 20 C° range. The ability to provide this adjustment can be explained as follows: With the unit filled with a known amount of fluid at a certain temperature, it is true from the thermodynamics of the closed system (Eq. 5) that there is a unique absolute volume of fluid associated with each and every temperature of the bracketed range. Therefore, by

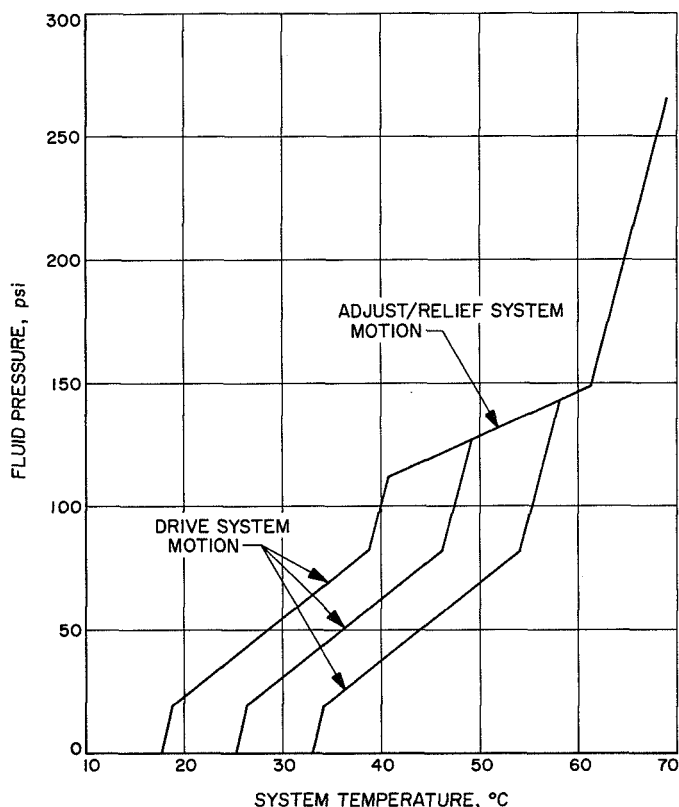


Fig. 4. Thermal actuator fluid pressure as a function of temperature

threading the adjusting nut, which simply expands or contracts the adjust/relief bellows and changes the internal physical dimensions of the actuator, any specific temperature can be selected below which the fluid has not reached a sufficient volume to be effective. This represents the temperature at the low end of the desired 20 C° range.

E. Design Considerations and Materials Selection

1. Prevention of metal-to-metal contact of moving parts. In developing the actuator, there were a number of design considerations, selections, and philosophies that were felt to be pertinent to meeting the outlined goals. Most of these were motivated by the requirement to guarantee operation for 1 year in space. For example, the use of nonlubricated Teflon/steel bearings was dictated to avoid the evaporative and contaminating characteristic of viscous lubricants.

This philosophy was more applicable to the design of the moving louver section of the active thermal controller, but it is reflected in the design of the Teflon rings upon which the drive and adjust/relief pistons

move. A related design philosophy is the use of nylon sleeves as guides for the springs and bellows. The design, in total, does not permit metal-to-metal contact of any moving parts.

2. Selection of bellows. The electrodeposited type of bellows was selected because it provided the best combination of available stroke, predictable spring rate, and wall homogeneity. Hydraulically formed bellows are stiffer and do not offer satisfactory available stroke per unit length. Welded bellows have a significant stroke advantage, but their noncontinuous construction does not provide the desired confidence against leakage.

In selecting a particular pair of bellows, the design procedure was iterative within the operating limits of the bellows and the defined parameters for the actuator. With the temperature requirements of range, adjust, and relief, and with a reasonably selected stroke, the design approach was one of selecting the bellows/spring combination to reach a proper balance of the following parameters:

- (1) Available force of drive system.
- (2) Bias relationship of drive and adjust/relief systems.
- (3) Maximum allowable pressure of bellows.

3. Minimizing contaminants. With consideration of a design of this type, it was readily concluded that the ability to predict the operation of the device and, furthermore, to have confidence in the operation was highly dependent on the selection of the fluid, the amount of contaminants introduced, and the sealing quality of the chamber. It was previously mentioned that silicone oil was selected for its low vapor pressure, stability of expansion coefficient β_T , and range of expansion coefficients as a function of viscosity. Other fluids of higher β_T were considered, but they did not offer the flexibility of selecting within their specie a range of expansion coefficients. It is also true that many of these fluids were of magnitudes higher in vapor pressure, which could not be allowed because of the natural compressibility of gaseous vapors.

Because the operation of the device is fundamentally based on the small expansion capability of a confined fluid and because the effect of pressure buildup in the system is to subtract from this effect, it was highly undesirable to introduce compressible contaminants into the device. Of particular concern were traces of volatile components and entrained air in the fluid, air trapped

in the bellows during filling, and air introduced during the final sealing procedure. Proper selection of fluid plus a vacuum de-aeration process negated the first concern of volatiles and entrained air.

The second concern of entrapped air during filling was felt to be minimized by a vacuum backfill technique wherein the fluid is introduced from a filling reservoir into the vacuum of the device. The problem of introducing air during the final seal was solved by use of the sealing mechanics shown in Fig. 2. The device may be sealed completely below the fluid level without the introduction of air.

III. Testing and Results

Testing of the actuator was done on a breadboard model identical to the flight model from the standpoint of operation and performance. Testing was carried out as a development program learning process with two objectives. The primary objective was to show that the actuator performed as designed and that the design goals, stated earlier, had been achieved. The secondary objective was an evaluation of the effect of certain unpredictable variables (mechanical compliance, entrapped air, and a variation in the fluid bulk modulus β_p) on the overall system performance.

All tests were performed in a temperature-controlled chamber. By the use of a potentiometer to monitor displacement and a temperature-compensated strain-type pressure transducer to check fluid pressure, the unit was evaluated over all temperature ranges. Freedom of range selection was demonstrated, as is shown on Fig. 4, which also shows the over-temperature relief capability to be in excess of the desired 60 C°.

Initial tests in the program indicated that the operating range of the actuator was 24 C°, instead of the predicted 20 C°. It was further shown that the operation of the device was identical for any selected range. From consideration of the four parameters (v_0 , β_T , Δp , β_p) of Eq. (5) which affect the $\Delta v/\Delta T$ relationship, it became evident that the value of the fluid bulk modulus β_p enjoyed our least confidence. Bulk moduli are typically published for high-pressure ranges, leaving low-pressure values to extrapolation and curve fitting.

Curve fitting from available manufacturer's data, however, resulted in an analytically determined compressibility that was one order of magnitude lower than that

originally used. Furthermore, continued testing led to a conclusion that, in fact, we were dealing with other factors that were operating collectively to give us what we now term an equivalent bulk modulus (β_{pe}). Such factors as entrained volatile fluid components, inherent bellows compliance, and air entrapped during the filling operation could all interact in the equivalent system.

An analytical evaluation of the β_{pe} reflecting this interaction would at best be difficult because of the interrelated variables listed above. Thus, to substantiate our conclusion and evaluate the equivalent modulus, an empirical approach was undertaken in the form of an over-temperature pressure test. The results of this test are shown on Fig. 4. Above 62°C, a region where $\Delta v \approx 0$, the graph indicates a finite change in pressure as a function of a change in temperature. Analysis of this data by Eq. (5) gives $\beta_{pe} = 17 \times 10^3$ psi.

To compensate for a decrease in β_{pe} , which (according to Eq. 5) manifests itself as a reduction in gain, a new fluid with a higher β_T was selected. Subsequent testing showed the operating range to be 20 ± 1.5 C° with a linearity of 2% maximum. With the operating range of 20 C°, the over-temperature relief became 60 C°, as predicted.

IV. Conclusion

The tangible result of the developmental effort was the local-sensing thermal actuator with the following characteristics, which met the earlier established design constraints imposed by requirements for ITOS:

- (1) Operating range provided was 20 ± 1.5 centigrade degrees.
- (2) Range selection was from -10 to $+10^\circ\text{C}$ up to $+35$ to $+55^\circ\text{C}$.
- (3) Over-temperature relief of 60 centigrade degrees was provided.
- (4) Stroke/temperature linearity was within $\pm 2\%$ of the full stroke.
- (5) Available force output was 4 to 7 lb.
- (6) Weight was 2 lb.
- (7) Reliability predicted was 0.995 for 1 year operation in space.

- (8) Minimum expected life is 10^7 cycles, based on bellows capability.
- (9) Ability to change operating range by changing β_T was provided.

More fundamentally, the effort reduced to hardware and proved through test the reality of a thermally actuated device based on the principle of controlled fluid expansion. Such a device is particularly suited to appli-

cations where the consumption of electrical power is not permitted and, at the same time, predictable high force outputs are desirable.

Acknowledgment

The authors acknowledge the assistance of Mr. John H. Hayden, senior design specialist, for his invaluable contribution to the design of this fluid thermal actuator.

N 69-11826

Development of Gravity-Gradient Dampers

M. E. Johnson and S. H. Marx

Philco-Ford Corporation

Space & Re-entry Systems Division

Palo Alto, California

The key functional component in a gravity-gradient stabilization system is the energy dissipation device, which, in most of these systems, is a lossy coupling. This paper describes some of the suspension and energy dissipation methods utilized in this type of component. Two of these couplings and their functional test methods are covered in detail.

I. Introduction

The ever-increasing life requirements of orbital systems have brought about increased interest in satellites which utilize the gravitational gradient for all or part of their orientation. These satellites are configured so that they are essentially gravitation pendulums. However, a simple pendulum would oscillate because of initial "tip-off" disturbances, orbital eccentricity, solar pressure, etc. Therefore, it is necessary to extract this libration energy by some means.

Thus far, two successful basic system approaches have been used. Both utilize relative motion between a primary and a secondary body. The first approach anchors a secondary body to the earth's magnetic field. This requires, first, the existence of the field and, secondly, that the field be predictable. The second approach utilizes a secondary body which, through a spring coupling, has

a null position at some fixed angle to the primary body. This inertia-spring system is tuned so that external disturbances will result in relative motion between the two bodies. In both approaches a damper, which dissipates the libration energy in the form of heat, is placed between the primary and secondary bodies. In the second approach above, the energy dissipation device and the spring are combined in a single coupling, referred to as a damper. This paper describes the design, development, and testing of two such dampers.

One of these devices was flown on a *Naval Research Laboratory* (NRL) satellite in mid-1967 and a second and different type is scheduled for launch in mid-1968 on the *NASA Radio Astronomy Experiment* (RAE) satellite.¹

¹For more information on the RAE satellite, see "The Radio Astronomy Explorer 1500-ft-Long Antenna Array" by E. Angulo and W. P. Kamachaitis, in these *Proceedings*.

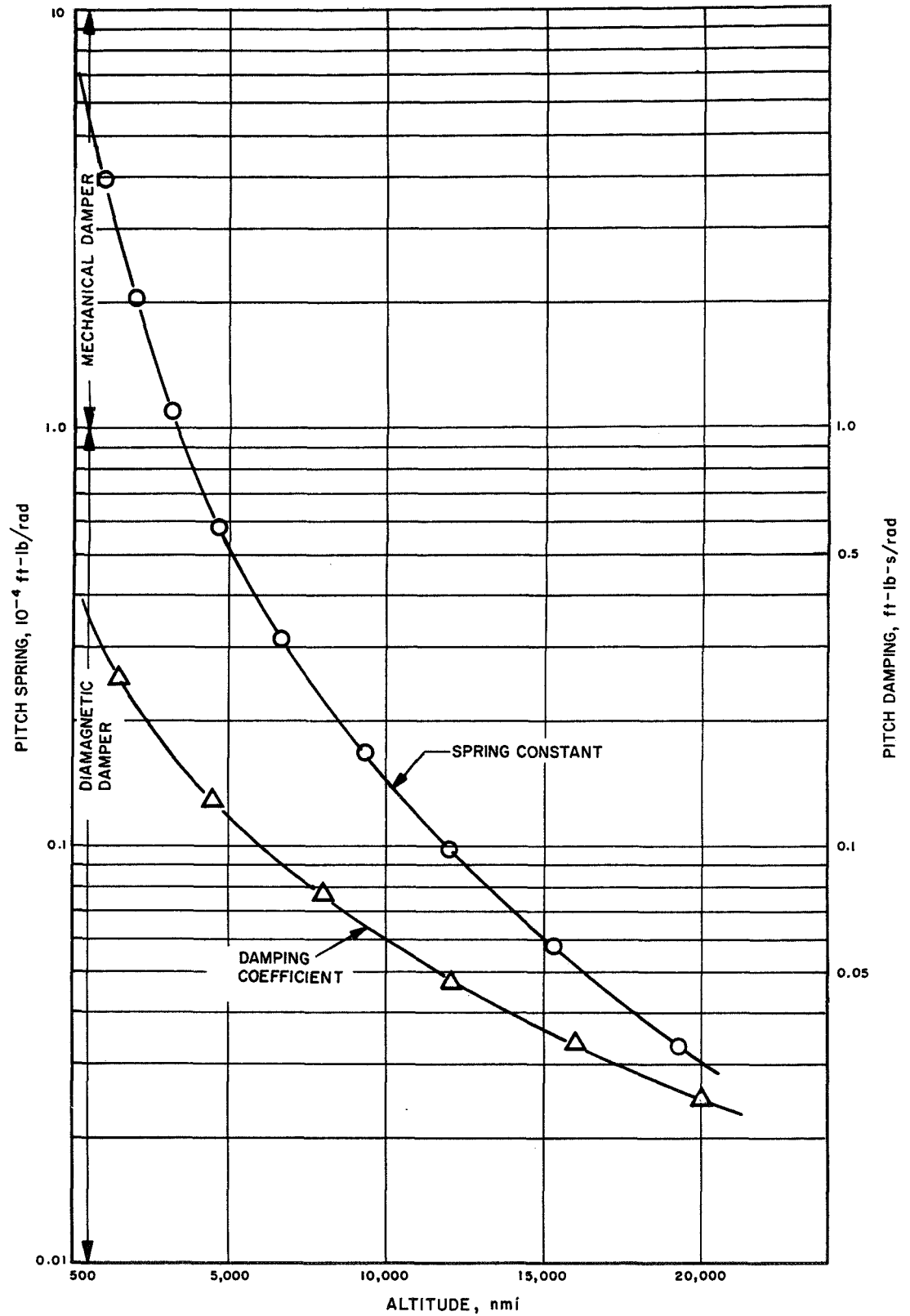


Fig. 1. Representative maxima for pitch damper parameters for pitch inertia $\cong 1000$ slug-ft²

The functional parameters of couplings such as those discussed here depend on a number of variables which include the altitude, steady-state excursion limits, etc. The analysis that determines these parameters will not be dealt with here, but, as a matter of general interest, the variation in functional parameters due only to orbit altitude is shown in Fig. 1.

II. Suspensions and Damping Methods Selected

Three basic spring suspensions (diamagnetic, torsion wire, and flexure pivots) and two different damping methods (magnetic eddy current and magnetic hysteresis) are used in various combinations in the dampers developed to date.

A. Diamagnetic Suspension

Materials that have a magnetic susceptibility less than that of free space are called diamagnetic. The most prominent of these materials are bismuth and carbon. The most useful is graphite (the crystalline form of carbon) and, most recently, pyrolytic graphite, because of its relatively low density and high strength. When these materials are partially immersed in a magnetic field, they experience an expulsion force. By shaping the magnetic field and the material, a spring characteristic and a suspension force can be obtained.

Since the difference between the magnetic susceptibility of diamagnetic materials and that of free space occurs in the sixth significant figure, the forces generated are very small. This factor, as well as other constraints, limits this suspension to applications requiring relatively low orthogonal force ratio and torsional spring constants of approximately 1×10^{-4} ft-lb/rad or less. Such a suspension is extremely rugged and relatively insensitive to mechanical damage during handling, launch, etc.

Philco-Ford's developments of diamagnetic suspensions are described elsewhere.² The present paper considers only torsion wire and flexure pivot applications.

B. Torsion Wire Suspension

Torsion wire suspension utilizes torsional stress resultants for rotational constraint. Location and suspension

² Marx, S., *Development of a Damper for Passive Gravity-Gradient Stabilization*, NASA SP-107. National Aeronautics and Space Administration, Washington 25, D. C., 1966.

forces are obtained by axial wire load. Although a large range of spring constants is obtainable, Philco-Ford experience has been concentrated in the range of 1×10^{-4} to 1×10^{-2} ft-lb/rad; however, this has been due to system constraints rather than suspension limitations.

C. Flexure Pivot Suspension

This suspension utilizes flexural stress resultants of very thin beams to obtain torsional spring characteristics. These beams are arranged so that a near-constant center of rotation is maintained. This suspension is particularly useful over approximately the same range as the torsion wire; moreover, it has the advantage of being much more compact for a comparable spring constant. It has the disadvantage of being easily damaged by relatively small displacements in the nonactive axes and requires specialized techniques and capabilities to manufacture in the size of interest here.

D. Magnetic Eddy Current Damping

The motion of a conductor in a magnetic field results in induced currents circulating throughout the volume of the conductor. Because of their general circulatory nature, these are referred to as eddy currents. The interaction between these currents and the field results in a braking torque on the conductor. Rotational energy is dissipated in the form of heat generated by the eddy current circulation. The damping experienced is "viscous" or velocity-dependent and therefore lends itself to straightforward analysis. This method has the disadvantage of having a relatively high weight-to-energy extraction ratio for the applications considered here.

E. Magnetic Hysteresis Damping

The magnetic domains in ferromagnetic materials are randomly oriented. When subjected to a strong external field, these domains become aligned with the field. If the field is reversed, the domains realign themselves; this results in a mechanical working of the material at the microscopic level and thereby dissipates energy in the form of heat. This process is analogous to mechanical elasto-plastic hysteresis. A typical torque-displacement curve is shown in Fig. 2.

Consider a ring that is rotating in a plane perpendicular to a pair of magnets as shown in Fig. 3; as an element passes under the magnet, a field reversal takes place. This process dissipates energy and thus a braking (or damping) torque results. This damping is displacement-dependent and does not readily lend itself to closed-form

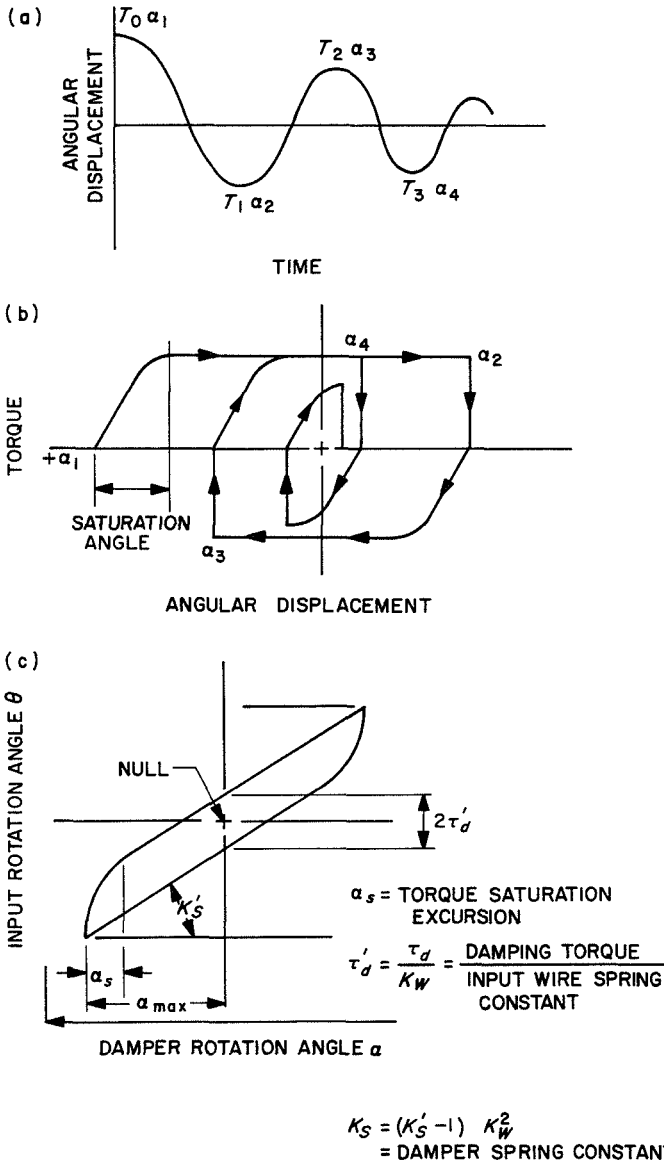


Fig. 2. Typical torque-displacement relationships

analytical methods. The ratio of energy dissipation to weight is relatively high.

F. Two-Axis Eddy Current Damper

The satellite configuration shown in Fig. 4 has one fixed vertical boom and tip mass attached to the spherical main structure. The secondary body, which is coupled through the two-axis damper to the primary body, consists of a V-boom with an included angle of 62 deg. Freedom of rotation about the pitch and roll axes is 30 deg. The damper assembly is shown in Fig. 5. Its pertinent performance parameters are shown in Fig. 4.

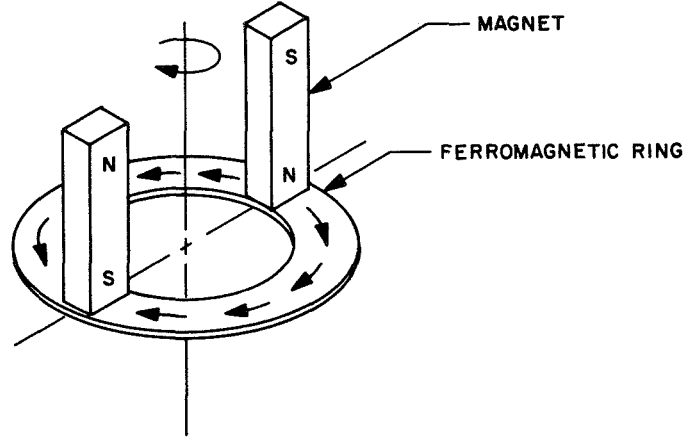


Fig. 3. Typical hysteresis circuit

SPRING CONSTANT
 PITCH AXIS = 2×10^{-3} ft-lb/rad
 ROLL AXIS = 4×10^{-4} ft-lb/rad
 DAMPING COEFFICIENT
 PITCH AXIS = 0.14 ft-lb-s/rad
 ROLL AXIS = 0.027 ft-lb-s/rad

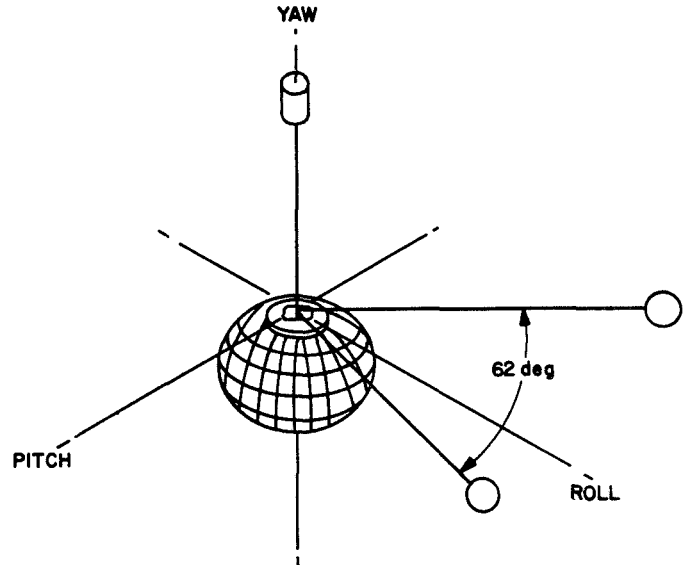


Fig. 4. NRL boom/satellite configuration

Because of the magnitude of the required spring constants, a totally mechanical suspension was used. The inner (roll) axis uses an Elgiloy torsion wire for the spring-restoring moment and suspension. Axial tension is provided by two cantilevered beryllium copper end springs. The pitch axis, which is exercised through the roll suspension, uses flexure pivots to conserve space. Damping in both axes is of the eddy current type, using copper rotating elements and matched Alnico V permanent magnets. The "railroad track" configuration of the pitch

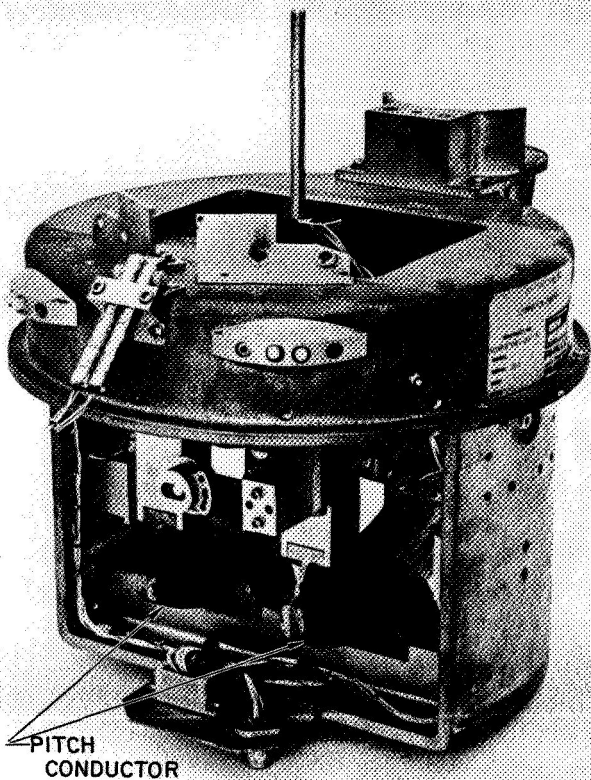


Fig. 5. Two-axis eddy current damper

ductor (Fig. 5) is to provide the eddy current return path, which is necessary for efficient damping. Magnetic pole control, which is essential with this configuration, is maintained by using soft iron pole shoes, precision air gaps, and a careful magnet-matching technique. The residual dipole was cancelled by a small additional magnet.

The damper assembly was caged during handling and released by a pair of clamps which secured both axes. These clamps were released by pyrotechnic pin-pullers. This mechanism is shown in Fig. 6. The main boom tip mass was secured by a pin-puller-released mechanism. The V-boom tip masses were caged by a lever/cable mechanism which was released by redundant pyrotechnic guillotine cutters. The independent caging and release mechanisms were required because of the system deployment sequence.

Because of the nature of the suspensions and the relative size of the damping coefficients, all functional parameters were tested at the component or subassembly level. Testing on the assembly consisted of dipole mo-

ment cancellation and residual determination and environmental tests.

Damping tests were run using auxiliary suspensions and the flight rotating elements and magnets. The decay of the rotating element from an initial displacement is recorded, and from this recording the damping coefficient is determined. To monitor the position of the rotor, an illuminated slit is projected onto a mirror on the rotating element. The mirror reflects the slit onto a photosensitive potentiometer. The voltage drop across the potentiometer is recorded. The test setup is statically calibrated before every run.

The spring constants of both axes are determined by using a known inertia and measuring the oscillation period induced by a step function input.

Dipole moment testing is done at a specially constructed facility. This facility is remotely located to eliminate external magnetic noise from vehicles and power lines, etc. A magnetometer is used to map the external magnetic field, and the magnetic dipole is obtained by a Fourier analysis.

G. Single-Axis Damper for Radio Astronomy Experiment (RAE) Satellite

A single-axis damper, shown in Fig. 7, was developed for use on the RAE satellite. This damper was specified to be a hysteresis unit with a spring constant of 9.5×10^{-3} ft-lb/rad and a saturated damping torque of 1×10^{-3} ft-lb. This unit also uses an Elgiloy torsion wire suspension with beryllium copper end springs. The damper is located in the proximity of a magnetometer, and control of the external magnetic field was necessary. For this reason, the closed magnetic circuit previously described was used. The magnetic circuit used matched Alnico V magnets with soft iron pole shoes and 416 stainless steel hysteresis material. Precise ring thickness was required to minimize torque ripple. Magnet matching and minimizing the air gap kept the stray field at 500 gammas with a peak-to-peak ac component of less than 5 gammas at a distance of 12 in.

Because the damping torque is displacement-dependent and because of requirements to determine the excursion to damping torque saturation as well as the torque ripple, it was necessary to construct a special test stand. The test stand uses a calibrated input torsion wire to drive the damper and an optical servo drive to track the damper excursion. The input torsion wire rotation is

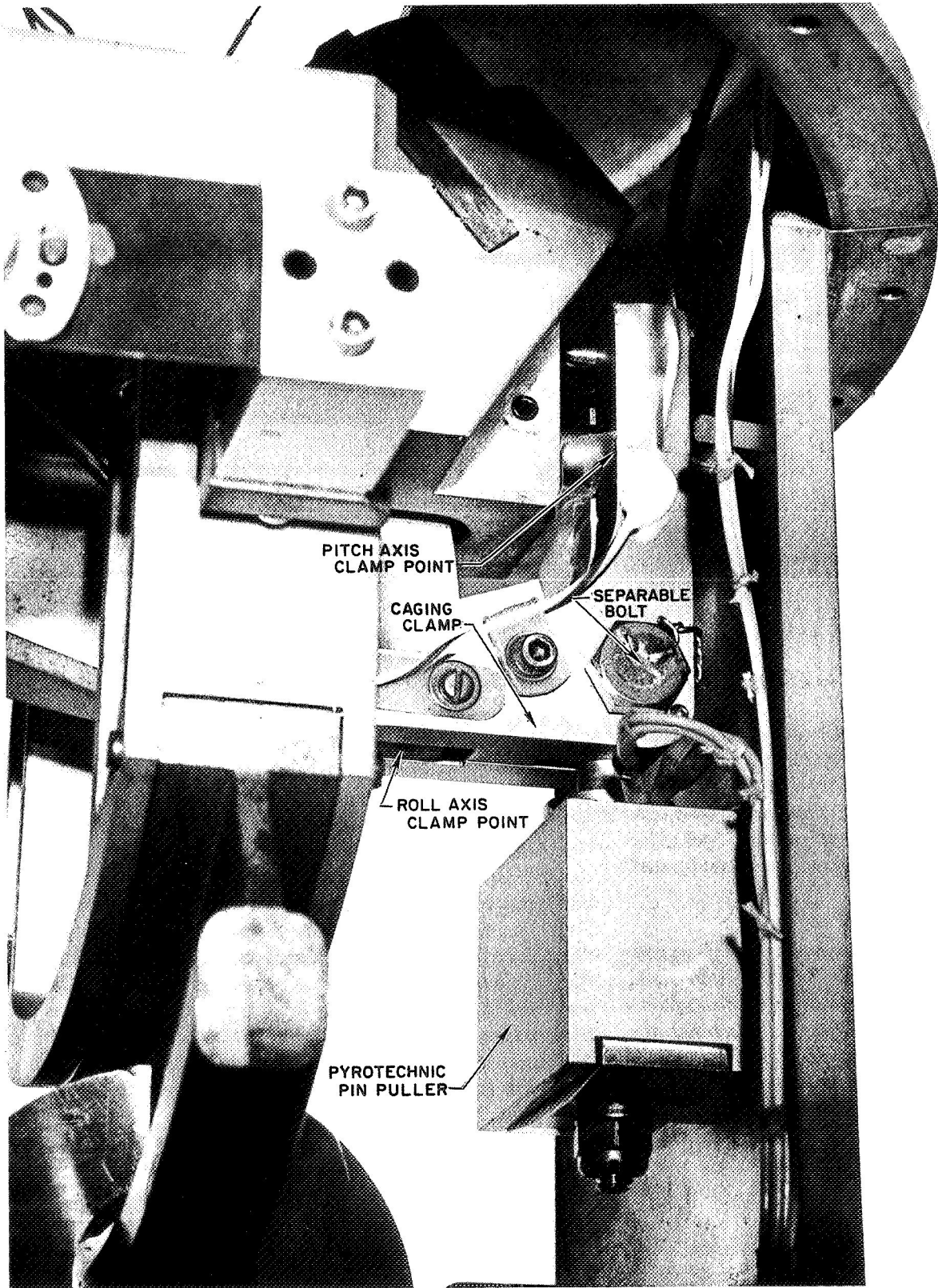


Fig. 6. Pyrotechnic pin-puller mechanism on two-axis eddy current damper

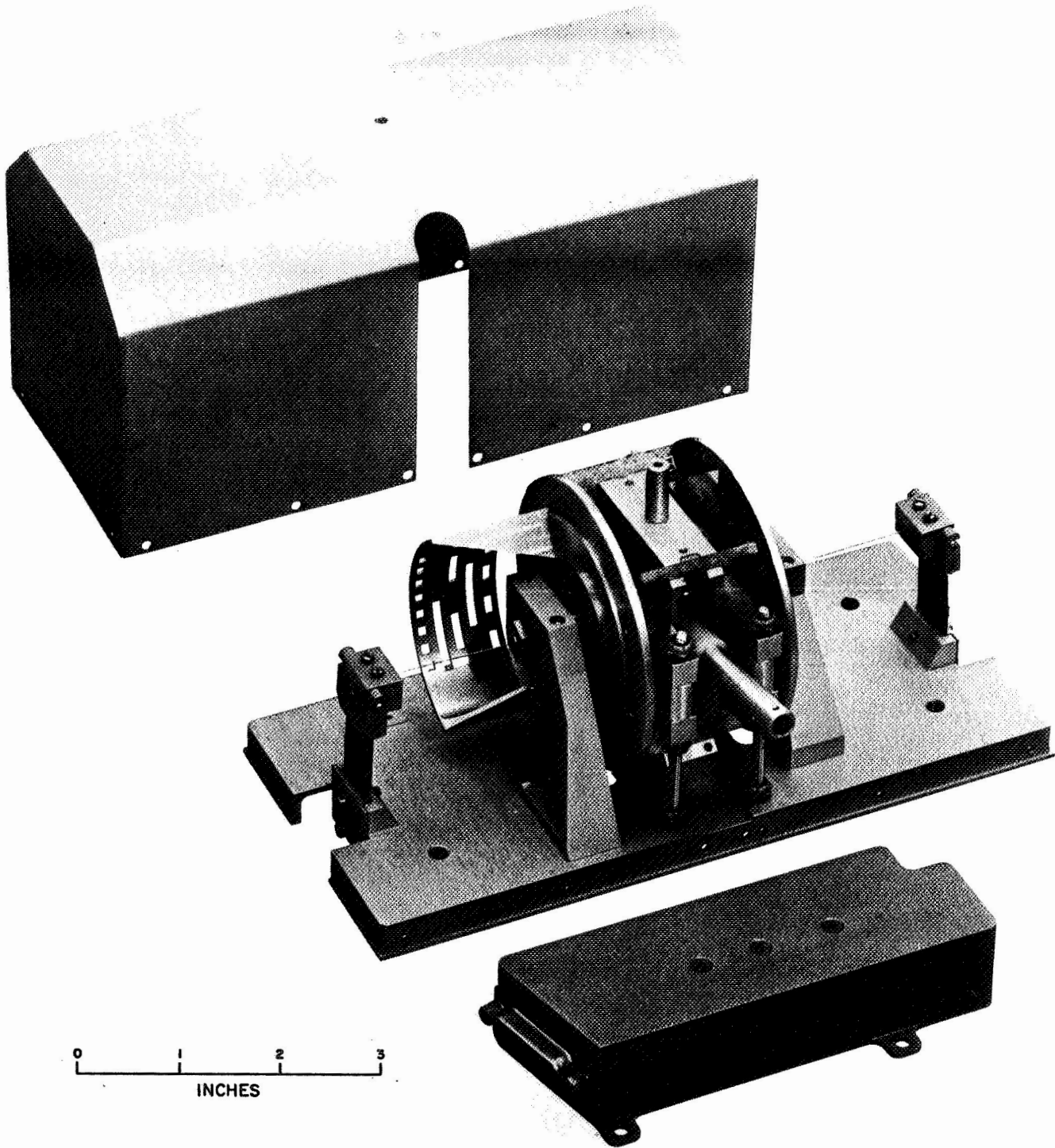


Fig. 7. Single-axis damper developed for the RAE satellite

orded on one axis of an $x-y$ plotter simultaneously
h the optical tracker (damper) excursion on the other
. The resulting plot displays all the pertinent func-
tional parameters. A typical output is shown in Fig. 2.

III. Conclusions

Gravity-gradient stabilization systems have been flight-
proven at selected altitudes. Components for systems to

be used at earth orbits up to synchronous altitude, and comparable orbits of other bodies, can be built using methods and procedures already developed.

The optimum method or system to be used is a function of mission requirements and each case must be individually examined.

List of Attendees

- AARDAHL, CLEDITH
Jet Propulsion Laboratory
- ABBOTT, HELEN M.
Lockheed Missiles & Space Company
- ABBOTT, RALPH E.
SPAR Aerospace Products, Ltd.
- ABSHERE, B. G.
Hughes Aircraft Company
- ACKER, ROY M.
TRW Systems Group
- ADAMS, JAMES L.
Stanford University
- ALEXANDER, EDWARD L.
TRW Systems Group
- ALEXANDER, HOSEA
Jet Propulsion Laboratory
- ANGULO, E. D.
NASA Goddard Space Flight Center
- AQUILERA, E. P.
General Dynamics Corporation
Convair Division
- BAISLEY, RONALD L.
Jet Propulsion Laboratory
- BAMFORD, ROBERT M.
Jet Propulsion Laboratory
- BARNETT, MORRIS A.
The Garrett Corporation
- BARTON, MILLARD V.
TRW Systems Group
- BAYLESS, JOHN C.
Ball Brothers Research Corporation
- BEAL, ROBERT T.
Naval Research Laboratory
- BELL, CURTIS C.
Hughes Aircraft Company
- BEYLIK, CALVIN M.
Jet Propulsion Laboratory
- BOCHARY, MICHAEL E.
TRW Systems Group
- BOHLING, RAYMOND F.
NASA Headquarters
- BOMKE, PAUL W.
Jet Propulsion Laboratory
- BRESNIKER, ROBERT L.
United Technology Center
- BROOKSON, GEORGE A.
Aerospace Corporation
- BROTKEMARKLE, DON W.
Aerospace Corporation
- BROWN, JERRY C.
Lockheed Missiles & Space Company
- BOYLES, HOWARD G.
Jet Propulsion Laboratory
- BUCHNER, MARY FRAN
Jet Propulsion Laboratory
- BURNEY, HAROLD W.
Metal Improvement Company
- BURNS, GENE C.
McDonnell Douglas Corporation
- CABLE, W.
Radio Corporation of America
- CALTA, M. C.
Aerospace Corporation
- CANTON, ROBERT
General Precision, Inc.
- CARDOSO, JOHN B.
Aerospace Corporation
- CARLEY, WILLIAM J.
Jet Propulsion Laboratory
- CARLSON, J. ALLEN
Electro-Optical Systems, Inc.
- CARMAN, ROBERT R.
Goodyear Aerospace Corporation
- CARR, W. F.
McDonnell Douglas Corporation
- CARROLL, FRANCIS J.
NASA Electronics Research Center
- CASABIANCA, CLIFFORD
Jet Propulsion Laboratory
- CHAMNESS, O. VAUGHAN
General Precision, Inc.
- CHASE, DAVID R.
Lockheed Missiles & Space Company
- CHOBOTOV, V.
Aerospace Corporation
- CHRONES, C.
TRW Systems Group
- COLLINS, GARY
Jet Propulsion Laboratory
- COLLINSON, J. A.
Bell Telephone Laboratories, Inc.
- COOK, J. S.
Bell Telephone Laboratories, Inc.
- CORRIGAN, HARRY G.
Consultant
- COYLE, GARY G.
Jet Propulsion Laboratory
- CROSS, D. G.
TRW Systems Group
- CROSSLEY, G. ERSKINE
Georgia Institute of Technology
- CSEBNAY, JOHN
SKF Industries, Inc.
- CULVER, JOHN S.
Hughes Aircraft Company
- CUNDALL, DONALD R.
Philco-Ford Corporation
- DAHL, P. R.
Aerospace Corporation
- DANKO, EDWARD A.
TRW Systems Group
- DARE, ALAN R.
TRW Systems Group
- DAVIDSON, JOSEPH K.
Ohio State University
- DAVIS, ROBERT R.
Jet Propulsion Laboratory
- DAVIS, THOMAS V.
The Boeing Company
- DAWSON, FREDERICK W.
Martin Marietta Corporation
- DAY, JOHN
McDonnell Douglas Corporation
- DEAL, T. E.
Hughes Aircraft Company
- DEBS, R. J.
NASA Ames Research Center
- DELAND, R. E.
TRW Systems Group
- DILLARD, PAUL A.
TRW Systems Group
- DIXSON, JOHN E.
TRW Systems Group
- DRUMMOND, OLIVER E.
Aerospace Corporation
- DUBOWSKY, STEVEN
Perkin-Elmer Corporation
- DUNK, ALLAN C.
Jet Propulsion Laboratory
- EDSTROM, ANDREW H.
Quantic Industries, Inc.
- ENGELBERT, DAVID F.
NASA Ames Research Center
- FALKENTHAL, GEORGE E.
NASA Ames Research Center
- FAN, JASON H.
Hughes Aircraft Company
- FARRINGTON, WILLIAM B.
Farrington and Light Associates
- FERGER, H. L.
Aerospace Corporation
- FERRERA, JOHN
Jet Propulsion Laboratory
- FILLEBROWN, WILLIAM C.
McDonnell Douglas Corporation
- FITTON, JOHN A.
TRW Systems Group
- FITZGIBBONS, JAMES W.
Sylvania Electric Systems
- FLEMING, M. F.
Philco-Ford Corporation
- FLEMING, WILLIAM M.
Pyronetics, Inc.
- FLOYD, ELMER
Jet Propulsion Laboratory
- FORD, ALLEN
Jet Propulsion Laboratory
- FORD, JOHN P.
Sandia Corporation

List of Attendees (contd)

- FORTENBERRY, JAMES
Jet Propulsion Laboratory
- FRIEDFELD, S. J.
TRW Systems Group
- FUCHS, H. O.
Stanford University
- GAEFCKE, R. L.
Hughes Aircraft Company
- GATCOMBE, E. K.
United States Naval Postgraduate School
- GEHRIS, J. D.
McDonnell Douglas Corporation
- GELMAN, MORRIS
NASA Goddard Space Flight Center
- GIBBONS, GLEN
Lockheed Missiles & Space Company
- GIBSON, GARY C.
Lockheed Missiles & Space Company
- GILBREATH, WILLIAM
NASA Ames Research Center
- GLIKSMAN, J. A.
TRW Systems Group
- GLUCK, R.
TRW Systems Group
- GOLDWARE, M. B.
Aerospace Corporation
- GOODWIN, FRANK A.
Jet Propulsion Laboratory
- GOYETTE, NORMAN
TRW Systems Group
- GRAM, MARSHALL B.
Jet Propulsion Laboratory
- GREENBERG, HARRY S.
North American Rockwell Corporation
- GROSKOPFS, ERNIE
SPAR Aerospace Products, Inc.
- GUDIKUNST, JAMES B.
General Electric Company
- GUY, JACK H.
General Electric Company
- HAAG, G. E.
Autonetics Division, North American
Rockwell Corporation
- HABERMAN, CHARLES M.
California State College at Los Angeles
- HALEY, J. M.
Lockheed Missiles & Space Company
- HARTHAN, L. JOHN
TRW Systems Group
- HAUSAUER, RUDOLPH J.
Hughes Aircraft Company
- HAUSHALTER, CARL H.
Emerson Electric Company
- HAYNIE, H. T.
The Boeing Company
- HENRIKSON, STANLEY M.
Lockheed Aircraft Corporation
- HERTEL, ROBERT H.
Electro-Optical Systems, Inc.
- HERZL, GEORGE G.
Lockheed Missiles & Space Company
- HORIUCHI, HARVEY
Jet Propulsion Laboratory
- HOWARD, DARNLEY M.
Johns Hopkins University
- HOWEY, CHARLES K.
Aerospace Corporation
- HUTMACHER, JOHN J.
McDonnell Douglas Corporation
- HWANG, C. M.
TRW Systems Group
- IBSON, CLIFFORD T.
Hycon Manufacturing Company
- IMUS, ROBERT E.
Jet Propulsion Laboratory
- JACKSON, DON E.
United States Air Force
- JAHNKE, EDGAR M.
Hughes Aircraft Company
- JAMES, JACK W.
Ball Brothers Research Corporation
- JENNINGS, W. A.
Philco-Ford Corporation
- JOHNSON, KENNETH G.
Jet Propulsion Laboratory
- JOHNSON, M. E.
Philco-Ford Corporation
- JONES, CALVIN L.
ESSA National Environmental
Satellite Laboratory
- KAHLER, A. E.
Lockheed Missiles & Space Company
- KAMACHAITIS, W. P.
Fairchild Hiller Corporation
- KELLEY, ROBERT E.
Aerospace Corporation
- KELSEY, GEORGE
Aerospace Corporation
- KENNEDY, BRIAN C.
Electro-Optical Systems, Inc.
- KIRKPATRICK, D. L.
General Electric Company
- KNIGHT, SHELDON A.
Quantic Industries, Inc.
- KOCIS, ROBERT W.
Jet Propulsion Laboratory
- KOK, J. C.
Lockheed Missiles & Space Company
- KOLEHMAINEN, L.
Aerospace Corporation
- KOOL, B.
Fairchild Hiller Corporation
- KOFF, EDWARD H., JR.
Jet Propulsion Laboratory
- KRAMER, NATHAN R.
Hughes Aircraft Company
- KURZEKA, W. J.
Atomics International Division
North American Rockwell Corporation
- LACY, G. T.
General Dynamics Corporation
- LAFFERTY, LANNY A.
Jet Propulsion Laboratory
- LAINE, DONALD D.
TRW Systems Group
- LASSEN, H. A.
TRW Systems Group
- LAYMAN, WILLIAM E.
Jet Propulsion Laboratory
- LEAR, T. C.
Jet Propulsion Laboratory
- LEDBETTER, D. R.
AC Electronics, Defense Research
Laboratories, General Motors
Corporation
- LEONARD, KIRKE
TRW Systems Group
- LIKINS, PETER W.
University of California, Los Angeles
- LITMAN, JAMES
Hughes Aircraft Company
- LOCATELL, FRANK C.
Jet Propulsion Laboratory
- LOHNES, R. A.
General Electric Company
- LONBORG, JAMES
Jet Propulsion Laboratory
- LOOP, FRANCIS E.
Jet Propulsion Laboratory
- LYMAN, PETER T.
Jet Propulsion Laboratory
- MACKENZIE, DONALD W.
Mechanics Research, Inc.
- MACNAUGHTON, JOHN
SPAR Aerospace Products, Ltd.
- MACK, R. A.
Hughes Aircraft Company
- MACK, THOMAS H.
Jet Propulsion Laboratory
- MAJORS, HARRY, JR.
Seattle University
- MALEK, ALBERT
The Marquardt Corporation
- MANKOVITZ, ROY J.
Jet Propulsion Laboratory
- MANN, GEORGE E.
California State College at Los Angeles
- MAROTT, R. A.
Aerospace Corporation

List of Attendees (contd)

- MARSH, PHILIP H.
Jet Propulsion Laboratory
- MARTIN, ROY J.
Sandia Corporation
- MARX, S. H.
Philco-Ford Corporation
- MATHEWS, RICHARD G.
Ball Brothers Research Corporation
- MATTEO, D. N.
General Electric Company
- MAURIC, GERHARD
Consultant
- MAYER, R. W.
Ball Brothers Research Corporation
- McDOUGAL, ALLAN
TRW Systems Group
- McFADDEN, W. C.
DynaMetric, Inc.
- McGLINCHEY, L. F.
Jet Propulsion Laboratory
- McSHERRY, JAMES C.
United States Air Force
- MEEKS, CRAWFORD R.
Hughes Aircraft Company
- MERRICK, VERNON K.
NASA Ames Research Center
- MIATECH, GERALD J.
NASA Ames Research Center
- MILIK, SAM
Hughes Aircraft Company
- MILLER, DAVID C.
Jet Propulsion Laboratory
- MILLER, RICHARD
Western Gear Corporation
- MILLIKEN, S. A.
Hughes Aircraft Company
- MOORE, RICHARD L.
Electro-Optical Systems, Inc.
- MORRIS, W. L.
Hughes Aircraft Company
- MOSS, ROBERT
Jet Propulsion Laboratory
- MOULTON, J. I.
Quantic Industries, Inc.
- MOUNTEER, CARL
Mounteer Instrument Company
- NEITZEL, F. J.
Santa Barbara Research Center
- NELSON, HARRY
Hughes Aircraft Company
- NISHIZAKA, T. J.
Aerospace Corporation
- NORMAN, ROBERT M.
Jet Propulsion Laboratory
- NOVICK, M. W.
TRW Systems Group
- O'NEILL, J. P.
TRW Systems Group
- OCKEY, T. J.
TRW Systems Group
- OLIVER, ROBERT E.
Jet Propulsion Laboratory
- OLSON, JAMI L.
Hughes Aircraft Company
- PALMER, G. DAN
TRW Systems Group
- PALMER, W. B.
TRW Systems Group
- PEFLEY, R. K.
University of Santa Clara
- PERKINS, GERALD S.
Jet Propulsion Laboratory
- PERRIN, B. J.
Ball Brothers Research Corporation
- PERRY, NORMAN V.
Applied Research Laboratories
- PETERSEN, R. S.
AC Electronics, Defense Research
Laboratories, General Motors
Corporation
- PHINNEY, D. D.
Ball Brothers Research Corporation
- POPE, D. L.
Bell Telephone Laboratories, Inc.
- POPE, ALAN
Sandia Corporation
- PRATER, C. R.
Lockheed Missiles & Space Company
- PRESCOTT, SHERBOURNE N.
Jet Propulsion Laboratory
- PUTNAM, RICHARD E.
Purdue University
- RAIT, JOHN C.
Hughes Aircraft Company
- RAMOS, DANIEL O.
General Electric Company
- RANGUS, JOHN
TRW Systems Group
- REHAK, JOHN
Philco-Ford Corporation
- RENNIE, BRUCE B.
The Boeing Company
- RICHTER, DONALD H.
North American Rockwell Corporation
- RINALDO, A. L.
Lockheed Missiles & Space Company
- ROBERT, R. D.
California State College at Los Angeles
- ROBILLARD, GEOFFREY
Jet Propulsion Laboratory
- ROBINSON, RALPH L.
Philco-Ford Corporation
- ROSENBERG, LAWRENCE M.
Jet Propulsion Laboratory
- ROTH, BERNARD
Stanford University
- ROTH, WILLIAM S.
Aeroflex Laboratories, Inc.
- RUCKER, ROBERT R.
Hycon Manufacturing Company
- RUSSELL, W. J.
Aerospace Corporation
- SACCO, STEVEN B.
Lockheed Missiles & Space Company
- SAMUELS, R. L.
TRW Systems Group
- SCHIMANDLE, WILLIAM J.
Jet Propulsion Laboratory
- SCHMITT, ROBERT H.
TRW Systems Group
- SCHNEIDER, G. W.
General Dynamics Corporation
- SCHWARTZ, WILLIAM
Philco-Ford Corporation
- SCHWARZBECK, JOHN G.
Western Gear Corporation
- SECHLER, E. E.
California Institute of Technology
- SEELIG, F. A.
The Bendix Corporation
- SEIFERT, R.
Aerospace Corporation
- SELENE, LLOYD J.
Philco-Ford Corporation
- SESSLER, DONALD R.
DynaMetric, Inc.
- SHEPHERD, BRUCE
Radio Corporation of America
- SHIBATA, H.
Aerospace Corporation
- SHINBROT, C. H.
McDonnell Douglas Corporation
- SILVER, JAMES M.
NASA Ames Research Center
- SILVERSHER, H. I.
Lockheed Missiles & Space Company
- SIMON, A. B.
Westinghouse Electric Corporation
- SIMPSON, EDWARD H.
Hughes Aircraft Company
- SIPOS, RAY
Jet Propulsion Laboratory
- SKOLNIK, SOL
Aerospace Corporation
- SMALLEN, HAROLD
Aerospace Corporation
- SMITH, WEBSTER D.
TRW Systems Group
- SMITH, WILLIAM G.
Aerospace Corporation

List of Attendees (contd)

SORENSEN, VICTOR N.
Lockheed Aircraft Corporation

SPENNY, CURTIS H.
NASA Electronics Research Center

SPERLING, FRANK
Jet Propulsion Laboratory

STEELE, OLIVER, III
Atomics International Division
North American Rockwell Corporation

STEDEL, R. F.
University of California, Berkeley

STEPHENS, JAMES B.
Jet Propulsion Laboratory

STEVENS, JAMES H.
Jet Propulsion Laboratory

STEVENSON, RONALD D.
McDonnell Douglas Corporation

STICKLEY, ROSS A.
Martin Marietta Corporation

STOWITTS, H. TOM
Western Gear Corporation

STRIBLING, MAURICE D.
Hughes Aircraft Company

TAMI, JOHN I.
Jet Propulsion Laboratory

THOMSON, GRAHAM
Hughes Aircraft Company

THOSTESEN, THOMAS O.
Jet Propulsion Laboratory

THUNBERG, F. W.
Autonetics Division
North American Rockwell Corporation

TIMM, JULIAN C.
Quantic Industries, Inc.

TINLING, BRUCE E.
NASA Ames Research Center

TOOKER, WALTER C.
TRW Systems Group

TROENDLE, J. A.
Lockheed Missiles & Space Company

TURNER, W. N.
Hughes Aircraft Company

UPTON, DEAN
Santa Barbara Research Center

VALENTIJN, HERMAN
Jet Propulsion Laboratory

VAN VOOREN, ROBERT H.
TRW Systems Group

VESCELUS, GLENN E.
Jet Propulsion Laboratory

WALKER, W. W.
Lockheed Missiles & Space Company

WALLER, C. E.
Lockheed Technical Services

WANG, TOM C.
Applied Research Laboratories

WATERMAN, ALVIN W.
The Boeing Company

WATKINS, CHARLES L.
North American Rockwell Corporation

WATKINS, E. M.
Hughes Aircraft Company

WATTENBARGER, R. L.
TRW Systems Group

WEATHERS, T. M.
TRW Systems Group

WEBER, MORRIS W.
Hughes Aircraft Company

WECHSLER, JOSEPH W.
McDonnell Douglas Corporation

WEINER, H.
McDonnell Douglas Corporation

WEISSENBERGER, STEIN
University of Santa Clara

WHEELER, BRYCE A.
Hughes Aircraft Company

WIANT, H. ROSS
General Dynamics Corporation

WICHMANN, HORST
The Marquardt Corporation

WILLIAMS, DAVID R.
Ryan Aeronautical Company

WILSON, JAMES N.
Jet Propulsion Laboratory

WINFREY, RICHARD C.
Hughes Aircraft Company

WITTE, F. S.
TRW Systems Group

WOOD, DOUGLAS P.
TRW Systems Group

WOOD, LORIN A.
McDonnell Douglas Corporation

WOOD, N.
Machine Design Magazine

YOUNG, BRADLEY H.
Lockheed Missiles & Space Company